Auxin biosynthesis in pea:
A characterisation of mutants

by

Ariane Gélinas-Marion

B.Sc. (Hons)

School of Natural Sciences

Submitted in fulfilment of the requirements for the degree of Doctor of Philosophy

University of Tasmania

January 2019

Declaration of originality

This thesis contains no material which has been accepted for a degree or diploma by the University or any other institution, except by way of background information and duly acknowledged in the thesis, and to the best of my knowledge and belief no material previously published or written by another person except where due acknowledgement is made in the text of the thesis, nor does the thesis contain any material that infringes copyright.

Authority of access

This thesis may be made available for loan and limited copying in accordance with the *Copyright Act 1968*.

Statement of published works

The publishers of the paper comprising results included in Chapter 4 hold the copyright for that content and access to the material should be sought from the respective journals. The remaining non-published content of the thesis may be made available for loan and limited copying and communication in accordance with the *Copyright Act 1968*.

Ariane Gélinas-Marion
School of Natural Sciences
University of Tasmania
January 2019

List of published works

McAdam, S.A.M., Eléouët, M.P., Best, M., Brodribb, T.J., Carins Murphy, M., Cook, S.D., Dalmais, M. Dimitriou, T., Gélinas-Marion, A., Gill, W.M., Hegarty, M., Hofer, J.M.I., Maconochie, M., McAdam, E.L., McGuiness, P., Nichols, D.S., Ross, J.J., Sussmilch, F.C., Urquhart, S. (2017) Linking auxin with photosynthetic rate via leaf venation. Plant Physiology *175*, 351-360. DOI:10.1104/pp.17.00535

Results from this publication are located in Chapter 4

Author contributions: S.A.M.M. developed the research plans for and supervised measurements of anatomy, gas exchange and hydraulics and wrote the manuscript with contributions from J.M.I.H. and M.P.E. who designed the research plans for molecular and phenotypic characterisation of mutant alleles; A.G-M. performed auxin quantifications and auxin activity analyses, writing relevant sections and collected anatomical data; S.D.C. prepared phylogenetic analyses, writing relevant sections; F.C.S. molecularly characterised a mutant allele and wrote relevant sections; E.L.M. acquired lines for auxin activity analyses; M.B., T.D., M.M., S.U. and M.C.M. collected anatomical and physiological data; P.M. designed specialised software for anatomical analyses; M.D. developed a mutant allele; D.S.N. assisted in the quantification of auxin; W.M.G. undertook resin imbedding; M.H. supervised and assisted in the characterisation of a mutant allele; T.J.B. assisted in experimental design; and J.J.R first observed the *pss* allele and complemented the writing.

McAdam, E.L., Meitzel, T., Quittenden, L.J., Davidson, S.E., Dalmais, M., Bendahmane, A.I., Thompson, R., Smith, J.J., Nichols, D.S., Urquhart, S., Gélinas-Marion, A, Aubert, G. and Ross, J.J. (2017). Evidence that auxin is required for normal seed size and starch synthesis in pea. New Phytologist *216* 193-204. DOI: 10.1111/nph.14690

Author contributions: E.L.M. and L.J.Q. measured hormone and carbohydrate concentrations and examined starch granules; T.M. performed transgenic work, measured starch concentrations and performed time course studies on seed and embryo growth; S.E.D. genotyped the plants; M.D., A.I.B. and R.T. conducted TILLING; G.A. provided promoter sequences; J.J.S. and S.U. genotyped plants and assisted with analyses; D.S.N. conducted mass spectrometry and A.G-M. analysed AuxREs; and J.J.R. supervised the research, carried out genetic aspects and drafted the manuscript.

Acknowledgements

I wish to thank all those who have provided support with their time, interest and knowledge over the last 4 years. You are many…

First and foremost, I would like to deeply thank my supervisors Adjunct Professor John Ross and Dr. Eloise Foo for supporting me during my studies. Your focus, enthusiasm, generosity and animated conversations have been much appreciated.

I also want to thank all the lovely people from Administration, the Glasshouse, the Molecular lab, the Hormone lab, the CSL (Dr. David Nichols), the Flowering group (principally Dr. Valérie Hecht) the LEAF lab and the Department in general (from honours students to head of school) for your unwavering assistance and esprit de corps!

Importantly, I deeply thank my family and friends for their unconditional and constant support. I am grateful to have you all in my life.

Finally, I want to thank my husband Stephen for being so helpful. Also, my children: Béa, for your independence and resilience, and Vince, for your warmth and gentle nature – I am so proud of you both.

Abstract

The optimisation of auxin concentrations, or auxin homeostasis, is modulated through several mechanisms including *de novo* biosynthesis, transport and inactivation, mainly conjugation and catabolism. These mechanisms are thought to work in concert to spatiotemporally regulate auxin content at a cellular and tissue level. The principal focus of this thesis will be on auxin biosynthesis and inactivation.

At present, the indole-3-pyruvic acid (IPyA) pathway is the only fully characterised route for auxin biosynthesis. In the first step, the amino acid tryptophan (Trp) is converted to IPyA by members of the TRYPTOPHAN AMINOTRANSFERASE (TAA1/TAR) family. In the second step, IPyA is converted to indole-3-acetic acid (IAA) by the YUC family of flavin-containing monooxygenases (FMO).

Members of the two gene families are widely distributed across plant species and the IPyA pathway is now considered to be the principal biosynthetic source of IAA, the main bioactive auxin in plants. However, the evidence in support for this route is primarily based on findings from *Arabidopsis*. Interestingly, previous data from *Pisum sativum* (garden pea) suggest that other auxin biosynthetic pathways may also be active in root tissue. These results expose the necessity of investigating the auxin biosynthesis pathway in a broader range of species.

Loss-of-function mutants are invaluable tools to establish links between gene function, hormone content and morphological outputs. However, auxin-biosynthesis mutants are relatively rare in species other than *Arabidopsis*. Novel recessive mutants relating to the IPyA pathway, only recently available in pea, are the basis of this thesis. These comprise two alleles with disruptions in *PsTAR1* (*Pstar1-1* and *Pstar1-2*) and four alleles affecting *PsYUC1* (the *crispoid* mutants *crd-1* to *crd-4*).

The principal focus of this thesis will be two-fold. First, to investigate the potential contributions that the IPyA pathway may have on auxin biosynthesis in pea by

monitoring auxin precursors, conjugates and auxins content from several tissue types. Second, to examine the impacts that IPyA-derived auxin may have on pea morphology by characterising the phenotypes of the auxin mutants.

In the first experimental chapter, the two *Pstar1* mutant lines are isolated. No phenotypes were observed in the novel mutants and despite *PsTAR1* being previously reported to be highly expressed in young pea seeds, the mutant analyses suggested that *PsTAR1* is not required for auxin biosynthesis during early seed development. Complications experienced in the process of identifying the homozygous recessive mutants, lead to the hypothesis that a second gene, a duplicate of *PsTAR1,* nearly identical in sequence, is present in the pea genome, further suggesting the possibility of a fifth *PsTAR* member.

In Chapter 3, the PsYUC1 enzyme structure is characterised using *in silico* techniques. Important domains and the potential binding residues of PsYUC1 are predicted. A comparative approach using the previously reported leaflet phenotypes of the *crd* alleles and the 3-dimentional structure of PsYUC1, a novel C-terminal motif is uncovered and proposed to be critical for the functioning of the pea enzyme.

In Chapter 4, a survey of the *crd* phenotypes is conducted to investigate the influence of the *PsYUC1* gene on pea development in general. Severe phenotypes are exhibited in the mutants demonstrating the importance of *PsYUC1* for lateral organ formation and suggests a role in meristematic and/or primordial cell developmental modules. Supporting this, an auxin-reporter construct revealed that auxin activity is adversely affected in the mutants. However, IAA content while only mildly reduced in the apical bud, was not affected in several tissues despite the strong phenotypes. Interestingly, the reduction in IAA aspartate conjugate (IAAsp) content in all tissues tested, suggests that the rate of conjugation is a likely mechanism for auxin homeostasis.

The last experimental chapter investigates potential explanations for the apparent decoupling of the *crd* phenotype and IAA content. Results indicated that IAAsp is the main conjugate in the shoot of pea with 2-oxoindole-3-acetic acid (oxIAA) not

being detected. In addition, root growth assays refuted a previous proposition that IAAsp is biologically active *per se* in pea roots. Furthermore, the labile IAA precursor, IPyA, is demonstrated to break down non-enzymatically and to contribute substantially to the IAA pool post-extraction. Variations on well-established extraction protocols support the use of derivatisation for the stabilisation of labile compounds in order to reliably quantify auxin.

Table of content

Chapter 1 - A summary of auxin biology

1.1. General introduction

Plants adapt their growth and development to respond to ever-changing internal and external cues. The molecular machinery that regulates the response processes is coordinated internally by signalling molecules, principally, plant hormones (reviewed in Davies, 2010). Auxin is one of the classical hormones and is considered critical to plant life. Indeed, auxin participates in a vast array of developmental processes, including root and shoot architecture, organogenesis and reproductive output, principally by modulating cell differentiation, cell division and cell elongation in a tissue-specific context (Abel and Theologis, 2010).

As with all hormone classes, auxin is a naturally-occurring bioactive compound found at low concentration (reviewed in Hedden and Thomas, 2008) . The term auxin is generally used singularly but there are five known endogenous auxins, three of which are known to have bioactive properties. Widespread in higher plants, the most studied auxin is indole-3-acetic acid (IAA). Present in a few legumes, such as peas and lentils, 4-chloroindole-3-acetic acid (4-Cl-IAA) was reported to play a critical role in seed development (McAdam et al., 2017a). Phenylacetic acid (PAA) is thought to be necessary for effective root/symbiont interaction (Somers et al., 2005). The functions carried out by indole-3-butyric acid (IBA) and indole-3-propionic acid (IPA) remain unclear. They may possibly serve as stable forms of IAA storage and can be conjugated and hydrolysed back to their original form (Ludwig-Muller, 2011), but to date, have no known specific auxin activity (reviewed in Normanly, 2010; Woodward and Bartel, 2005). All have simple chemical structures (Calderón-Villalobos et al., 2010) comprising an aromatic indole ring and a terminal carboxylic acid group.

Being integral to plant life, the regulation of auxin concentrations at a spatial and temporal level is therefore highly dynamic and finely tuned, through several processes including auxin biosynthesis, transport, and metabolism (for reviews, see

Adamowski and Friml, 2015; Korasick et al., 2013; Ljung, 2013; Zhao, 2018). Indeed, plants must constantly maintain auxin homeostasis to respond appropriately to endogenous and environmental signals.

1.1.1. IAA biosynthesis

IAA is thought to be biosynthesised in the cytosol from precursors produced by the shikimate pathway, or indole-3-glycerol phosphate (IGP), indole (Normanly et al., 1993; Ouyang et al., 2000; Zhang et al., 2008) and tryptophan (Trp) (reviewed in Davies, 2010). IGP and indole, both precursors of Trp, are also considered to be direct precursors of IAA in the "Trp-independent" route, which has been implicated in *Arabidopsis* early embryo patterning (Wang et al., 2015). However, key components, functions and developmental impacts of the Trp-independent pathway remain uncertain. On the other hand, the role of tryptophan (Trp) as the main precursor for IAA is now well established in a range of species (Kriechbaumer et al., 2006; Mashiguchi et al., 2011; Tivendale et al., 2014; Zhao, 2018).

In the past, four Trp-dependent pathways have been proposed, with each being named based by the precursor downstream of Trp: indole-3-pyruvic acid (IPyA), indole-3-acetamide (IAM), tryptamine (TRA) and indole-3-acetaldoxime (IAOx) (reviewed in Tivendale et al., 2014). Certain *in vivo* and *in vitro* experimental data have demonstrated that several compounds involved in these pathways are able to participate in auxin production. For example, labelled-TAM was shown to be converted to IAA in pea roots (Quittenden et al., 2009) and in *Arabidopsis*, the IAOx-related mutants had altered IAA synthesis (Barlier et al., 2000; Boerjan et al., 1995; Ljung et al., 2005).

In recent years, the IPyA pathway has been fully characterised and IAA is now thought to be principally biosynthesised via this route (Figure 1.1) (Won et al., 2011; Mashiguchi et al., 2011; Stepanova et al., 2011). Genes were first identified from mutant screens using the model species *Arabidopsis* (Cheng et al., 2006; Stepanova et al., 2008; Tao et al., 2008; Zhao et al., 2001) and the IPyA pathway to IAA was revealed to be a simple linear two-step process (Won et al., 2011). In the IPyA pathway, the precursor Trp is first converted to IPyA by aminotransferase enzymes

coded for by the *TRP AMINOTRANSFERASE OF ARABIDOPSIS1* (*TAA1*) and *TAA1-RELATED* (*TAR*s) gene family (Stepanova et al, 2008; Tao et al, 2008). The intermediate IPyA is then converted to IAA by flavin monooxygenases (YUCCA) enzymes (Mashiguchi et al., 2011; Won et al., 2011) encoded by the *YUC* gene family (Cheng et al, 2006; Zhao et al, 2001). Mounting genetic and biochemical evidence indicates that the IPyA pathway is most likely a major contributor to the IAA pool in higher plants due to its involvement in a range of vegetative and reproductive developmental processes (Dai et al., 2013; Mashiguchi et al., 2011; Stepanova et al., 2011; Won et al., 2011; Zhao, 2012). Many of these are described in the experimental chapters of this thesis.

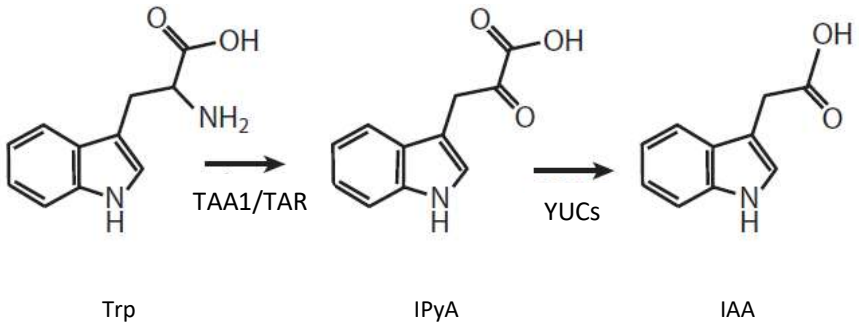

Figure 1.1. The 2-step IPyA pathway. The TAA1/TARs transaminase Trp to IPyA and the YUCs decarboxylase IPyA to IAA.

1.1.2. Sites of production and IAA transport

IAA is produced in developing tissues, such as apical buds and young leaves and is generally described as being transported downwards, in a polar fashion, towards the roots. It is transported in two distinct fashion: passively through the phloem for long-distance transport (Swarup et al., 2001) and actively between cells, assisted by efflux and influx membrane transport proteins for short-distance transport (Friml, 2003). Indeed, due to its chemical nature, IAA is less polar (or more protonated) under low pH conditions, such as in the apoplast, and diffuses readily into cells. Once in the cytosol, the pH is higher and IAA becomes unprotonated. Being

negatively charged, IAA can no longer diffuse across membrane and remains in the cell (Ljung, 2013). Active IAA transport was therefore proposed as a prerequisite for the formation and the distribution of the differential auxin concentration required by plants (Benková et al., 2003; Zažímalová et al., 2010).

The chemiosmotic model for auxin transport proposes that auxin content is modulated by the asymmetric localisation and the amount of AUXIN1/LIKE-AUX1(AUX/LAX) and PIN-FORMED (PIN) transport proteins at the cell membrane (reviewed in Friml and Palme, 2002; Swarup and Péret, 2012). Indeed, the efflux carriers, visualised with GFP, accumulated at the membrane of cells (Friml et al., 2002) and correlated with auxin-reporter constructs activity revealing that novel organs eventually emerged from sites where auxin signalling was most active (Benková et al., 2003; Dubrovsky et al., 2008). Furthermore, the *pin1* mutant of *Arabidopsis*, with altered efflux carrier distribution, formed very few organs at the shoot (Blilou et al., 2005; Petrášek et al., 2006). The polar transport of shoot-derived IAA was thought to generate the appropriate gradients and maxima required by the various sinks for growth and development to occur (reviewed in Adamowski and Friml, 2015; Robert and Friml, 2009).

However, IAA can also be locally synthesised at sites where it will be perceived. In other words, this locally produced auxin is not destined for transport but to trigger molecular changes *in situ*, at the site of production (reviewed in Zhao, 2018). Indeed, expression profiles, *in situ* hybridisation and mutant studies demonstrated that *TAA1*/*TAR*s and *YUC*s do not have ubiquitous activity but have localised and dynamic expression patterns in specific cells both at a spatial and temporal level (Cheng et al., 2006, 2007; Stepanova et al., 2008; Tao et al., 2008). Mounting evidence further supports that local auxin biosynthesis is integral to a plethora of development processes and to the capacity of a plant to respond to its changing environment (reviewed in Zhao, 2018).

Polar auxin transport and local auxin biosynthesis are two essential modes of delivery that ensure that auxin is present at the right concentration in the responding tissues.

1.1.3. Auxin perception and signalling

Auxin homeostasis is of paramount importance for growth and development to occur normally but auxin must also be perceived for any change to take place. Research in auxin perception and signalling has progressed immensely and much of the molecular machinery underpinning the mechanism has been identified, principally in *Arabidopsis*.

Nuclear auxin perception and the ensuing signalling molecular cascade relies on the ubiquitination of the AUXIN/INDOLE ACETIC ACID (Aux/IAA) proteins by the SKP-Cullin-F box (SCF) TRANSPORT INHIBITOR RESISTANT1/AUXIN SIGNALING F-BOX (TIR1/AFB) complex, referred to as the AFB receptor, once auxin is perceived (Dharmasiri et al., 2005; Kepinski and Leyser, 2005). In summary, when auxin binds to an AFB receptor, Aux/IAA docks in the pocket and is carried away for proteolysis. This derepresses the Auxin Response Factors (ARFs), liberating the associated Auxin Response Elements (AuxRE) located in the promoter region of an auxin-inducible gene and in turn, allows transcription to occur (for reviews, see Guilfoyle and Hagen, 2007; Salehin et al., 2015).

The auxin signalling machinery imparts versatile output capacity to the auxin signal. In *Arabidopsis*, there are six nuclear receptors (Dharmasiri et al., 2005), 23 ARFs (Liscum and Reed, 2002) and 29 Aux/IAAs (Tiwari et al., 2001), many of which have differing functions, half-lives and binding specificities (for reviews, see Luo et al., 2018; Parcy et al., 2016; Wang and Estelle, 2014). In addition, both ARF and Aux/IAA protein families are able to form homo-and hetero-dimers interchangeably, increasing the signalling network complexity (Del Bianco and Kepinski, 2011; Guilfoyle and Hagen, 2007). Indeed, the auxin signal can be diversified into specific responses when ARF and Aux/IAA proteins are paired into different arrangements. For example, when ARF7 is paired with Aux/IAA12 hypocotyl development is impaired but when paired with Aux/IAA3 root growth is affected (Tatematsu et al., 2004). This example demonstrates how combinations amongst the components of the signalling network can deliver a multitude of developmental output in response to auxin.

Interestingly, once Aux/IAA is degraded, the auxin molecule is released from the receptor and maintains its bioactive function (Calderón-Villalobos et al., 2012; Tan et al., 2007). Other mechanisms, such as transport and inactivation, are required to reduce the auxin signal at a cellular/tissue level.

1.1.4. Auxin metabolism

Auxin metabolism has been proposed to participate in the fine tuning of auxin homeostasis by optimising the IAA gradients at a cellular and tissue level (reviewed in Ludwig-Müller, 2011; Korasick et al., 2013). The metabolism of auxin is regulated by several mechanisms including conjugation, storage and catabolism (reviewed in Ljung, 2013). Indeed, much of the auxin, up to 75% depending on the species studied, is modified in form and is biologically inactive (reviewed in Ludwig-Müller, 2011). IAA can be conjugated to sugars or amino acids via ester links (IAA Glucose, IAGlc) and amide links (IAA-AA) respectively (reviewed in Ljung, 2013). IAA can also be oxidised (2-oxoindole-3-IAA, oxIAA) (reviewed in Stepanova and Alonso, 2016) and methylated (ester methyl IAA, MeIAA) (Qin et al., 2005; Yang et al., 2008).

Several inactive auxins, such MeIAA and IAA-Leucine (IALeu), are thought to act as storage forms of IAA, potentially rapidly delivering auxin as it is required at a cellular level (reviewed in Korasick et al., 2013). Indeed, the 'storage conjugates' can be hydrolysed to IAA (Bartel and Fink, 1995; Yang et al., 2008) and when applied exogenously, some amide-linked conjugates were demonstrated to have auxin-like activity (Ljung et al., 2002). Other inactive auxins, such as the amide-linked IAA-Aspartate (IAAsp) and oxidised IAA (oxIAA) are irreversibly inactivated and considered to be catabolites (Ljung et al., 2002; Woodward and Bartel, 2005). The auxin inactivation pathways are depicted in Figure 1.2.

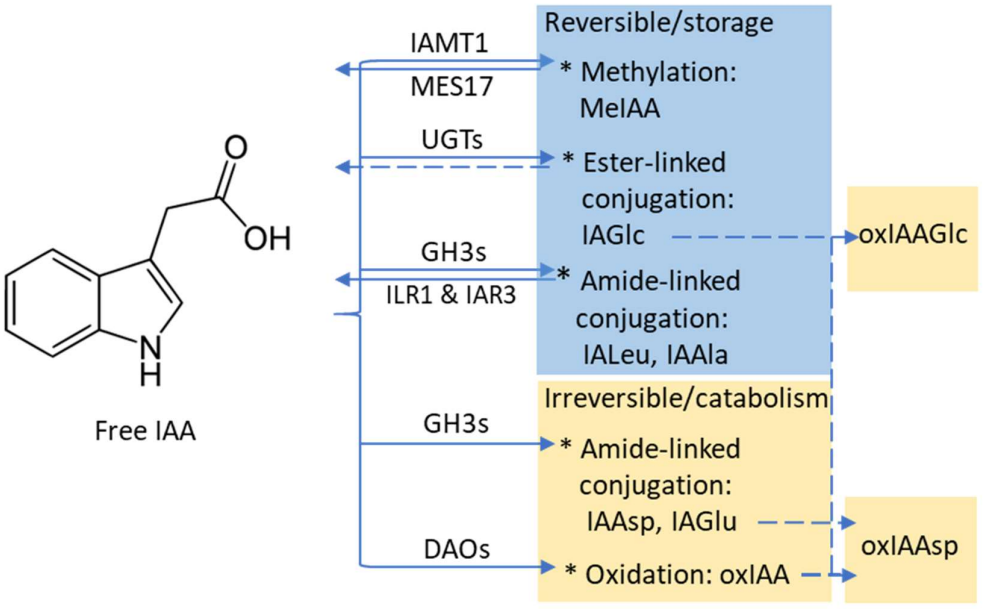

Figure 1.2. IAA metabolic pathways. IAA is methylated to MeIAA by IAMT1 and hydrolysed by MES17. The UGTs are responsible for ester-linked conjugation of IAGlc. The GH3s conjugates the amide-linked conjugates, ILRs and IAR3 hydrolyse IALeu and IAAla respectively and the DAOs oxidise IAA to oxIAA. IAAsp and oxIAA are proposed to be further broken down to oxIAAsp and oxIAA and IAGlc, to oxIAGlc. Solid arrows represent demonstrated conversions and dashed arrows indicate pathways where genes and enzymatic activity are uncertain.

Again, the pathways are complex with some of the enzyme families responsible for the conversions containing large numbers of members: hundreds for the UGTs and 19 GH3s in *Arabidopsis* (Caputi et al., 2012; Staswick et al., 2005). The function of many of the enzymes remains unknown, however, and our understanding of the biochemistry of several compounds is still incomplete (Korasick et al., 2013; Ludwig-Muller, 2011; Stepanova et al., 2011). Complicating the investigation relating to the contribution of each pathway to developmental outputs, the levels of the various metabolites vary considerably between species and in the different tissues of a single species. Furthermore, how the metabolism mechanisms communicate with one another and with the other auxin homeostasis regulatory pathway is still unclear. Indeed, much remains to be discovered.

1.1.5. *Pisum sativum* as a model species

Pisum sativum, referred to as pea hereafter, is classified as belonging to the Hologalegina clade, the 'cool-season legumes', of the Papilionoideae subfamily. The papilionoid lineage underwent a whole genome duplication event at the beginning of its speciation approximatively 50 Mya (Shoemaker et al., 2006). Duplication events are not unique to legumes and lead to paralogous duplicates with new gene copies gaining novel or diversified/specific functions over time, when compared with the ancestral genes (Cannon, 2013). The pea genome has experienced several duplication events post speciation from Medicago. Indeed, despite sharing a high degree of chromosome-based synteny with Medicago, pea has a much larger genome (up to 10 times bigger or ~4770 Mbp) (Zhu et al., 2005).

Pea and several legumes, such as soybean, lentil, chickpea, peanut, and the common bean, to name a few, are of great economic and agronomic importance (Duke, 2012). These crop species are significant resources for human nutrition, animal feed and several industries. In a scientific context, legumes are the third largest family of flowering plants and are efficient at fixing nitrogen. It is therefore imperative that model legumes be integral to studies pertaining to genetics, development biology, biochemistry, physiology and plant-microbe interactions.

Pea, in particular, due to its size, lends itself particularly well to physicochemical studies. Its short life cycle (3 to 4 generations per year) permits the crossing and selection of genetic material relatively rapidly.

1.1.6. Thesis overview

Results from mutant and phylogenetic analyses suggest that the *TAA1/TAR* and *YUC* gene families have expanded in both eudicots and monocots with extensive functional diversification in different species (Cheng et al., 2006; Fujino et al., 2008; McAdam et al., 2017a; McAdam et al., 2017b; Stepanova et al., 2008; Woo et al., 2007). Novel mutant alleles affecting *PsTAR1* (*Pstar1-1* and *Pstar1-2*) and *PsYUC1* (the *crispoid* mutants, *crd-1* to *crd-4*) are now available in pea. It is therefore of great interest to investigate their impacts on the development of a legume species.

The current thesis will concentrate on the TAR/YUC route of auxin biosynthesis in pea, addressing questions pertaining to IAA biosynthesis and metabolism and their effect on pea development.

The focus of this thesis will therefore be two-fold. First, to investigate the potential contributions that the IPyA pathway may have to auxin biosynthesis in pea by monitoring auxin precursors, conjugates and auxins content from several tissue types. Second, to examine the impacts that IPyA-derived auxin may have on pea morphology by characterising the phenotypes of the auxin mutants.

In the first experimental chapter, the strategy to identify two novel *Pstar1* homozygous recessive mutants is outlined. Obtained from the reverse genetic technique TILLING (Dalmais et al., 2008), the mutants had to be genotyped based on the identification of their respective point mutations. This goal was complicated by the fact that contradictory results were obtained from the different genotyping techniques used. One hypothesis to explain this is that a second gene, a duplicate of *PsTAR1*, nearly identical in sequence, is present in the pea genome. High-resolution melt analysis (HRM), cloning techniques and segregation ratios over several generations supported this 'Two Genes' hypothesis. Once the *Pstar1* homozygous lines were identified, phenotypes and auxin content were examined. Despite *PsTAR1* being previously reported to be highly expressed in young pea seeds, the mutant analyses revealed that *PsTAR1* is not required for auxin biosynthesis during that developmental stage. In fact, there were no obvious phenotypes attributable to these mutations.

In Chapter 3, the enzyme structure of PsYUC1, belonging to the YUC family of flavin-containing monooxygenases (FMO), is characterised using *in silico* techniques and published FMO crystal structures from bacteria. This enabled the visualisation of regions of interest and gave novel insight into the interactions between the binding pocket and the cofactors of the protein. Important domains and the potential binding residues of PsYUC1 are predicted. In addition, the similarity of severity of the leaflet phenotype across the *crd* mutants (McAdam et al., 2017b) was used to determine which PsYUC1 regions are likely to be required for the normal functioning of the enzyme. Indeed, novel regions, not previously defined as

important, are proposed to be critical for the stability and functioning of the pea FMO enzyme.

In Chapter 4, the *crd* phenotypes are further characterised to investigate the influence of the *PsYUC1* gene on pea development in general. Lateral root number, rate of node and leaflet formation, floral organ morphology and seed yield were negatively impacted when compared with wild type lines. Visualisation of auxin activity with an auxin-reporter construct from actively developing tissues in the mutants and the WTs demonstrated that auxin activity is adversely affected in the mutants. However, IAA content was not affected in root and flower tissues and only mildly reduced in the apical bud despite strong phenotypes being exhibited. Differences in IAA aspartate conjugate (IAAsp) content between the WT and the mutants suggest that the rate of conjugation is a likely mechanism for auxin homeostasis. Based on phenotypic evidence and hormone profile, I propose that *PsYUC1* is principally active at the meristematic and/or the primordial cells of root, shoot and inflorescence meristems where it participates in lateral organ formation. However, the IAA in *crd* mutants was often quite similar to that of the WT.

The last experimental chapter investigates potential explanations for the apparent decoupling of the *crd* phenotypes and IAA content. First, to test if other deactivation products are present in pea, 2-oxoindole-3-acetic acid (oxIAA), now considered to be the main auxin deactivation product in *Arabidopsis* (reviewed in Stepanova and Alonso, 2016), was monitored in pea apical portions. However, oxIAA was not detected and results demonstrated that IAAsp is the main conjugate in the shoot. In addition, the potential biological properties of IAAsp, previously proposed to be growth-promoting in pea roots (Ostrowski et al., 2016), were tested in root growth assays. This was done to ascertain that the reduced IAAsp content found in the *crd* mutants does not influence the phenotypes. The assays refuted the theory that IAAsp is biologically active *per se*. Furthermore, the unstable IAA precursor, IPyA, was previously shown to accumulate in *Arabidopsis* higher-order *yuc* mutant and its nonenzymatic breakdown was proposed to partially restore IAA content in mutant samples post-extraction. The present results do not support this proposition as the *crd-4* mutant did not contain higher levels of IPyA when compared with WT. However, and of great interest to the field of auxin quantification, IPyA is confirmed

to break down nonenzymatically and to contribute substantially to the IAA pool post-extraction in all biological samples tested. A well-established extraction protocol, involving derivatisation for the stabilisation of IPyA, was adapted here in order to reliably quantify IAA.

Chapter 2 - The auxin biosynthesis gene *PsTAR1*

2.1. Introduction

Indole-3-acetic acid (IAA), the principal auxin in plants, is now thought to be principally biosynthesised via the two-step indole-3-pyruvic acid (IPyA) pathway (Mashiguchi et al., 2011; Won et al., 2011). In the first step, tryptophan (Trp) is converted to IPyA by the Trp aminotransferase enzymes. The Trp aminotransferases were first identified in *Arabidopsis* from two independent forward genetic screens (Stepanova et al., 2008; Tao et al., 2008).

2.1.1. The tryptophan aminotransferases

Phenotypic analysis of two allelic mutants with disruptions in the *TRYPTOPHAN AMINOTRANSFERASE OF ARABIDOPSIS1* (*TAA1*) gene indicated that TAA1 is a key enzyme involved in auxin-dependent developmental processes and in auxin biosynthesis. The shade-avoidance *sav3* mutant has reduced auxin biosynthetic activity and diminished auxin response or hypocotyl elongation when compared with the WT under shade conditions (Tao et al., 2008). The ethylene-insensitive *wei8* mutant does not exhibit obvious morphological defects when compared with WT apart for root-specific defects when an ethylene precursor (ACC) is applied during growth (Stepanova et al., 2008). Four extra *TAA1*-related genes (*TAR1-4*) were also identified. Similarly to *taa1*, single *tar* mutants do not have obvious phenotypes, but multiple mutant combinations containing *taa1* exhibit severe defects in meristem maintenance, root gravitropism, apical hook and gynoecium development. Results from the mutant combination analysis indicate a level of functional redundancy within the TAR family in *Arabidopsis* (Stepanova et al., 2008).

Additional *taa1* mutant alleles were subsequently characterised. The auxin transport

inhibitor N-1-napthylpthalamic (NPA) -resistant *tir2* plants have reduced auxin activity under high temperature treatment. Root gravitropic defects, reduced root meristem and hypocotyl auxin response phenotypes were observed in the mutant (Yamada et al., 2009). Lastly, the cytokinin-induced root curling 1 (*ckrc1*) mutant is insensitive to cytokinin. The addition of cytokinin did not induce the expression of *TAA1* in the mutant but did so in the WT. The *ckrc1* mutant has defective root gravitropic response and reduced primary root growth (Zhou et al., 2011). The pleiotropic phenotypes of the mutant alleles demonstrate the importance of the TARs for plant development and the extent to which the enzymes contribute to multiple regulatory processes and interacts with a range of phytohormone pathways.

The TARs have strong sequence similarities with the alliinases found in *Allium* species (Kuettner et al., 2002) and belong to the super-family of the α class of pyridoxal-5-phosphate (PLP) dependent enzymes (reviewed in (Percudani and Peracchi, 2003). Structural crystal studies of TAA1 proteins in bonded configuration with ligands revealed important residues for interaction with the PLP cofactor and confirmed that Trp is the preferred substrate for TAA1 (PDB code: 3BWN, www.rcsb.org; Tao et al., 2008). *In vitro* assays of the WT and the mutant purified proteins tested in the presence of PLP confirmed that TAA1 has Trp aminotransferase activity while activity in the mutant proteins was reduced (Stepanova et al., 2008). Furthermore, the levels of IPyA extracted from *Arabidopsis* seedlings and flower buds from higher order mutants had a 32% and 62% reduction respectively when compared with WT (Mashiguchi et al., 2011).

The Trp aminotransferases are highly conserved in angiosperms. The TARs have been identified in *Arabidopsis* (Tao et al. 2008; Stepanova et al. 2008), maize (*Zea mays*) (Phillips et al., 2011), rice (*Oriza sativa*) (Abu-Zaitoon et al., 2012; Yoshikawa et al., 2014), pea (*Pisum sativum*) (Tivendale et al., 2012) and wheat (*Triticum aestivum*) (Shao et al., 2017). Unlike in *Arabidopsis*, single *tar* mutants outside of the *Brassicaceae* have strong phenotypes when grown in normal conditions. For example, in maize, *vanishing tassel2* (*vt2*), a *TAA1* co-orthologue, is semi-dwarf, has reduced leaf numbers due to defects in leaf initiation, barren inflorescences and overall reduced cell elongation (Phillips et al., 2011). Similarly, the *fish bone* (*fib* and *fbl*) rice mutants have severe vegetative and reproductive

phenotypes due to a reduction in IAA levels (Yoshikawa et al., 2014). This indicates that the genetic and functional redundancy amongst the TARs in *Arabidopsis* appears to be less prevalent in other species and stresses the importance of investigating gene function at a multi-species level.

2.1.2. Specific roles for the TARs in seed development

The TARs are now well established as being central to auxin biosynthesis. There is also increasing evidence demonstrating the importance of the generation and maintenance of auxin gradients through *de novo* auxin synthesis during embryogenesis and seed growth (reviewed in (Robert et al., 2015). The *TAR* gene family has been shown to be required during embryogenesis but expression patterns and spatial and temporal contribution of the specific TARs is variable across species. Indeed, in *Arabidopsis*, triple mutants are required to obtain embryo defects (Stepanova et al., 2008). Discriminating between the developmental effects of the five TARs is challenging due to their apparent functional overlap.

Rice contains only two TARs (Abu-Zaitoon et al., 2014). A 50-fold increase in IAA was recorded during grain development and so, an increase in the expression of auxin biosynthetic genes was predicted. *OsTAR1* (*FBL*) expression was weak in the early developmental stage (1 day after pollination, DAP) but increased dramatically at the beginning of the major starch synthesis phase (7 DAP) and was maintained until starch deposition was complete (21 DAP). On the other hand, *OsTAR2* (*FIB*) was highly expressed throughout seed development (Abu-Zaitoon et al., 2014). Interestingly, *OsTAR2* was also constitutively expressed throughout the plant in all tissues tested while *OsTAR1* was only expressed in anthers, ovaries and seeds (Yoshikawa et al., 2014). These results suggest that *OsTAR1* codes for a grain-specific TAR.

2.1.3. TARs in pea seeds

The common garden pea, *Pisum sativum*, is an important model organism. It can represent higher plants in general and commercially important legume crop species

in particular. As pea seeds are an important protein-rich source of food and feedstock, understanding how the TARs affect seed development has the potential to enhance yield and productivity.

There are four sequenced *TARs* in pea; three are annotated in GenBank (*PsTAR1, PsTAR2, PsTAR3,* www.ncbi.nlm.nih.gov/) and the forth *TAR* (PsCam057706) can be found in the Pea RNA gene atlas (bios.dijon.inra.fr/FATAL/cgi/pscam.cgi). Data from the Pea RNA Atlas show a clear delineation of gene expression amongst the *PsTAR* members. *PsTAR1* and *PsTAR3* are close homologues, sharing a high sequence similarity. However, they are differently expressed spatially with *PsTAR1* being mainly expressed in young pods and immature seeds, while *PsTAR3* is predominantly expressed in the root system. *PsTAR2* and its closely related PsCam057706 are expressed in all tissues tested (Table S2.1).

Expression profiles of *PsTAR1*, *PsTAR2* and *PsTAR3* in developing seeds have been described (McAdam et al., 2017a; Tivendale et al., 2012). Similarly to rice, expression profiles of the *PsTAR*s were also temporally partitioned but somewhat differently (Tivendale et al., 2012). *PsTAR1* was predominantly expressed in the early stages of seed development unlike *OsTAR1* that predominated in the later stages (Abu-Zaitoon et al., 2014). The high expression of *PsTAR1* also correlated with elevated levels of IAA. As seed development progressed, at 12 days post anthesis (DPA), IAA levels decreased substantially as did *PsTAR1* expression. A reversal of the pattern occurred with *PsTAR2* (Tivendale et al., 2012). Low expression levels in the early stages correlated with low levels of the highly bioactive seed-specific chlorinated form of auxin found in pea (4-Cl-IAA) (Lam et al., 2015; Reinecke, 1999). At 16 DPA, *PsTAR2* was highly expressed and high levels of 4-Cl-IAA were recorded. In the later stage (35 DPA), 4-Cl-IAA content had substantially decreased, *PsTAR2* expression had decreased by 60% and *PsTAR3* was marginally expressed, but still only about 5% of the *PsTAR2* expression level (Tivendale et al., 2012). *PsTAR3* does not appear to be an important contributor during seed development.

Furthermore, hormone analysis of a *Pstar2* mutant allele demonstrated that IAA content in young seeds was not decreased when compared with WT but 4-Cl-IAA

had decreased by 90% in the later developmental stages (Tivendale et al., 2012). Reduced auxin content was subsequently linked to seed phenotype. Indeed, mature seeds of the *Pstar2* mutant alleles are smaller, in part due to smaller cell size, and *Pstar2-1* seeds are wrinkled, with significantly decreased starch content and starch granule morphology resembling that found in immature WT seeds (McAdam et al., 2017). These results indicate that *PsTAR2* is a key determinant in starch synthesis and accumulation during the later stages of seed development and is most likely involved in 4-Cl-IAA synthesis (McAdam et al., 2017a). This raises the question; does *PsTAR1* function as an important auxin biosynthesis gene in early pea seed development? And is *PsTAR1* required for successful embryo development?

2.1.4. The *Pstar1* mutant alleles

Eleven uncharacterised *Pstar1* mutant alleles were previously obtained from an ethyl methanesulfonate collection using the Target-Induced Local Lesions in Genome (TILLING) screening method (Table S2.2). TILLING is a forward and reverse genetics protocol developed for species that are recalcitrant to *Agrobacterium*-based transformation, such as pea (Dalmais et al., 2008). Two of those lines, line 905 and 2601, were predicted to produce truncated proteins while five had SIFT scores below the accepted threshold and were therefore predicted to be aberrant.

Several lines with a range of predicted impacts were grown to obtain mutants and to compare the effects of the different mutations: line 784, 1240, 2121 and 1424, predicted as aberrant and line 970 and 2374, predicted to be WT-like. However, no obvious phenotypes were perceivable, and no homozygous recessive individuals were detected from any of the *Pstar1* populations (R. Ali, unpublished).

Similarly, no phenotypes or mutants were detected from the two lines predicted to produce truncated proteins (line 905 and 2601). The lack of homozygous mutant seeds in the *Pstar1* lines led to a model proposing that *PsTAR1* is required for successful reproduction to occur (Ross et al., Auxins and Cytokinins in Plant Development 2014, conference abstract 01-9, p.23).

The requirement of specific genes to the process of fertilisation has previously been demonstrated in *Arabidopsis* mutants. The *abstinence by mutual consent* (*amc*) mutant has disrupted male/female gamete interaction during fertilisation (Boisson-Dernier et al., 2008). Recessive pollen tube growth and discharge is impaired when interacting with a recessive female gametophyte, thus preventing the production of homozygous mutant seeds. Boisson-Dernier and colleagues (2008) proposed that 'a diffusible signal emanating from either gametophyte' is required for pollen tube reception. In this model, the impaired production or release of an unknown molecule from a recessive gametophyte can be rescued by the presence of the molecule produced by another functional gametophyte (Boisson-Dernier et al., 2008). The phenomenon of a second pollen tube rescuing an earlier failed attempt at fertilisation by a previous dysfunctional gamete was termed 'fertilisation recovery' by Kasahara and colleges (2012). The fertilisation rates of the gametophytic fertility mutant *duo pollen3-2* (*duo3-2*; also called *g21)* were higher than expected due to WT pollen fertilising an ovule after a failed attempt by a mutant pollen (Kasahara et al., 2012).

This similar line of logic was extended to our system as the novel *Pstar1* mutant lines did not appear to be able to produce homozygous mutant seeds. The *Pstar1* pollen tube and female gametophytes could have impaired *de novo* auxin biosynthesis. If auxin directly or indirectly modulates a signal required for male-female interaction, a decrease in auxin content would prevent the recessive gametes from fertilising one another. However, if gametes were viable and an essential auxin pool derived from *PsTAR1* was impaired in the mutants, seeds may be formed but abort during the early embryo stages.

This led to speculation regarding potential reasons for the apparent lack of homozygous recessive seeds/plants for either of the two mutations concerned.

Three potential explanations are:

1. Recessive pollen fertilises recessive ovule, a homozygous recessive zygote is produced but subsequently aborts.

2. One of the recessive gametes is not viable and the one that is, gets fertilised by a dominant one.

3. The two recessive gametes are viable, but their interaction is impaired for an unknown reason.

2.1.5. Aims

The aims of this chapter are to investigate the roles that *PsTAR1* may have in pea development in general with a particular focus on seed production and development. Based on previous methods employed to examine *PsTAR2* function in auxin biology and seed development (Tivendale et al., 2012; McAdam et al., 2017), similar strategies will be used to address the goals of this project. A multidisciplinary approach comprising genetic and molecular techniques, auxin quantification and morphological characterisations will be used to tackle the next three specific goals.

The first goal, with a focus on the two truncated lines (905, *Pstar1-1* and 2601, *Pstar1-2*), is to isolate and obtain novel *Pstar1* mutant and to characterise the mutant alleles. Gamete viability and rate of seed abortion will also be investigated to further test the impacts of the *Pstar1* mutations on those developmental processes. A polymerase chain reaction (PCR), restriction fragment length polymorphism analysis (RFLP) and sequencing based approach will be used to genotype the segregating populations and identify the *Pstar1* mutants.

The second goal is to characterise the phenotypes of the novel *Pstar1* mutants. Morphological phenotypes will be examined for each genotype. All apparent vegetative phenotypes will be monitored, with an emphasis on reproduction and early seed development.

The third goal is to investigate if *PsTAR1* has a temporal auxin biosynthesis role during seed development. IAA and 4-Cl-IAA content, two auxins relevant to seed development (Reinecke et al., 1999; Tivendale et al., 2012; Lam et al., 2015; McAdam et al., 2017), will be quantified in *Pstar1* mutants and WT seeds. Analysing auxin patterns in *Pstar1* mutants will help to test if the *Pstar1-1* and *Pstar1-2* mutations physiologically affect seed development.

2.2. Materials and Methods

2.2.1. Plant materials

The *Pstar1-1* (line 905) and *Pstar1-2* (line 2601) alleles (the mutant alleles) are on the dwarf Caméor background (line JI 3253) and were back-crossed six times to remove any other mutations potentially present in the genome. The wild-type (WT) plants used for this study were the dwarf (*le-1*) *cv*. Caméor, the tall (*LE*) *cv*. Torsdag (JI 3167) and the WT progeny segregating from heterozygous parents. All plants used were the progeny from the sixth backcrosses. Seeds were nicked to allow for even germination rate and treated with a fungicide at sowing time. All plants were grown individually in slimline 14 cm sterilised pots containing a 1:1 ratio of vermiculite and gravel then topped with 3 cm of potting mix. Seeds were germinated and grown in a heated greenhouse under natural photoperiod conditions (Hobart, Tasmania).

Of importance to note and to clarify nomenclature, *Pstar1-1* and *Pstar1-2* are referred as the '905 SNP' (Single Nucleotide Polymorphism) and the '2601 SNP', respectively, in some of the experiments included in this chapter.

2.2.2. Genomic DNA extraction

Genomic DNA extraction of all plant material was performed using a modified version of a CTAB protocol described in (Doyle and Doyle, 1987). Young expanding leaves were harvested (~100 mg), immediately frozen in liquid N_2 and stored at -80°C until needed. Material was grinded for 2 minutes (30Hz) with a Tissue Lyser in 1.7ml screw-cap Eppendorf tubes containing Tungsten carbide beads (3mm, Qiagen) without lysis buffer. This step is critical as it disrupts the cells, releases the nucleic content and shears proteins and carbohydrates contained in the plant material. Extraction buffer (500 µl; 100 mM TRIS-HCl pH 8, 1.4 M NaCl, 20 mM EDTA, 2% w/v CTAB) was added to each tube, thoroughly mixed and incubated at 60°C for 30 min. Two purification steps were then performed

sequentially where 500 µl of chloroform/Isoamylic alcohol (24:1 ratio) was added to the tubes, mixed by gentle inversion, centrifuged at 14000 rpm for 1 min and the upper aqueous phase was transferred to new 1.5 ml tubes. After the majority of the organic content was removed from the samples, 1ml of precipitation buffer was added (50 mM TRIS-HCl pH 8, 10 mM EDTA, 1% w/v CTAB), mixed by gentle inversion, incubated at room temperature for 10 min and centrifuged at 14000 rpm for 10 min to form a pellet. Supernatant was discarded, RNAse A buffer added to the tubes containing the pellet (300 µl; 1.5M NaCl, 25mg/ml Rnase A) and incubated for 30 min at 50°C. To precipitate the DNA, 600 µl of 100% ethanol was then added to the tubes, inverted gently, centrifuged at 14000 rpm for 10 min and the supernatant discarded. Pellet was washed (200 µl; 70% ethanol), centrifuged at 14000 rpm for 5 min, air-dried and resuspended in 100 µl of water. All DNA samples were kept at -18°C.

2.2.3. Sequencing primer design

All primers were designed using Primer 3 (fokker.wi.mit.edu/primer3/input.htm) with an optimal primer size of 30±2 base pairs (bp), melting temperature (*Tm*) of 70±1°C and a GC nucleotide % of 35 to 55. Primer efficiency and secondary structures were tested for with Net Primer (premierbiosoft.com). Hairpins of -0.64, 3' dimmers of -8 and 5' dimmers of -6 were tolerated. All primers used for sequencing are included in Table 2.2. Once sequenced, data were organised with the Sequencher software (5.1), which also provided the predicted coding protein sequences necessary for further analyses. The genomic sequence of *PsTAR1* is included as a reference (Figure S2.1).

Table 2.2. Full-length and nesting primers used for sequencing *PsTAR1*.

Gene	Primer name	Sequence (5' to 3')
PsTAR1	67g Fw (gDNA)	TCCAAACACAAGAACTAAAACCAACAACTA
	90 Fw (cDNA)	ATGGTGGTTGCTAGAGACGGTTCATCATCT
	126Nest Fw (cDNA)	TACCTCTCTCCAATCTCTCATACGA
	836 Rev (cDNA)	CGAAAAAGAGGCGGTCTGATGGAGTG
	1418Nest Rev (cDNA)	CATCACAAATCACTTCAATAATCTTAGCAG
	ENTR_R1 (cDNA)	TCATTCTATTTTAGCATTTTCC

2.2.4. Phylogenetic analysis

The phylogeny of *Pisum sativum TAR*s was inferred using alignments of full- length translated TAA1/TAR protein sequences. The phylogeny tree was rooted using the canonical garlic alliinase (Rabinkov et al., 1994). Sequences can be found under the relevant accession numbers in the GenBank/EMBL database, the Arabidopsis information resource TAIR (www.arabidopsis.org/) and the pea RNA-seq gene atlas (bios.dijon.inra.fr/FATAL/cgi/pscam.cgi). The sequences were aligned using clustalW (www.genome.jp/) with BLOSUM matrices as these are the most efficient at carrying out protein database homology searches.

2.2.5. Genotyping

Due to the lack of visual phenotypes in the two mutant lines, genotyping protocols based on PCR and restriction fragment length polymorphism analysis (RFLP) were developed for the *Pstar1* alleles (Dr S.E. Davidson and Dr L.J. Quittenden) (Table 2.3). Prior to digest, gDNA was extracted, as above, and amplified with the Advantage 2 polymerase mix (Clontech) or the proofreading polymerase (Velocity DNA polymerase; Bioline). In some instances, seedling tissue was amplified with the Terra PCR Direct Polymerase Mix (clontech.com). For both strategies, allele specific CAPS markers designed using the dCAPS Finder 2.0 (helix.wustl.edu/dcaps/dcaps.html) were used to amplify the desired amplicons

(Table 2). Aliquots from the PCR products (5 µl) were digested using the CutSmart Buffer protocol (NEB.com) with template specific restriction enzymes (Table 2.4). NEB recommended protocols for each enzyme were followed.

Table 2.3. RFLP specific primers for each allele in line 905 and line 2601.

Line	allele	Primer name	Sequence (5' to 3')
905	WT	905dCap Fw	GGGTGATCCAGTGGGATTCAGGAAATTCCG
		391 Rev	CAGCAACAACATTGAAGGGAATATGAGAGG
	mutant	67gFw	TCCAAACACAAGAACTAAAACCAACAACTA
		391 Rev	CAGCAACAACATTGAAGGGAATATGAGAGG
2601	WT	133 Fw	GGAGAAATTGAGTGAAGAAGCAAAAGTGG
		91 Rev	TGACACACCAATGGAGCTTAGGTGCAAG
	mutant	1071dCAP Fw	GGAATGTTGTTTATGACTTGGCCTATTCTT
		91 Rev	TGACACACCAATGGAGCTTAGGTGCAAG

Table 2.4. *PsTAR1* lines with respective enzymes used, amplicons size from PCR product and cut patterns expected for each allele.

Line	Cleaved allele	Amplicon size	Enzyme required	Cleaved product
905	WT	290 bp	HpaII	270/20bp
	mutant	526 bp	DdeI	267/258
2601	WT	1100 bp	BsII	838/262
	mutant	292 bp	DdeI	272/30

2.2.6. Inferred protein structure and binding sites

The *PsTAR1* and mutant alleles protein architectures were predicted using the Phyre2 server (Kelley and Sternberg, 2009). For visualisation and presentation, structures generated with RaptorX were used due the manipulation capacity of the server (http://raptorx.uchicago.edu). To identify the potential binding residues, MAMMOTH (Ortiz et al., 2002) was used to perform a full structural scan of the modelled structure against a library of protein structures with bound ligands.

Homologous structures were then aligned with TMalign (Zhang and Skolnick, 2005) which resulted in the identification of the ligand clusters. Residues that were within a distance threshold (0.8 ångström) of the clustered ligands were predicted to be part of the binding site. Data were then compared to the *Arabidopsis* TAA1 (Tao et al, 2008) to infer the relevant binding residues of PsTAR1.

2.2.7. Reciprocal crosses

Reciprocal crosses were performed to assess if the female or the male *Pstar1-1* and *Pstar1-2* recessive gametes are viable or if the interaction between the two recessives is impaired, thus preventing fertilisation. Torsdag (line 107, *LE*) was used to ascertain that our original crosses were successful, as *LE*, in Torsdag, would rescue the dwarf phenotype of Caméor in the F1 generation.

All plants used in the crosses were emasculated prior to anther dehiscence. Mature pollen from Torsdag (line 107) was used to pollinate *PsTAR1.Pstar1* flowers and mature *PsTAR1.Pstar1* pollen was used to pollinate Torsdag. Resulting F1 seeds were grown. If the male recessive gametes are not functional, heterozygotes should not be obtained when crossed to Torsdag and if the female gametes are not viable, heterozygotes should not be produced when fertilised by Torsdag pollen. If interaction between the two recessive *Pstar1* gametes is impaired, the F2 generation originating from the heterozygotes carrying the *Pstar1* alleles should not produce any homozygous recessive seeds. All plant material was sequenced and genotyped using RFLP protocols.

2.2.8. Caméor and Torsdag SNP segregation

The complete cDNA sequences of *PsTAR1* found in Genbank (ncbi.nlm.nih.gov) were aligned using ClustalW (genome.jp) to find the presence of single nucleotide polymorphisms (SNPs) between the Caméor and Torsdag cultivars. As a positive control, the inheritance and segregation of SNPs were monitored for in the sequenced progeny originating from the reciprocal crosses.

2.2.9. High resolution melt analysis

High resolution melt (HRM) analysis was conducted using a SensiFAST HRM Kit (Bioline) with gene specific primers (Table 2.5). Each reaction contained 2 µL of sample gDNA (~ 50 ng µL), 5 µL of Sensifast mix, 1 µL each of forward and reverse primer (10 mM) and dH2O. Reactions were mixed using a CAS- 1200 liquid handling robot (Corbett) and amplified using a rotorgene Q real time PCR cycler (Qiagen). All cycling runs were as follows: 95°C for 5 minutes, 50 cycles of (95°C for 10 seconds, 60°C for 30 seconds), 95°C for 5 minutes, 50°C for 5 minutes. HRM analysis included a 90 second first step and then, between 65°C and 85°C, temperature was incrementally increased by 0.1°C every 2 seconds. Only samples with confidence level of 95% and above were included in the results.

Table 2.5. Primers used to genotype line 905, line 2601 and SNP2 contained in *PsTAR1* using high resolution melt analysis (HRM).

Gene	SNP	Primer	Sequence (5' to 3')	Amplicon size
PsTAR1	905	126 Fw	TACCTCTCTCCAATCTCTCATACGA	301 bp
		303 Rev	CTTATCTTCTGTGTTTGCATTCCCA	
		242g Fw	GTGATCCAGTGGGATTCAGG	138 bp
		379g Rev	TTGCATTCCTCATTTGTGGT	
	2601	1066g Fw	CTGATGGAGAAGGGAATGTTG	134 bp
		1200g Rev	CGATACGAGAACCGGCGTGA	
	SNP2	334 Fw	TTGGGAATGCAAACACAGAA	139 bp
		453 Rev	TAATGAGGAGCAGCAGCAAC	

2.2.10. Transformation

Pisum sativum gDNA was extracted from apical portions of 4-week-old Caméor, *PsTAR1-1* and *Pstar1-1* seedlings. PCR with Advantage 2 polymerase mix (Clontech) and ThermoPol (NEB) and gene specific primers (Table 2.6) resulted in PCR fragments with the expected bands (227 base pairs) on agarose gel. The PCR

products were purified (PCR clean-up system; Promega), ligated into pGEM-T-easy, and transformed into JM109 competent *Escherichia coli* (Promega). Plasmid DNA was isolated from individual colonies (Wizard plus SV minipreps; Promega) and sequenced by Macrogen DNA sequencing services (dna.macrogen.com/eng/). Nucleotide sequences were analysed and cleaned up using the Sequencher software version 5.1 (genecodes.com).

Table 2.6. *PsTAR1* specific primer used to transform line 2601.

Gene	Line	Primer name	Sequence (5' to 3')	Amplicon size
PsTAR1	2601	1081 FW	CTGATGGAGAAGGGAATGTTG	227 bp
		1304g Rev	CGATACGAGAACCGGCGTGA	

2.2.11. Phenotypic characterisation

Internode and stem length, shoot to root dry weight ratios, flowering node, time of flowering, number of pods, seeds per pod and seed weight were quantified and recorded.

2.2.12. Quantification of free auxins and UPLC-MS

Endogenous IAA and 4-Cl-IAA levels were measured from excised immature seeds (7 days post anthesis; 5mg each) from single pods. Seeds numbers ranged between 5.5 and 6.5 for each sample. Seeds were pulverised with a physcotron (Microtech) in 1 ml of 65% isopropanol containing 250 mg L-1 of butylated hydroxytoluene (BHT) along with the labelled internal standards [$^{13}C_6$] IAA (Cambridge Isotope Laboratories) and [$^{2}H_4$] 4-Cl-IAA (generously supplied by Prof. Jerry Cohen). Samples were extracted overnight at 4°C then centrifuged to form pellets. The supernatants were transferred to clean eppendorfs and dried in a sample concentrator. Hormones were resuspended in 1% acetic acid in dH2O before being analysed by LC-MS.

Samples were analysed as previously (Cook et al., 2016) with a solvent combination of 1% (v/v) acetic acid in water (solvent A) and acetonitrile (solvent B). The modified UPLC program, 'Phenylalanine Method' or PA Method, was 95% A: 5% B to 50% A: 50% B at 4.5 min, followed by immediate re-equilibration to starting conditions for 3 min. The flow rate was 0.35 mL min^{-1} with the column held at 35°C, and the sample compartment was at 6°C. The mass spectrometer was operated in positive and negative ion electrospray mode with a needle voltage of 2.8 kV, and MRM was used to detect all analytes (Table 2.7). The ion source temperature was 130°C, the desolvation gas was N_2 at 950 L per $hour^{-1}$, the cone gas flow was 100 L per $hour^{-1}$, and the desolvation temperature was 450°C. Data were processed using MassLynx software.

Endogenous hormone level contained within each sample was calculated by comparing the endogenous hormone transition peak area from and corresponding internal standard peak area.

For IAA:

$$\frac{\text{endogenous peak area}}{\text{exogenous peak area}} \times \frac{\text{ng of internal standard added}}{\text{g of fresh weight (FW)}} = \text{ng of IAA per g FW}$$

The levels of 4-Cl-IAA were calculated in the same manner, however, a correction factor had to be used prior.

To correct endogenous 4-Cl-IAA:

uncorrected peak area – 0.06 x uncorrected internal standard peak area

To correct internal standard [$2H_4$]4-Cl-IAA:

uncorrected peak area – 0.035 x uncorrected endogenous peak area

Table 2.7. MRM transitions monitored to identify and quantify endogenous auxins and labelled standards.

mode	Analyte	Primary transition	Approximate RT (min)
+	Indole-3-acetic acid	176.7 to 130.1 m/z	2.5
+	[$^{13}C_6$] Indole-3-acetic acid	182.1 to 136.1 m/z	2.5
+	4-Chloroindole-3-acetic acid	210.1 to 164.1 m/z	3.4
+	[$^{2}H_4$] 4-Chloroindole-3-acetic acid	214.1 to 168.1 m/z	3.4

2.3. Results

2.3.1. *PsTAR1* is a Trp aminotransferase

PsTAR1 belongs to the *Arabidopsis TAA1* clade (Tivendale et al., 2012) and similarly to *TAA1*, *TAR1* and *TAR2*, clusters separately from the canonical garlic alliinase (Figure 2.1). The translated PsTAR1 protein shares greatest homology with TAA1 from *Arabidopsis* (Table 2.8). The alliinase C-terminal /aminotransferase class I and II domains are conserved in PsTAR1 as are important binding and catalytic amino acids (Figure S2.1) (Tao et al., 2008).

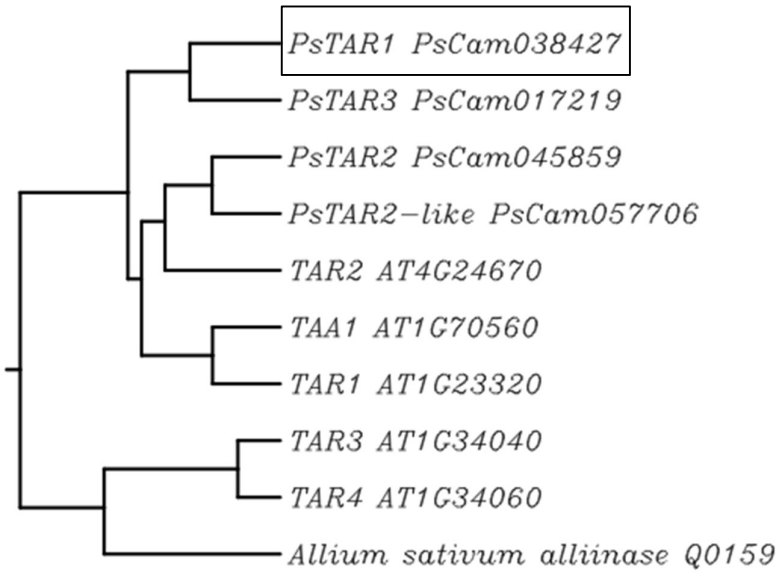

Figure 2.1. Inferred phylogenetic tree of the *Arabidopsis* and *Pisum TAR* family members. cDNA sequences and appellation from TAIR (www.arabidopsis.org/index.jsp) and the pea RNA-seq gene atlas (bios.dijon.inra.fr/FATAL/cgi/pscam.cgi). Rooted tree generated using ClustalW (www.genome.jp) with the default parameters.

Table 2.8. Similarity scores of the TAR proteins generated by ClustalW (www.genome.jp). Arabidopsis sequences originate from TAIR and pea sequences from Genbank (ncbi.nlm.nih.gov) and the Pea Gene Atlas

Proteins	PsTAR1	PsTAR2	PsCam01719	PsCam057706
AtTAA1	49	51	51	49
AtTAR1	47	50	50	51
AtTAR2	45	55	46	56
AtTAR3	33	33	38	30
AtTAR4	31	33	35	30

Several pea lines carrying mutations in the *TAR1* gene were obtained from a TILLING programme. Two lines were selected because they had point mutations resulting in premature truncation in the coding region. The *Pstar1-1* mutation (line 905) contains a G to A substitution early in the second exon and the *Pstar1-2* mutation (line 2601) contains a G to A substitution halfway through the third exon (Figure 2.2). Both mutations convert the affected Trp residue (W45 and W200, respectively) to a stop codon. Truncation occurs prior to the important catalytic lysine residue necessary to the transamination of pyridoxal-5-phosphate-dependent aminotransferases (Figure 2.2) (Ferreira et al., 1993; Hennig et al., 1997). The *Pstar1-1* and *Pstar1-2* mutations are therefore considered to be null alleles.

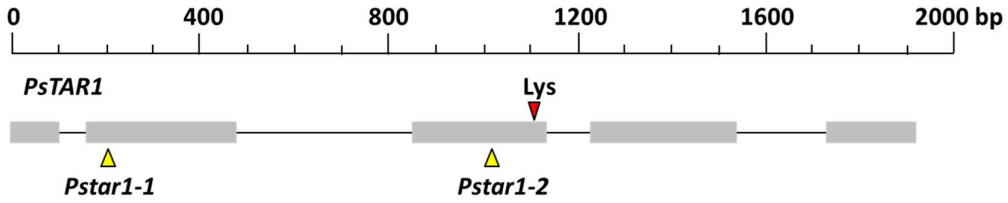

Figure 2.2. Schematic representation of *PsTAR1* genomic sequence from the ATG start to the TGA stop. The grey boxes are the exons. The two pea mutant alleles are marked *Pstar1-1* (L905, G203A) and *Pstar1-2* (L2601, G1041A). The three nucleotides (starting at 1103) coding for the catalytic PLP binding site are marked as Lys.

2.3.2. Inferred mutant proteins functionality

As the two *Pstar1* mutant alleles harbor stop codons prior to the PLP binding site, very little protein functionality should to be retained by the truncated proteins. Inferred protein structures based on the *Arabidopsis* TAA1 crystal structure revealed little capacity for catalytic activity to occur (Figure 2.3). Indeed, based on the *Arabidopsis* TAA1 protein NMR in solution with several ligands, predicted binding residues are missing in the pea mutant alleles, including the Alliinase C-Terminal (Figure S2.1).

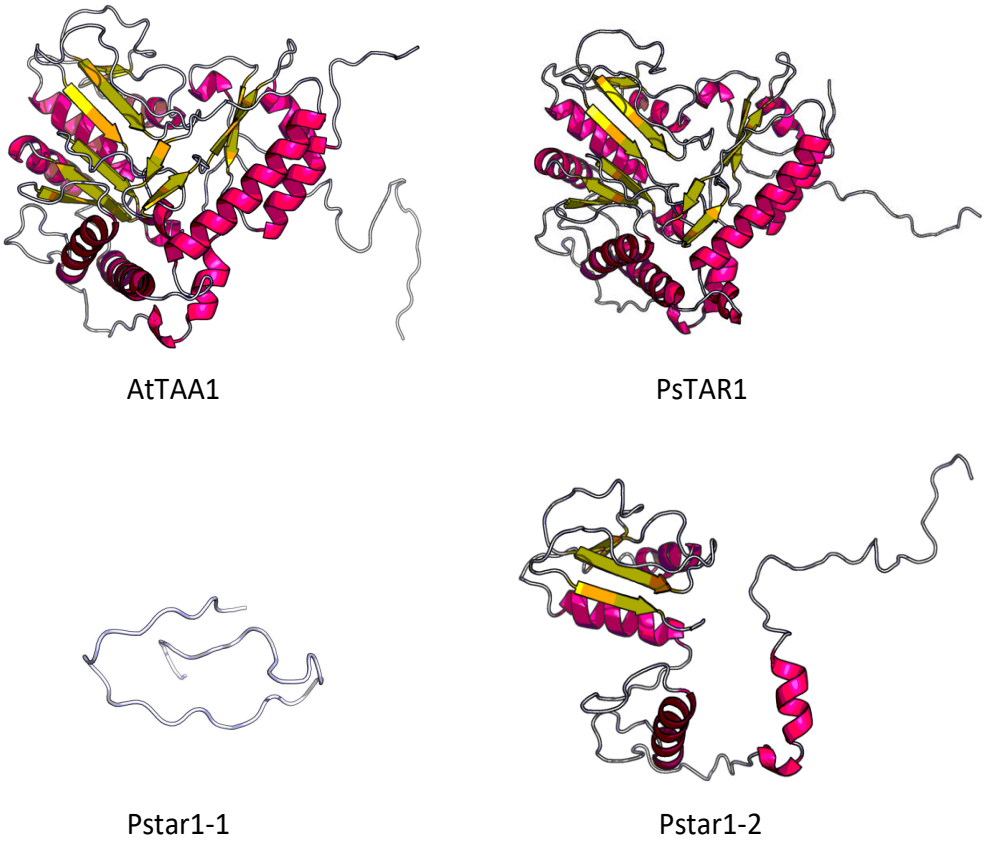

Figure 2.3. 3D protein architectures of *Arabidopsis* TAA1, inferred PsTAR1 and Pstar1 mutants. The proteins are shown as ribbon diagrams. The well-characterised AtTAA1 is included for comparison. (structural models generated with http://raptorx.uchicago.edu/StructurePrediction/).

2.3.3. *Pstar1-1* and *Pstar1-2* homozygous recessives are not detected

The original accessions of line 905 (which carries the *Pstar1-1* mutation) and line 2601 (*Pstar1-2* mutation) had no visual phenotypes permitting discrimination between WT and mutant plants. Therefore, heterozygosity of these lines was considered a possibility. RFLP and sequencing protocols were developed and used to genotype the subsequent populations as this strategy had been previously successful for *Pstar2* (Tivendale et al., 2012) and *Pstar3* (Davidson and Ross, unpublished). However, after crossing line 905 and line 2601 to the parental Caméor line, populations appeared to consist only of heterozygous and WT progeny. The two lines were backcrossed six times. At each sowing and genotyping efforts, WT and heterozygotes were consistently detected. The mutations were maintained in heterozygous plants. In excess of 300 plants originating from the crosses were genotyped for the purpose of this chapter. However, homozygous recessive plants were never detected.

Under the RFLP protocol used, in line 905, the mutant allele does not cleave (290 bp) and a single band of that weight is expected if a plant is homozygous recessive for the 905 mutation. The WT allele cleaves into two products (270 and 20 bp). The smaller of the two products (20 bp) is not generally visible on the gel and so, a single band at the 270 bp mark on the ladder is interpreted as being WT. Two bands being present on the gel (290 and 270 bp) suggests that both the WT and the mutant alleles are contained in the sample's genome. This plant would be defined as being heterozygous. Several band 'profiles' were obtained in line 905 (Figure 2.4). WT always consisted of a strong single lower band while a heterozygote had two bands of close to equal strength with the WT (lower) band being stronger or, a strong upper mutant band and a weak lower WT band. This could be due to a different rate of amplification during the PCR between the two alleles.

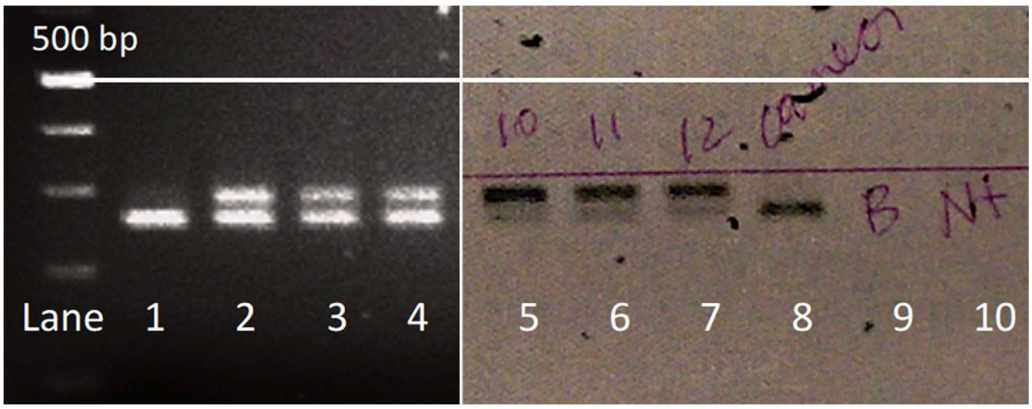

Figure 2.4. Examples of typical RFLP electrophoresis gels of segregating samples from line 905. Lane 1 is defined as WT; lanes 2 to 7 are defined as 'heterozygous'; lane 8 is a positive control and line 9 and 10 are negative controls. Note: lanes 5 to 7, the upper band (290 bp) is stronger than the lower (WT, 270 bp) band.

When the samples were sequenced, a similar pattern occurs (Figure 2.5). The WT allele, a single black peak (G), was sequenced in WT plants but in plants defined as heterozygous, the WT black peak (G) could be stronger, or close to equal to the 905 mutation green peak (A). However, in many instances, the green peak appeared stronger than the WT black peak. Again, the difference between the peaks of the sequenced nucleotides could be due to a different rate of amplification between the two alleles during the PCR.

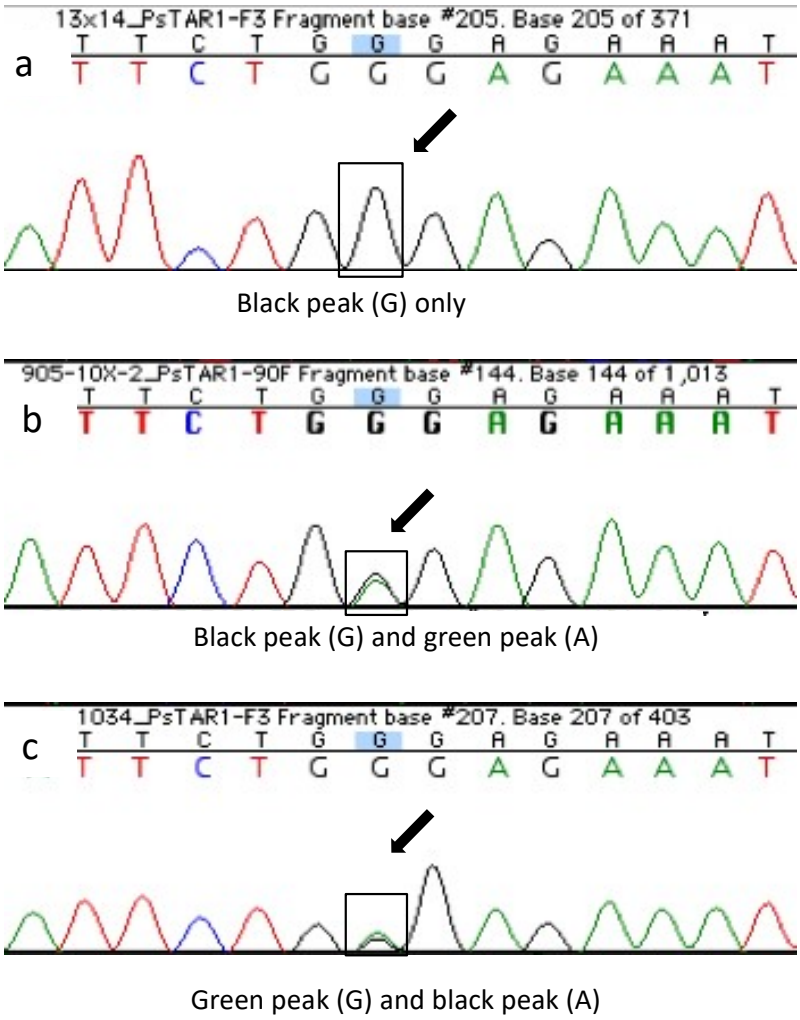

Figure 2.5. Examples of sequencing chromatograms of segregating samples from line 905 carrying the *Pstar1-1* mutation. a) Only the WT (G, black peak) is present in samples defined as WT. b and c), chromatograms clearly demonstrating the WT (G, black peak) and mutant (A, green peak) alleles in the samples defined as heterozygotes. c) The mutant (A, green peak) is slightly stronger than the WT (G, black peak). No homozygous recessives were detected in line 905.

Similar patterns of band profiles were obtained in line 2601 (Figure 2.6). The WT allele is cleaved into two products (838 and 262 bp) and the mutant allele does not cleave (1100 bp). Again, in heterozygotes, the 2601 mutation band could appear of weaker strength to that of the WT band or appeared stronger (Figure 2.6, lane 7).

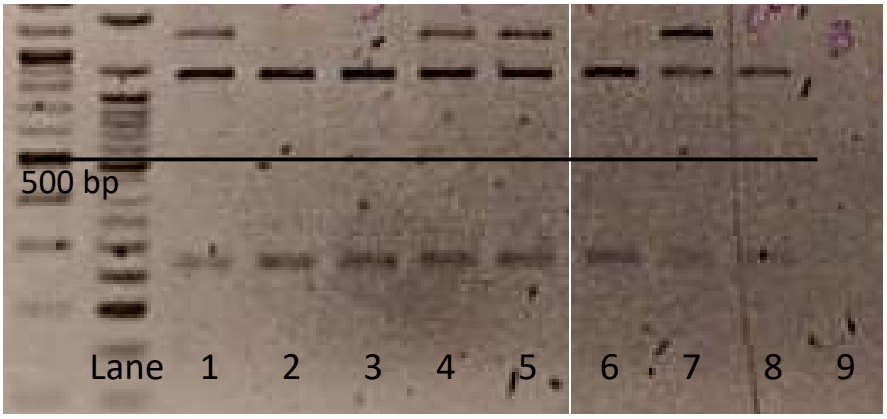

Figure 2.6. Examples of typical RFLP electrophoresis gels of segregating samples from line 2601. Lane 1, 4, 5 and 7 are defined as 'heterozygous'; lane 2, 3 and 6 are defined as WT; lane 8 is a positive WT control and line 9 is a negative control. Note lane 7, the upper band (1100 bp) is stronger than the lower band (WT, 838 bp).

Similarly to sequencing results from line 905, no homozygous recessive plants were detected in sequenced samples from line 2601 (Figure 2.7). WT samples always had a clear black peak (G) while samples defined as heterozygous, had either a stronger WT allele black peak (G) and weaker green peak (A) or the opposite.

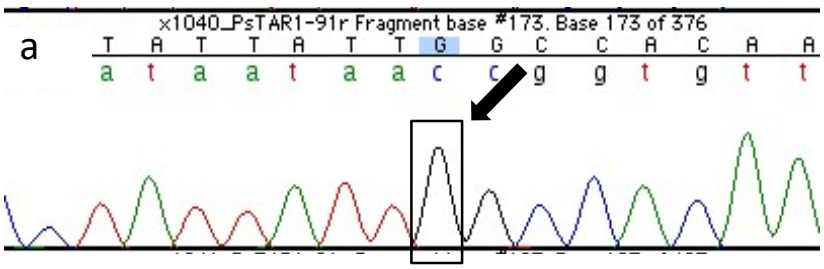

Only the black peak is present in WT samples

Black peak (G) only

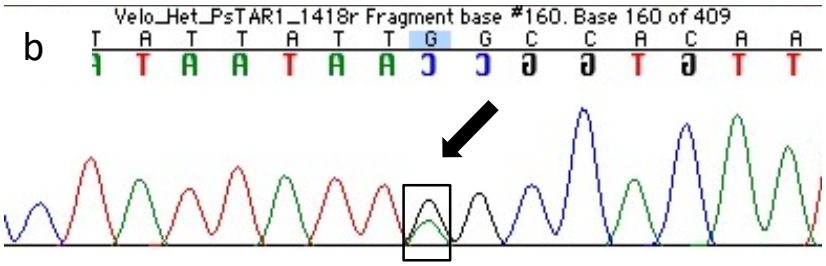

Both peaks are present but the black peak is slightly stronger

Black peak (G) and green peak (A)

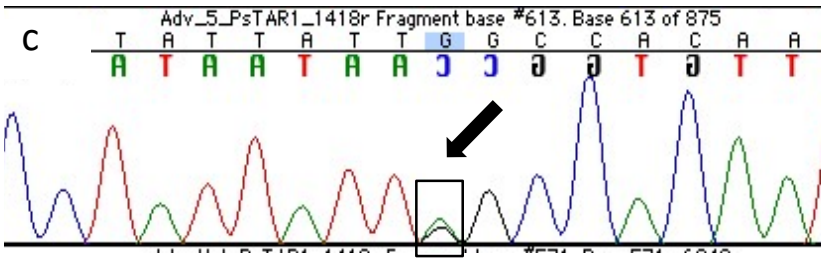

Both peaks are present but the green peak is slightly stronger

Green peak (A) and black peak (G)

Figure 2.7. Examples of sequencing chromatograms of segregating samples from line 2601 carrying the *Pstar1-2* mutation. a) Only the WT (G, black peak) is present in samples defined as WT. b and c), chromatograms clearly demonstrating the WT (G, black peak) and mutant (A, green peak) alleles in the samples defined as heterozygotes. c) The mutant (A, green peak) is slightly stronger than the WT (G, black peak). No homozygous recessives were detected in line 2601.

2.3.4. Abortion rates are not affected in the mutant lines

As homozygous recessive plants could not be detected in segregating populations, mutant seeds may abort early during development. To test this possibility, abortion rates in heterozygous and WT plants were quantified. To do so, the following were scored: the number of viable seeds (VS), the number of central abortions (CA) or the number of aborted seeds located between two viable seeds and the total number of possible seeds (PS); VS + CA = PS. In pea, seeds at either end of a pod are often aborted. These were not included in the scoring and calculations. In a segregating population originating from a heterozygote, a 1:2:1 ratio of WT, heterozygotes and homozygous recessive is expected. In other words, a quarter of the progeny is expected to be homozygous recessive. Following this line of logic, if fertilisation occurs between the two *Pstar1* gametes and the seeds subsequently abort, an increase in abortion rate is expected in heterozygous plants when compared with WT plants. However, the percentage of aborted seeds did not differ between heterozygous and WT plants (Table 2.9). These results indicate that homozygous recessive seeds do not abort post fertilisation and that explanation 1 (above in the introduction) does not apply.

Table 2.9. Percentage of aborted seeds from WT plants and 'heterozygous plants carrying the *Pstar1* mutations in line 905 and line 2601

Defined by RFLP as carrying:	Viable seeds + central abortions	Number of abortions	Percentage of aborted seeds
905 WT	154	22	14.3%
905 'heterozygote'	943	128	13.6%
2601 WT	134	45	33.6%
2601 'heterozygote'	182	51	28%

2.3.5. *Pstar1-1* and *Pstar1-2* recessive gametes are viable

To test the viability of the *Pstar1* recessive male and female gametes, reciprocal crosses were made between the cultivar Torsdag (line 107) and 905 and 2601 plants carrying their respective *Pstar1* alleles. Torsdag was selected as it carries *LE*, which controls internode length via the gibberellin pathway (Lester et al., 1997; Potts et al., 1982). The F1 progeny resulting from the crosses would be heterozygous for *LE* and be of tall stature, as opposed to the dwarfism of Caméor, line 905 and 2601. This was the case (data not presented) and the crosses were considered successful (n=10 for each cross; a total of 40 plants). In the F1 generation, a ratio of 1:1 WT to heterozygotes was obtained. As reciprocal crosses produced heterozygotes, both the female and the male recessive gametes are viable when crossed with dominant alleles originating from Torsdag (Table. 2.10). Recessive *Pstar1* pollen could fertilise ovules from Torsdag and recessive *Pstar1* ovules could be fertilised by Torsdag pollen. Therefore, the lack of homozygous recessive progeny in line 905 and 2601 cannot be explained by dysfunctional recessive gametes. In other words, explanation 2 does not apply.

Table 2.10. Punnet square demonstrating that heterozygotes are detected in the F1 generation originating from reciprocal crosses between line 905 or line 2601 and Torrsdag (line 107). Gametes highlighted in yellow originate from line 905 or line 2601.

Gametes originating from:		Line 905 and line 2601	
		PsTAR1 ♀	*Pstar1* ♂
Torsdag line 107	*PsTAR1* ♀		*Pstar1* ♂ *PsTAR1* ♀
	PsTAR1 ♂	*PsTAR1* ♀ *PsTAR1* ♂	

Crossing pollen from 905 or 2601 that carries *Pstar1* to WT ovules from107

Gametes originating from:		Line 905 and line 2601	
		Pstar1 ♀	*PsTAR1* ♂
Torsdag line 107	*PsTAR1* ♀		*PsTAR1* ♂ *PsTAR1* ♀
	PsTAR1 ♂	*Pstar1* ♀ *PsTAR1* ♂	

Crossing WT pollen from 107 to 905 or 2601 that carries *Pstar1* ovules

The F2 seeds originating from heterozygotes carrying *Pstar1-1* or *Pstar1-2* were grown on to observe the inheritance of the mutant alleles (n=30 for each cross; 30x2x2 = 120 plants in total). Again, no mutants appeared to be present in the segregating population (Table 2.11). A ratio of 1:3 WT to heterozygotes was obtained. These results indicate that the interaction between the two recessive gametes may be impaired, preventing fertilisation to occur. The results also imply that WT pollen may rescue failed fertilisation attempts by defective recessive pollen, as previously reported in the Arabidopsis *duo3-2* mutant (Kasahara et al., 2012) and *amc* mutant (Boisson-Dernier et al., 2008). In other words, explanation 3 might apply.

Table 2.11. Segregation of the *PsTAR1* alleles from the heterozygous F2 generation originating from the F1 generation (above). a) Homozygous recessives are not detected. b) A ratio of 3:1 heterozygote to WT is obtained Alleles highlighted in yellow originate from line 905 or 2601.

a

F2 generation	*PsTAR1*	*Pstar1*
PsTAR1	*PsTAR1* *PsTAR1*	*Pstar1* *PsTAR1*
Pstar1	*PsTAR1* *Pstar1*	*Pstar1* *Pstar1*

Homozygous recessives are not detected in the F2 generation

b

F2 generation	*PsTAR1*	*Pstar1*
PsTAR1	*PsTAR1* *PsTAR1*	*Pstar1* *PsTAR1*
Pstar1	*PsTAR1* *Pstar1*	*PsTAR1* *Pstar1*

A 3:1 ratio of heterozygous to WT is obtained

2.3.6. Unexpected SNP segregation

Next, it was decided to exploit the presence of single nucleotide polymorphisms (SNPs) found between Caméor and Torsdag in the *PsTAR1* gene. Their inheritance and segregation were followed as a positive control. There are seven SNPs in the coding region of *PsTAR1*, referred to as the 'Cam SNPs' when derived from line 905 and line 2601 or the 'Tor SNPs' when originating from Torsdag (line 107). These SNPs are numbered SNP1-7 in Figure 2.8. I opted for this nomenclature to distinguish between the SNPs that do not segregate on their respective background (i.e. Caméor and Torsdag) and, the SNPs that segregate in line 905 and 2601; and can either be WT (*PsTAR1*) or mutant (*Pstar1*). These SNPs are referred as the '905 SNP' and the '2601 SNP'. In the F1 generation, all the crosses were heterozygous for the Cam SNPs and the Tor SNPs (data not presented).

Figure 2.8. Alignment of Caméor and Torsdag *PsTAR1* cDNA with present SNPs highlighted in yellow. The locations of *PsTAR1-1* (905 SNP) and *PsTAR1-2* (2601 SNP) are highlighted in green. Sequences obtained from Genebank. Alignment generated with ClustalW (www.genome.jp).

Surprisingly, in the F2 generation from 'heterozygous' plants for 905 or 2601, the Cam/Tor SNPs segregation did not reflect the segregation of the 905 or 2601 mutations. In line 905 and as expected, nearly a quarter (22%, 13 plants out of 60) of

the progeny were homozygous for the Tor SNPs and 56% (34 plants out of 60) were heterozygous for the Cam/Tor SNPs. However, 13 out of 60 plants were homozygous for the Cam SNPs despite being 'heterozygous' for 905. A similar pattern of segregation occurred in the Cam/Tor SNPs in the F2 generation of line 2601 (data not presented). These results were unexpected because if a plant is heterozygous for the Cam/Tor SNPs, it must also be heterozygous for 905 or 2601. However, what was observed was that plants that carried the 905 mutation (originating from Caméor), and the WT 905 SNP (*PsTAR1* originating from Torsdag, line 107), only carried the Cam SNPs and not the Tor SNPs (Table 2.12).

Table 2.12. Segregation of line 905 and the Cam/Tor SNPs from a representative sub-sample (8 plants) of the sequenced F2 generation progeny. Nucleotides in grey originate from Caméor. Highlighted in yellow are samples in which Cam/Tor SNPs did not segregate as expected.

F2 generation progeny	Line 905 G: WT A: mutant	Cam SNP/Tor SNPs		Expected result
		SNP1: A/C	SNP2: T/G	
905 SNP (WT)	G G (WT)	A A (Cam)	T T (Cam)	Yes, control
107 (WT)	G G (WT)	C C (Tor)	G G (Tor)	Yes, control
(Tor♂X905/10)1/1	G A (het)	A A (Cam)	T T (Cam)	No, should be het for SNP1/2
(Tor♂X905/10)1/2	G G (WT)	C C (Tor)	G G (Tor)	Yes
(Tor♂X905/10)1/3	G A (het)	A C (het)	T G (het)	Yes
(905/12♂XTor)1/1	G A (het)	A C (het)	T G (het)	Yes
(905/12♂XTor)1/2	G G (WT)	C C (Tor)	G G (Tor)	Yes
(905/12♂XTor)1/3	G A (het)	A A (Cam)	T T (Cam)	No, should be het for SNP1/2

2.3.7. HRM genotyping finally reveals *Pstar1* mutants

Next, it was decided to use high resolution melt analysis (HRM) to genotype F1 and F2 generation samples originating from the reciprocal crosses to confirm whether the

results obtained from previous genotyping protocols (RFLP and sequencing) were erroneous or could potentially be replicated and confirmed. 24 out of the 34 F1 samples sequenced as 'heterozygous' were analysed and HRM confirmed that indeed the samples were heterozygous for 905 (*PsTAR1 Pstar1*) (Figure 2.9a). The Cam/Tor SNP2 was selected, as the T to G difference between the two cultivars would allow for a greater melt and better detection. The same 24 samples were 100% heterozygous for the Cam/Tor SNP2 (Figure 2.9b). HRM results from the F1 generation mirrored those obtained through sequencing.

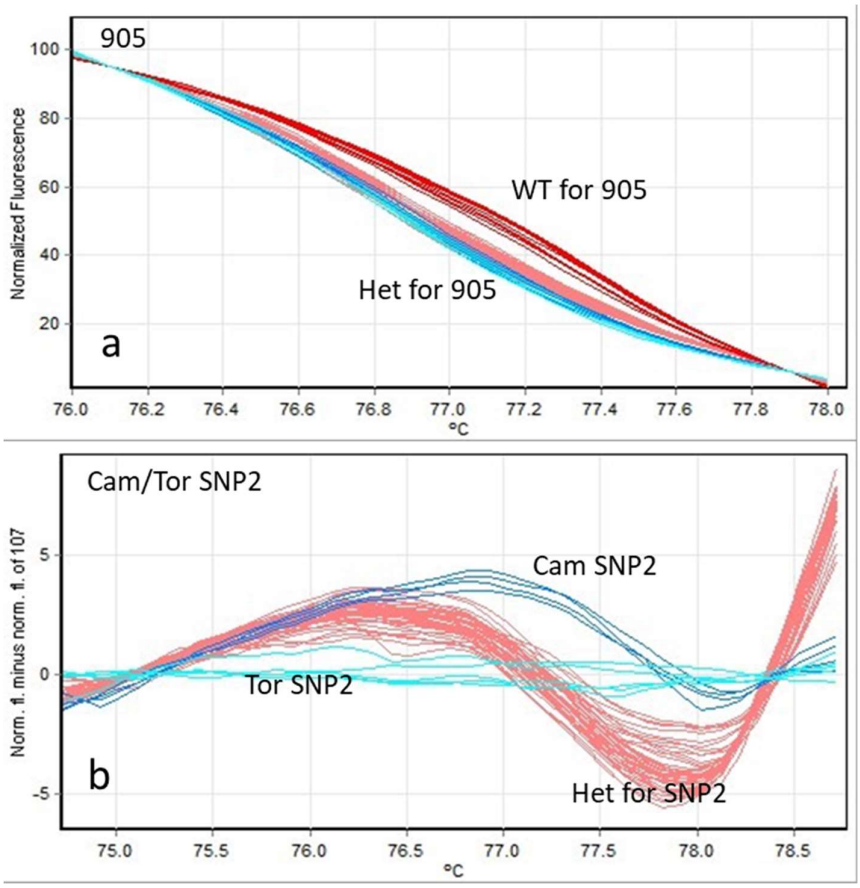

Figure 2.9. HRM melt curves plots (fluorescence over temperature) of 24 samples from the F1 generation sequenced as heterozygous for 905 originating from the reciprocal crosses between line 905 (*Pstar1-1*) and line 107 (Torsdag). a) All the F1 progeny was heterozygous (bottom, pink and blue) for line 905. Controls, 905 WT in red (top). b) Genotype of the monitored Cam/107 SNP2. Fluorescence normalised to the 107 SNP2. All the samples were heterozygous for Cam/107 SNP2 (pink lines). Controls, Cam SNP2 are in dark blue (top) and 107 SNP2 are in light blue (straight lines).

The 60 samples from the F2 generation (above) were analysed under the same HRM conditions. Out of the 60 samples, 13 were defined as WT for 905 and 34 as heterozygous. Some samples were defined as being *Pstar1* homozygous mutant (13 out of 60) (Figure 2.10a). The 13 samples were also defined as homozygous WT for the Cam SNPs analysed, (Figure 2.10b). These results were in accord with the Cam/Tor SNPs sequencing results obtained earlier (Table 2.12). This indicated a strong likelihood of *Pstar1* homozygous mutant plants being present in the population, that somehow, could not be identified through RFLP-based sequencing.

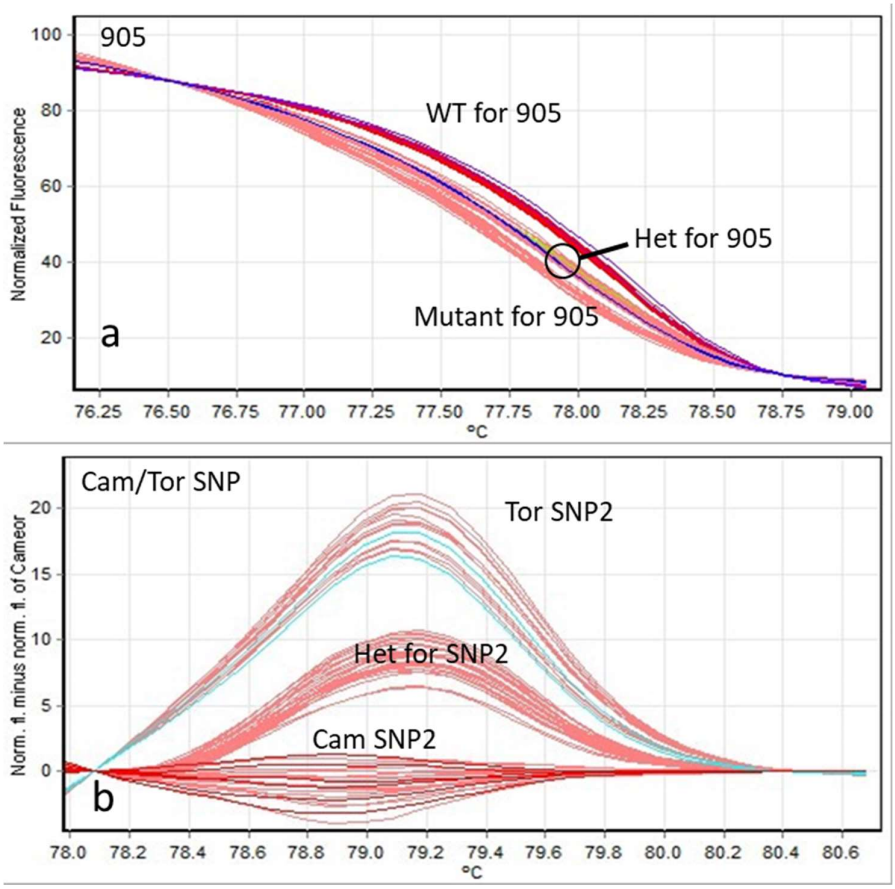

Figure 2.10. HRM melt curves plots (fluorescence over temperature) of 30 samples from the F2 generation genotyped under HRM conditions. a) 8 samples are genotyped as homozygous recessive for *Pstar1-1* (bottom, pink). 15 heterozygotes (middle, pink/purple) and 7 WT (top, red) are also present. b) Genotypes of the monitored Cam/Tor SNP2. Fluorescence normalised to the Cam SNP. The three genotypes are present. Samples are homozygous dominant for the Cam SNP2 (bottom, red) and the Tor SNP2 (top, red and blue) or heterozygous for SNP2.

One plausible explanation for the discrepancy between the results obtained from the different genotyping protocols is that there might be another gene with an almost identical sequence to *PsTAR1* present in the pea genome. In this explanation, 'gene 1' (*PsTAR1*) can segregate for the 905 SNP or the 2601 SNP and can therefore carry the WT (G) and/or the mutant (A) alleles. '*Gene 2*' however, is always homozygous WT at that SNP (G). The primers used in our RFLP protocol would amplify both genes and the enzymes would also cleave both genes. Indeed, the enzymes would always digest '*Gene 2*' as it carries the WT allele. In other words, a *Pstar1* mutant plant that carries two mutant alleles (A A) would also carry the two WT alleles (G G) from '*Gene 2*'. All the alleles of the two 'quasi-identical' genes would be amplified but only the WT alleles would be cleaved. A *Pstar1* 'mutant' would therefore be genotyped as a heterozygote.

2.3.8. *PsTAR3* is not '*Gene 2*'

The first contender considered to potentially be '*Gene 2*', was *PsTAR3*. Amongst the four *PsTAR* present in the pea genome, *PsTAR1* and *PsTAR3* share the highest sequence similarity (Figure 2.1). Nucleotide sequences obtained from Genbank (ncbi.nlm.nih.gov) were aligned to confirm that all the primers were specific to *PsTAR1* (Figure S2.2). *PsTAR1* primer sequences were dissimilar and do not amplify *PsTAR3*. All *PsTAR1*-specific primers and their resulting amplified sequences were also analysed through the Basic Local Alignment Search Tool (BLAST) from the NCBI and the pea RNA atlas portals. No other genes were calculated as statistically significant in their sequence similarity. Furthermore, *PsTAR3*-specific primers were used to successfully genotype *Pstar3* mutants in combination with RFLP (Davidson and Ross, unpublished) indicating that the two genes can be separated by PCR protocols.

2.3.9. Transformation supports the two genes hypothesis

To test the 'two genes' hypothesis, clones from each genotype were sequenced to see if *Pstar1* mutants also carry WT alleles. Bacterial transformation followed by

Sanger sequencing of individual colonies permits to sequence single alleles. Indeed, when cloning genomic DNA strands, amplicons are inserted singly in a vector before being introduced into a host. As the host, in this instance *E. coli*, multiplies and colonies are selected for sequencing, the single allele of interest is kept separated from any other alleles that may have been amplified in the original PCR. In other words, if sufficient colonies are selected randomly, some colonies should contain only *PsTAR1* alleles (G, WT or A, mutant) while other colonies containing alleles from '*Gene 2*' should only contain the WT-like nucleotide (G). As expected, sequences from transformed Caméor clones were all WT (G) and sequences from 905 heterozygote samples were mainly WT (G) with a low proportion of *Pstar1-2* mutant alleles (A) (data not presented). However, from the defined-by-HRM 2601 homozygous mutant sample, six out of the 14 clones were sequenced as WT (G) and eight out of 14 as mutant, (*Pstar1-2,* A) (Figure 2.11). In both instances, the primers used in the cloning protocols annealed at different locations when compared to those used in the RFLP and in the HRM analyses. These results support the hypothesis that a second gene with an almost similar sequence to *PsTAR1* is present in the pea genome.

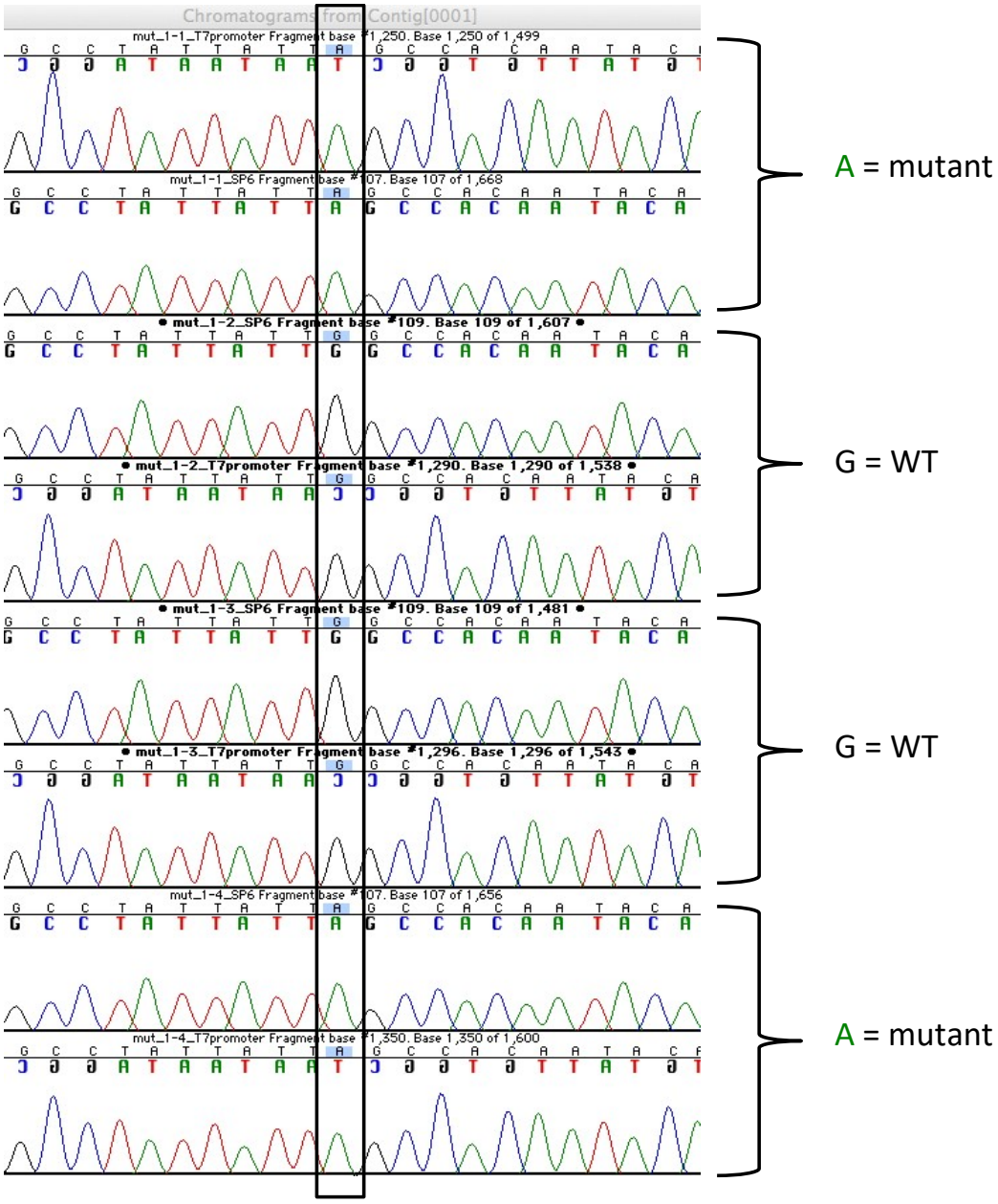

Figure 2.11. Representative chromatograms from *Pstar1-2* clones. WT 2601 and mutant 2601 alleles are sequenced from forward and reverse sequences in 2601, *Pstar1-2* clones (amplicon size of 227 bp). Nucleotides of interest are boxed.

2.3.10. Plants breed true-to-type

The next line of inquiry was to test whether genotypes defined by HRM breed true-to-type. Seeds produced by two putative homozygous mutants defined by HRM were grown and genotyped by HRM (n=30). If WT or heterozygotes segregate in the two populations, results from the HRM protocol would be considered unreliable. However, if the progeny breeds true-to-type and only mutants are genotyped, we can state that the results obtained by the HRM protocol are reliable. All F3 samples originating from two putative mutant parents were defined as mutants by HRM (Figure 2.12).

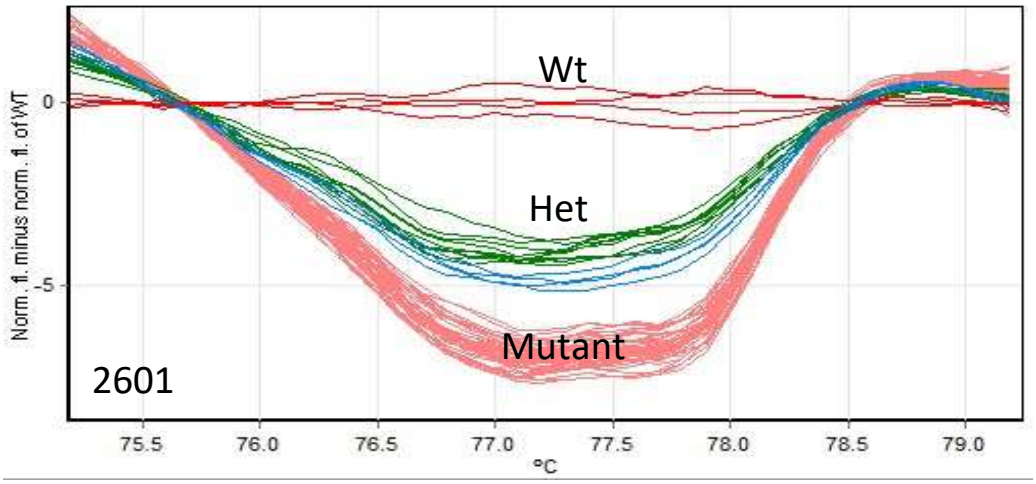

Figure 2.12. HRM chromatogram of 30 F3 generation plants originating from *Pstar1-2* mutants defined by HRM. All the progeny is defined as being homozygous recessive for *Pstar1-2* (bottom, pink). Control WT (top, red) and control heterozygotes (middle, green and blue).

The same samples now considered as mutant, were then tested under RFLP conditions to see how they behaved. All samples defined as mutants with HRM were genotyped as heterozygotes by RFLP (Figure 2.13.a). It must be noticed that the upper 'mutant' band (1100 bp) is stronger than the lower WT band (838 bp). This band profile had been obtained before (see Figure 2.4 for line 905 and Figure

2.6 for line 2601). Experimental HRM heterozygotes and controls were genotyped in the same manner under the two protocols (Figure 2.13b). This discrepancy implies that we may have always had mutants in our populations but had never identified them as such.

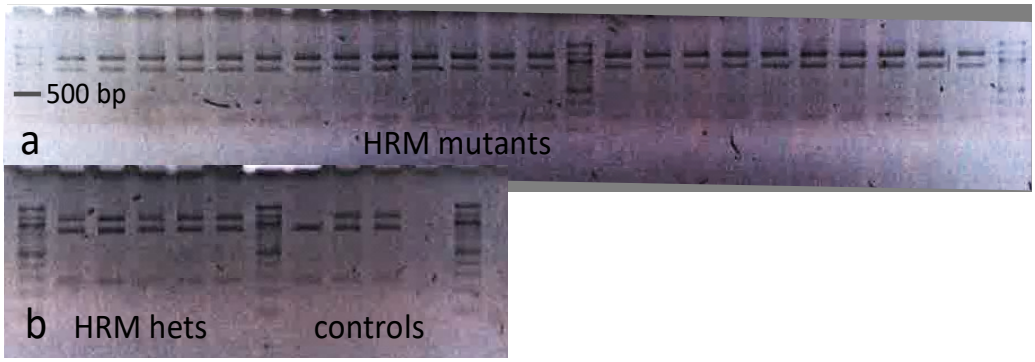

Figure 2.13. RFLP gel of putative homozygous recessive *Pstar1-2*. a) All experimental 'mutants' are genotyped as heterozygotes under the RFLP protocol. b) Bottom row includes experimental heterozygotes and controls; WT and heterozygotes defined from previous HRM, RFLP and sequencing protocols.

The progeny from two heterozygous plants defined under HRM protocol were also grown and genotyped (n=22). The three genotypes were detected. The segregation was skewed towards heterozygosity (two mutants, six WT and 15 heterozygotes out of 22 plants) (Figure 2.14). However, observed values did not deviated from expected values ($\chi 2$ (2) = 3.7; critical value of 5.99; p=0.15) indicating that the progeny derived from the two heterozygotes segregated as expected.

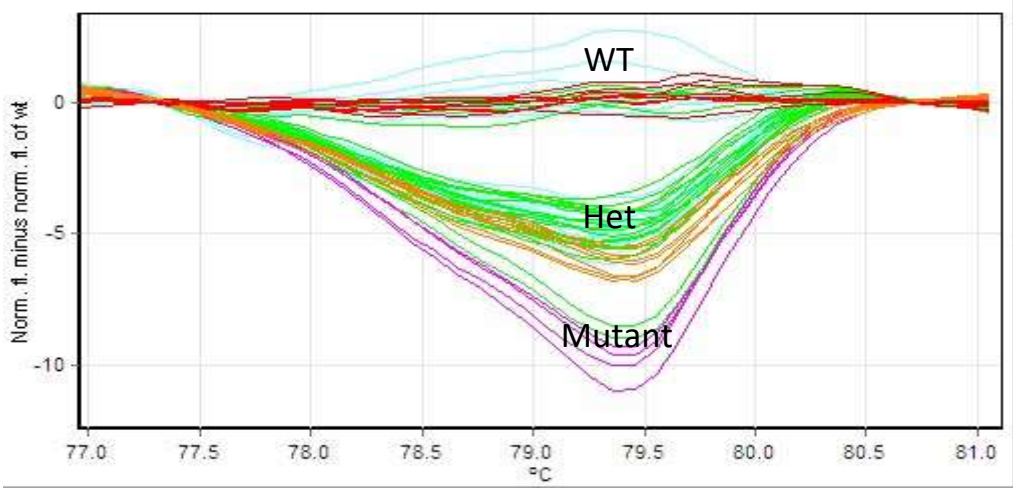

Figure 2.14. HRM melt curves plots of the F3 generation originating from two putative Pstar1-2 heterozygotes defined by HRM. WT (top, green and blue; controls in red), heterozygotes (middle, green; controls in orange) and mutants (bottom, pink; controls in green) are present.

2.3.11. Phenotypic characterisation

The newly identified *Pstar1* mutants were phenotypically characterised. However, no visible phenotypes were present in neither of the mutants (*Pstar1-1* presented in Figure 2.15). There were no significant differences in internode and stem length, shoot to root dry weight ratios, flowering node, time of flowering, number of pods, seeds per pod and seed weight when mutants were compared with WT plants (data not presented).

Figure 2.15. *Pstar1-1* (905) and Caméor (WT) mature plants (top) and seeds (bottom). No visible phenotypes are present in the mutant line when compared with the WT.

2.3.12. Seed auxin content is not reduced in *Pstar1-1*

IAA and its chlorinated form (4-Cl-IAA) was quantified from young pea seeds as the *TAR*s in *Arabidopsis* were reported to be required for maintaining auxin concentrations during embryogenesis (Stepanova et al., 2008) and *PsTAR1* was shown to be highly expressed in immature seeds (Tivendale et al, 2012). There was no significant difference in the IAA and 4-Cl-IAA content between the *Pstar1-1* mutants and the WT in young seeds (Figure 2.16). Similarly to previous findings, IAA was elevated in the young seeds while 4-Cl-IAA was low (Tivendale et al., 2012).

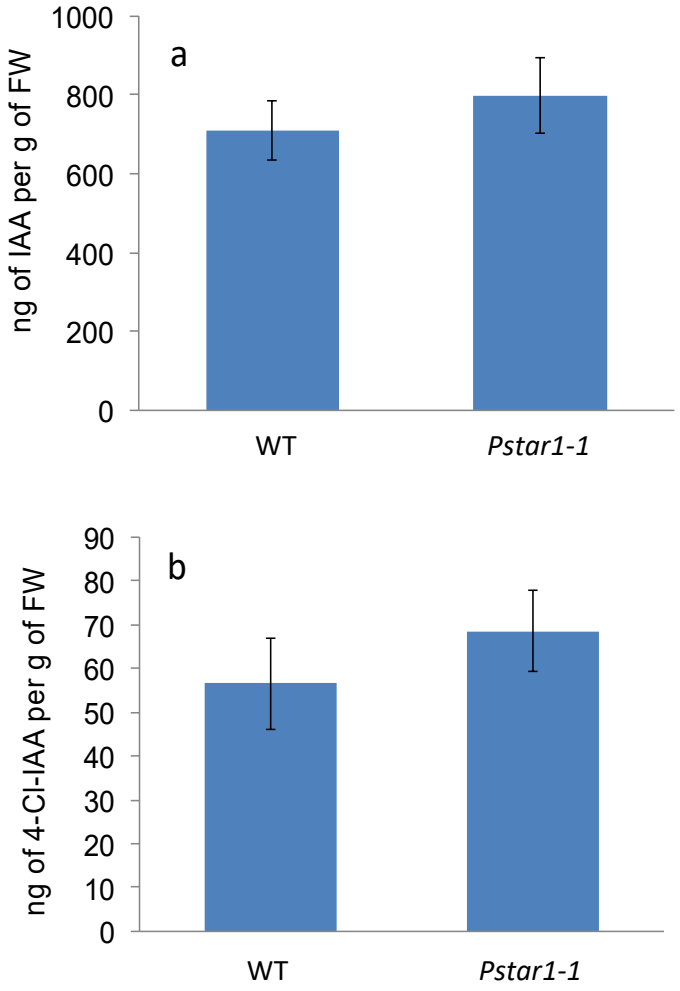

Figure 2.16. IAA and 4-Cl-IAA content in *Pstar1-1* and WT young seeds (5mg/seed, 6 seeds per samples, n=6).

2.4. Discussion

The aims of this chapter were to investigate the potential roles of *PsTAR1* in pea development in general and in pea seed development more specifically. To be able to do so, homozygous recessive plants needed to be obtained. The PCR followed by RFLP genotyping methodology had been used successfully in pea previously with two *Pstar2* mutants identified and characterised (McAdam et al., 2017) as had *Pstar3* mutants (Davidson and Ross, unpublished). However, when using the well-established RFLP methodology, *Pstar1* homozygous mutant plants were not detected from the novel TILLING lines.

The gene *PsTAR1* (or a paralog) was shown to be highly expressed in young pea seeds with expression levels correlating with high IAA content (Tivendale et al., 2012). Furthermore, *ZmTAR1* and *OsTAR1* were shown to be required for normal grain growth (in maize and rice respectively), implicating auxin as an important signal for seed development (Phillips et al., 2011; Abu-Zaitoon et al., 2014).

2.4.1. *Pstar1* gametes and rate of seed abortion are not affected in heterozygotes

As the genotyping protocols used at the onset of the research failed to detect homozygous recessive individuals from *Pstar1-1* and *Pstar1-2* populations, a previously proposed model, proposing that *PsTAR1* is required for successful fertilisation, was considered (Ross et al., Auxins and Cytokinins in Plant Development 2014, conference abstract 01-9, p.23). Abortion rates were quantified and ascertained that embryo development was not detrimentally affected in *tar1 tar1* mutant seeds (Table 2.9). In addition, gamete viability was tested and demonstrated that the two recessive gametes are viable (Table 2.10).

Fortuitously, the reciprocal cross experiments lead to intriguing sequencing results that exposed some unknown phenomenon occurring in our biological system (Table 2.11). Indeed, the inheritance of SNPs present in *PsTAR1* between the Caméor (line

905 and line 2601) and the Torsdag (line 107) cultivars in segregants from reciprocal crosses, questioned our first model (Table 2.11).

2.4.2. *Pstar1* mutants are finally obtained

Using HRM genotyping protocols permitted the detection on *Pstar1-1* and *Pstar1-2* mutants. When using HRM, the two *Pstar1* mutants could be reliably genotyped from segregating populations. The results in this chapter points to the likelihood of a 'second gene', such as a psedogene nearly identical in sequence to *PsTAR1*, being present in the pea genome. In this scenario, a 'gene' on a distinct locus appears to have been amplified, cleaved and sequenced during RFLP genotyping protocols. HRM primers are situated differently on the *PsTAR1* sequence, indicating that SNPs between *PsTAR1* and '*Gene 2*', may be present in these regions.

Genes sharing sequence similarity are common in all plant species. As discussed in the General Introduction, whole genome duplication events have occurred pre- and post-speciation of *Pisum sativum* (Zhu et al., 2005). Indeed, pea, with its large genome, has a high prevalence of pseudogenes, repetitive DNA, transposable elements and chimeric genes (Macas et al., 2007). The possibility that '*Gene 2*' may be a fifth member of the pea aminotransferase family must be considered. Another plausible explanation is that within the pea genome, several 'fragments' of DNA, identical to 'fragments' of *PsTAR1*, are included, in chimeric genes for instance. The products of these chimeric genes may or may not be biologically functional. However, they are unlikely to carry PsTAR1 identical function, or convert Trp to IPyA. Nonetheless, *PsTAR1*-like fragments may have been amplified during RFLP protocols, confounding results.

Once *Pstar1* homozygous recessive individuals were identified, inquiries into the nature of '*Gene 2*' were cast aside to focus on the principal goal of this chapter: the characterisation of the novel *Pstar1* mutants. Future research with a focus on the *PsTAR* family would require the elucidation of the '*Gene 2*' phenomenon. Is it indeed a fifth member of the family or is an unknown number of repetitive DNA or chimeric genes being amplified? Being able to discriminate between the various

products and ascertain that all experimental data solely focus on *PsTAR1* is paramount to confidently interpret results.

2.4.3. The novel *Pstar1* mutants do not exhibit any obvious phenotypes

Most importantly, having access to *Pstar1* mutants permitted to characterise their phenotypes. However, no phenotypic differences were observed between the *Pstar1* mutants and their respective WT (Figure 2.15a). Furthermore, despite *PsTAR1* being principally expressed early in seed development (Tivendale et al., 2012; Table S2.1), *Pstar1* mutants had no seed phenotype (Figure 2.15) and IAA and 4-Cl-IAA, two auxins known to be required for pea seed development did not vary between the *Pstar1-1* mutant and the WT (Figure 2.16). Indeed, in the present chapter, there was no evidence that *PsTAR1* is contributing significantly to the synthesis of *de novo* auxin or to the maintenance of adequate auxin content in young pea seed. However, the putative 'Gene 2' may compensate for the disrupted *PsTAR1* during early seed development in the mutant alleles is a possibility that must be considered. Again, being able to discriminate between the two genes is paramount.

Furthermore, functional redundancy and overlap amongst members of a gene family is a recurring theme in biology. In *Arabidopsis*, single *tar* mutants do not exhibit any observable phenotypes when grown under normal conditions suggesting that there is a high degree of functional redundancy amongst the *TAA1/TAR*s (Stepanova et al., 2008; Tao et al., 2008). As mentioned in the Introduction, the pea *TAR* family has four members, two of which are highly expressed in all tissues tested (Table S2.1). Potentially, other *PsTAR*s compensate for the disrupted *PsTAR1* in the mutant alleles.

In conclusion

In conclusion, it does not appear that *PsTAR1* function as a critical auxin biosynthesis gene during fertilisation and early pea seed development or that it is required for successful fertilisation. However, these results do not necessarily

indicate that *PsTAR1* carries no IAA biosynthetic function during early seed development. Indeed, in a WT functional plant, *PsTAR1* may contribute to the IAA pool, but when disrupted, as it is predicted to be in the *Pstar1* mutants, other members from the family may compensate and rescue auxin content to the required level for development to progress normally.

In the future, isolating the 'Second Gene' and sequencing the promoter regions of the two genes may show functionality has been lost, completely or in part, in one of the genes i.e. pseudogene or the '*Gene 2*' is in fact an uncharacterised *PsTAR* gene. Furthermore, producing *Pstar* higher order mutants may reveal additive or synergistic effects of the mutations.

Chapter 3 - Characterising the YUC1 pea enzyme and obtaining a novel *crd* mutant

3.1. Introduction

In the second step of the IPyA pathway, the intermediate IPyA is converted to IAA by flavin-containing monooxygenase-like (FMO) enzymes (Won et al., 2011; Zhao et al., 2001). The *YUCCA*s (*YUC*s) were first isolated from *Arabidopsis* (Zhao et al., 2001). The term YUCCA was coined due to the growth habits of the first identified mutant which resembled those of the common yucca plant (Agave sp.) (Zhao et al., 2001). The *Arabidopsis yucca* mutant (now known as *yuc1-D*, At4g32540) (Cheng et al., 2006) is a dominant gain of function mutant obtained through an activation tagging screen where cauliflower mosaic virus (CaMV 35S) enhancer repeats were inserted to promote the transcription of genes proximally located (Weigel et al., 2000).

The *yuc1-D* mutant exhibited hallmark phenotypes of auxin overproduction as defined by the *superroot* mutants of *Arabidopsis* (Boerjan et al., 1995; Delarue et al., 1998). The *yuc1-D* mutant is fertile with elevated auxin content at all developmental stages (up to 50%), has elongated hypocotyls under all light spectra, increased apical dominance and shorter roots with increased and longer root hairs when compared with WT plants. A combination of physiological, molecular, and biochemical experiments determined that the phenotypes were caused by auxin overproduction. For instance, auxin-induced genes, such as *GH3* and *Aux/IAA*, were up-regulated in *yuc1-D*, as was the *DR5::GUS* auxin reporter (Zhao et al., 2001).

The *Arabidopsis* genome contains 29 putative FMO-encoding genes, eleven of which are *YUC*s genes involved in auxin biosynthesis (Zhao et al., 2002). The *YUC*s phylogenetically divide into three clades, two of which divide into two sub-clades (Cheng et al., 2006). Similarly to the *AtTAR*s, single loss-of-function *yuc* mutants do

not have observable phenotypes (Cheng et al., 2006; Stepanova et al., 2008). However, specific combinations of different mutants (*yuc1 yuc4* and *yuc2 yuc6*), principally those belonging to the same sub-clade, exhibited abnormal floral and vascular phenotypes while combinations of mutants belonging to different sub-clades do not (*yuc1 yuc2* and *yuc4 yuc6*, for instance) (Cheng et al., 2006). Higher order mutants including *yuc10* and *yuc11*, were also shown to have increasingly aberrant phenotypes affecting leaf and flower vasculature, floral organ identity and placement, and embryogenesis when combined with mutants from the *YUC1*/*YUC4* sub-clade (Cheng et al., 2007).

The remaining *YUC*s (*YUC3*, *YUC5*, *YUC7*, *YUC8* and *YUC9*) are principally expressed in various root tissues. Consistent with this, the *yucQ* mutant (disrupted in all five genes) had severe defects in the roots but not in the shoot (Chen et al., 2014). Taken together, these findings suggest a level of overlapping functionality and redundancy amongst subsets of *YUC* members but also distinct tissue-specific physiological roles across clades (Cheng et al., 2006, 2007; Chen et al., 2014). However, these *yucQ* mutant phenotypes could have been the result of disrupted auxin-related transcription or conjugation genes and not necessarily of disruption to auxin biosynthesis exclusively. Extra biochemical evidence was required to clarify which step was disrupted.

Critical findings demonstrated that the *YUC* members are involved in IAA biosynthesis of *Arabidopsis* and are essential to a vast range of developmental programmes. The phenotypes of the *yuc1 yuc4* mutant could not be rescued by auxin application but were rescued by expressing, *in vivo*, the bacterial auxin biosynthetic gene *iaaM* under the control of a *YUC* promoter (Cheng et al., 2006). Cheng and colleagues (2006) hypothesised that a tightly regulated temporal and spatial production of IAA through the *YUC*s was required for successful tissue and organ development (Cheng et al., 2006). In other words, auxin has to be present in the right amount, in the right cells and at the right time for a developmental programme to proceed normally. Applying exogenous auxin through external means did not meet the auxin requirements of developing cells.

3.1.1. A paradigm shift

Originally, the YUCs were placed in the tryptamine (TAM) pathway due to *in vitro* results suggesting that the enzymes had the capacity to convert TAM to *N*-hydroxytryptamine in a rate limiting fashion (Zhao et al., 2001). However, evidence challenged this model. In another model species, *Pisum sativum*, metabolism experiments showed that labelled tryptamine fed to pea roots was not converted to *N*-hydroxytryptamine (Quittenden et al., 2009). In another experiment, when young pea seeds (demonstrated to express a *YUC*-like gene) were fed with labelled tryptamine, no labelled IAA was recovered (Tivendale et al., 2010).

Then, in 2011, several papers reported that the YUC family members of *Arabidopsis* operate in a different biosynthetic route: the IPyA pathway (Mashiguchi et al., 2011; Phillips et al., 2011; Stepanova et al., 2011; Won et al., 2011). Indeed, overexpressing *yuc* mutants had a 33% decrease in IPyA when compared to control plants while loss-of-function triple mutants had a 1.8 time increase in IPyA in young flower buds when compared with WT (Mashiguchi et al., 2011). Furthermore, enzymatic assays of GST-fused YUC2 proteins expressed in *E. coli* converted IPyA preferentially to IAA when in solution with NADPH (Mashiguchi et al., 2011). Similar results were obtained when using recombinant YUC4 variants where IPyA was converted to IAA but TAM was not (Kriechbaumer et al., 2012). These findings shifted the consensus and unambiguously supported that YUCs are key auxin biosynthesis enzymes that converts IPyA to IAA and that the auxin produced through the YUCs is required for plant development.

Finally, the biochemical mechanisms of the YUC FMOs were characterised. Expressed and purified from *E. coli*, YUC6 proteins were shown to contain a flavin adenine dinucleotide (FAD) which uses nicotinamide adenine dinucleotide phosphate (NADPH) and oxygen to catalyse the oxidative decarboxylation of IPyA to IAA (Dai et al., 2013). Fluorescence experiments indicated that the FAD cofactor is buried in the pocket of the enzyme. In a three-step fashion, the FAD cofactor is reduced to FADH- by NADPH which in turn forms a C4a-(hydro)peroxy FAD intermediate by binding with oxygen. The C4a-intermediate had a half-life of ~20 seconds in the

absence of the IPyA substrate. In the last step, IPyA is decarboxylated to IAA by an irreversible reaction with the C4a-intermediate. Interestingly, Dai and colleagues (2013) demonstrated that YUC6 was also able to use another physiological α-keto acid as a substrate or phenyl-pyruvate (PPA) to produce phenyl acetic acid (PAA). Several FMOs found in animals and bacteria tolerate a wide range of substrates (Eswaramoorthy et al., 2006) and this appears to be the case with the YUCs. YUC6 did not, however, react with benzoylformic acid, indicating that the YUC FMO may require substrates to have a methylene group (H_2C) in the side chain (Dai et al., 2013).

Homologues of the *Arabidopsis YUC*s are widely distributed through plants. Representatives of the *YUC*s are present in lycophytes, moss, gymnosperms, eudicots and monocots (Poulet and Kriechbaumer, 2017) and were demonstrated to be essential for normal plant development. In tomato, six *YUC* genes (*ToFZY1-6*) have been identified. Comparatively to *Arabidopsis*, all are differentially expressed spatially and temporally with overlap amongst certain members (Expósito-Rodríguez et al., 2007). The expression of *ToFZY1* was principally in leaf and flower tissues while *ToFZY4* was preferentially expressed in flower and fruit tissues. Both are orthologues of *AtYUC1/AtYUC4*, respectively (Expósito-Rodríguez et al., 2007). In pea, 11 members can be found in the pea gene atlas portal (Alves-Carvalho et al., 2015). The pea genes exhibit spatiotemporal expression with overlap amongst certain members (Table S3.1). For instance, two members, *PsYUC1* and *PsYUC2*, homologues of *AtYUC1* and *AtYUC2*, were shown to both be expressed in the apical portion at a similar level (Tivendale et al., 2011). However, *PsYUC1* was highly expressed in the developing seed but was not expressed in the mature leaf while the opposite occurred with *PsYUC2*, highly expressed in the leaf but not in the seed (Tivendale et al., 2010). In rice, 14 members are found (*OsYUCCA1-14*). However, expression patterns varied substantially: *OsYUC1*, a homologue of *AtYUC1/AtYUC4*, had very poor to no amplification in a semi-quantitative RT-PCR experiment, while several *OsYUC*s could not be detected and others had very localised expression (Abu-Zaitoon et al., 2012).

Plants with the appropriate mutations, or levels of gene expression, are required to definitively link expression and protein function to physiological and morphological phenotypes. But *YUC* mutants in species other than *Arabidopsis* are not widely available. Gain of function mutants or overexpressing mutants are invaluable tools due to the fact that phenotypes may be obtained despite functional overlap or redundancy amongst members of a gene family. However, loss-of-function mutants are of critical importance to establish the direct effects of a disruption to a specific gene with a developmental process. In *Arabidopsis*, mutants with disruptions in single *YUC* genes do not exhibit morphological defects. Yet, in several other species, single mutants are found to have extensive effects. The *floozy* (*flz*) mutant of petunia, identified from a transposon mutagenesis screen has aberrant flower and leaf venation architecture (Tobeña-Santamaria et al., 2002). In maize, the *de18* and *spi1* mutants, clustering with *AtYUC1/AtYUC4* and *AtYUC2/AtYUC6*, have strong phenotypes (Bernardi et al., 2012; Gallavotti et al., 2008). This indicates that redundancy may not be as prevalent in species other than *Arabidopsis*.

3.1.2. A novel *yuc1* mutant allele

In the garden pea (*Pisum sativum*), four mutant recessive alleles, disrupted in an orthologue of *AtYUC1/AtYUC4*, are available (Figure 3.1). The *crd-1* (JI2460) mutant was first identified from induced mutations on the dwarf (*le*) *cv*. Paloma with NEU (N-ethyl-N-nitroso urea) treatments (Swiecicki, 1989). Waved leaf surfaces and toothed stipule bases are diagnostic characteristics of a few pea mutants defined as having a 'crispoid' phenotype, such as *crispa* (*cri*, WT 11297) and *curled* (*curl*, WT 15855). Locus identity tests revealed that the *crd-1* crispoid-like phenotypes were the result of a mutation at a locus independent of the other crispoid-like loci. The novel gene was named *Crd* (Swiecicki, 1989).

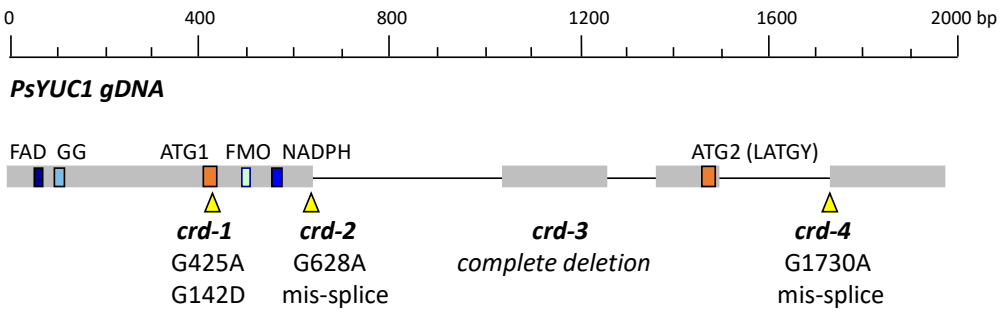

Figure 3.1. Four mutant alleles for *PsYUC1* (McAdam et al., 2017b). The grey boxes represent exons. The four types of motifs are in coloured boxes: The FAD and NADPH cofactors binding sites are in blue (Eswaramoorthy et al., 2006), the GG motif in light blue (Vallon, 2000), ATG1 and ATG2 (LATGY) motifs in orange (Expósito-Rodríguez et al., 2007; Schlaich, 2007) and the YUC/FMO -identifying motif in light blue (Ziegler, 1993). The *PsYUC1* mutant alleles are pointed out with yellow triangles (McAdam et al., 2017b).

The *crd-whip* mutant (originally on the SG background, now on SGE), referred to as *crd-2*, arose from an EM mutagenesis screen (Berdnikov et al., 2000). On the SG background, the *crd-2* mutant was reported to have stronger leaf phenotypes than *crd-1* with leaves often dramatically reduced in size and sometimes missing (Berdnikov et al., 2000). The *crd-2* also exhibited aberrant flower morphology (Berdnikov et al., 2000). The *Crd* locus was mapped to chromosome 1 and was linked to *Aatp* and *His(2-6)* of the linkage group II (Swiecicki, 1989; Berdnikov et al., 2000).

The *crd-3* mutant (FN1522-1) was obtained from a fast neutron mutant population (McAdam et al., 2017b) and consequently, large gene-size deletions were expected (Domoney et al., 2013). Accordingly, a next generation RNA approach was used to identify the disrupted gene in the *crd-3* mutant (McAdam et al., 2017b). A 435 base pair deletion in the *crd-3* mutant, when compared with the parental WT line (JI 2822), was observed and found to correspond to the previously identified *PsYUC1* (Tivendale et al., 2010). The *crd-3* allele is therefore considered to be a null mutant.

Finally, the *crd-4* mutant allele was identified incidentally. One plant with an abnormal leaf vasculature phenotype was observed from a segregating *Pstar1-1* (line 905, WT Caméor, Chapter 2) population of 96 plants. Due to the reduced vein density, the novel mutant was first named *pipes in short supply* (*pss*). The phenotype was not rescued when crossed to the previously described *crd-1* mutant (McAdam et al., 2017b). The non-complementation results revealed that the novel mutation is allelic to *crd-1* and carries a disruption at the *Crd* locus. The *pss* mutant line was therefore renamed *crd-4* to reflect this (McAdam et al., 2017b).

3.1.3. Aims

The aim of this chapter is to establish an understanding of the nature of *PsYUC1* and its mutant alleles. In the next chapter, the effects of disrupting the normal functioning of *PsYUC1* on several developmental processes and organs will be investigated.

Firstly, in a comparative approach utilising the well-described *Arabidopsis* FMO1 (Hou et al., 2011) and available FMO crystal structures, the *PsYUC1* enzyme structure will be characterised *in silico*. The potential effects of the *crd* mutations on the protein structure will also be inferred. The three-dimensional visualisation of the FMO structures will permit a comparison of secondary structures amongst the WT and mutant enzymes. Predicted binding amino acids, the way in which they pack in the binding pocket and how they interact with known ligands will assist in determining the motifs relevant to the functioning of PsYUC1.

Secondly, the steps taken to obtain the novel *crispoid* mutant (*crd-4*) will be described. Indeed, mutagen-based mutagenesis experiments are indiscriminate and mutations occurring in multiple random genes are expected. Thorough crossings over many generations are generally required to keep the mutation/phenotype of interest and remove other unwanted genomic mutations from the background. The novel *crd-4* mutant allele originates from a line targeting another auxin-biosynthesis gene, *PsTAR1* (Chapter 2), despite having been backcrossed five times. The possibility that the *crd-4* mutant also carries the *Pstar1-1* mutation is considered.

3.2. Materials and methods

3.2.1. Plant material

The progeny from the first observed *crd-4* plant was grown, backcrossed to the parental Caméor line and propagated by single plant selection for five generations. The wild-type (WT) plants used for this study were the dwarf (*le-1*) *cv*. Caméor and the WT progeny segregating from heterozygous parents. All plant material was grown as described in Chapter 2.

3.2.2. Phylogeny

The phylogeny of *Pisum sativum YUC*s was inferred using alignments of full- length translated YUC protein sequences. The phylogenetic tree was rooted using a genbank *Rhodococcus sp.* protein sequence (accession WP051637449.1). *Arabidopsis* sequences can be found under the relevant accession numbers in the *Arabidopsis* information resource (TAIR) database (www.arabidopsis.org/). The pea sequences were obtained from BLAST searches in the pea RNA-seq gene atlas (bios.dijon.inra.fr/FATAL/cgi/pscam.cgi) (Alves-Carvalho et al., 2015) using the published *PsYUC1* sequence available in genbank (accession HQ439907) (Tivendale et al., 2010). The sequences were aligned using clustalW (www.genome.jp/) with BLOSUM matrices as these are the most efficient at carrying out protein database homology searches.

3.2.3. Mutant alleles SIFT score

SIFT (Sorting Intolerant From Tolerant) was used to predict whether the amino acid substitution in the *Psyuc1* alleles may have a deleterious effect. SIFT is a multistep procedure that searches and chooses closely related sequences that may share similar function to the query sequence and then calculates probabilities for all possible amino acid substitutions from the alignment. Positions with probabilities less than

0.05 are predicted to be deleterious and those that are greater than or equal to 0.05 are predicted as being tolerated (sift.jcvi.org/) (Kumar et al., 2009; Sim et al., 2012).

3.2.4. Inferred protein structure and binding sites

The *AtYUC1*, *PsYUC1* and mutant alleles protein architectures and important binding residues were predicted using the Phyre2 server (Kelley and Sternberg, 2009) and a range of services offered by the RaptorX server (as described in Chapter 2) (Källberg et al., 2012). However, the crystal structure of a YUC protein, in *planta*, is not available in databases. The protein structure homology-modelling server Swiss-Model was used to test and select published crystal structures of high similarities and significant global (the whole sequence) and local (individual amino acids) scores as defined by the programme (swissmodel.expasy.org/) (Waterhouse et al., 2018). Models with a Global Model Quality Estimate (GMQE) score closest to '1' (scores range between 0 and 1) and a composite of four monitored parameters (QMean) score above '-4' were considered of reliable quality (Benkert et al., 2010; Biasini et al., 2014). The templates used in this instance were of published structures derived from monooxygenases from bacteria, or *Thermocrispum municipal* (PDB # 5M0Z) (Romero et al., 2016) and *Rhodococcus sp.* HI-31, (PDB # 3UCL, 3GWD) (Mirza et al., 2009; Yachnin et al., 2012).

3.2.5. Genotyping the *crd-4* allele

Segregating *crispoid* mutants were mainly identified based on leaf vasculature and floral phenotypes. However, to accelerate the generational progress arising from crosses to different cultivars, a RFLP analysis protocol was designed to identify *crd-4* heterozygotes and *CRD-4* homozygous dominants in backcross generations. Primers and enzymes are included in Table 3.1 and Table 3.2 respectively. All genomic DNA extraction, primer design, PCR and digest protocols were followed as described in Chapter 2. Furthermore, the likelihood that the novel *crd-4* mutant carried the *Pstar1-1* mutation was considered and tested for with the HRM protocol described in Chapter 2 (Table 2.5).

Table 3.1. RFLP specific primers used to genotype the *CRD-4* allele.

Gene	Primer name	Sequence (5’ to 3’)
PsYUC1	3' RACE F11	GGAAGGTGTGAAGGAGATAACAAGGAATGG
	ENTR R2	CTAAACATTATTAAGAGTAGTAGTACTAAT

Table 3.2. Enzyme used, amplicon size from PCR product and cut patterns expected for the *crd-4* allele.

Line	Cleaved allele	Amplicon size	Enzyme required	Cleaved product
CRD-4	Mutant	600 bp	PsiI	360/240 bp

3.3. Results

3.3.1. One in a 100

One plant with an abnormal phenotype was identified from a segregating *Pstar1-1* (line 905, Chapter 2) population of 100 individuals. From the third node, the fully expanded leaves exhibited an unusual venation pattern (Figure 3.2). The progeny bred true to type and an observable reduction of secondary veins led to the novel mutant being called *pipes in short supply* (*pss*). The leaves also had a 'crinkled' or 'waved' surface towards the apex and in between the veins. A cross with the previously described *crd-1* mutant (Swiecicki 1989) revealed that *pss* is a novel *crispoid* mutant allele (McAdam et al., 2017b). The *pss* mutant was renamed *crd-4* accordingly (McAdam et al., 2017b). Using a next generation RNA sequencing approach and taking advantage of the complete deletion of the *crd-3* allele transcripts, it was ascertained that *Crd* belongs to the *YUCCA* gene family and corresponds to the *PsYUC1* sequence published in genbank (HQ439907.2) (Tivendale et al., 2010; McAdam et al., 2017b).

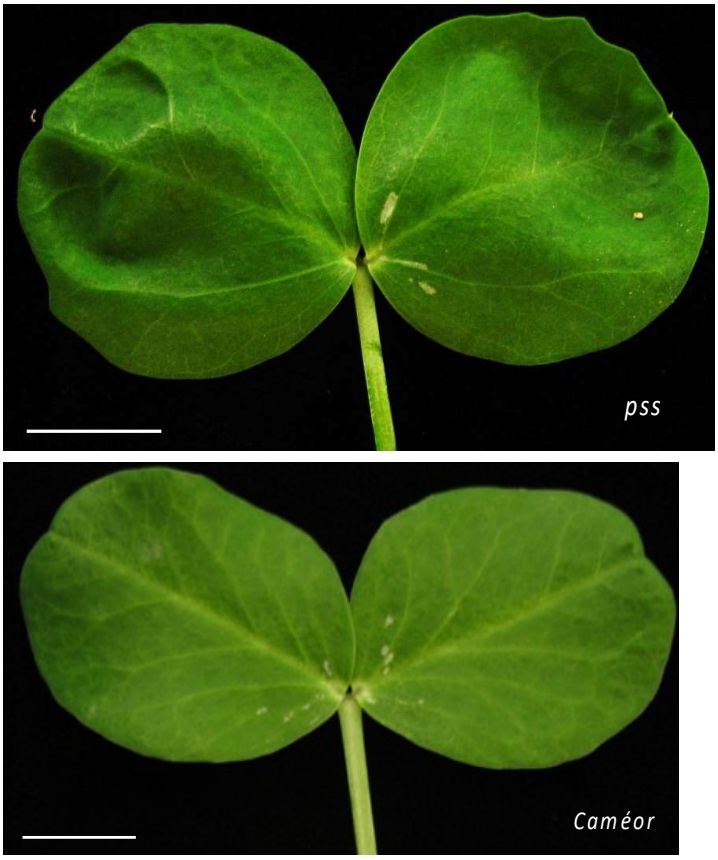

Figure 3.2. The *pss* mutant (now referred to as *crd-4*) has altered leaf vein structure and waved surface when compared with the parental line Caméor. First fully expanded leaf at the third node. Scale bar represent 1cm.

3.3.2. Inferred phylogeny

Phylogenetic analysis of the 12 pea YUC protein sequences available in genebank (ADP88696.2) (Tivendale et al., 2010) and the pea RNA gene atlas (Alves-Carvalho et al., 2015), and including the 11 FMO of *Arabidopsis*, confirmed that the *Crd* locus-*PsYUC1* is homologous to *Arabidopsis YUC1/YUC4*. Pea has representatives in the five sub-clades defined by analysis of *Arabidopsis* sequences (Figure 3.3). The PsYUC1 protein sequence shares highest similarities with the *Arabidopsis* YUC4 and YUC1 (Table 3.3). No other pea YUC protein clusters in the YUC1 sub-clade.

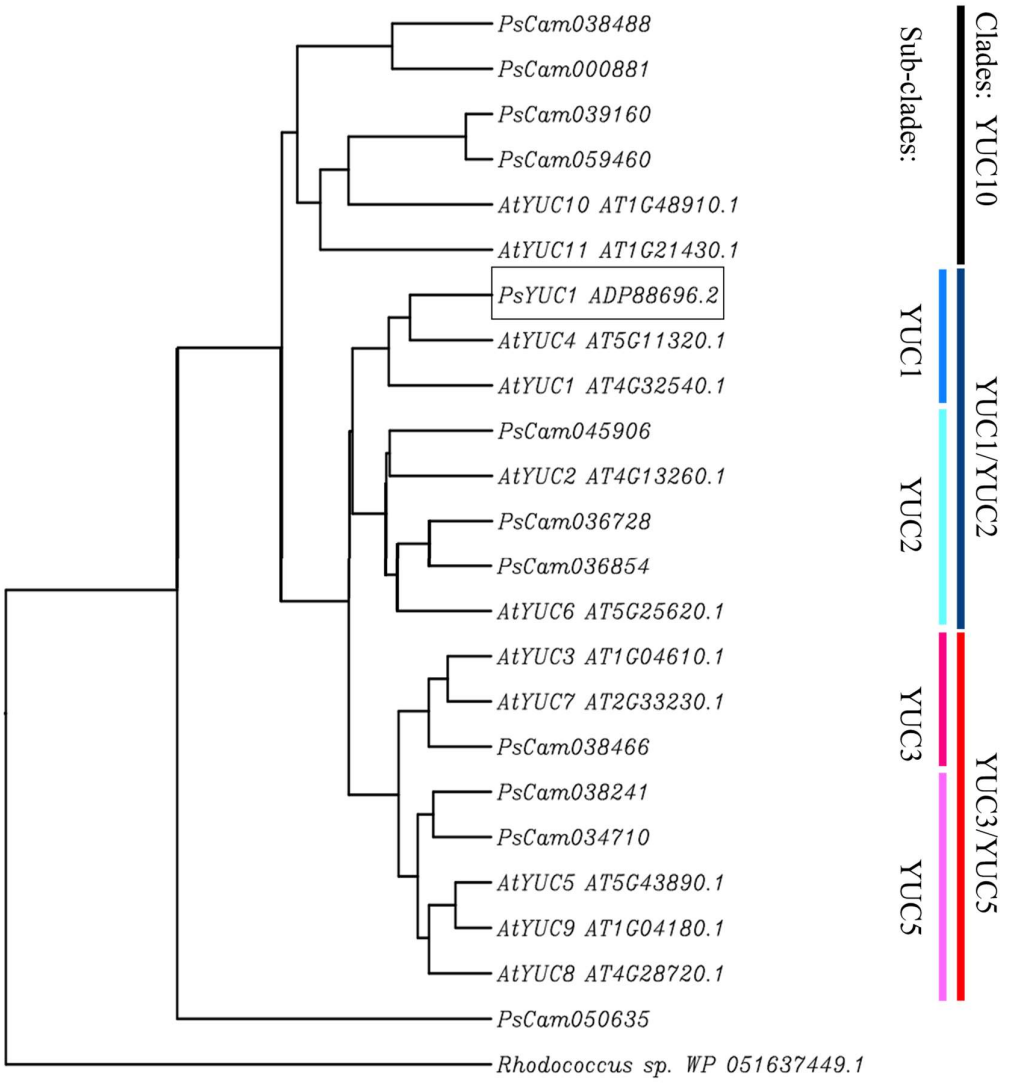

Figure 3.3. Inferred phylogenetic tree of the *Arabidopsis* and *Pisum* YUC protein family members. PsYUC1/Crd is boxed. Sequences and accession numbers from TAIR (arabidopsis.org/index.jsp), genebank (ncbi.nlm.nih.gov) and the pea RNA-seq gene atlas (bios.dijon.inra.fr/FATAL/cgi/pscam.cgi). Rooted tree (UPGMA) generated using ClustalW (www.genome.jp) with default parameters. At represents *Arabidopsis thaliana* and Ps, *Pisum sativum*. The bars represent the *Arabidopsis* clades and sub-clades.

Table 3.3. Sequence similarity scores for pea and *Arabidopsis* YUC proteins. Generated with ClustalW (www.genome.jp/). Highest similarity scores are highlighted in bold.

	PsYUC1 ADP88696.2 PsCam000833	PsCam036728	PsCam036854	PsCam045906	PsCam038466	PsCam038241	PsCam034710	PsCam039160	PsCam059460	PsCam038488	PsCam000881	PsCam050635
AtYUC1	**60**	53	54	53	49	52	47	40	32	41	41	32
AtYUC2	55	**65**	**65**	**63**	54	55	47	39	33	44	43	33
AtYUC3	53	54	54	52	**74**	67	56	44	30	45	46	30
AtYUC4	**68**	55	54	56	53	54	48	41	32	42	42	32
AtYUC5	52	56	56	51	67	**68**	**61**	42	32	42	44	32
AtYUC6	54	**68**	**66**	**62**	54	57	49	40	34	44	45	34
AtYUC7	52	56	55	52	**73**	66	55	38	31	43	45	31
AtYUC8	53	53	53	50	67	**72**	**62**	36	32	42	42	32
AtYUC9	53	57	56	52	65	**69**	**62**	39	32	44	45	32
AtYUC10	42	44	44	44	44	44	38	**54**	**42**	**47**	**46**	**43**
AtYUC11	42	47	45	43	46	45	41	48	**42**	44	**46**	**42**

3.3.3. PsYUC1 protein structure

In silico protein structures were generated to understand the nature of functional AtYUC1 and PsYUC1 proteins. An *in silico* structure of the rice YUC1 protein was previously published (Fujino et al., 2008) but the levels of details did not allow the investigation of the impacts of the *crd* mutation may have on the protein. All structures included have a significant confidence level with more than 95% of the sequences modelled at >90% accuracy (Kelley et al., 2015). Published bacteria monooxygenase crystal structures in bonded formation with the FAD and NADPH cofactors (PDB # 5M0Z, 3UCL and 3GWD) (Mirza et al., 2009; Romero et al., 2016; Yachnin et al., 2012) were used to generate templates using the Swiss-Model server (swissmodel.expasy.org/) (Figure 3.4a, c). Both the bacteria FMO and the *Arabidopsis* YUC1 tertiary structures are reminiscent of a 'bird nest' with the FAD and NADPH binding pocket in the centre (Figure 3.4a, b). When looking from the top, the α-helices and β-strands are all located at the periphery in the shape of the

'nest' with a single and short α-helix (the second α-helix, αB) at the base of the structure forming a 'floor' (Figure 3.4c, d).

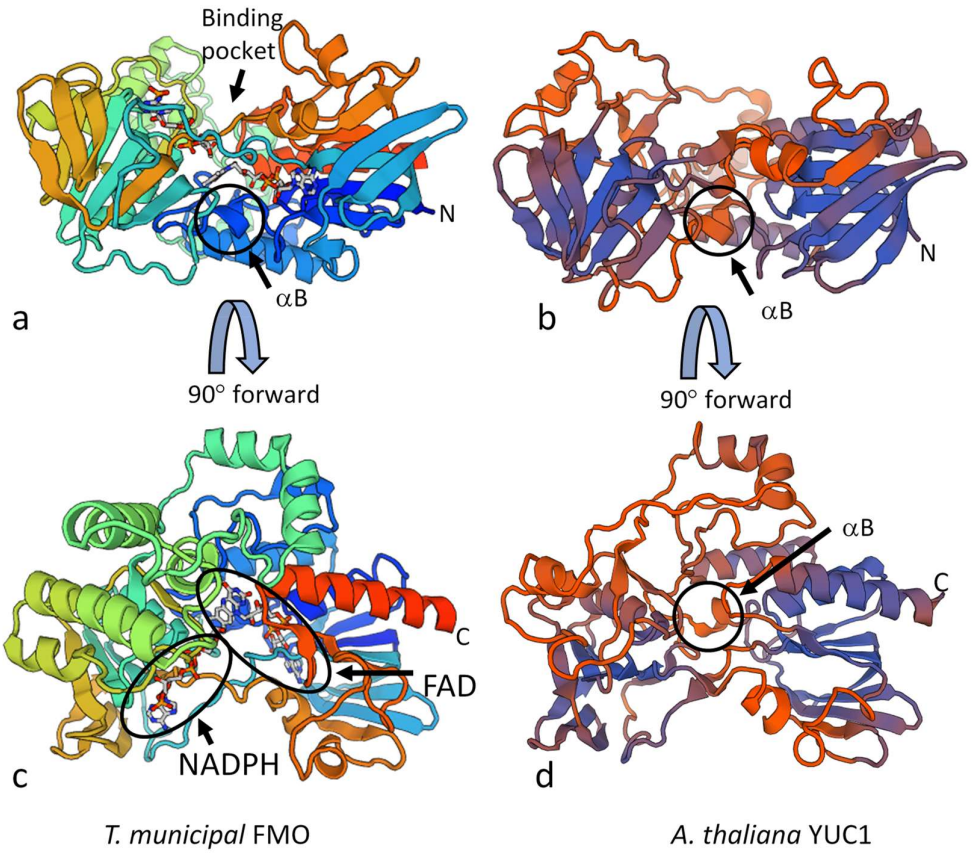

Figure 3.4. Bacterial FMO crystal structure and *in silico Arabidopsis* YUC1 protein structure. The proteins are presented as ribbon diagrams and *T. municipal* is shown in the rainbow format with the N-terminus (N) being blue and the C-terminus red (C). a) The binding pocket is accessible from the top. a and b) The proteins resemble a 'bird nest'. The FAD and NADPH cofactors are both in bonded formation inside the binding pocket of T. municipal. Generated with the Swiss-Model server (swissmodel.expasy.org/).

The two proteins are of similar length (AtYUC1, 414bp and 5M0Z, 457bp). Structurally, the proteins resemble one another but differences in folding patterns and secondary structures are apparent. The first 17 bp and the last 21 bp of AtYUC1 are not modelled resulting in a shorter AtYUC1 sequence when compared with the

bacteria FMO (Figure 3.5). As the bacteria FMO sequence is 81 bp longer in the alignment, centrally located gaps are introduced in the AtYUC1 sequence. Consequently, seven extra α-helices are introduced in the bacteria FMO, giving its 3-D structure a 'fuller' appearance (Figure 3.4b).

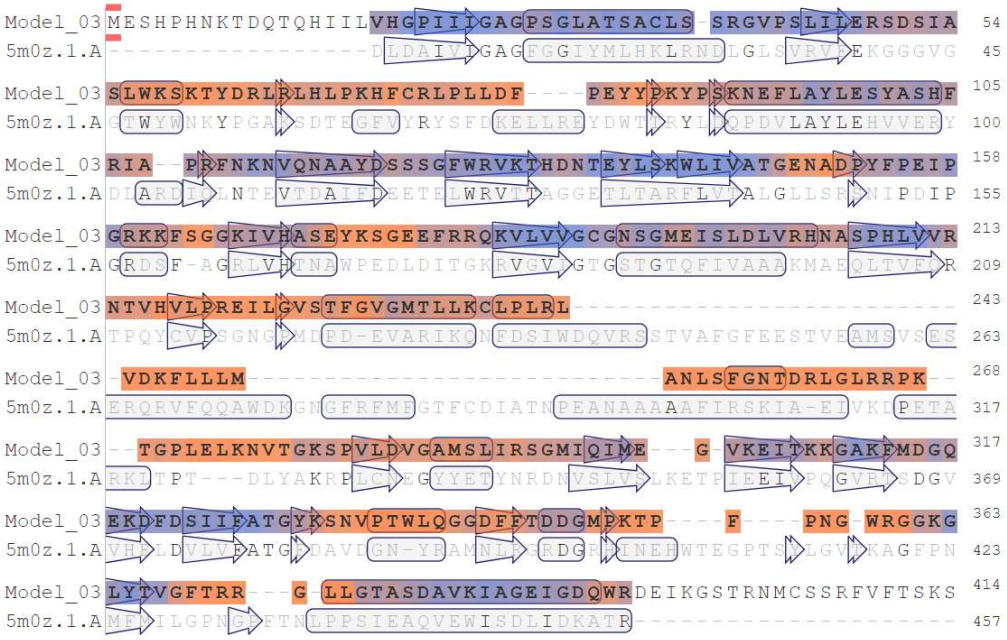

Figure 3.5. Alignment of AtYUC1 (model_03 in the figure) and bacteria FMO (5m0z.1.A). The amino acids in bold are modelled, the ones encircled represent alpha-helices (α) and the arrows, beta-strands (β). Small arrows only comprising a single amino acid represent strong torsion in the loops. Alignment generated with Swiss-Model.

As with Arabidopsis, the pea YUC1 in silico predicted protein contains 14 α-helices and 17 β-strands (Figure 3.6 and 3.7). Numerous loops of varied lengths are located between the principal secondary structures. From the N-terminus to the C-terminus, the six conserved FMO domains are present. The PsYUC1 FAD binding motif (GxGxxG) (Schlaich et al. 2007) and the associated GG motif (ExxxxxAS) (Vallon, 2000) are positioned C-terminally on short loops post β1 and β2 respectively. The plant-specific ATG1 domain (YxxxWL(I/V)VATGENAE) (Expósito-Rodrígez et al., 2007) is located on the second half of β6, the same location of the *crd-1* mutation

(G142D). The FMO defining motif (FxGxxxHxxxY/F) (Fraaije et al., 2002) overlaps over β7 and αF, and the NADPH binding motif is on the short loop after β8. In the *crd-2* mutant allele, the frame-shift is located on the short loop prior to β10 and adversely affects the sequence downstream with a premature termination well before the second ATG motif (Dxxx(L/F)ATGYxxxP) (Vallon, 2000). The second ATG motif, often referred to as the LATGY motif in YUC proteins (Hou et al., 2011), encompasses β16 and the majority of the following long loop. In *crd-4*, the frame-shift start is located post αL, well after any of the previously defined motifs, but does detrimentally affect several secondary structures and terminates the sequence prematurely.

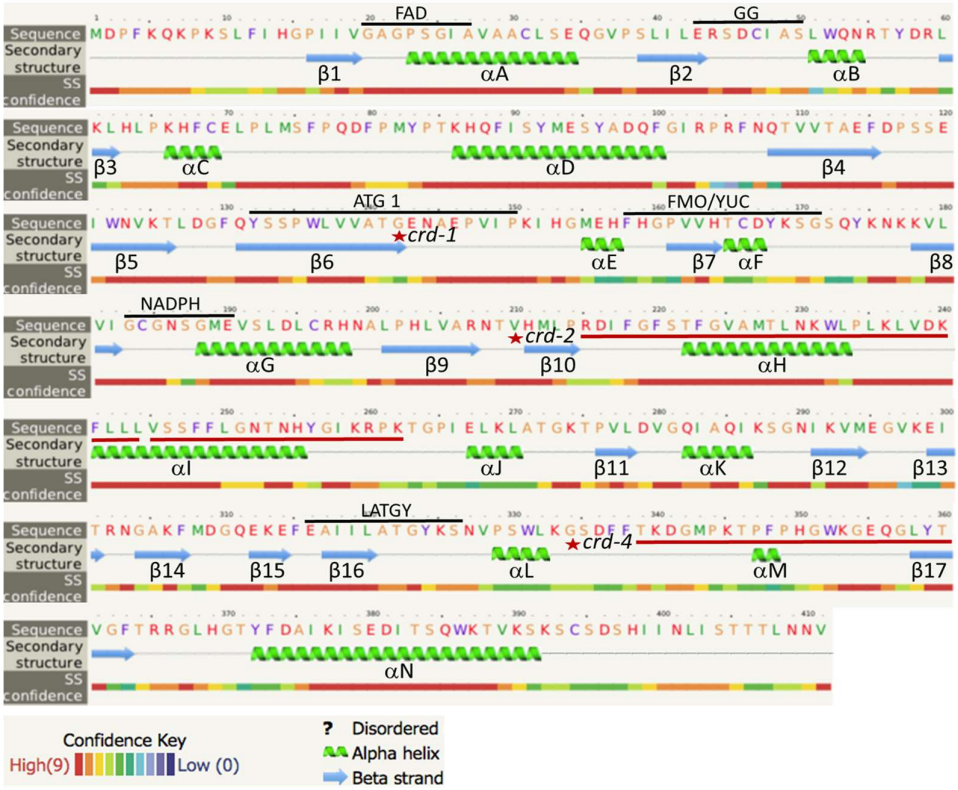

Figure 3.6. The predicted secondary structures of the YUC1 protein of pea. The locations of the known FMO motifs are marked with a black line and the *crd* mutations with a red star. The sequence sections affected by the *crd-2* and *crd-4* frame-shifts are underlined with a red line. Confidence levels are colour coded. Secondary structures generated with the Phyre2 web portal (sbg.bio.ic.ac.uk/~phyre/).

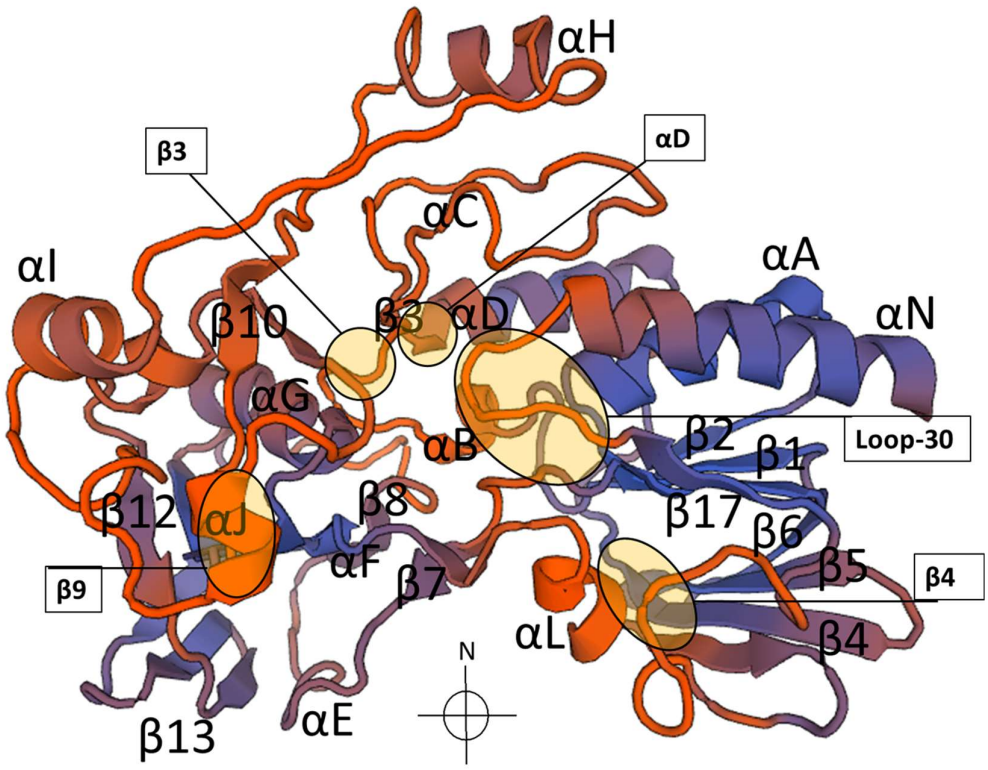

Figure 3.7. The PsYUC1 predicted 3-D protein architecture and its secondary structures. α-helices are alphabetised and β-strands are numbered. The protein is shown as a ribbon model. Generated with Swiss-Model.

3.3.4. Important PsYUC1 binding amino acids

Next, the potential FAD and NADPH binding amino acids of the pea YUC1 protein were predicted (Table 3.4). The *T. municipal* FMO sequence was selected as a reference due to the high similarity scores given by the binding prediction web servers. The bacteria binding residues included in Table 3.4 were obtained by X-ray diffraction of proteins in bonded solution with ligands at 1.60 ångström (Romero et al., 2016). The pea YUC1 protein has fewer predicted binding residues overall when compared with those present in the bacteria FMO. Two servers were used to compare and confirm results obtained for PsYUC1. The majority of predicted residues were in agreement and represented highly conserved amino acids clustering to areas defined by the consensus FMO domains. Intriguingly, no amino acids were

predicted for the FMO -identifying motif. The 3-D ligand prediction server (sbg.bio.ic.ac.uk/3dligandsite/) predicted fewer binding residues than did the RaptorX-Binding site (raptorx.uchicago.edu/BindingSite/). Most discrepancies related to interactions of PsYUC1 with the NADPH cofactor. Of interest, several regions of the bacteria and pea sequences, not characterised as core FMO motifs, were predicted as having important binding residues. The section between the GG motif and the first ATG motif had three clusters of amino acids defined as having binding roles. The region between the NADPH binding motif and the second ATG (LATGY) motif had three areas with predicted binding residues. Furthermore, and of relevance to this study, one area downstream of the LATGY motif was predicted to have binding properties.

Table 3.4. Predicted binding amino acids of PsYUC1 compared with bacteria FMO binding residues from crystallographic studies (Romero et al., 2016). Results from two independent ligand prediction servers are included: 3dligandsite and RaptorX-Binding. Residues in bold are present in bacteria and predicted by both servers.

FMO/YUC motifs and secondary structures	Function	Important residues defined by bacteria FMO*	PsYUC1 predicted residues	
			3DLigand Site lnE score=23.5	RaptorX p=4.38e-10
FAD motif: Loop-2 and α-helix A	Binds the Adenine moiety of FAD cofactor	I12, **G15**, A16, **G17**, G20, I21	V19, G20, G22	V19, **G20, G22,** P23, S24
GG motif: Loop-4 and α-helix B	May stabilise FAD cofactor	G32, **E39**	L42, **E43**, R44, S45, S50, L51, **W52**	**E43**, R44, S50, L51, **W52**
β-strand 3	Unknown	W48, Y53, K57	N54, R55, **Y57**, L60, **K61**, L62, H63	**Y57**, L60, **K61**, H63
α-helix D	Unknown	Y83, Y92, E94	K86	K86
β-strand 4 and β-strand 5	Unknown	N109, **V112**, A115, F117, D118/ W124, V126, T128	Q108, T109, **V110**	Q108, T109, **V110**
ATG1 Motif: β-strand 6	May provide linkage between FAD and NADPH	L139, V140, **A142**, **G144**, I151, **P152**	**A140**, T141, **G142**, E143, N144, A145	**A140**, T141, **G142**, E143, **P150**
FMO/ YUC motif: α-helix E and β-strand 7	Baeyer-Villiger motif motif found in all FMOs. May contribute to NADPH binding	I154, G156, F160, G162, V165, T167		

NADPH motif: Loop-14 and α-helix G	Binds to NADPH cofactor. Reduction of FAD	V181, V183, **I184, G185, G187**, G190	S187, E190	**I182, G183**, C184, **G185**, N186, S187, E190
β-strand 9 and α-helix J	Unknown	**R209**/ P216 S305, P322/ K328, P330		A206, **R207**, N208 K269
LATGY motif: β-strand 16 and loop-27	Present in N-hydro-xylating enzymes. May assist in NADPH linkage	A379, T380, G381	Y324	**A321**, **T322**, **G323**, Y324, N327
Loop-28 and 29	Unknown	D398, G399, G420	S335	
Loop-30 and α-helix N	Unknown	I444, S449, I452		G362, R365, R366, G367, L368

*PDB #5M0Z (Romero et al., 2016).

The data from the two binding prediction servers can also be visualised in 3-D (Figure 3.8 and 3.9). The majority of the pea α-helices and β-strands form the 'nest' with α-helix B forming the 'floor'. When spun 90° forward and viewed from the top, the 'floor' of the 'bird nest' can be seen at the centre of the structure (Figure 3.8a). As with AtYUC1, the shorter PsYUC1 sequence (411 bp) folds slightly differentially than the bacteria FMO structure, resulting in fewer α-helices and β-strands. The predicted binding residues are located within the pocket (Figure 3.8b). These represent the critical binding region present in bacteria FMO (Schlaich et al., 2007). Furthermore, when the whole structure in bonded formation is viewed in space-filling mode, nearly all the predicted binding residues are incorporated, and the FAD cofactor is quenched in the pocket. However, a substantial part of the NADPH ligand remains exposed, potentially to permit the interaction with molecular oxygen, which leads to the formation of the C4-intermediate (Figure 3.8d).

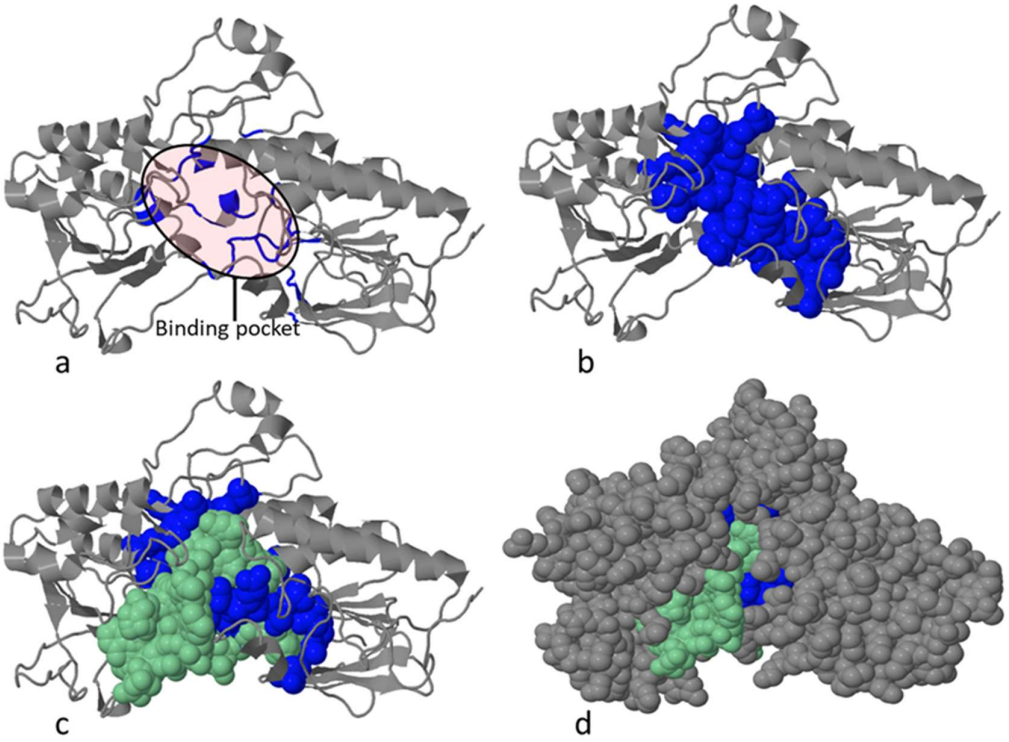

Figure 3.8. The PsYUC1 protein architecture and the FAD and NADPH binding amino acids predicted *in silico* with Phyre2. a) Viewed from above, the PsYUC1 protein is presented in ribbon mode. The binding pocket is encircled, and the predicted binding residues are in dark blue. b) The predicted amino acids presented in space-filling mode. c) The FAD and NADPH ligand in space-filling mode and green. d) The whole structure in space-filling mode. Generated with Phyre2.

When viewed with the RaptorX binding prediction tool, the two principal ligands are placed as expected (Figure 3.9). From the top of the structure, NADPH interacts with the secondary structure on the left side of the protein (Figure 3.9a). Focussing on the interactions of PsYUC1 with the cofactor FAD (Figure 3.9b), the core residues of the FAD binding motif interact with the purine ring of FAD. The amino acids predicted to bind at the tail-end of the protein (Loop-30 and a-helix N) can be clearly seen coming in contact with the central region of the FAD cofactor (Figure 3.9c).

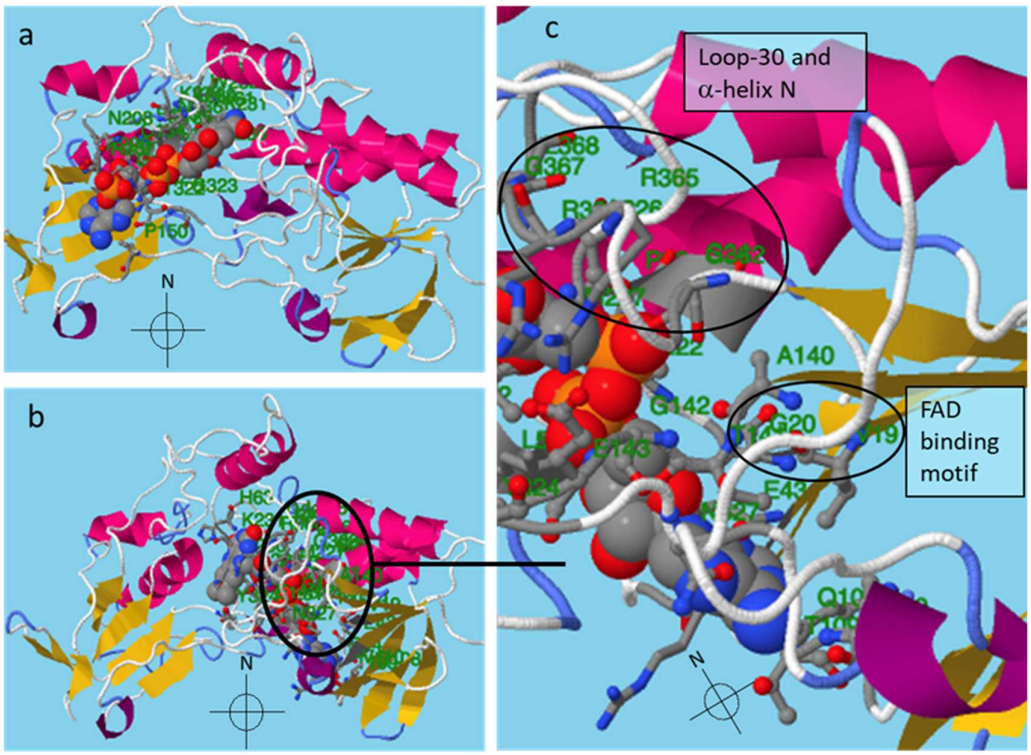

Figure 3.9. The PsYUC1 protein architecture and the FAD and NADPH binding amino acids predicted *in silico* with RaptorX-Binding site. A) NADPH in the binding pocket. B) FAD and predicted binding amino acids. C) Close-up of FAD cofactor in the binding pocket. The FAD binding motif region and the C-terminus Loop-30 and α-helix N predicted binding residues are boxed. Generated with the RaptorX-Binding site.

Next, the potential amino acids preferential interactions with the FAD and NADPH cofactors were then accessed *in silico* (raptorx.uchicago.edu/BindingSite/) (Figure 3. 10). Amino acids tended to cluster in groups which were primarily associated with one cofactor or the other. However, two regions were predicted to bind with both cofactors. Seven regions of the sequence were principally targeting the FAD cofactor. The majority were in the first half of the protein sequence with one C-terminally located cluster. Three areas centrally located targeted NADPH.

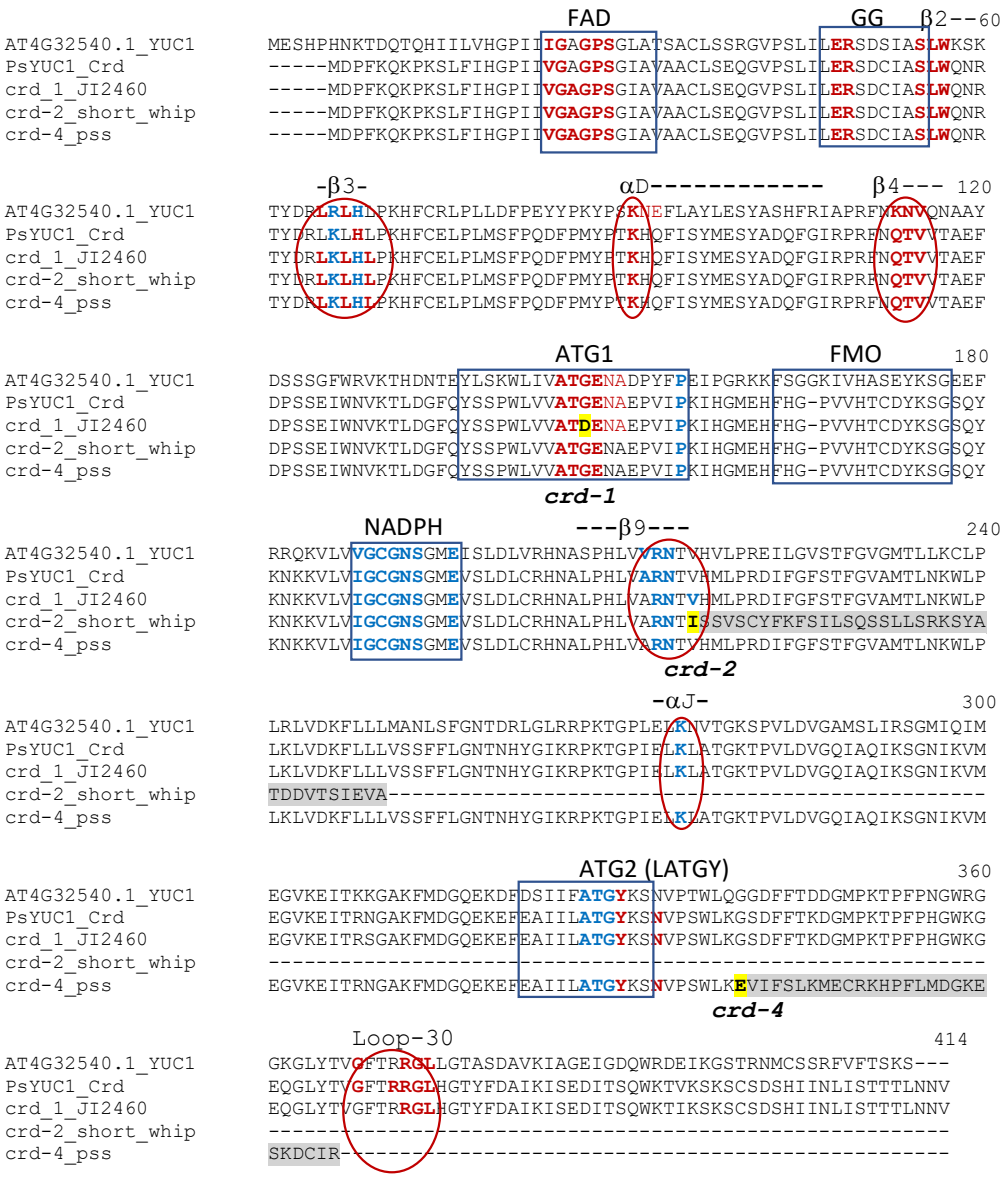

Figure 3.10. Predicted binding residues of the AtYUC1, PsYUC1 and the *crd* mutant proteins. Previously described FMO motifs are in boxes. Amino acids in red are predicted to interact with FAD and residues in blue with NADPH. Amino acids in red circles are predicted to be important binding residues but have not been previously defined as such. The mutated residues in the *crd* mutants are marked in yellow. Sequence alignment generated with ClustalW and binding residues predicted with 3-D Ligand site (sbg.bio.ic.ac.uk/3dligandsite/) and RaptorX-Binding (raptorx.uchicago.edu/BindingSite/).

The uncharacterised clusters of amino acids defined as binding to the FAD and NADPH cofactors were placed on the 3-D PsYUC1 protein structure to assess whether the predictions were physically plausible. The five predicted areas, despite not being associated with known FMO domains, are located in the binding pocket and could therefore have the capacity to interact with the relevant ligands (Figure 3.11). The residues defined as being FAD-associated are in regions that are likely to interact with the FAD cofactor. FAD tightly fits in the Eastern portion of the protein and is likely to come in contact with β-strand 4, α-helix D and Loop-30. NADPH locates in the Western side of the binding pocket increasing the likelihood of interaction with β-strand 9. Furthermore, and strengthening the case of the predictions being credible, β-strand 3, predicted to contain amino acids binding to both cofactors, is located at the junction where FAD and NADPH meet.

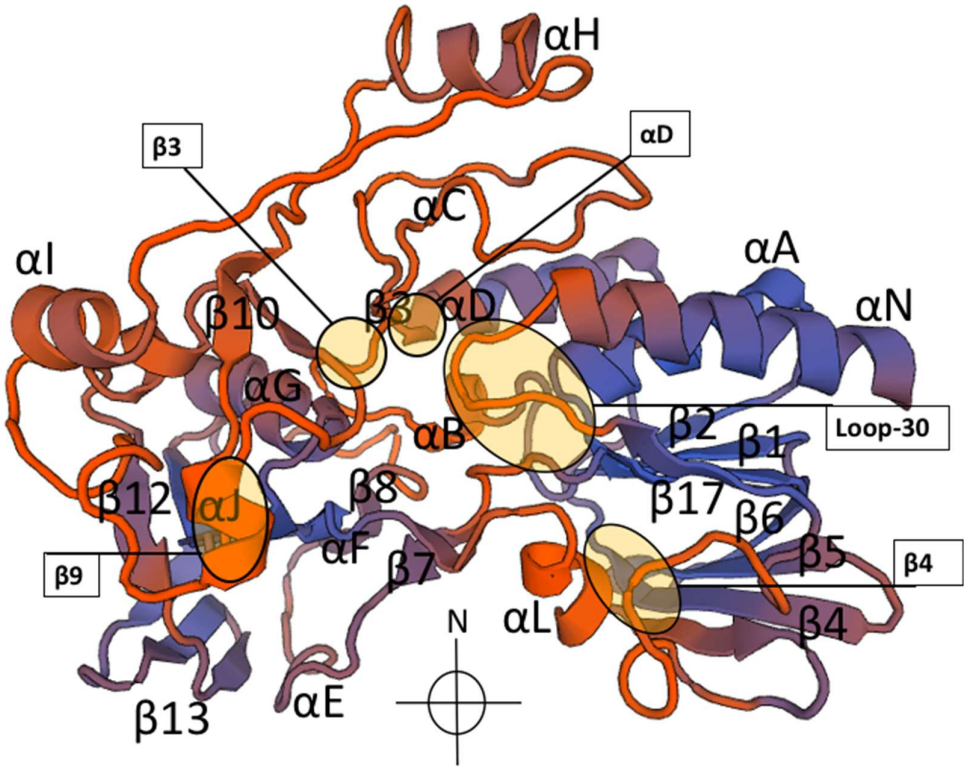

Figure 3.11. Uncharacterised PsYUC1 regions predicted as containing important binding residues. The protein is shown as a ribbon model. Potential novel binding regions are highlighted. Structure generated with Swiss-Model server.

3.3.5. The effects of the *crd* mutations on PsYUC1

The 3-D models also allow to visualise the structural consequences that the *crd* mutant alleles impart to the PsYUC1 protein. The *crd-1* mutant has leaf vasculature phenotypes (McAdam et al., 2017b; Swiecicki, 1989). However, no change in overall structure and folding pattern are predicted at the tertiary protein level. The *crd-1* point mutation, located at the first ATG motif (McAdam et al., 2017b), changes a glycine to an aspartic acid residue (G142D) (Figure 3.12). Glycine does not have any side chain, increasing the flexibility of the polypeptide chain at that location. Glycine, being neither hydrophilic nor hydrophobic, can be found in either environment but is generally considered non-polar (McMurry and Simanek, 2007). Residues in the vicinity of Gly 142 are mainly hydrophobic (Val 138 and 139, Ala 140 and Ala 145). However, the amino acids directly flanking Gly142 are polar (Thr 141 and Asn 144) and negatively charged (Glu 143) implying that Gly 142 may assist in increasing contact with water.

The change of glycine to aspartic acid (G142D) does not appear to affect the PsYUC1 folding pattern or torsion angle at the location of the amino acid change (Figure 3.12). Aspartic acid, the amino acid coded for by *crd-1*, has a negatively charged side chain. Potentially, having two negatively charged amino acids side-by-side may increase polarity within that specific area, allowing too much water to be incorporated thus preventing Thr 141 and Asn 144 from forming efficient hydrogen bonds with the ligand. Furthermore, at position 142, all other 19 amino acids have a SIFT score (sift.jcvi.org/sift) of 0.00 (<0.05 considered deleterious), with the exception of glycine being the only amino acid present and tolerated in the 48 sequences included in the alignment. Any changes to glycine at position 142 is expected to have aberrant consequences on the functionality of the protein.

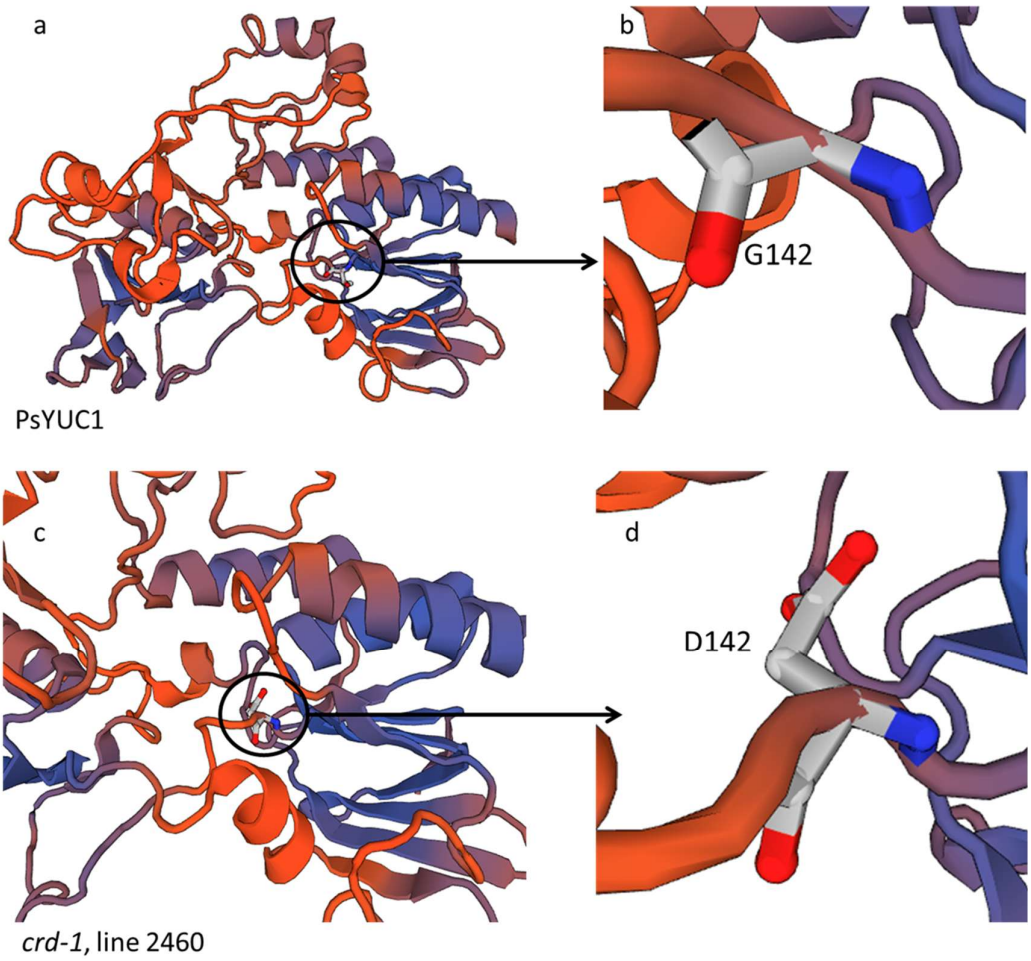

Figure 3.12. PsYUC1 and crd-1 predicted protein structure. a and b) PsYUC1 structure with close-up of location of G142. c and d) The location of the altered amino acid D142. Generated with Swiss-Model server.

The *crd-2* mutation, originally referred as *crd-whip* (Berdnikov et al., 2000), has a single nucleotide substitution (G628A) resulting in a frameshift at position 210 in the translated protein sequence. Two principal protein products, with altered sequences and premature termination are produced due to alternative splicing of the mutant RNA: the longer product terminates at position 262 and the shorter product, the most abundant of the two, terminates at position 244 (McAdam et al., 2017b). The products have several amino acids predicted as deleterious. The shorter product has five amino acid out of 35 with SIFT scores below 0.05 and the longer product, has eight out of 53. Both frameshifts and early truncations adversely affect the proteins

folding patterns and structures. The secondary structures of the most abundant product, the shorter *crd-2*, and the product used in all proceeding predictions, is disrupted from α-helix H onwards (Figure 3.13). The second ATG motif (Hou et al., 2011) is missing as are the last five α-helices and seven β-strands.

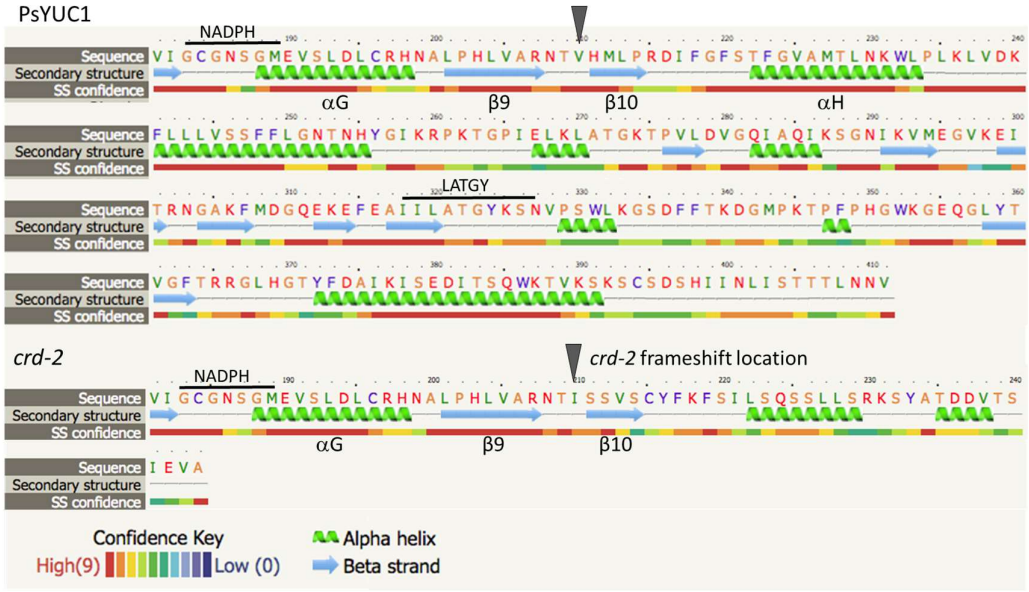

Figure 3.13. Comparison of the predicted secondary structures of the C-terminal section of the PsYUC1 and *crd-2*. The sequence section affected by the *crd-2* is shown with grey triangles. Confidence levels are colour coded. Secondary structures generated with the Phyre2 web portal (sbg.bio.ic.ac.uk/~phyre/).

The C-terminal section of the *crd-2* protein sequence is missing, which consequently translates to the 3-D *in silico* structure having fewer FAD and NADPH binding residues being predicted (Figure 3.14). Many of the FAD-related binding amino acids can be seen in the pocket as these principally occur in the 'Eastern' side of the protein (Figure 3.11b, c). However, in space-filling mode, much of the FAD cofactor and its associated binding residues are not fully incorporated in the *crd-2* pocket when compared with the WT PsYUC1 structure (Figure 3.11d). The PsYUC1 protein from the *crd-3* mutant (line FN1522-1) cannot be modelled due to

the complete deletion of *PsYUC1* from the genome. Consequently, *crd-3* can be confidently presumed to be a null mutant (McAdam et al., 2017b).

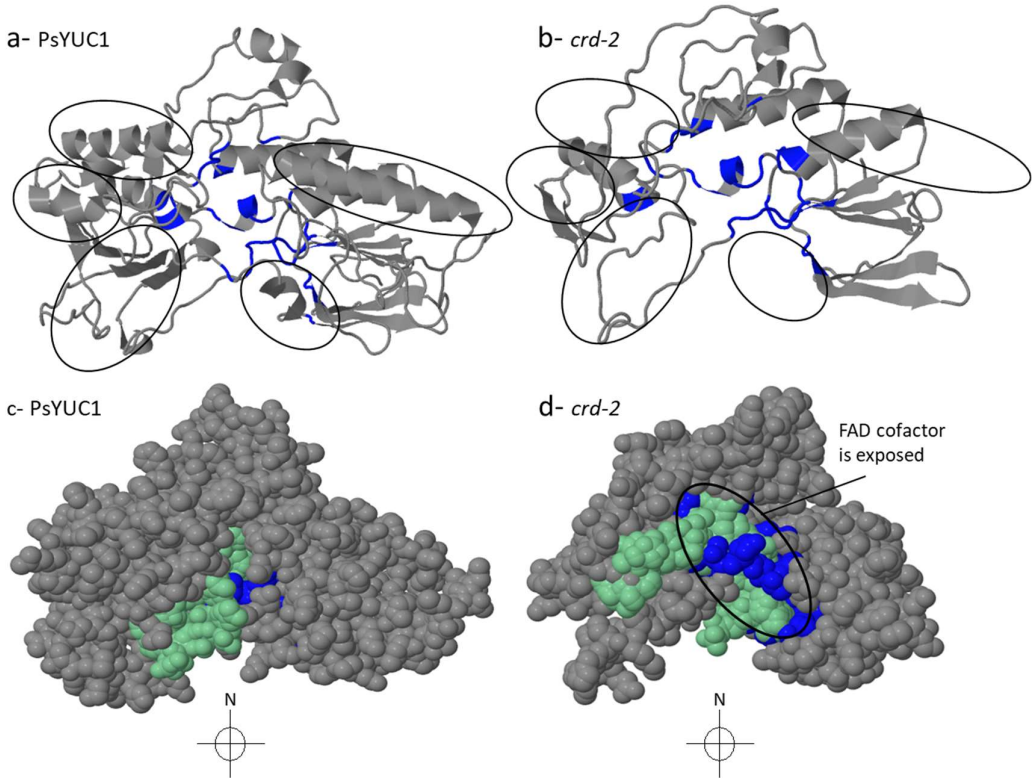

Figure 3.14. The protein structure of the *crd-2* mutant and its predicted binding amino acids for the FAD and NADPH cofactors. a) Viewed from above, the WT protein is presented in ribbon mode. The predicted binding residues are in dark blue and areas that are affected in *crd-2* are encircled. b) The *crd-2* protein presented in ribbon. Areas where secondary structures are missing are encircled. c and d) The structure (grey), the binding residues (blue) and the FAD and NADPH ligands (green) in space-filling mode for PsYUC1 and crd-2 respectively. d) FAD and associated binding residues are not quenched in the pocket. Generated with Phyre2.

For *crd-4*, a single-point mutation (G1730A) results in a frameshift at position 334 of the protein sequence (McAdam et al., 2017b). The resulting product has a premature termination at position 361 and 27 altered amino acids, 12 of which are predicted as deleterious with SIFT scores < 0.05. Despite the fact that the *crd-4* mutation occurs

downstream of the consensus FMO domains, the protein structure is nonetheless adversely affected (Figure 3.15). The last two α-helices and β17 are missing.

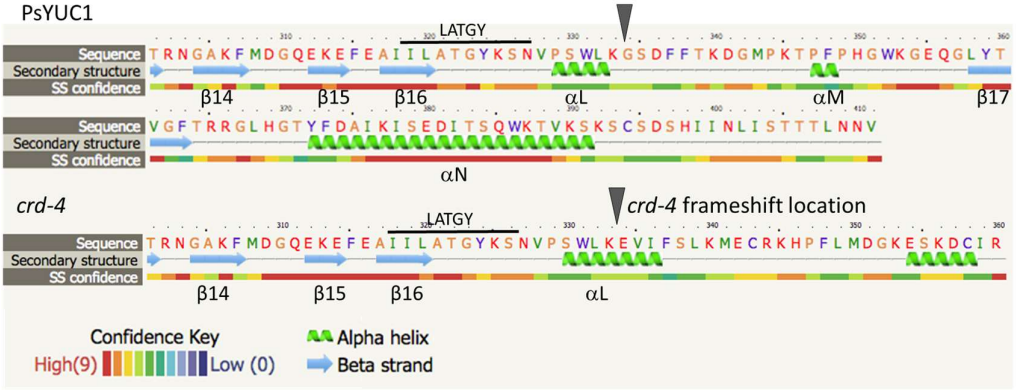

Figure 3.15. Comparison of the predicted C-terminal secondary structures of PsYUC1 and *crd-4*. The sequence section affected by the *crd-4* is shown with grey triangles. Confidence levels are colour coded. Secondary structures generated with the Phyre2 web portal (sbg.bio.ic.ac.uk/~phyre/).

The physical changes caused by the *crd-4* allele alter the secondary structures at the C-terminal end of the PsYUC1 protein (Figure 3.16a, b). Folding patterns are not substantially modified but the missing β-strand and α-helices may affect the capacity of the binding pocket to interact efficiently with the ligands. Indeed, in space-filling mode, much of the FAD cofactor and its associated binding residues are not fully incorporated in the *crd-4* pocket (Figure 3.16c, d).

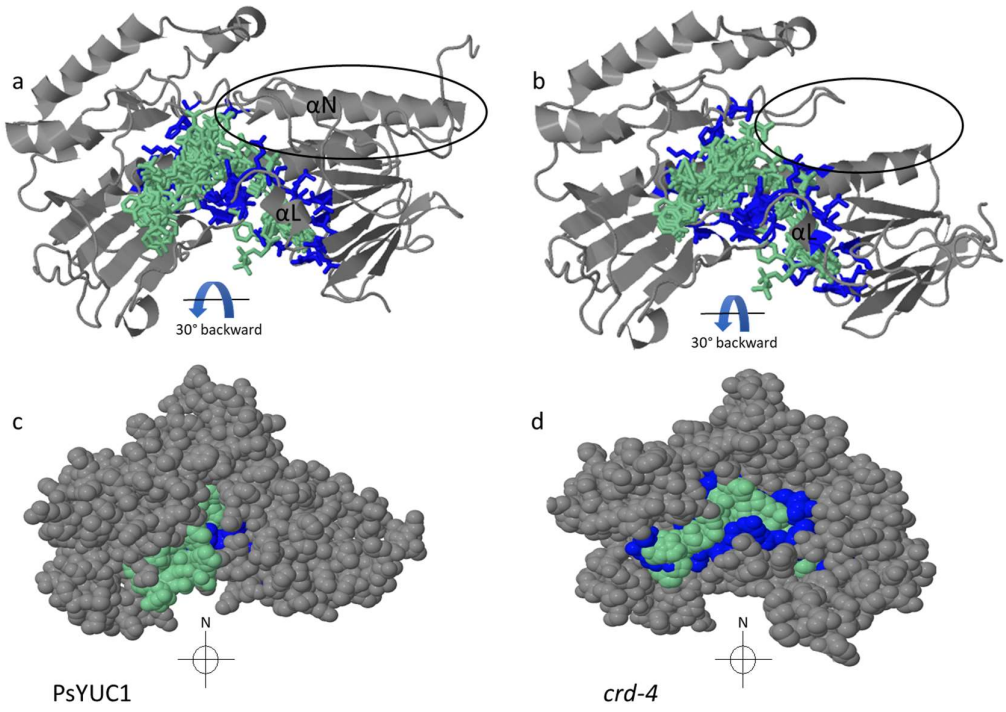

Figure 3.16. The effects of the *crd-4* mutation on the PsYUC1 architecture. a and b) Tilted 30° backwards, the PsYUC1 and *crd-4* proteins are presented in ribbon mode. The predicted binding residues (dark blue) and FAD and NADPH ligands (green) are shown as stick models. The region affected in the *crd-4* mutant is encircled. c and d) The whole structures are viewed from the front in space-filling mode. Generated with Phyre2.

In the WT PsYUC1 protein, Loop-30, found between β-strand 17 and α-helix N, is located above the floor of the binding pocket, α-helix B, and folds back onto the area where the FAD cofactor locates (Figure 3.17a). The 'folding back' of Loop-30 appears to form a 'roof' or a 'lid' above the binding pocket. The hydrophobic amino acids associated with Loop-30 (Val 361, Phe 363 and Leu 368) face down towards the pocket (Figure 3.17b). Val 361 is proximally placed above Gly 20, a canonical FAD binding residue of FMOs (Eswaramoorthy et al., 2006). The two arginine (Arg 365 and 366) side chains outstretch over the binding site. Arginine is amphipathic, meaning that the positively charged head of the side chain possibly interacts with the

environment outside of the protein while the hydrophobic hydrocarbon chain may interact with the interior and the FAD cofactor.

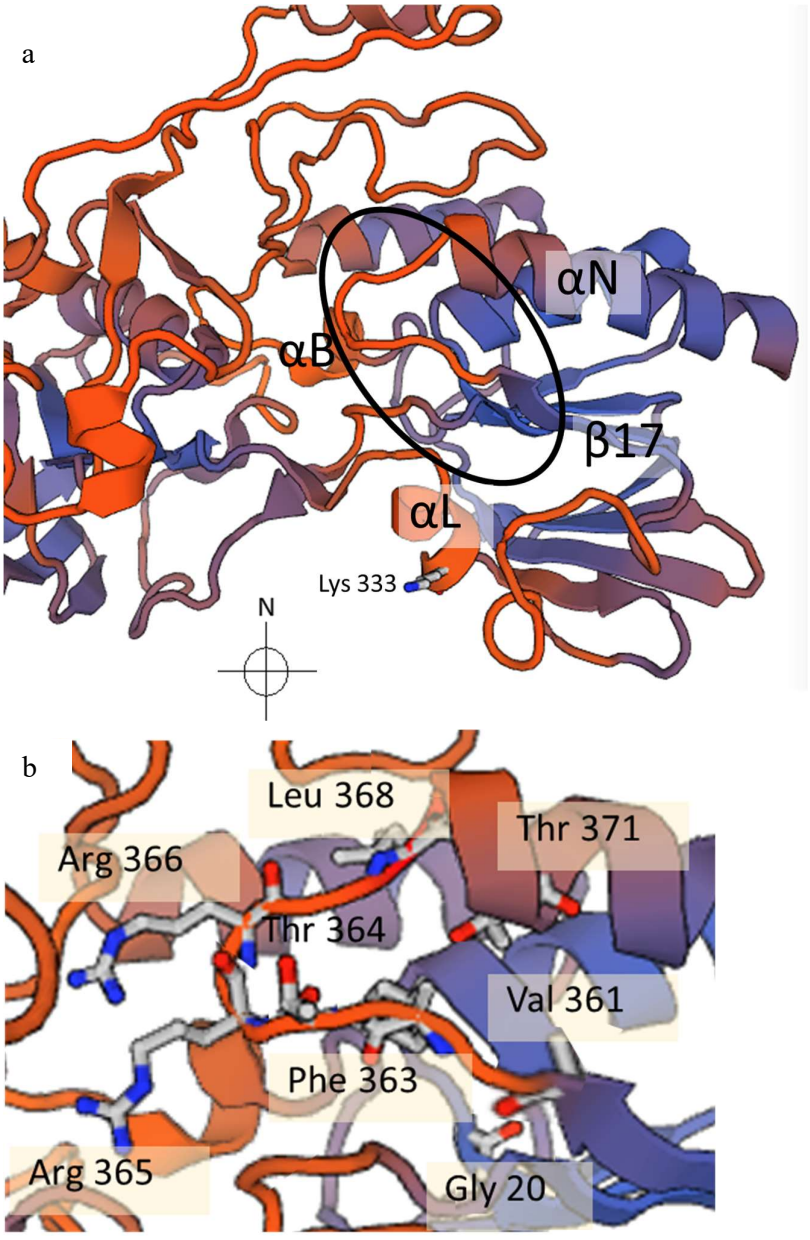

Figure 3.17. Loop-30 may be important to the functionality of the PsYUC1 protein. a) Loop-30 is situated above the binding pocket. Lys 333 is selected because Gly 334, the start of the *crd-4* frameshift, is located behind Lys 333 and cannot be seen in this orientation. b) Amino acids that form Loop-30. Oxygen in red, nitrogen in blue and hydrogen in light grey. Generated with Swiss-Model.

Loop-30, and the amino acids flaking each side, are highly conserved in plants but not in bacterium or in animals, represented here by a rabbit FMO (Figure 3.18). Potentially, in plant species, Loop-30 and its flanking residues, behave in a similar fashion as another protein with a 'lid'. Indeed, a simpler protein, Hsp70 or DnaK, a chaperone involved in protein export destined for secretion in *E. coli* (Hartl, 1996; Wild et al., 1992), has a lid located above the binding pocket. The lid did not appear to have binding properties *per se*, but was demonstrated to 'capture' the substrate within the binding domain (Zhu et al., 1996). Further studies demonstrated that the removal of the lid drastically reduced the binding capacity of the protein by destabilising the pocket and reducing its affinity for the substrate (Moro et al., 2004).

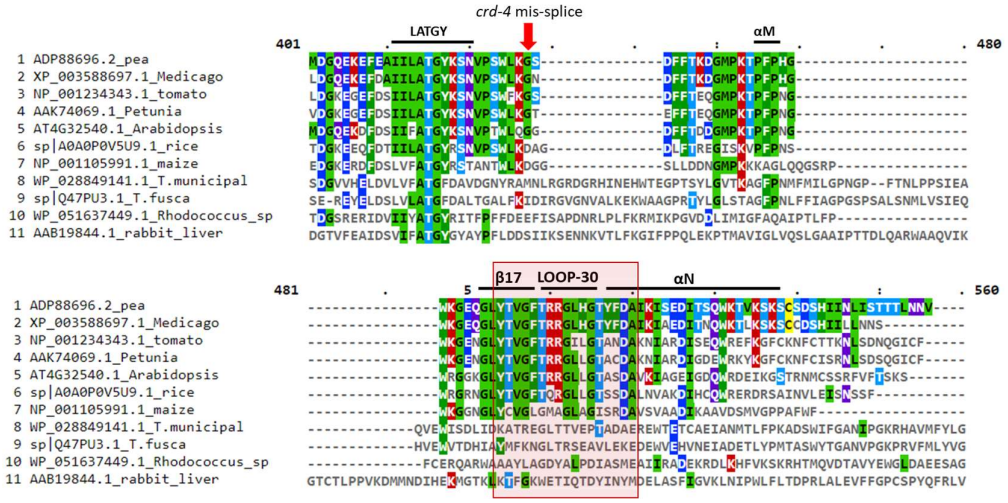

Figure 3.18. Sequenced alignment of the C-terminal end of YUC1-related proteins from a range of species, including eudicots, monocots, bacterium and mammal. The second ATG motif (LATGY), the location of the *crd-4* mutation (red arrow) and several tertiary structures are included as references. The pink box marks the amino acids that form the binding pocket 'lid' and include β-strand 17, Loop-30 and part of α-helix N. The two Arginine, in red, are located at the centre. Colouring scheme represents the amino acid family. Aligned with ClustalW and presented with the EMBL-EBI MVIEW website.

3.3.6. The *crd-4* mutant also carries the *Pstar1-1* mutation

The novel *crd-4* mutant allele originates from a *Pstar1-1* segregating population. The possibility that the *crd-4* line that was observed in this study also carried the *Pstar1-1* mutation was considered. The HRM protocol used to genotype *PsTAR1-1* (Chapter 2) revealed that indeed the *Pstar1-1* mutation was present in *crd-4* and *CRD-4* individuals selected as an isoline for the mutant (Figure 3.18). The *Pstar1-1* mutation was therefore removed from *crd-4* by crossing the double mutants to the parental *cv*. Caméor and genotyping subsequent generations until the lines only carried the *Psyuc1* mutation.

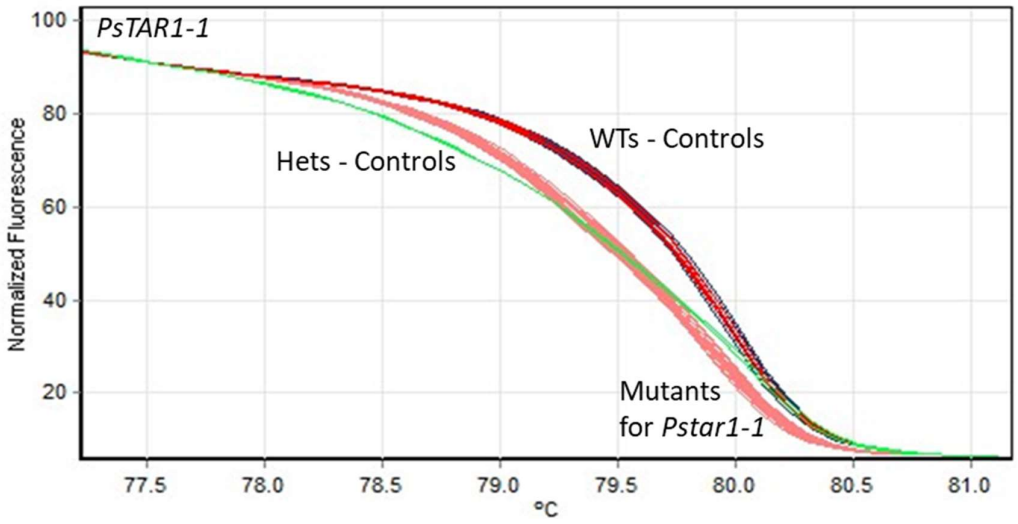

Figure 3.18. Genotyping *crd-4* and *CRD-4* for *Pstar1-1*. HRM melt curves plot (fluorescence over temperature) of four *crd-4* and four *CRD-4* samples genotyped under HRM conditions for the *Pstar1-1* mutation, line 905. All samples are genotyped as homozygous recessive for *Pstar1-1* (bottom, pink). Controls: heterozygotes (middle, green) and WT (top, red).

In the subsequent F2 generation, individuals that were genotyped as WT for *PsTAR1*, were also genotyped for *PsYUC1* using a RFLP protocol (Figure 3.19). In this protocol, the WT allele does not cleave, producing a single 600 bp product. The mutant cleaves once, producing two bands (360/240 bp) and the heterozygote,

carrying both alleles, has three bands. This was done to ensure that the phenotype co-segregated with the mutation, and that only heterozygotes for *PsYUC1* were selected, to expediate the progress of the single plant selection programme.

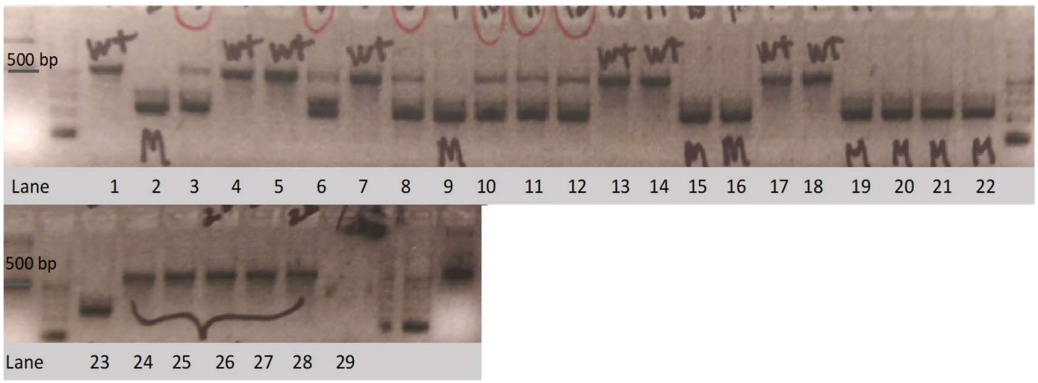

Figure 3.19. Genotyping for heterozygotes (*PsYUC1Psyuc1*). RFLP electrophoresis gel from a segregating F2 population originating from a cross between *crd-4* and Caméor. Lane 1, 4 and 5 are examples of WT individuals, lane 2, 9 and 15 of mutants and lane 3, 6 and 8 of heterozygotes. Controls: lane 23, homozygous recessive; lanes 24-29, WT and Caméor; lane 29, negative control.

3.4. Discussion

The principal catalytic function of the flavoprotein monooxygenase superfamily is to transform the lipophilic nature of xenobiotic compounds by inserting an oxygen atom to their structure, making them soluble and easier to excrete (Eswaramoorthy et al., 2006; Fraaije et al., 2002). The superfamily includes N-hydroxylating monooxygenases (NMOs), Baeyer-Villiger monooxygenases (BVMOs) and flavin-containing monooxygenases (FMOs) (Fraaije et al., 2002). The mechanism of the catalytic activity is underpinned by the reduction of the prosthetic cofactor FAD by the coenzyme/cofactor NADPH. Two ADP-binding motifs responsible for forming βαβ super-secondary structures with nucleotide binding properties (the Rossmann fold) are responsible for binding the two cofactors. Once reduced, $FADH_2$ binds to oxygen and forms a reactive intermediate (C4α-hydroperoxy-flavin) making the enzyme ready to oxidise the substrate (Fraaije et al., 2002). FMOs, however, do not require a substrate to begin their catalytic cycle. While the enzyme is in the intermediate phase, the enzyme complex is stable and is considered promiscuous to a range of substrates (Ziegler, 1993; Eswaramoorthy et al., 2006).

3.4.1. The PsYUC protein structure is well conserved

FMO sequences are highly conserved across kingdoms, generally containing six consensus domains and several core binding amino acids (Krueger and Williams, 2005; Schlaich, 2007; Vallon, 2000). In the WT PsYUC1 protein, the six consensus domains were present at the sequence level, five of which were predicted to contain binding residues at the tertiary structure level. Principally, the two ADP-binding motifs (GxGxxG), the FAD and NADPH motifs, are located inside the binding pocket and situated in areas that would allow contact with the associated cofactors. In both instances, amino acids predicted to have binding capacity clustered and located to the ADP-motifs. Furthermore, each residue cluster was predicted to specifically bind to its respective cofactor. The FAD binding motif only contained residues predicted to bind to FAD and the NADPH motif only had residues predicted to bind with NADPH. Interestingly, the FAD cofactor was located deeper in the

pocket than NADPH. In the WT protein, FAD and its associated residues were fully integrated, suggesting that FAD binds more strongly to the enzyme than NADPH does. This prediction is in agreement with the prosthetic nature of FAD.

Indeed, the crystal study of the FMO-FAD complex, from the bacterium *Schizosaccharomyces pombe*, revealed that the adenine portion of FAD anchors to the FAD-binding motif of the enzyme, forming strong hydrogen bonds. The riboflavin group of FAD was also incorporated in the pocket, forming further hydrogen bonds with nearby residues. Furthermore, a network of water molecules was demonstrated to facilitate the interaction and contact of FAD with the protein (Eswaramoorthy et al., 2006). In *Arabidopsis*, data from spectrophotometry of isolated and purified YUC6 proteins in bonded complex, eluded to this aspect of the FAD-AtYUC6 interaction (Dai et al., 2013). The fluorescence of the FAD-protein complex was substantially less than that of the FMN cofactor from lactase-2-monooxygenase. This result lead to the suggestion that the fluorescence is diminished because FAD buries deep in the pocket and is quenched by proximally located amino acids (Dai et al., 2013).

At the sequence level, the motif located downstream of FAD is the GG motif, which was proposed to stabilise FAD within the pocket (Hou et al., 2011). The *in silico* PsYUC1 3-D structure supports this proposition. Indeed, the GG motif, locating to Loop-4, was next to α-helix B, the 'floor' of the binding pocket, and was situated underneath where the riboflavin part of FAD positioned. Furthermore, several amino acids clustering to the GG motif were predicted to bind to FAD, suggesting that this motif may also assist in stabilising FAD in PsYUC1. Similarly, the two ATG motifs are present in the sequence and in the binding pocket of the 3-D structure. Amino acids clustering to the first ATG motif are predicted to bind to FAD while amino acids predicted to bind to both cofactors clustered to the second ATG motif. These motifs were proposed to stabilise the cofactors in the protein complex (Krueger and Williams, 2005).

Most monooxygenases, including plant FMOs, were shown to contain a highly conserved motif: the FMO-identifying motif (FXGXXXHXXXY) (Fraaije et al.,

2006; Schlaich et al., 2007). Numerous highly conserved residues clustering to the motif suggested that the FMO motif may be important for catalysis (Fraaije et al., 2006). Site-directed mutagenesis of amino acids contained in the FMO-identifying motif abolished the enzyme activity, indicating that the signature motif is essential for the protein function (Choi et al., 2003). In the crystal study of a cyclohexanone monooxygenase from a *Rhodococcus* strain, the signature motif did not appear to play a direct role in catalysis. However, several residues (H166 in particular) binding with NADPH, were proposed to have a structural role in modulating the conformation of the protein to accommodate NADPH (Mirza et al., 2009). The functional role of this motif was also unclear in crystal studies of *Schizosaccharomyces pombe* FMO and a role for 'substrate capture' was proposed (Eswaramoorthy et al., 2006).

In PsYUC1, the FMO-identifying motif is present at the sequence level and within the binding pocket proximal to where NADPH locates. However, no amino acids with binding properties were predicted to be contained in the motif or near it. In *Arabidopsis*, 29 genes code for FMO-like protein with roles as diverse as pathogen defence (Koch et al., 2006), glucosinolates metabolism (Hansen et al., 2007) and IAA biosynthesise (Zhao et al., 2002). This clearly indicates that the function of plant FMOs has diverged substantially from that of the other FMOs. This also opens the possibility that the FMO-identifying motif, despite being maintained at the sequence level, has lost its binding and/or putative conformational role. Divergence of roles has been previously demonstrated in yeast FMO. The only identified FMO in *Saccharomyces cerevisiae* does not contribute to xenobiotic excretion but participates in protein folding involved in maintaining the redox buffer ratio at the ER and cytoplasm interphase (Suh et al., 1999).

3.4.2. The *crd* mutations demonstrate the importance of several motifs

The two ADP-binding motifs are required for the catalytic function of FMOs. In plants, the majority of reported recessive mutants, shown to have morphological defects, have lesions in either of the two motifs or near them (Gallavotti et al.

2008). In pea, the first identified *crd-1* has a missense mutation that alters the first ATG motif, prior to the NADPH motif (Figure 3.1). The protein structure is modified at that site (G142D) suggesting that the first ATG motif is important for the pea protein catalytic function. In maize, a mutation in the FAD binding motif of *Sparce Inflorescence1* (*SPI1*), a YUC homologue, had strong developmental and reproductive phenotypes (Gallavotti et al. 2008). Furthermore, a screen for double yuc1 yuc4 mutant of *Arabidopsis,* with a focus on the effects of YUC1, identified five mutants (Hou et al., 2011). Three had point mutations in the ADP-binding motifs and the other two were located between the two binding motif sites, one of which coded for a stop codon. No mutant alleles locating downstream of the NADPH site were identified from the screen. Hou and colleagues (2011) suggested that alterations downstream of the catalytic sites may not completely disrupt the function of the protein, producing leaky mutants with weak phenotypes. This in turn would make the leaky mutants harder to identify.

However, in pea, mutations occurring downstream of the NADPH site suggest that other motifs are required. The *crd-2* mutation occurs after the NADPH binding site but before the second ATG motif thought to be essential to N-hydroxylating enzymes (Hou et al., 2011; McAdam et al., 2017b). The second ATG was proposed to interact with NADPH (Vallon, 20000). The strong phenotypes exhibited by *crd-2* indicates that the second ATG site is indeed required for the function of the protein. In the WT PsYUC1, amino acids locating at the second ATG motif were predicted to bind to both NADPH and FAD (Figure 3.10). Furthermore, when visualised in the 3-D protein, this motif was situated in the binding pocket where the two cofactors could make contact with the motif.

Furthermore, the frameshift caused by the *crd-4* mutation disrupts the PsYUC1 protein sequence downstream of the six consensus FMO domains and does not affect any of the characterised binding residues (Schlaich et al., 2007). If the FMO domains are exclusively required for the protein to function, then mutations that do not impact the core domains should have milder phenotypes (or none) when compared with mutations that alter the sequence upstream of the domains. However, *crd-4* has phenotypes that are as severe as those exhibited by the other *crispoid*

mutants (McAdam et al., 2017b). This indicates that motifs locating to the C-terminal region of the protein must be required for the normal functioning of PsYUC1.

Indeed, predictions of PsYUC1 in bonded formation with the FAD and NADPH cofactors indicated numerous amino acids as having binding roles, all of which were located within the substrate binding pocket. The majority grouped into distinct clusters associated with specific secondary structures. Five of the six consensus FMO domains were included in the predictions. However, unlike bacteria FMOs, the FMO/YUC-identifying domain of PsYUC1 was not predicted as containing any binding residues. Interestingly, five more regions were predicted to have amino acids binding with the FAD and NADPH cofactors. These regions have not been previously described in the literature, but phenotypic evidence from the *crispoid* mutants suggests that the predictions, or at least some of the predictions, may be accurate.

3.4.3. The *crd-4* mutant reveals a novel region required for PsYUC1 function

In silico data from this chapter predicted several regions, previously undescribed, to bind to the two cofactors (Table 3.4 and Figure 3. 10). Whether these regions are in effect participating in stabilising the protein in complex, contributing to the substrate specificity or are critical to the protein function is uncertain as no biochemical data are available. However, phenotypic, histochemical and hormone quantification evidence unequivocally demonstrate that the *crd-4* mutation adversely affects the physiology and morphology in mutant individuals (McAdam et al., 2017b). These results indicate that the C-terminal region is required for the functionality of the PsYUC1 enzyme.

Indeed, the frameshift caused by the *crd-4* mutation completely abolishes the fourth exon and disrupts the PsYUC1 protein sequence downstream of the six consensus FMO domains. None of the previously characterised binding residues are affected (Schlaich et al., 2007). If the FMO domains are exclusively required for the protein

to function, then mutations that do not impact the core domains should have milder phenotypes (or none) when compared with mutations that alter the sequence upstream of the domains. However, *crd-4* has a leaf venation phenotype that is as severe as that exhibited by the other *crispoid* mutants (McAdam et al., 2017b).

A combination of phenotypic and hormonal analyses with structural studies have defined novel binding regions of potential importance. These indicate that domains that have not been previously described may be required for the normal functioning of the PsYUC1 enzyme. Loop-30 is such a contender, with amino acids overarching over the binding site and forming a lid above the pocket opening. As discussed previously, the FAD and NAPHD binding sites are located inside the pocked and the prosthetic FAD, in particular, buries deeply, most likely being quenched by the surrounding residues (Dai et al., 2013). Loop-30 and principally the double arginine residues may assist in that quenching function. Alternatively, missing portions of the protein, as is the case in both *crd-2* and *crd-4*, could potentially destabilise the enzyme catalytic capacity. However, Loop-30 and the positioning of the 'lid' may be artefacts of modelling. To validate the structural model, enzymatic assays should be performed in vitro on recombinant proteins with substitution mutations in the critical regions of the structure.

3.4.4. Obtaining a novel *crd* allele

Four *crispoid* alleles, with alterations in *PsYUC1* and observable leaf and floral phenotypes are available in pea. All were obtained from mutagenesis programmes which are indiscriminate and can alter multiple genes in the genome (Dalmais et al., 2008; Domoney et al., 2013). This opens the possibility that phenotypic traits attributed to the gene of interest may in fact be caused by another unknown mutated gene. To minimise this possibility, back-crossing programmes are required to remove unwanted and unknown mutations from a line. However, genes that are linked to the gene of interest, are generally maintained as they are inherited through the generations. With the *crispoid* mutants, the four alleles are on different genetic backgrounds, rendering the likelihood of gene linkage, as an explanation for the association between the *YUC1* genotype and phenotype, highly improbable.

The *crd-4* mutation originated from an EMS mutagenesis programme targeting *PsTAR* genes on the Caméor background (Chapter 2). The *crd-4* mutation was one such 'unknown mutation' present alongside the *Pstar1-1* mutation in at least some of the seeds originally received. Through back-crossing the presence of *crd-4* was reduced to one 'sub-line' out of 10. One seed from this 'sub-line', when grown, had an observable leaf phenotype unlike all the other *Pstar1-1* individuals. The progeny from the abnormal '*Pstar1-1*' were found to carry a lesion in *PsYUC1*and in *PsTAR1*. Removing the *Pstar1-1* mutation from the background was critical as the two auxin-biosynthesis may have additive effects on the phenotypes, confounding results. Once *Pstar1-1* was removed from the background, the progeny from subsequent generations became the *crd-4* line utilised in all the following experiments. This episode highlights the importance of stringent plant selection and thorough genetic screening.

Chapter 4 - Characterisation of the *crd* mutant phenotypes

4.1. Introduction

As sessile organisms, plants have evolved the capacity to adapt to their ever-changing environment by modulating their growth accordingly. Depending on environmental cues, two plants, sharing the same genome, can produce different phenotypes if grown under different conditions. Developmental and phenotypic plasticity involves a range of molecular strategies in response to environmental pressures such as light, gravity, nutrient availability and pathogen or herbivore attack. A classic example, phototropism, elegantly demonstrated in stem curvature experiments by Darwin and Darwin (1880) is now known to involve asymmetric auxin distribution (Ding et al., 2011; Tanaka et al., 2006). Similarly, gravitropism requires differential auxin distribution to modify growth orientation (Friml et al., 2002; Wolbang et al., 2007). On the other hand, many processes, such as embryogenesis and phyllotaxy, are considered to be developmental programmes (Byrne et al., 2003). These autonomous pathways are genetically predetermined, regulated by endogenous signals, and are generally not responsive to external factors. The body plan of a simple leaf for instance, will not become compound to increase the light harvesting capacity of a plant.

Auxin modulates, directly or indirectly, many externally driven phenotypic responses and intrinsic developmental programmes, rendering it critical to plant life. Indeed, auxins are potent hormones with strong morphogenic and growth action throughout all life stages from germination, root and shoot formation to reproduction and senescence (reviewed in Davies, 2010). Auxin-related mutants, whether affecting biosynthesis, transport or perception, often exhibit similar phenotypes highlighting the developmental modules in which auxin action participates. Indeed, phenotypes are generally pleiotropic in nature, affecting a

range of developmental processes, such as root and shoot architecture (Gallavotti, 2013), vascularisation (McAdam et al., 2017b), branching (Ligerot et al., 2017), floral tissues, reproductive organs (Cheng et al., 2006) and seed formation (McAdam et al., 2017a). For example, the pea *rms2-1* mutant, disrupted in the auxin signalling AFB4/5 receptor (Ligerot et al., 2017) has increased branching (Arumingtyas et al., 1992), reduced internode length and root growth (Beveridge et al., 1994) and reduced seed size and yield (A. Gélinas-Marion, unpublished data)

The IPyA pathway is now considered to be the principal auxin biosynthetic pathway and its impact on plant growth and development has been experimentally demonstrated, especially with *Arabidopsis* as the model species (Won et al., 2011; Zhao, 2012). However, in other species, the contribution of IPyA-derived auxin to several aspects of plant growth and development remains to be demonstrated. For example, a link between the pea *TAR2* gene, starch accumulation and mature seed phenotype was made using a loss-of-function mutant (McAdam et al., 2017a). No other phenotypes were reported, suggesting that *PsTAR2* does not participate in the development of other tissue/organ-types. Furthermore, *Pstar1* mutants, described in Chapter 2, had no effect on pea development and growth. In this chapter, the role of *PsYUC1*, an auxin biosynthesis gene of the IPyA pathway, will be used to investigate auxin action on several aspects of growth and development that distinguish pea from *Arabidopsis*.

4.1.1. Auxin and root development

Roles for auxin in the determination of root architecture have been recognised since the 1930s (reviewed in Overvoorde et al., 2010). When a seed germinates, the primary root, comprising the root apical meristem, is the first organ to emerge and develop. Subsequently, secondary and higher-order lateral roots are produced in a regular pattern from the primary root to establish the root system architecture. The distal tip of the primary root and the tip from each new emerging lateral root contain high levels of auxin that is both actively transported from the shoot and locally produced in the apical meristematic tissue (Blilou et al., 2005; Liu et al., 2017; Ljung et al., 2005).

The specific contribution of the IPyA pathway to auxin in the root has been demonstrated in *Arabidopsis*, rice and maize, using knock-down/knock-out and overexpressing mutants (Bernardi et al., 2016; Chen et al., 2014; Stepanova et al., 2008; Stepanova et al., 2011; Woo et al., 2007; Yamamoto et al., 2007). For example, *Arabidopsis* mutants with disruptions in genes from the *TAR* family, responsible for converting L-Trp to IPyA, had a range of primary root defects. The primary root of the weak ethylene insensitive *taa1* and the double mutant *wei8 tar2* exhibited a decrease in gravity response while *taa1 tar1 tar2* triple mutants did not produce primary roots (Stepanova et al., 2008). The *taa1 tar2* primary root phenotypes were phenocopied in certain mutant combinations with disruptions in *YUC* genes, responsible for the conversion of IPyA to IAA (Won et al., 2011). The primary root of the *yucQ* mutant, disrupted in all five genes from the *YUC3*/*YUC5* clade, was shorter, agravitropic and resistant to ethylene (Chen et al., 2014). Indeed, in *Arabidopsis*, the expression of the *YUC*s appears to separate into two distinctive functional groups: the four genes from the *YUC1/YUC2* and *YUC10* clades act in the shoot and the five genes from the *YUC3/YUC5* clade, in the taproot (Cheng et al., 2006, 2007; Won et al., 2011). However, shoot to root ratio, a measure of general root growth, was affected in the loss-of-function *oscow1* mutant, a rice homologue of *AtYUC1* and *AtYUC4* (Woo et al., 2007) demonstrating that differences in YUC spatial functions exist between species.

In pea, auxin was reported to be active during root development. Indeed, a *DR5::GUS* auxin reporter demonstrated that auxin transcription, through GUS staining, was present in the main root tip and the lateral root prior to and after lateral tip emergence from the cortex (DeMason and Polowick, 2009). However, with GUS staining, auxin activity is detected but the biosynthetic 'provenance' of the auxin is not defined. In pea roots, metabolism experiments demonstrated that labelled tryptamine (a proposed auxin precursor) was converted to IAA, suggesting that, at least in part, the tryptamine pathway might contribute to the auxin pool in pea roots (Quittenden et al., 2009). Subsequently, a Trp aminotransferase mutant of pea (*tar2-1*) was reported to have seed phenotypes but did not have altered shoot growth, and root morphology was not described (McAdam et al., 2017a). No

evidence to date, and to our knowledge, has demonstrated that auxin produced from the IPyA pathway is present or active in the pea root system.

4.1.2. The compound leaf of pea

Auxin has important morphogenic properties pertaining to positional and initiation information in leaf development (reviewed in Conklin et al., 2018). Put simply, the down regulation of meristem maintenance transcription factors, such as *KNOX1* genes, by auxin maxima at the SAM periphery establishes the site of leaf initiation (Long et al., 1996; Reinhardt et al., 2003). Numerous plant species have leaves with various degrees of structural and developmental complexity. A reactivation of *KNOX1* genes, at the leaf primordia, was shown to participate in compound leaf development in several species by promoting indeterminacy at the leaf primordia (Kim et al., 2003). However, in the Fabaceae, this developmental module does not occur. In pea and *Medicago*, *KNOX1* genes are not reactivated at the leaf primordia (Di Giacomo et al., 2008; Hofer et al., 2001; Wang et al., 2008). Instead, orthologues of the *Arabidopsis LEAFY* (*LFY*), *UNIFOLIATA* (*UNI*) in pea and *SINGLE LEAFLET1* (*SGL1*) in *Medicago*, are expressed and proposed to be required for lateral leaflet initiation and formation (DeMason et al., 2013; DeMason and Schmidt, 2001; Hofer et al., 1997; Wang et al., 2008).

Analysis of auxin transport mutants and auxin application experiments have revealed pivotal roles of auxin gradients in leaf formation (Benkova et al., 2003; Reinhardt et al., 2003). The sources of auxin production were however not defined. Evidence that auxin produced by the YUCs participates in simple leaf formation was obtained from *yuc* mutants of several species. Principally, a quadruple mutant of *Arabidopsis* and *floozy* of petunia had aberrant venation patterns (Cheng et al., 2007; Tobeña-Santamaria et al., 2002) while the maize *spi1* produced fewer leaves compared with WT (Gallavotti et al., 2008) and *yuc1* rice alleles (*cow1* and *nal7*) produced narrow leaf blades (Woo et al., 2007; Fujino et al., 2008). However, unlike simple leaves, compound leaves maintain organogenic activity, producing novel and distinct organs (leaflets and tendrils in the case of pea), after their initial emergence from the stem (Barkoulas et al., 2007; Blein et al., 2008). This

distinction between the two developmental strategies renders compound leaves species of particular value when studying developmental diversification and gene function.

A role for auxin in the development of compound leaf of pea was first alluded to by the phenotypic characterisation of several leaf mutants under a range of TIBA concentrations (2,3,5-triiodobenzoic acid, an auxin transport inhibitor) (Gould et al., 1991). A follow-up paper using a similar approach but including additional auxin transport inhibitors, electron scan microscopy, gene expression and radiolabelled auxin transport assays suggested that auxin is 'the driving force' for compound pea leaf development and leaflet determination and initiation (DeMason and Chawla, 2004). These findings demonstrated the involvement of auxin in compound leaf development but again, the biosynthetic 'provenance' of the auxin was unknown and direct evidence from characterised auxin-related loss-of-function mutants was not available.

As mentioned above and in chapter 2, loss-of-function mutant alleles of *PsTAR1* and *PsTAR2* (McAdam et al., 2017a) genes did not exhibit shoot or leaf phenotypes. The *crd* mutant alleles however, with disruptions in *PsYUC1*, had vasculature defects. Vein density was reduced, and the secondary veins and free-ending veinlets were abnormally placed (McAdam et al., 2017b). Interestingly, primary and secondary veins are formed early in leaf development 'spreading-out' as the leaf expands while minor veins are initiated subsequently during leaf expansion (Aloni et al., 2003) suggesting that *PsYUC1*-derived auxin participates in several stages of leaf development.

4.1.3. Pea shoot ontogeny

Pea is described as heteroblastic due to sudden and significant changes in leaf form, size and arrangement depending on developmental stages (Hofer and Ellis, 1998). Throughout its life history, a pea plant will produce different leaves depending on ontogenetic stages regardless of environmental factors (Bäurle and Dean, 2006). As a seedling emerges, leaf formation is initiated at regular intervals from the shoot

apical meristem (SAM). As node development progresses, leaves of increasing complexity are produced. The first two nodes have reduced leaves (described as scale leaves). At the third node, the first true leaf emerges, consisting of a pair of stipules, a rachis and a pair of leaflets. During the next several nodes, a plant is in a juvenile vegetative growth phase, and continues to produce similar leaves with a pair of proximal leaflets, one pair of distal tendrils and a single terminal tendril. As growth progresses, a transition from one pair to two pairs of leaflets and tendrils occurs.

These changes are genetically controlled and denote the transition from the juvenile to the adult vegetative growth phase at which point the shoot response to the flowering signals may become competent (reviewed in Poethig, 2013; Weller et al., 2009). Certain microRNAs, proposed to interact with the auxin signalling pathway, are thought to modulate the juvenile to adult vegetative transition switch (Wang et al., 2009). However, our understanding of the molecular machinery regulating the vegetative phase change is still incomplete.

The next ontogenetic phase in pea shoot development pertains to reproduction. That is, when the SAM of a plant switches identity and becomes an inflorescence meristem (IM) (Bernier et al., 1993). Pea plants, as do most legumes, have compound inflorescences, that is, lateral secondary inflorescence branches (I_2) that bear flowers, are produced on the primary inflorescence (I_1) (Berbel et al., 2012). The link between the adult vegetative phase and the induction to flowering phase is also unclear (Poethig, 2013). Genetic studies of developmental mutants of pea suggest that the pathways regulating the two programmes may be uncoupled (Wiltshire et al., 1994). However, many genes and modules regulating the transition to flowering in plants have been described in detail (reviewed in Jung et al., 2017). In pea, the autonomous *LateFlowering* (*LF*) determines the node of flowering by modulating the responsiveness of the apical portion to the flowering signal (Foucher et al., 2003; Weller et al., 2009). The *LF* gene is one of three orthologues of the *Arabidopsis TERMINAL FLOWER1*, *TFL1*, and is proposed to inhibit the transition to flowering. Indeed, low transcript levels of *LF* correlated

with early flowering while high transcript levels correlated with late flowering (Foucher et al., 2003).

4.1.4. The flowering programme of pea

The ABCDE or ABCE model of floral organ identity, based on *Arabidopsis* and *Antirrhinum*, specifies that the primordia of each flower organ-type, or the four whorls, are initiated in sequential steps and in a centripetal fashion, or from the outer to the inner whorl (Coen and Meyerowitz, 1991; Irish, 2017). Each primordium, spatially located in a specific area (field/domain) of the developing flower, is formed prior to the initiation of the next (Bowman et al., 1991). Homeotic genes that primarily encode for MADS-box transcription factors, described as having A, B, C, D or E functions, confer organ identity by working in their specific domains, with a level of overlap between certain genes (Ditta et al., 2004; Pelaz et al., 2000).

An important aspect to this model, is that the A and C genes are mutually antagonistic, preventing them from being active in the same domains (Bowman et al., 1991; Coen and Meyerowitz, 1991; Wollmann et al., 2010). In *Arabidopsis,* the *APATELA1* and *APATELA2* genes carry the A function, *APETALA3* and *PISTILLATA* the B function, *AGAMOUS* the C function, *AGAMOUS-LIKE11* the D function and the *SEPALLATA* gene family, the E function (Becker and Theißen, 2003; Colombo et al., 1995; Theißen et al., 1996). First the sepal primordia are formed (A), then the petals (A+B+E), followed by the stamens (B+C+E), the carpel (C+E) and lastly, the ovules (C+D+E) (reviewed in Bowman et al., 2012). This classical model has been tested and demonstrated to occur in several gymnosperm and angiosperm species (Kater et al., 2006; Kramer et al., 2004; Litt and Kramer, 2010).

However, in pea and in *Medicago*, the initiation of primordia overlaps, with common primordia containing different identity information, resulting in the differentiation of organs belonging to different whorls (for reviews, see Benlloch et al., 2003; Tucker, 2003). In other words, multiple organ-types are initiated

simultaneously. Furthermore, the order of initiation of the different types of organs starts at the abaxial side of the flower and progresses in a unidirectional fashion in all the whorls through to the adaxial side. This overlapping and unidirectional initiation of primordia results in the development of common primordia from which different types of organs will subsequently differentiate. How the various classes of floral identity genes are regulated in these legumes remains uncertain.

Auxin has been demonstrated to participate in the regulation of the flowering programme. In *Arabidopsis*, maize and petunia, disruption in IPyA pathway genes had detrimental effects on flower development (Cheng et al., 2006; Gallavotti et al., 2008; Tobeña-Santamaria et al., 2002). How and if these genes participate in the pea flowering programme is uncertain.

4.1.5. Reproductive output

The development of seed and fruit is pivotal to the reproductive success of flowering plants. When the female gametophyte is fertilised, the early stages of seed development begin. Two fertilisation events take place. The fusion of the egg cell and the central cell with the sperm cells result in two zygotic products: the embryo, and the endosperm, which serves as a source of nutrient to the growing embryo (Sun et al., 2010). The zygote undergoes a series of asymmetrical cell divisions leading to the globular stage when the positioning and specification of the shoot and the root stem cell niche is clearly defined. Lastly, at the heart stage, all the organs and meristematic tissues necessary for embryo growth and maturation are present (for reviews, see Heidstra and Sabatini, 2014; Robert et al., 2013).

Dynamic patterns of auxin biosynthesis, transport and signalling are observed during early seed development (for reviews, see Lau et al., 2012; Robert et al., 2015). Indeed, auxin biosynthesis enzymes, efflux carriers and transcription activators are all highly transcribed in young embryos (Belmonte et al., 2013). In the early stages, the biosynthesis *YUC* genes are expressed in the suspensor and are thought to produce auxin *de novo*, which is then transported by *PIN* efflux carriers towards the embryo (Robert et al., 2013). The accumulation of auxin is likely to

trigger gene transcription and activate auxin responses in the embryo. Loss-of-function *Arabidopsis* mutants with disruptions in the biosynthetic *TAR* and *YUC* gene families have altered embryo morphology and cell specification (Cheng et al., 2007; Stepanova et al., 2008). Early in pea embryo development, *DR5::GUS* staining was located in the procambial strands in the cotyledons and epicotyl, and in the root tip, demonstrating the importance of auxin in the early stages of pea seed development (DeMason and Polowick, 2009).

Auxin is thought to participate in cell differentiation events during late seed development. In most eudicots, cotyledon cell number and size are responsible for final seed size since the embryo replaces most of the endosperm as the embryo grows to full size and matures (Sun et al., 2010). The switch from the mitotic cycle to the endocycle (genomic replication without division, i.e. ploidy) in the developing embryo is considered to be essential for normal seed development (Atif et al., 2013). The transition coincides with a shift from cell division to cell differentiation (Ishida et al., 2010). The process of endoreduplication is therefore proposed to be an integral part of seed filling and maturation. The mechanism results in cell size increase (Inzé and De Veylder, 2006). In *Medicago*, seeds had prolonged cell division when grown with the exogenous auxin NAA. The seeds also had sustained endoreduplication. As a result, Medicago seeds grown on the auxin medium were bigger and heavier when compared with controls (Atif et al., 2013). In pea, a *tar2* loss-of-function mutant had reduced auxin content in the seed (up to 10-fold less 4-Cl-IAA). Cell size was smaller in the seed and starch granule formation and accumulation were compromised (McAdam et al., 2017a). As a result, the seeds produced were smaller, heavily dimpled and had reduced starch content when compared with WT.

There are clear links between seed and fruit developmental programmes. Once fertilised, the quiescent ovary rapidly grows into a young fruit. Growth occurs first through cell division and then through cell expansion (De Jong et al., 2009). Auxin, transported from the seeds to the ovary, is proposed to promote cell division and expansion of the fruit tissues (Ozga et al., 2002; Sundberg and Ostergaard, 2009). Indeed, in a diverse range of species, auxin concentrations were shown to be higher

in seeds compared to other fruit tissues (Devoghalaere et al., 2012; Tiwari et al., 2013). For example, in capsicum, an increase in carpel cell diameter correlated with a peak in IAA levels. In seedless capsicum however, carpel cell size was significantly reduced, and the expected auxin peak was not reported (Tiwari et al., 2013). Furthermore, in pea, a positive correlation between the number of seeds and the ability of a plant to maintain fruit growth has been demonstrated (Ozga et al., 1992), highlighting the vital influence of seeds on fruit development. In young pea pods, cell division and expansion were regulated and maintained by auxin originating from the seeds. Pea pods could not grow in the absence of seeds and the application of the halogenated auxin 4-Cl-IAA restored growth in the deseeded pods (Ozga et al., 2002).

4.1.6. Aims

Pea lends itself favourably to physicochemical studies rendering the species as an invaluable model to the investigation of growth-promoting and developmental responses of plants to hormones (Cannon, 2013; Ozga et al., 2003). Pea also serves as an alternative to *Arabidopsis*, with several aspects relating to growth and development (mentioned in the present introduction), differing in both species.

The use of loss-of-function mutants is a reliable way of linking a gene to a specific function. However, until recently, no mutants were available to investigate the contribution of the IPyA pathway to pea development. The *crispoid* mutants used in the present study are only the second known IPyA-related knock-down and knock-out mutants in pea; the first being *tar2-1* (McAdam et al., 2017a). Indeed, the *crd* mutants, and *tar2-1*, are the only auxin biosynthesis mutants in pea with reported phenotypes. Seed and some shoot phenotypes were described for the *tar2-1* mutant and in-depth leaf phenotypes for the *crd* alleles (McAdam et al., 2017a and b). However, a detailed survey of the *crd* phenotypes remains to be performed.

As auxin action pertains to most plant growth and developmental processes, the principal focus of this chapter is to describe the effects of *PsYUC1* disruption on pea development in general. By extension, the contribution of a genetically

characterised IPyA-pathway gene to several growth processes and its interaction with other genes known to affect well-defined developmental modules will be investigated. A multidisciplinary approach comprising genetic and molecular techniques, auxin quantification and morphological characterisations will be used.

Firstly, morphological characterisation of any observable phenotypes will be described. Several aspects relating to plant development in general and others that are more specific to pea in particular will be monitored, including root architecture, compound leaf development, shoot ontogeny, and reproductive traits. To do so, the *crd-1* mutant on an extreme dwarf background will be crossed onto a background shared with other *crd* mutants to allow for comparison amongst the different alleles.

Secondly, the *crd-4* allele will be crossed to a tall (*LE*) background. Indeed, auxin is not the only growth promoting hormone in plants. Gibberellins (GAs) promote cell elongation and cell division during vegetative growth (Claeys et al., 2014). Dwarfism, for example, is a classical phenotype of GA-deficient mutants (Lester et al., 1997). However, auxin is thought to induce GA biosynthesis. Indeed, pea and tobacco plants that have lost their source of apical auxin through decapitation had decreased contents of bioactive GA in the stem when compared with intact plants, while the application of auxin to the apex restored wild-type levels of GAs (Ross et al., 2000; Wolbang and Ross, 2001). As the *crd-4* mutant is on a dwarf (*le-1*) background with disruptions to GA biosynthesis, it was important to rectify that situation by crossing onto the *LE* background. In the process, the recessive *lf* allele, a key determinant in the timing of the transition to flowering (Foucher et al., 2003) was crossed out of the *crd-4* mutant background.

Thirdly, a comparison of the flower phenotypes in *crd* alleles is made. Indeed, the three alleles are located in different regions of the *PsYUC1* gene (McAdam et al., 2017b). The *crd-4* mutation, occurring late in the sequence, affects a region of the YUC protein that has not been previously reported as critical to the function of the enzyme. In Chapter 3, the C-terminal region affected in the *crd-4* structure was proposed to (1) form a lid above the binding pocket, (2) potentially stabilise the ligand-protein interaction and (3) be required for the proper functioning of PsYUC1. If phenotypes present in the *crd-4* mutant are similar and as severe as

those exhibited in the loss-of-function *crd-3*, the allelic comparison will support, at least in part, the propositions described in Chapter 3.

Lastly, auxin activity and auxin content will be monitored from several tissues to test whether these correlate with morphological defects. A *DR5::GUS* construct will be used to visualise the potential differences in auxin activity between the mutant alleles and the WTs. Furthermore, auxin will be monitored in several of the organs and tissues exhibiting phenotypes. IAA, the main product of the IPyA pathway, and IAAsp, an important conjugate of IAA in pea will be quantified from *crd* mutants and WT plants.

4.2. Materials and Methods

4.2.1. Plant material

Two *crispoid* mutant alleles were used to characterise the effects of disrupting *PsYUC1* on pea vegetative development: the *crd-3* mutant (line FN 1522-1) on the JI 2822 background and the *crd-4* mutant, on the *cv*. Caméor background (McAdam et al., 2017b). Further lines used were the tall (*LE, LH*) *cv*. Torsdag (line 107) and the gibberellin-biosynthesis mutant *lh-2* (line NGB 5843; Reid and Potts, 1986; Yaxley et al., 2001). The *crd-1*, on the Paloma background, and *crd-3* lines were provided by Julie Hofer (Aberystwyth University, United Kingdom). The WT JI 2822, Caméor and Paloma are dwarf (*le-1*). The other lines were obtained from the Hobart seed collection. Furthermore, the RTP9 transgenic *DR5::GUS* line (WT W6 22593) was generously provided by Patricia Polowick (National Research Council of Canada). All plants were grown as described in Chapter 2.

4.2.2. Controlled crosses

The *crispoid* mutants were crossed, as described in Chapter 2, to other lines to obtain the mutations on genetic backgrounds of interest. First, the *crd-3* mutant (line FN 1522-1), originally on the JI 2822 background, was backcrossed three times to the *cv*. Caméor to allow for comparison between *crd-4* and *crd-3* individuals. Plants were phenotyped based on leaf and flower morphology at each generation. The *crd-4* mutant was also backcrossed four times to *cv*. Torsdag (line 107) to remove the potentially confounding influence of the gibberellin-biosynthesis disruption present on the dwarf background. In this instance, the RFLP protocol described in Chapter 3 was used to identify heterozygotes from the F1 generations (Table 3.2). Results originating from those new lines are based on plant material derived from *crd-3*(CAM) 3rd backcross and *crd-4*(TOR) 4th backcross segregants, unless specified otherwise.

4.2.3. Phenotypic characterisation

To investigate the effects of the *crd* mutation on pea development, vegetative and reproductive phenotypes were monitored and characterised, grown as described above. First, root development phenotypes, including tap root length, secondary and tertiary root number and length of the *crd-3*(CAM) and the WT *CRD-3*(CAM) were quantified. Secondly, *crd-4*(TOR) and the WT *CRD-4*(TOR) were used to characterise several aspects pertaining to the compound pea leaf morphology, including leaflet vasculature, stipules, leaflet placement and number and turgor. Furthermore, *crd-4*(TOR) growth and shoot ontogeny were investigated, including the juvenile to adult vegetative transition timing, the rate of leaf expansion, stem and internode length. The *lh-2* mutant was included in several of the quantified phenotypes to test the potential influence of GA. Thirdly, flower phenotypes are described in *crd-1*, *crd-3*(CAM) and *crd-4* as is the reproductive output of *crd-4*(TOR), *lh-2* and the tall WT. All data were statistically analysed with unpaired T-tests.

4.2.4. Shoot dry weights

To test the effects of the *crd-4* mutation on plant biomass, shoot dry weight and stem weight to length ratio (representing stem thickness) were recorded. Whole shoots from mature *CRD-4* and *crd-4* plants (n=3) on the Caméor background, were harvested 28 d after sowing and dried at 70°C for 62 h before being weighed (± 0.0001 g). For the stem weight to length ratio, seven randomly selected portions of stem from *crd-4* and *CRD-4* (n=3) were weighed and measured. The same procedures were repeated with plants on the *LE* background, or *crd-4*(TOR) and co-segregating WT *CRD-4*(TOR) (n=12 in both experiments). Unpaired T-test were used to analyse the data.

4.2.5. DR5 construct

The transgenic *DR5::GUS* lines carrying the *CRD-4* and *crd-4* alleles were obtained by crossing the RTP9 line (DeMason and Polowick, 2009) with pollen from

heterozygous plants (*CRD-4 crd-4*). The segregating F1 generation was phenotyped for the RTP9 insert by examining GUS activity in developing leaves. The RTP9 insert was also monitored by PCR to ascertain that the two protocols were equally reliable at detecting all individuals that contained the insert. In this instance, primers and cycling protocols previously described in DeMason and Polowick (2009) were utilised (Table 4.1). In subsequent generations, both methods were used interchangeably. Only lines that did not segregate for the insert were grown through to the next generations. In other words, progeny that were homozygous for the *DR5::GUS* construct (carried two copies of the insert) were grown and used in experiments.

Table 4.1. Primers used to amplify the *DR5::GUS* construct and ascertain its presence in the genome of an individual.

Construct	Primer name	Sequence (5' to 3')	Amplicon size
DR5::GUS	DR5_Fw	GGTGTTCGGCGTGGTGTAGAGCAT	549 bp
	DR5_rev	GGGCCCCGTCCGTCCTGTAGA	

To classify *CRD-4* and *crd-4* individuals, two methods were used. First, leaf morphology of segregating individuals discriminated *crd-4* plants from those with a WT phenotype (WT and heterozygous genotype). To identify heterozygotes, the RFLP protocol described in Chapter 3 was used. A single plant selection approach was used to progress the *DR5:CRD-4* and the *DR5:crd-4* lines for five generations. Experiments were conducted with tissue from several of those five generations and the generation used is specified when required.

4.2.6. Histological analysis of GUS activity

Leaflets and flower clusters were used to observe GUS activity in the *crd-4* mutant and the WT (homozygous for the DR5 transgene). For the leaflets, the segregating F2 generation consisting of 42 *Crd GUS*+: 15 *crd GUS*+: 14 *Crd GUS*-: 7 *crd GUS*- (9:3:3:1, $x^2 = 1.0$, $P = 0.8$, n.s.) was genotyped as described above. Young developing leaflets <8 mm in length were removed from within stipules enclosing

the apical meristem and immediately immersed in GUS staining buffer containing 2 mM 5-bromo- 4-chloro-3-indolyl b-D-glucuronidase (Gold BioTechnology), 100 mM sodium phosphate (pH 7.5), 0.5 mM potassium ferricyanide, 0.5 mM potassium ferrocyanide, 10 mM EDTA, and 0.1% (v/v) Triton X-100 (Jefferson et al., 1987). For the flower clusters, mutant and WT individuals from the segregating F5 generation were genotyped (as above) and clusters containing young unopened flowers were harvested and treated identically to the leaflets.

Samples were vacuum infiltrated on ice at 200mbar for 45 minutes then incubated for 24 to 48 hours at 37°C. The staining buffer was replaced with fresh solution after 24 hours when incubated for 48 hours. The samples were then cleared in 70% ethanol and dissected. Leaflets were photographed with a compound microscope (Zeiss Axioskop 2 plus). Mutant and WT samples (n=8) were histologically determined in a double-blind experiment to ensure that morphological analysis and interpretation were unbiased. Developing flowers from mutant and WT plants (n=4) were photographed using a compound microscope.

4.2.7. Analyte extraction

IAA and IAAsp were extracted and quantified from mutant and WT root tissues, apical shoot portion and developing flowers. For the roots, the first two millimetres of the apical portion (tip) of lateral roots from *crd-3* and co-segregating *CRD-3* WT were excised. A biological replicate (n=5) contained 10 tips pooled (averaging 15 mg ±0.001 g) from a single plant. Similarly, 10 two mm portions of fully differentiated (mature) root tissue proximally located to the tap root were pooled for each biological replicate (n=5) weighing approximately 120 mg ±0.01g. For the apical shoot tissue, the growing apical portion and all tissue immediately above to the uppermost fully expanded leaf of *CRD-4* and *crd-4* individuals (n=4), were harvested. A single apical portion was included per biological sample with approximately 25 mg (±0.001 g) harvested per replicate for both genotypes.

All tissues were treated in the same manner and compounds were derivatised and extracted according to Novák and colleagues (2012) with minor adjustments

(Novák et al., 2012). Tissue was weighed and placed intact in 1 mL of sodium phosphate buffer (50 mM, pH7). To quantify the endogenous compounds, stable isotope-labelled internal standards were added; these were [$^{13}C_6$]-IAA (Cambridge Isotope Laboratories) and [^{15}N, $^{2}H_5$]-IAAsp (OlChemim). Samples were pulverised with a physcotron homogeniser (Microtech). Aliquots (500 µl) were added to 3 mL of cysteamine solution (0.25M) and incubated at room temperature for one hour with agitation. The pH of the samples was reduced to ~2.7 with 10 N HCl before being loaded onto preconditioned SepPak for solid phase extraction under vacuum (with 3 ml methanol, 3 ml purified water and 500 µl sodium phosphate buffer at pH 2.7). Samples were then washed with 2 ml of 1% acetic acid and eluted into round-bottomed flasks with 2ml of 80% MeOH. Eluates were taken to dryness by rotary evaporation, re-suspended in 1% acetic acid (100 µl), transferred to a new Eppendorf tube and spun at 13000rpm for five minutes to remove any remaining debris. Supernatants (75 µl) were transferred to auto-sampling vials and analysed promptly.

4.2.8. UPLC-MS

All samples were analysed by ultra-performance liquid chromatography tandem mass spectrometry as described before (Cook et al., 2016) using a Waters Acquity H-Class UPLC instrument coupled to a Waters Xevo triple quadrupole mass spectrometer.

The UPLC programme used to separate the metabolites of interest, was the 'IAAsp-slow method'. The programme consisted of 95% A:5% B to 50% A:50% B at 4.5 min, followed by immediate re-equilibration to starting conditions for 9 min. The flow rate was 0.35 mL min−1, the column was held at 35°C, and the sample compartment was at 6°C. The mass spectrometer was operated in positive and negative ion electrospray mode (Table 4.2) with a needle voltage of 2.8 kV, and multiple reaction monitoring (MRM) was used to detect all analytes. The ion source temperature was 130°C, the desolvation gas was N2 at 950 L h−1, the cone gas flow was 100 L h−1, and the desolvation temperature was 450°C. Data were processed using MassLynx software.

Table 4.2. MRM transitions monitored to identify and quantify endogenous auxins and labelled standards.

Mode	Analyte	Primary transition	Approximate RT (min)
+	Indole-3-acetic acid	176 to 130	5.1
+	[$^{13}C_6$] Indole-3-acetic acid	182 to 130	5.1
+	Indole-3-acetyl-L-aspartic acid	289 to 132/174	3.7
+	[^{15}N, $^{2}H_5$] Indole-3-acetyl-L-aspartic acid	295 to 133/134	3.7

4.3. Results

4.3.1. Disruption in *PsYUC1* affects root development

To observe the effects of disrupting the IPyA pathway on the root system of pea, firstly the *crd-3* mutant (on the Caméor background) was used. Using this mutant permitted observing the potential effects of completely knocking out *PsYUC1* (Figure 4.1). Taproot lengths did not differ between the WT and the mutant, but secondary roots were shorter and less numerous in the *crd-3*(CAM) mutant when compared with the co-segregating *CRD-3*(CAM) WT (Figure 4.2).

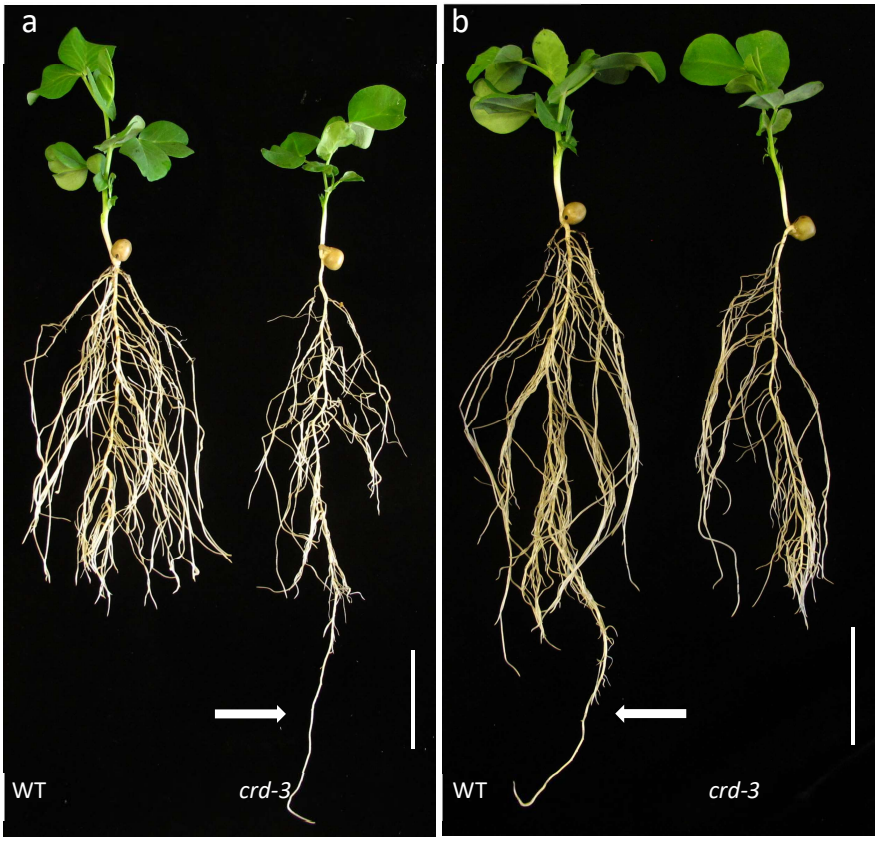

Figure 4.1. Root system of WT and *crd-3* on Caméor background. a and b) Both genotypes have five expanded leaves. Note the reduced number of secondary roots in the mutant. However, taproot length (white arrows) is not affected. Scale bars represent 5 cm.

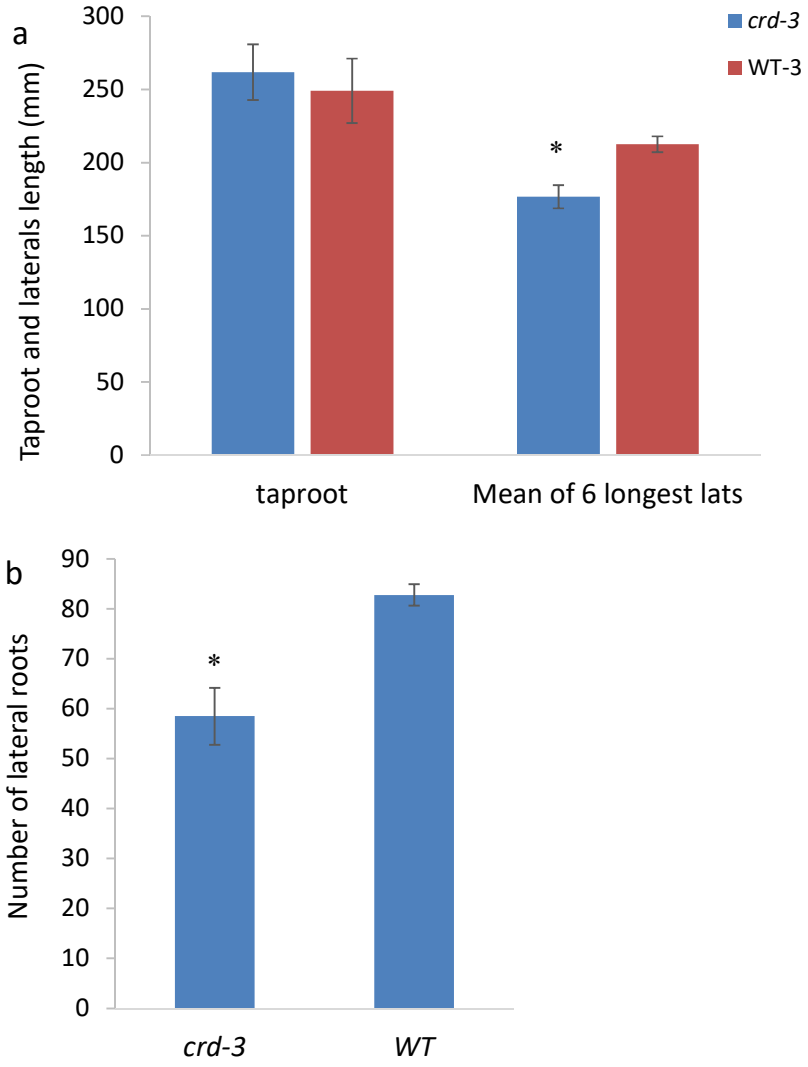

Figure 4.2. Tap root and secondary laterals of WT and *crd-3* on the Caméor background. a) Taproot length did not differ between genotypes, but length of secondary laterals did (n=10, secondary laterals length: p=0.002) and b) laterals number were reduced in the mutant (n=10, secondary laterals number: p=0.0009). Results are means ± S.E. and asterisks denote significant differences.

Next, tertiary roots were counted and measured. However, no differences in tertiary root length or tertiary root number were observed between the two genotypes (Figure 4.3).

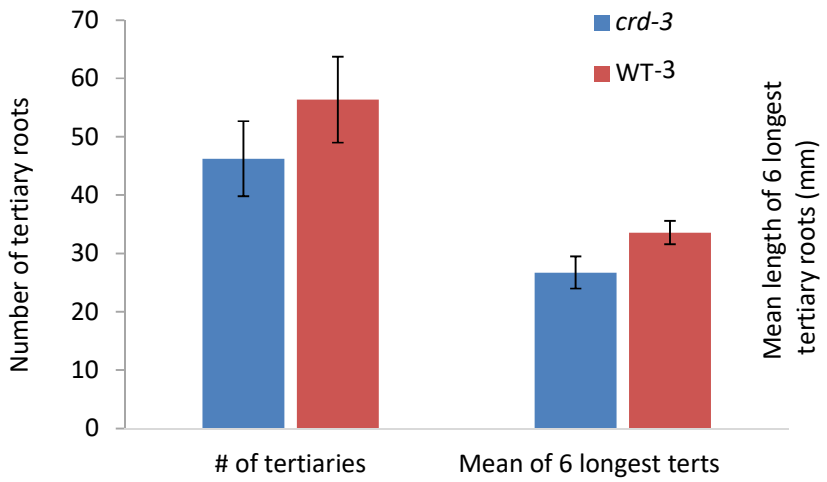

Figure 4.3. Tertiary root number and length of WT and *crd-3* on Caméor background. There were no differences in tertiary root phenotypes between genotypes (n=10). Results are means ± S.E.

Unexpectedly, an observable difference in secondary root initiation at the top-most portion of the taproot was noticed (Figure 4.4). Anatomically, there is no hypocotyl in *Pisum sativum*, as this region is defined as being the portion of stem below the cotyledon and above the root system. The term is nonetheless used in this chapter to describe the area situated below the cotyledons, but above the emergence of the first secondary lateral root. In the mutant, the top portion of the principal root proximal to the cotyledons was devoid of secondary roots, suggesting that root initiation in that region is impaired.

Figure 4.4. The region defined as the 'hypocotyl' had a decreased number of secondary lateral roots in the *crd-3* mutant when compared with the WT.

Several shoot growth traits were quantified from the *crd-3* mutants, at the same developmental stage. The number of expanded leaves was significantly reduced in the mutant when compared with the co-segregating WT while the "hypocotyl" length, or that of the proximal segment of the tap root without lateral roots, was increased (Figure 4.5a). However, internode and epicotyl length were not adversely affected in the mutant (Figure 4.5b).

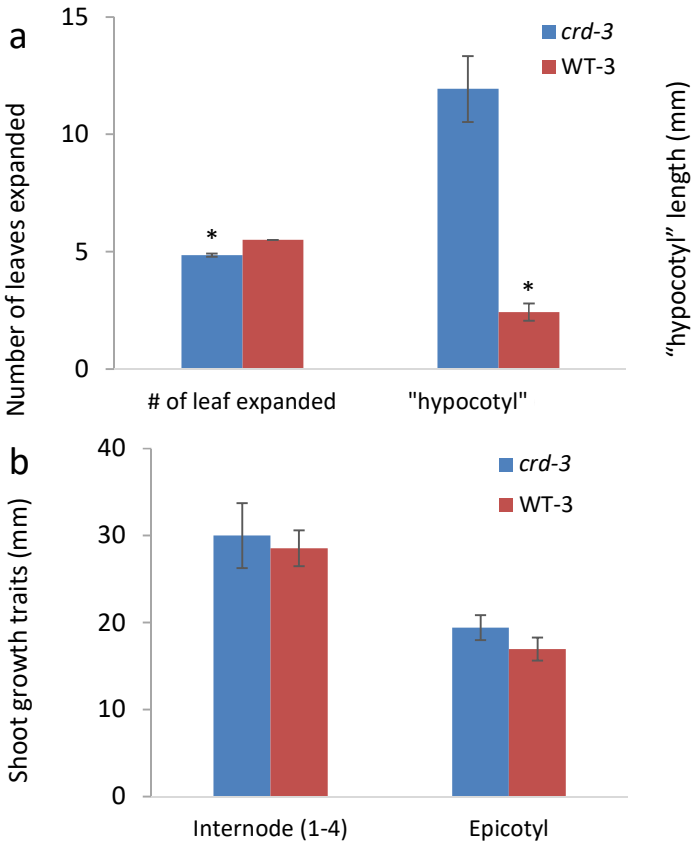

Figure 4.5. Shoot growth and developmental traits of *crd-3* plants on the Caméor background and co-segregating WT. a) In the mutant, the "hypocotyl" length was increased (n=10, p=3.7E-06) and number of expanded leaves was decreased (n=10, p=2.3E-06). b) Internode and epicotyl length did not differ between the two genotypes. Results are means ± S.E. and asterisks denote significant differences.

The same observations and quantifications were made using the *crd-4* mutant on the Caméor background. This time, data were collected from young seedlings (11 DAS, n=10) to observe whether the phenotypes present at the five nodes stage were also present at a less advanced developmental stage. The growth of the first true leaves (node 3) had been initiated but leaves were not yet fully formed and expanded (Figure 4.6a). Results from the young *crd-4* seedlings mirrored those obtained from the *crd-3* mutant. Taproot length (data not shown), epicotyl and internode lengths did not differ between the genotypes while shoot and "hypocotyl" lengths, the number of lateral roots and the mean length of the six longest laterals were significantly different (Figure 4.6b).

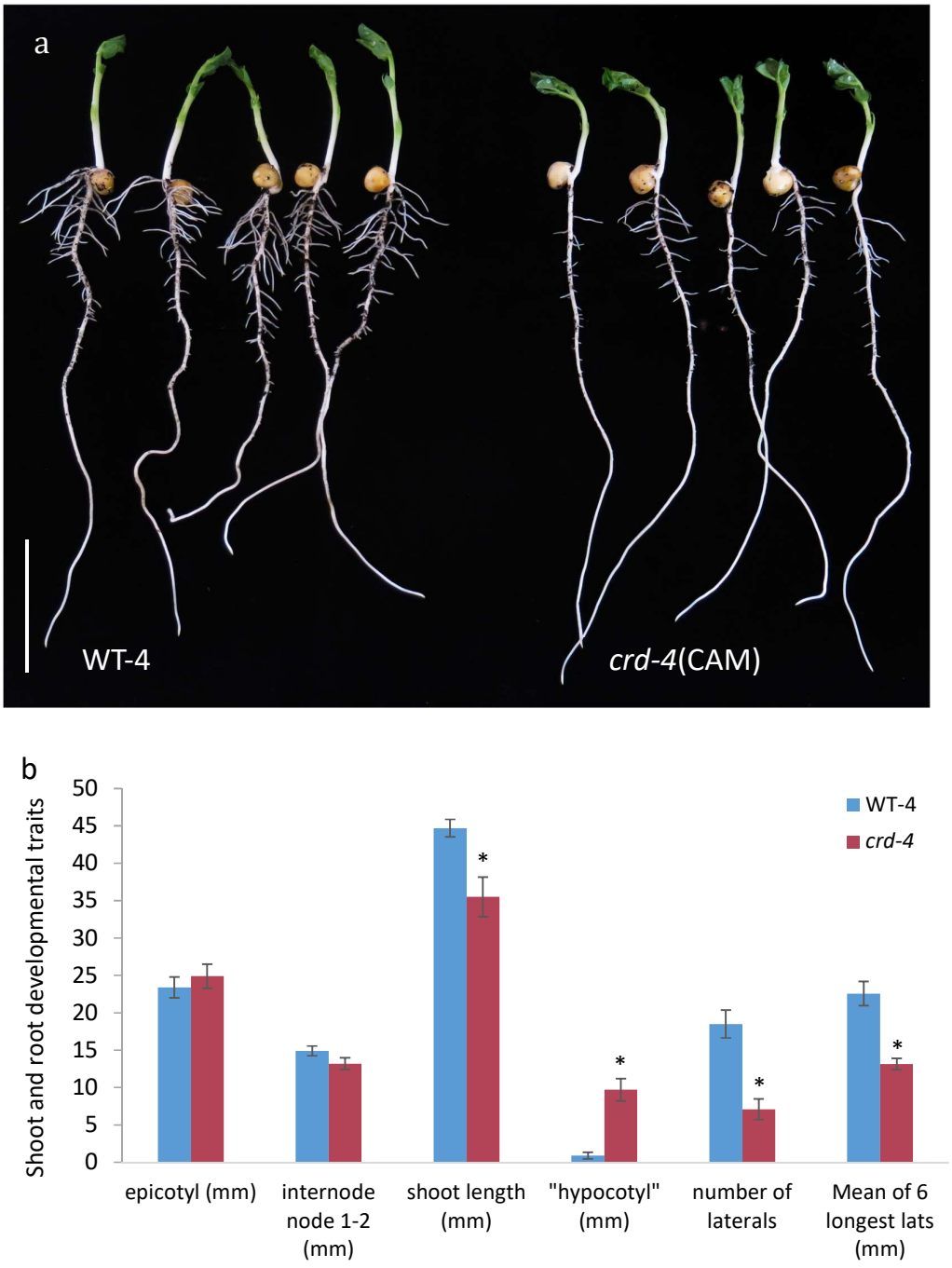

Figure 4.6. Root and shoot growth traits of *crd-4* plants on the Caméor background and co-segregating WT. a) 11 days old *crd-4* and WT-4 seedlings. Note the number of lateral roots in the WT on the left. Scale bar = 5cm. b) Epicotyl and internode lengths were not affected in the mutant but "hypocotyl" length was increased (n=10, p=2.5E-05) while shoot length, the number of laterals and length of the six longest laterals were decreased in the mutant when compared with the WT (n=10, p=0.006, p=0.0001 and p=5.1E-05 respectively). Results are means ± S.E. and asterisks denote significant differences.

4.3.2. The shoot vegetative development of *crd-4* is altered

Several aspects of shoot growth were affected in the *crd* mutants, including leaf vasculature, leaf morphology, stature and shoot ontogenetic transitions. However, a branching phenotype, previously observed in the *rms2* mutant, was not exhibited in the *crd* mutants.

Four alleles with mutations on the *Crd* locus are available in pea (McAdam et al., 2017b) all of which are on dwarf (*le-1*) backgrounds that have alterations to the biosynthesis pathway of gibberellin (GA). GA is known to participate in pea shoot growth (Ross et al., 1997). Therefore, to observe the effects of a *crd* mutation in plants with normal GA content, the *crd-4* mutation was crossed to the tall (*LE*, *LH*) Torsdag background. The *LE* gene is responsible for the conversion of GA_{20} to GA_1, a bioactive GA in pea shoots. The *lh-2* mutant is isogenic to Torsdag, has an "early" GA biosynthesis blockage (Davidson et al., 2004; Swain et al., 1997), has GA-deficient phenotypes and has reduced GA_1 levels (MacKenzie-Hose et al., 1998). For these reasons, the *lh-2* mutant was compared with *crd-4* on the Torsdag background in relation to several aspects of the pea vegetative development.

The crd *venation phenotypes are not attributable to the GA deficient background*

As previously demonstrated, the *crd* mutants have a reduction in vein density with abnormal secondary vein and free-ending veinlet formation and placement (McAdam et al., 2017b). Indeed, in the *crd-4* leaflets, leaf gas exchange is reduced and vein morphology and topology are negatively affected when compared with WT (McAdam et al., 2017b). The *lh-2* mutants did not exhibit leaf abnormalities when compared with the WT (Figure 4.7) indicating that the decreased leaf vein density is most likely directly attributable to auxin deficiency and is not mediated by effects of auxin deficiency on GA content.

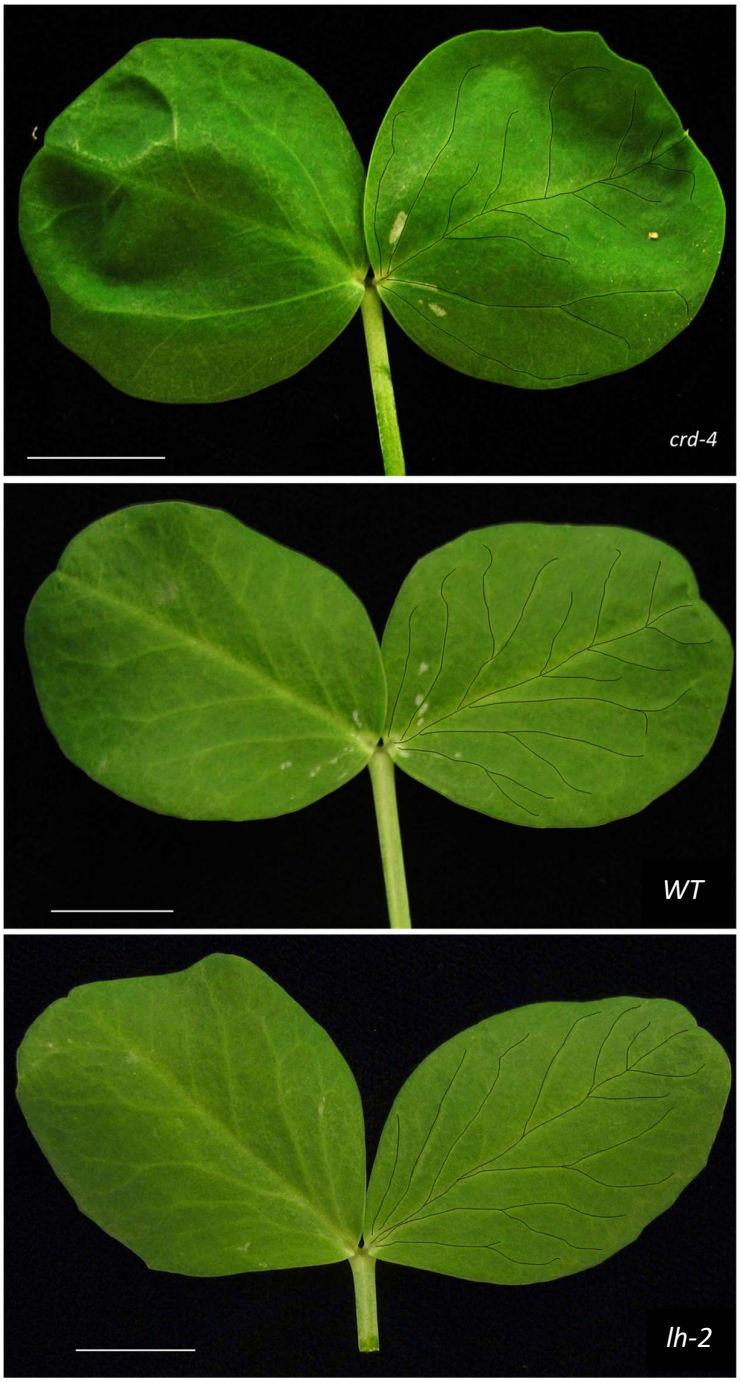

Figure 4.7. Leaf venation of *crd-4* and WT on the tall Torsdag background and of *lh-2* (line 5843), a dwarf mutant derived from Torsdag. Mid rib and secondary veins are traced in black in the right hand-sided leaflet. First expanded leaf from the 3rd node. Bars represent 1 cm.

The crd *mutants have strong compound leaf phenotypes*

Pea mutant alleles of the *Crd* locus were previously described to have compound leaf phenotypes: toothed stipules, waved leaf surface and reduced or missing leaflets (Swiecicki, 1989; Berdnikov et al., 2000). Having access to a *crd* mutant on a tall background, the phenotypes of the compound pea leaf, consisting of three different components (stipules, leaflets and tendrils), was re-assessed. The *crd-4*(TOR) mutant was affected in all three parts. The stipules had severely altered vasculature, giving the appearance of an abnormal body plan when compared with the WT (Figure 4.8). Furthermore, mutant stipules were generally bigger with 'rounded' distal ends when compared with those of the WT and asymmetry between opposite stipules of the same node was regularly exhibited. In addition, larger 'areas' devoid of visible veins were common in the mutant. The 'toothed' phenotype described by Swiecicki (1989) was present in both genotypes but appeared more marked in the mutant.

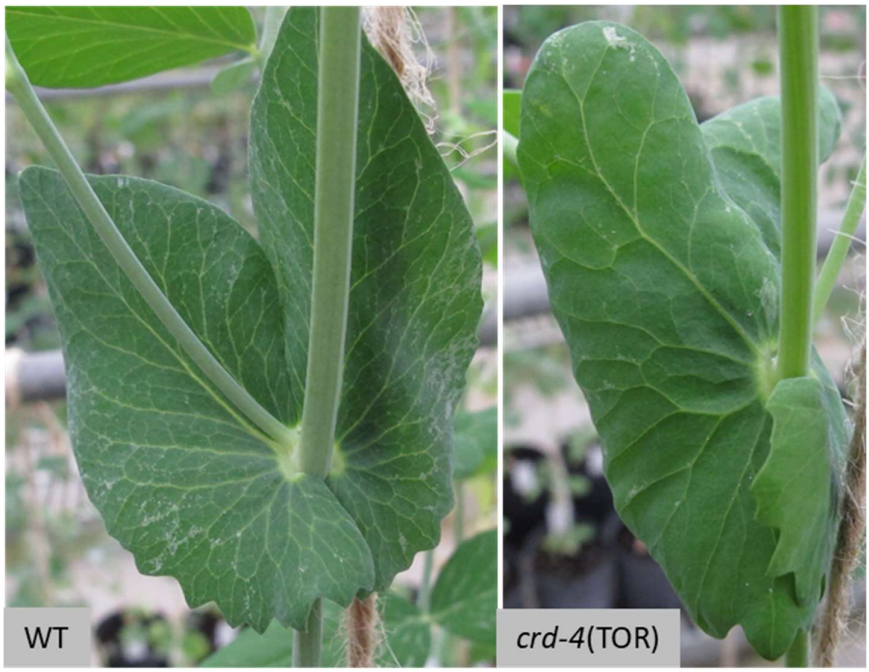

Figure 4.8. The WT and *crd-4* stipules on the tall Torsdag background. Vasculature is severely affected as is overall morphology in the *crd-4* mutant, when compared with the WT.

As on the Caméor background, homozygous recessive segregants on the tall (*cv*. Torsdag) background were easily identifiable based on leaf phenotype. Genotypes were also confirmed molecularly with RFLP protocols. Leaflet number and placement were disrupted in the tall *crd-4* mutant, with most leaves in an individual plant being affected. A leaflet may be reduced in size, may be absent with only the petiolule remaining, or there might be a 'protrusion/bulge' at the location where growth would normally occur (see below). In pea, as described earlier, a change in leaflet number (from two to four or more leaflets) occurs as the juvenile vegetative growth transits to the adult vegetative phase (Wiltshire et al., 1994). Leaflet numbers were counted after this transition in each genotype for a total of 6 nodes. This was done to ensure that results were not confounded by the leaflet number in the juvenile growth phase. The *crd-4* mutant had a 33% decrease in leaflet number when compared with the *CRD-4* WT and the dwarf *lh-2* (Figure 4.9). The WT and the *lh-2* mutant had on average five leaflets per leaf while the *crd-4* mutant had less than four leaflets per leaf indicating that a disruption in *PsYUC1* negatively affects leaflet initiation and normal compound leaf growth in pea.

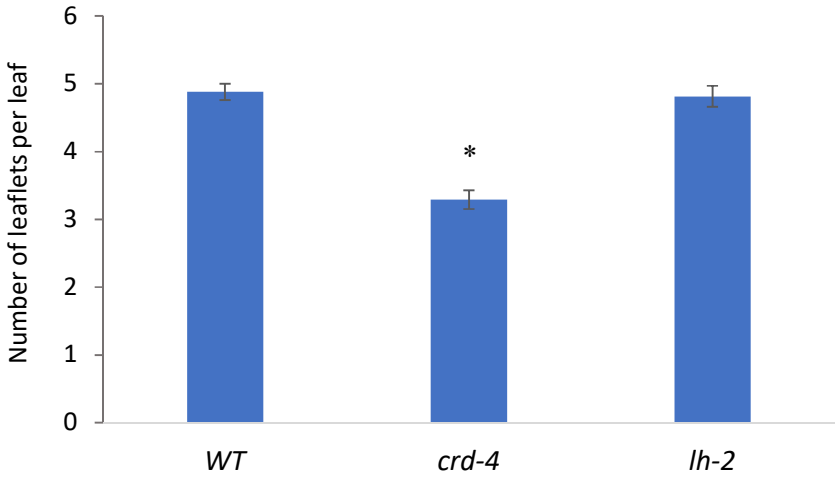

Figure 4.9. Leaflet number per leaf, after the juvenile/vegetative transition phase, in *crd-4* on the tall background, the co-segregating WT and the dwarf *lh-2* mutant. The *crd-4*(TOR) mutant leaflet number was significantly decreased when compared to the WT and the *lh-2* mutant (n-9; p = 3.6E-08 and p = 1.4E-05 respectively). Results are means ± S.E. and asterisk denotes significant difference.

However, the leaflet number and leaflet placement phenotypes were not always observed simultaneously on a leaf (Figure 4.10). For example, a plant may have a leaf with missing leaflets at node 6 while the leaf at node 7 may have displaced leaflets. The two phenotypes may also occur in the same leaf. Tendrils in the mutant also exhibited pleiotropic phenotypes mirroring those seen with leaflets. Pairs of distal single tendrils were often missing or placed in alternate positions instead of opposite. Tendrils were generally less 'curly', reducing their capacity to twine as growth progressed.

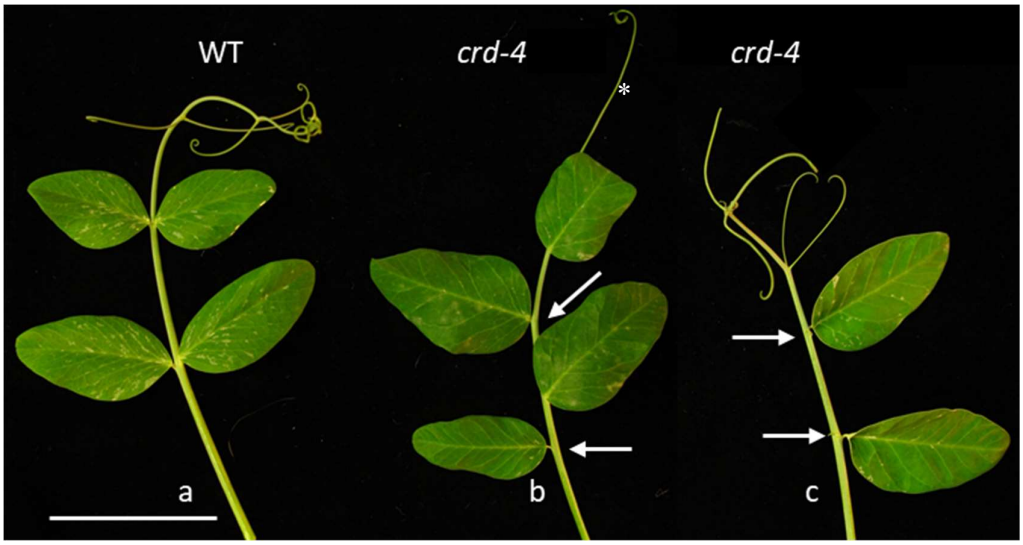

Figure 4.10. Leaf phenotypes of WT and *crd-4* mutant on a tall (*LE*, *LH*) background. a) A WT compound pea leaf at node 12. Two leaflet pairs (opposite positioning of leaflets) along the petiole/rachis and two opposite tendrils pairs with a terminal single tendril. b) The *crd-4* leaf development is affected. In this case, the leaflets are positioned in an alternate fashion (white arrows). The two pairs of tendrils are missing (*). c) Leaflets are missing. The locations where the leaflets are missing have petiolules only (white arrows). Tendrils are reasonably normal but do not spiral as in the WT. Scale bar = 5 cm.

Leaf turgor appeared to be affected in the *crd-4* mutant. Leaves were 'softer' and often 'drooping' (Figure 4.11b). Their attachment to the rachis, the petiolule, appeared frailer then that of the WT. Again, where leaflets were missing, small

protrusions on the rachis were clearly visible (Figure 4.11b). These indicated positions from which pairs of tendrils (proximal and distal) would have emerged.

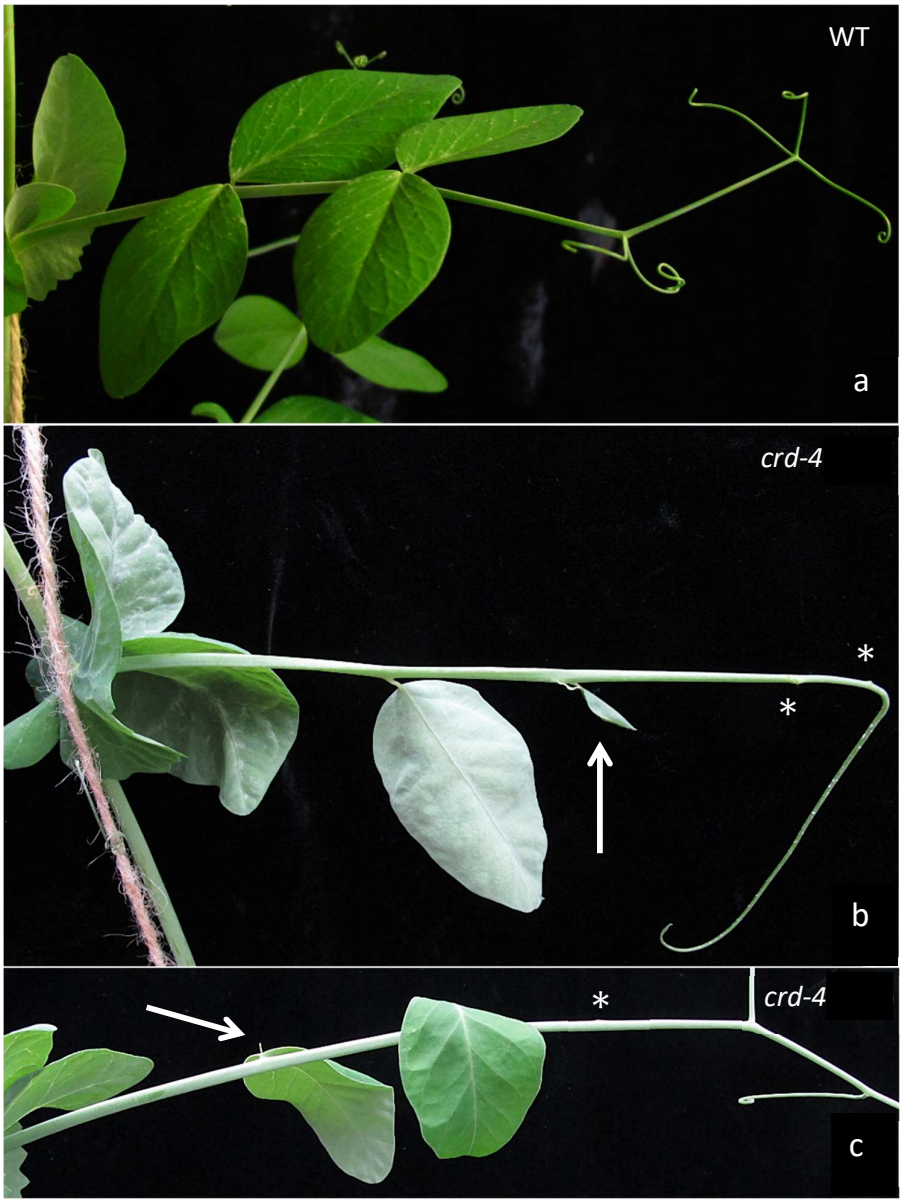

Figure 4.11. Leaflet turgor was affected in the *crd-4* mutant when compared with the WT. a) A typical WT pea leaf. b) The *crd-4* mutant leaf lacked turgor. An underdeveloped leaflet and petiolules are highlighted with arrows. * denote protrusions/bulges along the rachis. c) Again, a *crd-4* leaf with compromised turgor and missing leaflets. Leaves are from node 10.

Further vegetative abnormalities occurred but only on rare occasions. Fusion at the base of leaflets (cone-shaped leaflet) was occasionally exhibited by the *crd-4* mutant (Figure 4.12a). On rarer occasions the terminal tendril developed as a leaflet with mosaic organ identity (Figure 4.12b). Indeed, in a mutant population of 30 individuals, the cupping effect was only seen twice and the identity phenotype once.

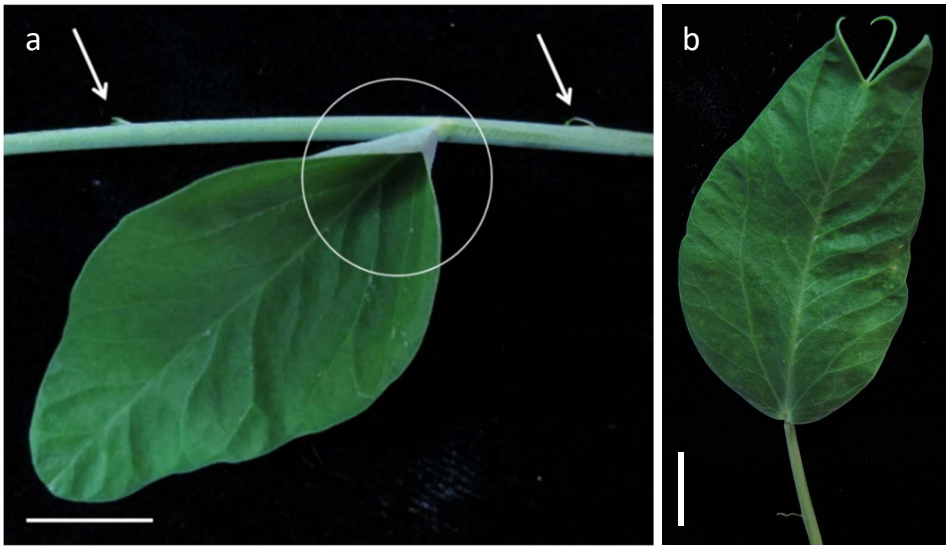

Figure 4.12. The tall *crd-4* mutant leaf has cupping and identity/mosaic phenotypes on occasion. a) Fusion at the base of *crd-4* leaflets (encircled). The leaf also exhibited a placement phenotype and was missing two leaflets, as demonstrated by the white arrows. b) Terminal tendril developed as a leaflet with tendril identity restored at the distal end of the leaflet. Scale bars = 1 cm.

Furthermore, the ontogenetic transition from the juvenile to the adult vegetative phase was affected in the tall *crd-4*, occurring at a lower node in the mutant than in Torsdag and segregating tall WTs (Figure 4.13). Ontogenetic transition in the *lh-2* mutant, isogenic to Torsdag, was not affected mirroring the WT. In the tall *crd-4* mutant, the transition occurred at (on average) node 10.6 while the transition in the WT and the dwarf *lh-2* mutant occurred at (on average) node 11.6 and 11.8 respectively.

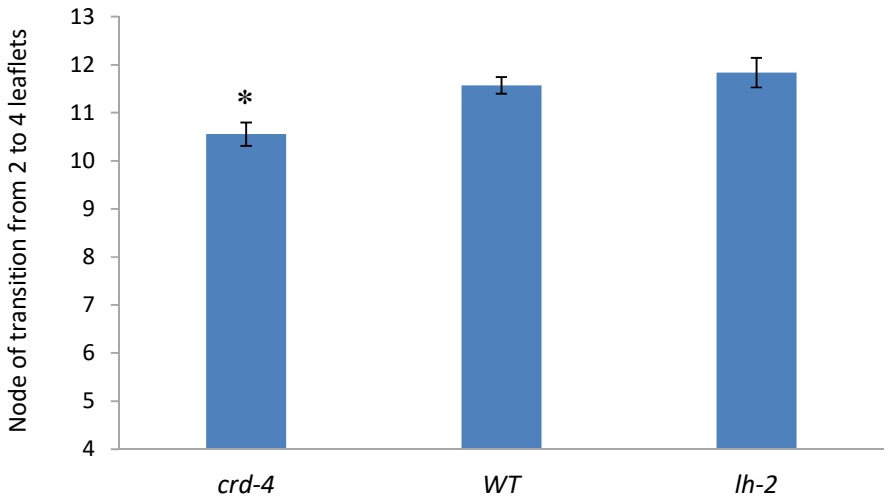

Figure 4.13. Node at which leaflets number transitions from two to four in the *crd-4* mutant, the segregating WT and the *lh-2* mutant (n=6–14). The transition occurs at a lower node in the *crd-4* mutant when compared with the other two genotypes (p=0.002). Results are means ± S.E. with asterisk denoting significant difference.

The crd-4 *has decreased shoot weight*

We previously proposed that the altered vasculature in the *crispoid* mutant leaf decreases the photosynthetic capacity of the plant (McAdam et al, 2017b). Consistent with that, the *crd-4* mutant shoot dry weight was reduced when compared with the WT on both the dwarf (n=3, p=0.0001, Figure 4.14a) and the tall backgrounds (n=15, p=0.007, Figure 4.14b). Root dry weight was also reduced but the shoot to root ratio was not (data not presented).

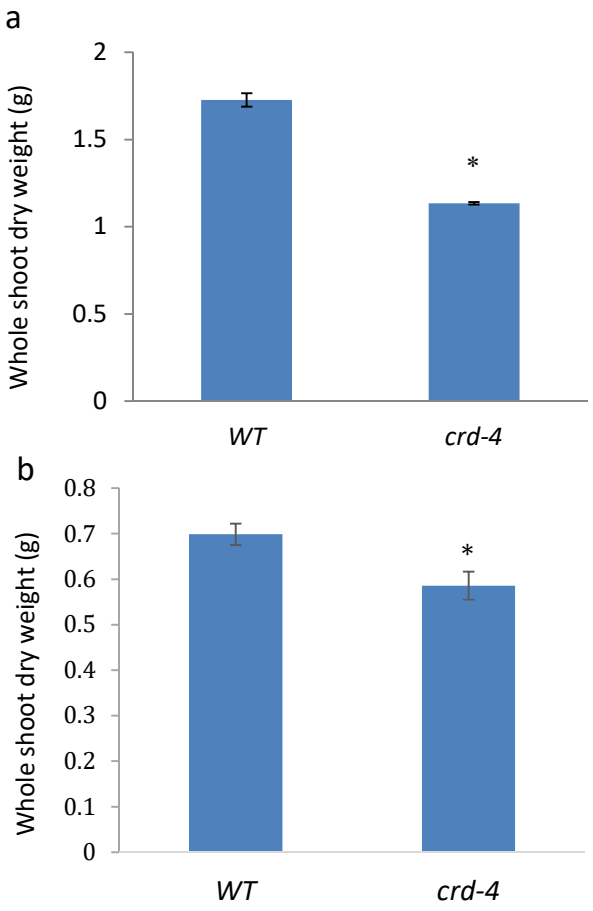

Figure 4.14. The *crd-4* mutant has reduced total shoot weight when compared with the WT. a) Whole shoot dry weight on the dwarf Caméor background, mature plants, n=3; p=0.0001. b) Whole shoot dry weight on the tall Torsdag background, juvenile plants, n=15; p=0.007. Results are means ± S.E. with asterisks denoting significant differences.

Stature is reduced in the crd-4 *mutant*

The stature of a plant is an important aspect that can affect weight/biomass. The *crd-4* mutants on the *le* background were regularly of shorter stature when compared with the WT (data not shown). When the mutation is carried onto the tall Torsdag background and the influence of reduced GA is removed, stature remained reduced in mutant plants (Figure 4.15).

Figure 4.15. The *crd-4* mutant on the *LE* background is of shorter stature when compared with the co-segregating WT. Nodes/leaves are numbered and highlighted with yellow arrows. White stars are located where nodes were tagged (at the uppermost fully expanded leaf) 27 days after sowing. Of note, in the top right corner: similarly to the WT, the *crd-4* mutant does not branch (white arrows) demonstrating that apical dominance is not affected in the mutant. Scale bar is graduated in 5 cm increments.

Rate of leaf expansion, and stem length, but not internode length, are affected in the crd-4 *mutant*

To examine the growth traits that drive the shorter stature in the mutant when compared with the WT, various growth parameters were quantified. First, the rate of node formation/number of leaves expanded in the tall *crd-4*, the co-segregating WT and the dwarf *lh-2* was counted. Second, the associated stem length was measured. In both instances, the traits were quantified by simultaneously recording the nodes reached by each individual after 27 days and the stem length from node 1 to that node. Third, two representative internodes located within the measured stem were selected and measured. Thus, the number of nodes with expanded leaves after 27 days represented the rate of node initiation/leaf expansion, the length between node 1 and the tagged node represented the stem length (reached at that point in time) and the internode length monitored the potential influence of the mutants on internode elongation.

Twenty-seven days after sowing, Torsdag and co-segregating WT plants had formed 10 or 11 nodes, while the *crd-4* and *lh-2* individuals had formed 8 or 9 nodes. In other words, the rate of node formation in the two mutants was significantly reduced when compared with WT (Figure 4.16a). The stem length between node 1 and the tagged node was also reduced in the two mutants, with *lh-2* recording a greater decrease than *crd-4* (Figure 4.16b). However, no difference in internode length (between node 7 and node 9) between the *crd-4* mutant and the co-segregating WT was recorded (Figure 4.16c). The *lh-2* mutant, being dwarf, behaved as expected with reduced internode length.

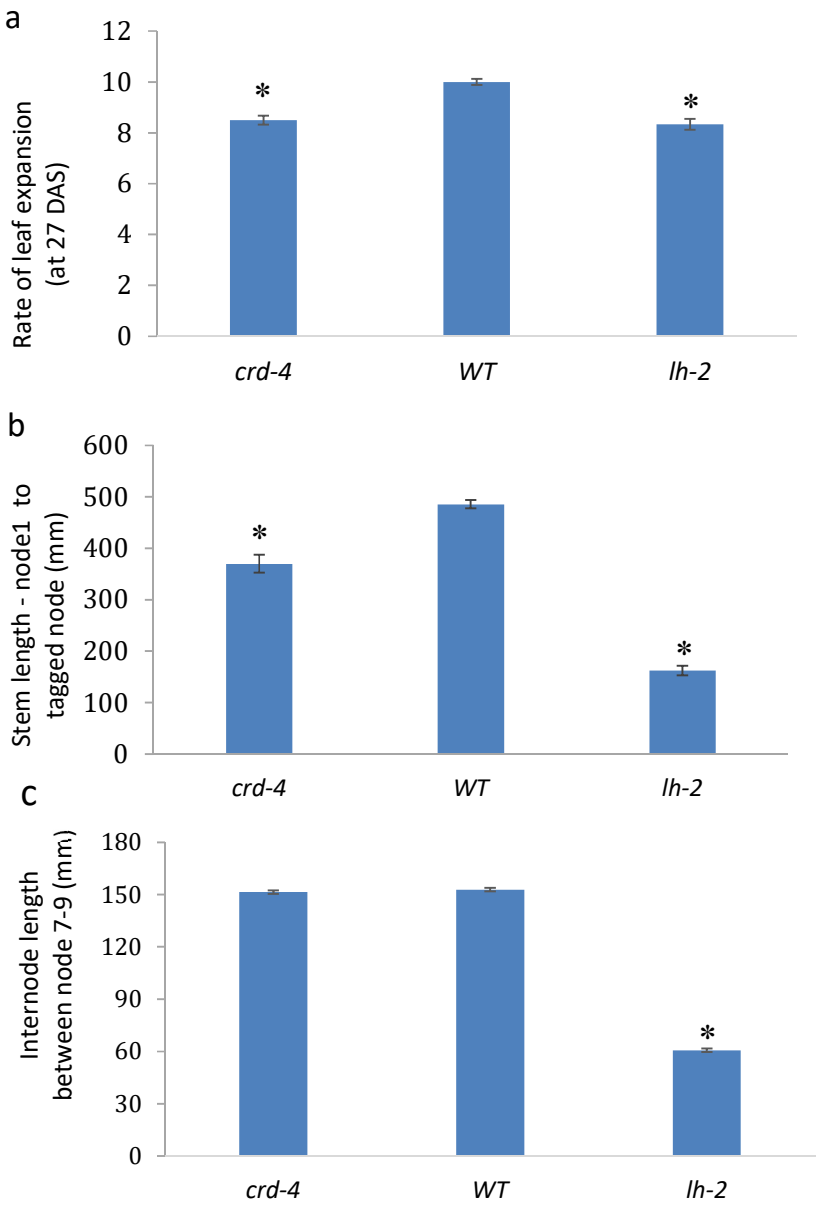

Figure 4.16. Growth traits of the tall *crd-4*, the co-segregating WT and the dwarf *lh-2* prior to the WT adult vegetative phase transition. a) Rate of leaf expansion at 27 days after sowing (DAS) was reduced in the *crd-4* and the *lh-2* mutants when compared with the WT (n=9, 6 and 14 respectively, p=7.8E-7 in both instances). b) Stem length (mm) between node 1 and the tagged node (27 DAS) is reduced in the *crd-4* and the *lh-2* mutants when compared to the WT (n=9-14, p=8.5E-07 and n=6-14, p=4.4E-13 respectively). C) The internode length (mm) between node 7 and 9 was measured in the same individuals. Internode length between *crd-4* mutant and WT did not differ (n=9-14, p=0.8) but that in *lh-2* was decreased (n=6-14, p=4.4E-13). Results are means ± S.E. with asterisks denoting significant difference.

Stem thickness

The number of expanded leaves and stem length can highly influence total shoot weight, but the thickness of these organs further contributes to total shoot weight. Stem weight to length ratio was measured in *crd-4* on the dwarf background to see if this aspect of shoot development contributed to the shoot weight decrease in the mutant. Stem sections from each genotype were randomly selected, measured and weighed. The stem weight to length ratio was decreased in *crd-4* when compared with the WT (n=7, p=1.35E-06) (Figure 4.17).

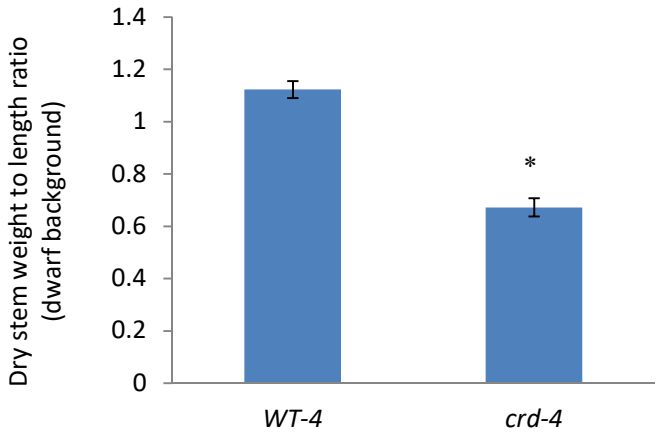

Figure 4.17. Stem thickness is affected in the *crd-4* mutant. Dry stem weight to length ratio is reduced in the dwarf background (n=7; p=1.35E-06). Results are means ± S.E. with asterisks denoting significant difference.

4.3.3. Allelic comparison of the *crd* flower phenotypes

Some aspects pertaining to flower morphology were mentioned previously but only for the effects of the *crd-2* mutation (Berdnikov et al., 2000). The flower phenotypes of the *crd-1*(Paloma), *crd-3*(Caméor) and *crd-4*(Caméor) mutants will therefore be used to compare the effects of the different alleles on that specific

developmental aspect. As mentioned in the introduction, the allelic comparison would serve two functions. First and foremost, it would ascertain that the *crd* phenotypes are consistently present in the three alleles, which in turn, would confirm that the flower phenotypes are directly attributable to a disruption of the *PsYUC1*/*CRD* gene, and not a mutation in a closely linked gene. Furthermore, similar phenotypes across alleles would also provide further support to the proposition, as discussed in Chapter 3 and the present introduction, that the C-terminal region, altered in the *crd-4* mutant, is required for the functioning of the PsYUC1 enzyme.

The crd *mutants have severe floral phenotypes*

All of the *crd* mutants have strong flower phenotypes, displaying defects in three whorls of the first flower and in all four whorls of the second flower. On the WT background, each secondary inflorescence emerging at a node produces two flowers/pods. The two flowers reach anthesis sequentially within a day. The first, more mature and physically closest to the stem is defined as the first flower while the youngest and distally located flower is defined as the second flower. In the *crd* mutants, every first flower produced on each second-order inflorescence exhibited abnormalities (see below). However, the severity and the range of defects varied between flowers (Figure 4.18a). Second flowers were rarely produced but when they were, had substantially more severe defects than the first flowers. All four whorls of the second flowers were affected, exhibiting mosaic organs, placement and identity defects and misshapen or missing organs (Figure 4.18b).

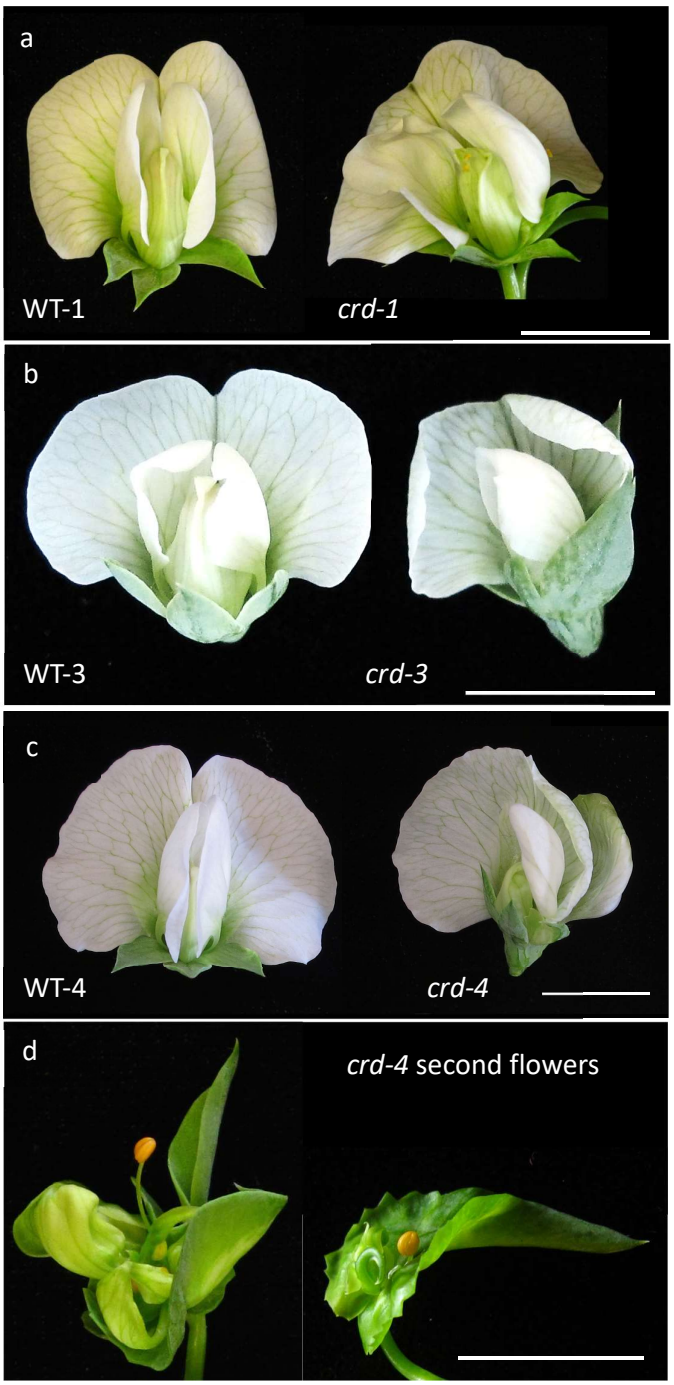

Figure 4.18. The *crd-1*, *crd-3* and *crd-4* mutants exhibit severe flower phenotypes. a) The WT-1 (Paloma) and the *crd-1*. b) The WT-2 (Caméor) and the loss-of-function *crd-3* mutant. c) The WT-4 (Caméor) and the *crd-4* mutant. d) Second flowers from *crd-4*. Scale bars represent 1 cm.

The first flower produced by the *crd-4* mutant on both dwarf and tall backgrounds was affected, with sepal, petal and stamen morphology and number defects (Figure 4.19). Morphology of one or more of the five sepals was abnormal with sepals often missing and on occasion developing as a petal, exhibiting a mosaic phenotype (Figure 4.19g). Whether this phenotype arose from identity or placement defects is uncertain. Similarly, petals were consistently affected. The standard (vexillum) was generally misshapen with asymmetric growth. The two wings and fused keel were often reduced in size and malformed. Often, a wing or a keel was missing. The male reproductive organs of *crd-4* were always reduced in numbers with only two to four stamens instead of 10. The staminal tube did not fuse (Figure 4.19i) and the pollen in the anthers was pale in colour when compared with the WT. However, the carpel developed normally with all expected reproductive organs present (carpel, style, stigma and ovules). On occasions, vasculature was affected in the carpel (Figure 4.19j).

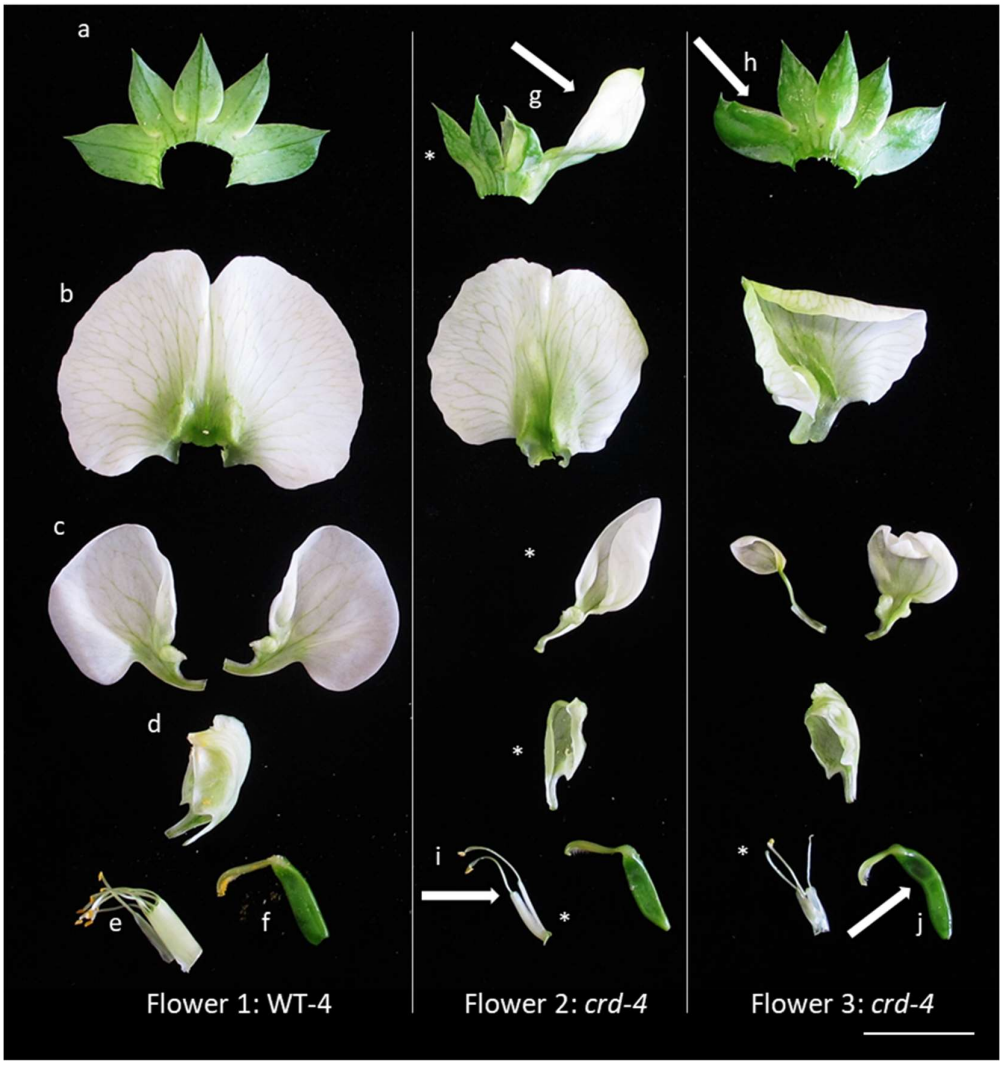

Figure 4.19. The *crd-4* mutant on the tall background exhibit strong flower phenotypes. Three representative flowers are 'deconstructed' and laid-out from the top of the figure to the bottom. Starting on the left, a WT flower: a) five sepals; b) the standard (vexillum); c) two wings (alea); d) two keels now fused; e) the fused staminal tube from which arises 10 filaments with associated anthers (containing the pollen grains) and f) the central carpel with a pericarp containing the ovules, the style and stigma. The next two 'deconstructed' flowers on the right are *crd-4*. The *crd-4* mutant exhibits a range of phenotypes including organ placement defects/mosaic (g), morphological deformities (h, i, j), and missing organs (*). The white arrows highlight areas of interest. Scale bar represent 1 cm.

To investigate if the vasculature phenotype observed in the leaf of *crd* mutants was present in the mutant flower, the venation pattern of the standard was qualitatively monitored. No marked or obvious observable differences in pattern or vein density were noticed in the standard of *crd-4* when compared with WT (Figure 4.20). As the standard was generally smaller in the mutant, the areas between the veins appeared less expanded. However, further microscopy and vein density measurements are required to adequately quantify any effects, if any, of *crd* on petal vasculature.

Figure 4.20. The venation patterning of the *crd-4* standard (vexillum) does not appear affected when compared with the WT. Scale bar = 1 cm.

4.3.4. Further reproductive traits are affected in the *crd* mutants

Other traits relating to reproduction have not been characterised previously. Several traits including time to initiation of flowering (as measured by nodes formed), time of flowering, pod development, seed phenotype and yield were monitored in the *crd-4* mutant on a tall background and compared with the co-segregating WT and the dwarf *lh-2* mutant.

Flower initiation is adversely affected in crd-4

The *LF* gene, or *PsTFL1c*, one of three pea homologues of the *Arabidopsis TFL1*, affects the timing of the flowering transition phase by lengthening the vegetative phases (Foucher et al., 2003). To ensure that the influence of *lf*, found in Caméor, was removed from the new tall *crd-4* line, careful plant selection was carried out. Only segregating mutants that flowered at the highest node within each F2 population were selected from each new generation for crossing to Torsdag (backcrossed four times). The *lh-2* mutant, isogenic to Torsdag, was included for comparison. Flowering occurred at an earlier node in the *crd-4* mutant when compared to the segregating WT and the dwarf *lh-2* mutant (Figure 4.21a). However, flowering time was delayed in both the *crd-4* and the *lh-2* mutants when compared with the WT (Figure 4.21b).

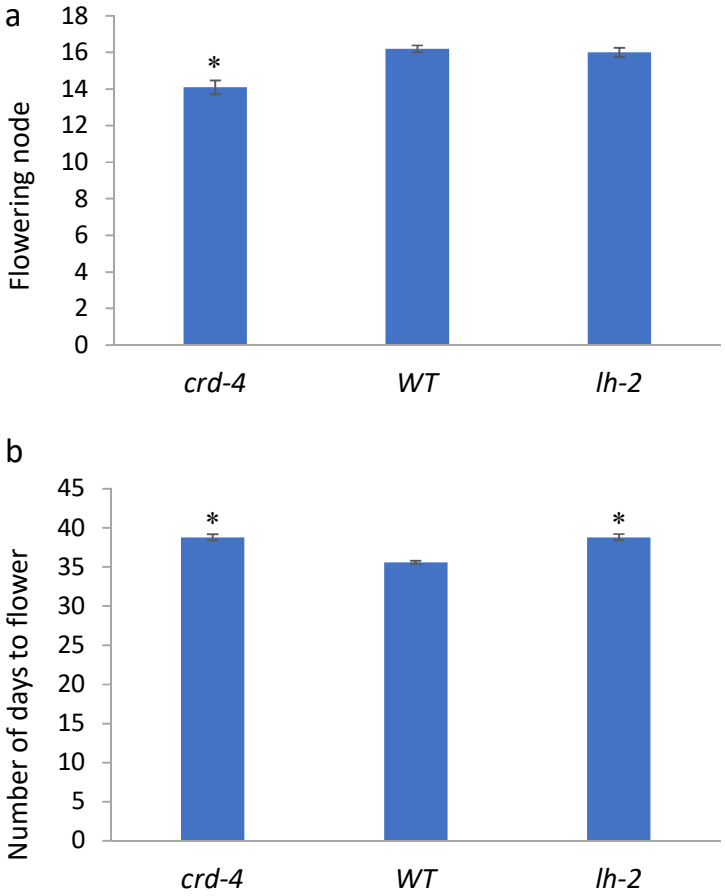

Figure 4.21. Flowering node and flowering time are affected in the *crd-4* mutant on a tall background. a) The *crd-4* mutant flowered on average two nodes before the WT and the *lh-2* mutant (n=9, 14 and 6 respectively, p=0.003). Both the *crd-4* and the *lh-2* mutants flowered on average 3 days after the WT (p=5E-8). Results are means ± S.E. with asterisks denoting significant difference.

The crd-4 *pod exhibit vasculature defects*

Pod phenotypes were affected in the tall *crd-4* mutant when compared with the WT and the *lh-2* mutant. A pea pod develops from one carpel that folds in two with two seams that run parallel to one another. The seam where the placenta and the seeds grow is the ventral vascular suture while the one at the opposite end, is referred to as the dorsal vascular suture (Figure 4.22). Both seams are important to the process of dehiscence and seed dispersal (Weeden et al., 2002). In the original, native pea, once the seeds are mature and the pod is dry, the pod splits along both sutures into

two halves, to release the seeds. On occasions, *crd-4* pods containing developing seeds exhibited suture defects. When present, the phenotype was consistent: the dorsal vascular suture and the associated median carpellary bundle developed normally starting at the distal end of the pod and a quarter to half way along the expected growth plane, both structures bifurcated. Growth changed orientation to cut across one side of the pod (Figure 4.22). From that point on and until the proximal end of the pod, along the dorsal plane, the dorsal vascular suture and the carpellary bundle were absent.

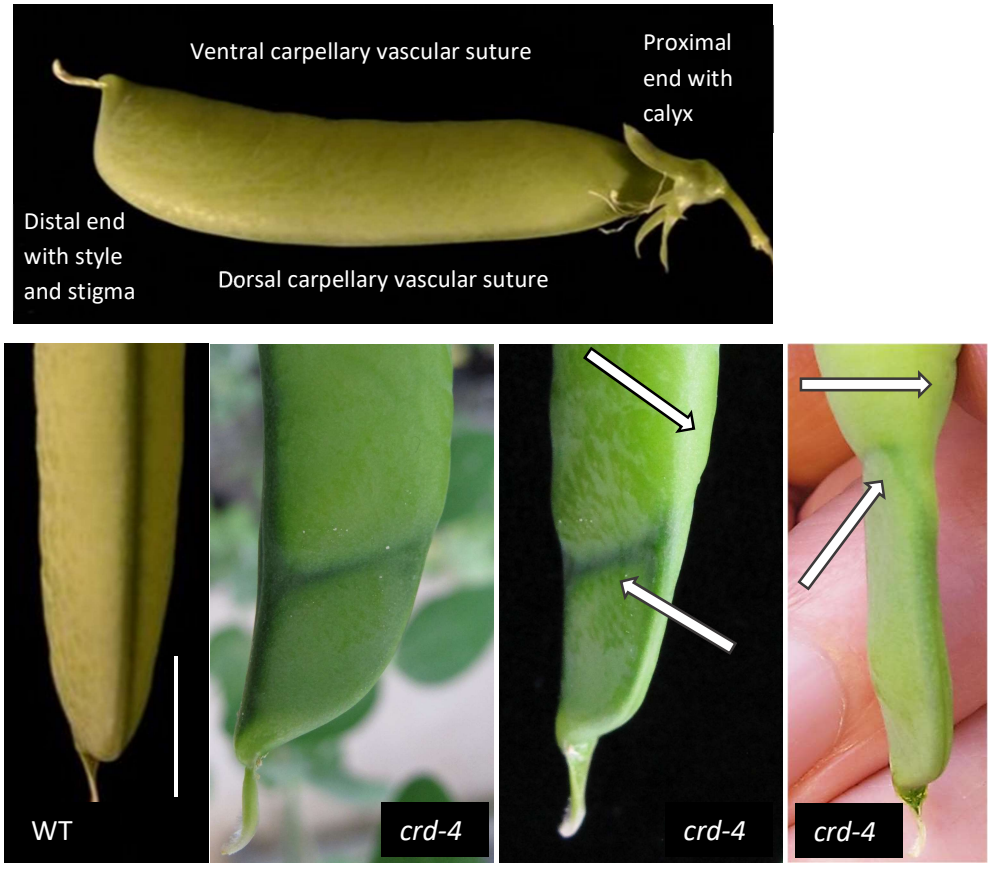

Figure 4.22. Pods of the tall *crd-4* mutant have vasculature defects. Top: a WT pea pod with the ventral carpellary vascular suture, the dorsal carpellary vascular suture, the distal end of the pod with the style and stigma and the distal end of the pod with the calyx. On the bottom left, a WT pod with the dorsal carpellary vascular suture clearly visible. On the right, three *crd-4* pods exhibiting dorsal suture defects (white arrows). Scale bar = 1 cm.

Seed yield is severely compromised in the crd-4 *mutant*

Furthermore, the number of pods per plant and seed number per pod were quantified to assesses if these reproductive output traits are adversely affected in the *crd-4* mutant (tall background). On average, the *crd-4* mutant produced as many pods as the WT while the *lh-2* mutant produced fewer (Figure 4.23a). However, the two mutants, *crd-4* and *lh-2*, produced many seedless pods significantly reducing seed number per pod while each pod carried by the WT contained seeds (Figure 4.23b). Indeed, the *crd-4* seedless pods remained green and fleshy as did their fertilised counterpart, but pod size was substantially reduced. The severely reduced yield of seeds in the *crd-4* mutant appeared to be driven by a combination of the high rate of seedless pods and decreased number of seeds per pod.

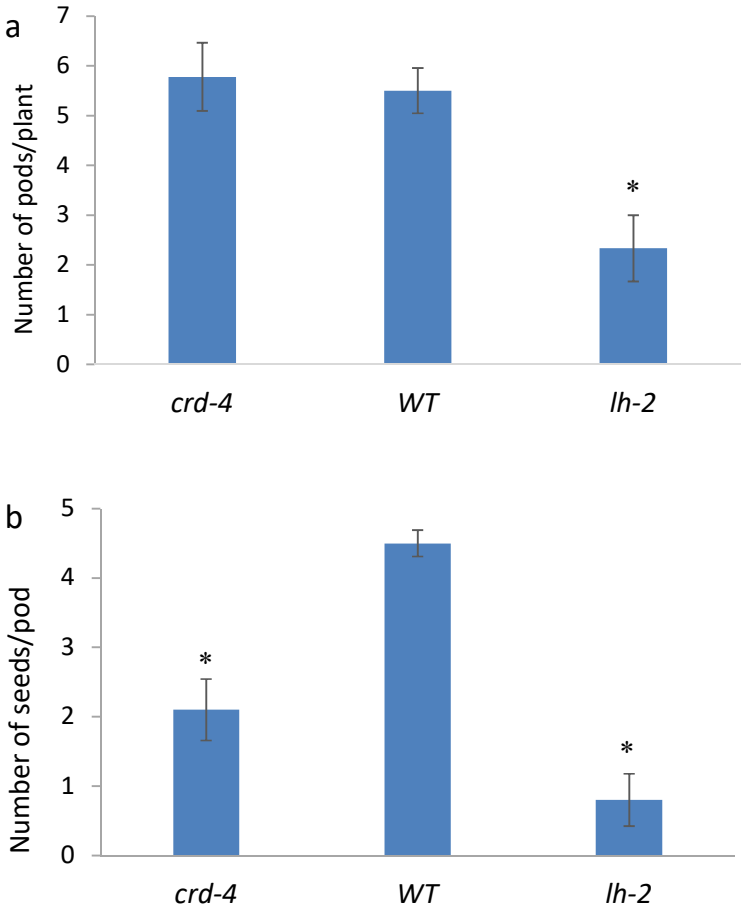

Figure 4.23. Reproductive output in the *crd-4* mutant on the tall Torsdag background, the segregating WT and the isogenic dwarf *lh-2* mutant. a) Number of pods per plant was not significantly different between *crd-4* and the WT (n=9-14; p=0.48) but the *lh-2* mutant produced fewer pods (n=6-14; p=0.001). B) The number of seeds per pod was decreased in the *crd-4* and the *lh-2* mutants when compared with the WT (n=9-14, p=5E-06 and n=6-14, p=2.8E-09 respectively). Results are means ± S.E. with asterisks denoting significant difference.

The crd-4 *mature seed phenotype appears normal*

Seed yield was adversely impacted in the *crd-4* mutant but the mature seed phenotype was not (Figure 4.24), indicating that auxin pool required for seed development to progress normally was not impacted by the *crd-4* disruption.

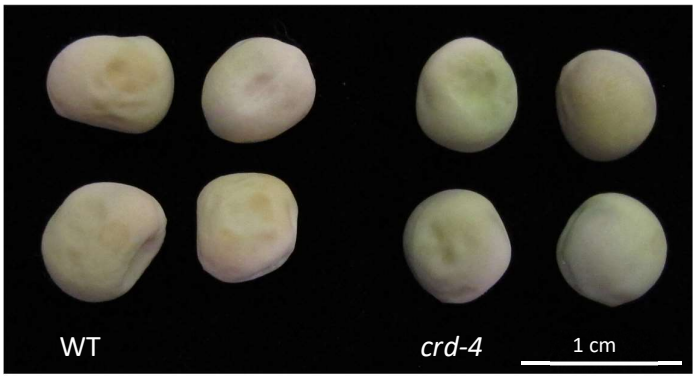

Figure 4.24. The *crd-4* mature seed phenotype is comparable to the WT.

4.3.5. Auxin activity is affected in the *crd* mutants

Auxin activity in pea can be qualitatively monitored by histochemical analysis of GUS staining under the control of the highly auxin-inducible synthetic *DR5* auxin response element (AuxRE) (DeMason and Polowick, 2009). Put simply, the *DR5::GUS* construct contains two critical parts: the DR5 promoter consisting of tandem direct repeats of the canonical TGTCTC AuxRE from the soybean *GH3* promoter region and a fused *gusA* gene originating from *E. coli* (Jefferson et al., 1987). The *gusA* gene (GUS) acts as a reporter of the *DR5* promoter activity. The *gusA* gene codes for β-glucoronidase, an enzyme that cleaves the chromogenic substrate X-gluc, in turn producing an insoluble blue stain. Furthermore, there is normally no detectable GUS activity in plants, making the assay suitable for detecting auxin-responsive transcription without confounding endogenous *gusA* activity (Ulmasov et al., 1997).

To investigate auxin activity in the *crd* mutants, a *DR5::GUS* construct (RTP9, DeMason and Polowick, 2009) was introduced in the dwarf *crd-4* line via crossing. Young leaflets and flowers were selected, as phenotypes were most marked in those organs.

Young crd-4 *leaflets have minimal GUS staining*

Apical portions of transgenic *crd-4* mutants on the dwarf background and of WTs from actively developing plants were harvested and treated with an X-gluc solution. All plant material was genotyped and homozygous for DR5. The level and pattern of staining in developing leaves of the WT-4 (WT segregant carrying the DR5 reporter) was similar to that of the RTP9 positive control. Strong staining saturated cells throughout the leaf, including the vasculature and the expanding leaf extremities. Unlike the WT, *crd-4* leaves had minimal GUS activity with occasional staining in the expanding extremities (Figure 4.25). Based on GUS staining, the genotypes of a segregating population could be identified and results mirrored phenotypes and RFLP data.

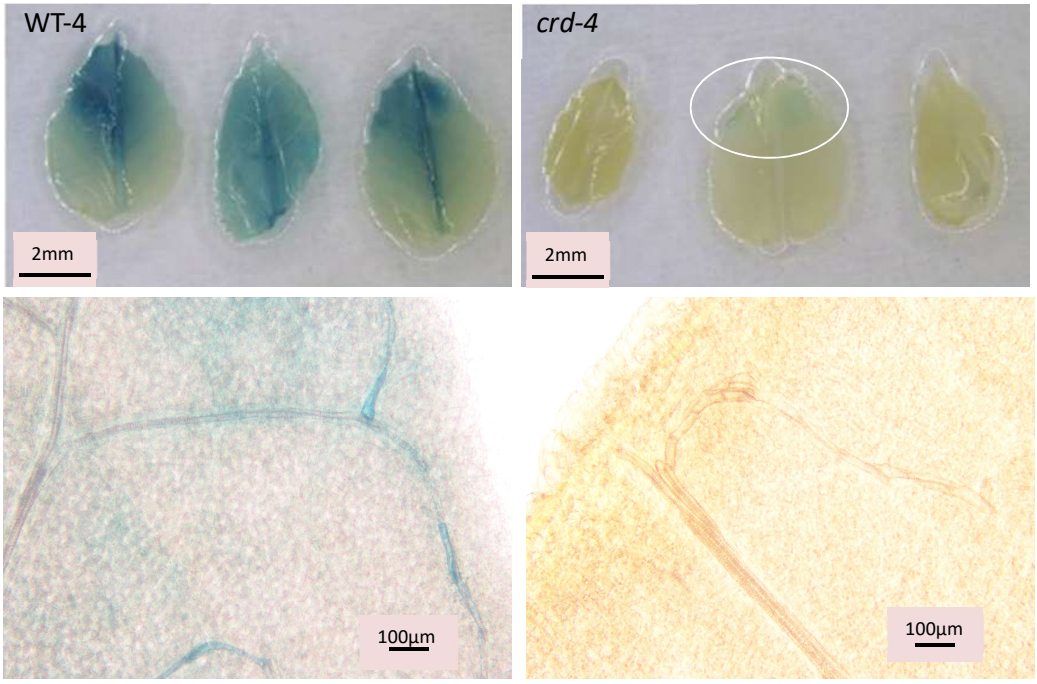

Figure 4.25. The *DR5::GUS* auxin reporter in *crd-4* and co-segregating WT. Top panel, young developing leaflets and stipules from stained WT-4 and *crd-4*. The WT exhibit strong staining particularly at the distal end and in the central vein. The *crd-4* has minimal staining at the expanding extremity (encircled). Bottom panel, the terminal veinlets of the WT-4 leaflet and the *crd-4* mutant. GUS staining is clearly visible in the WT but not in the mutant. Sections taken from the margins of young developing leaflets measuring less than 8mm.

GUS staining is decreased in developing crd-4 *flower buds*

Flower clusters from *crd-4* mutants carrying the *DR5::GUS* construct and co-segregating WT-4 were stained next. The apical portion subtending the inflorescence (bud cluster) was harvested prior to anthesis. At that stage, flower buds ranged in size from one to 10 mm. Petals were still contained within the sepals as the buds were still immature. Similar patterns of auxin activity as seen in the leaflets were exhibited in the developing flower buds. Stem, stipules and sepals from the WT stained strongly while apart for the stem, the mutant buds, had minimal staining (Figure 4.26).

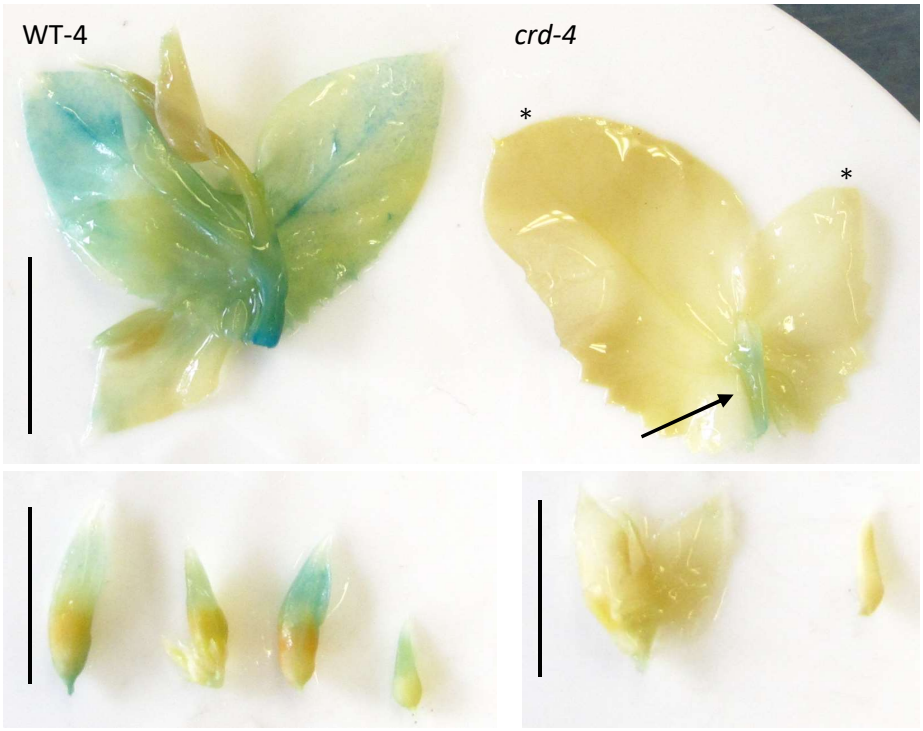

Figure 4.26. The apical portions of *DR5::GUS* carrying WT-4 and *crd-4* containing the young flower buds. Top panel, the apical portion with flower buds removed. GUS staining is present in the *crd-4* stem (black arrow) but not in the stipules. Note the size asymmetry between the two *crd-4* stipules (*). Bottom panel, the flower buds contained within the apical portion. No GUS staining was detected in the *crd-4* mutant. Scale bars = 1 cm.

4.3.6. IAA and IAAsp contents are affected in *crd* mutants

Free IAA and IAAsp were quantified from *crd-3* root tissues and from the apical portions of *crd-4* seedling and inflorescence clusters containing young floral buds. These tissues were selected as actively growing root tips, the shoot apex of seedling and developing floral organs are active sites of auxin responsiveness (Aloni et al., 2006; Vanneste and Friml, 2009).

IAAsp content is reduced in crd-3 *root tip*

To test whether the decrease in lateral secondary root number in the mutant correlated with auxin content, IAA was quantified from actively developing lateral secondary apical root portions (root tip) and from the associated tissue of fully differentiated roots (mature root) of the *crd-3* mutant and the segregating WT. IAAsp was quantified as well to assess if auxin conjugation was affected in the mutant roots. No difference in IAA content was detected between the genotypes in either tissue-type. Fully differentiated mature root tissue contained approximately 125ng per gram of IAA less than actively developing root tip tissue (Figure 4.27a). However, root tip tissue from the *crd-3* mutant on the Caméor background had decreased levels of the conjugate IAAsp when compared with the segregating WT (Figure 4.27b). This decrease in IAAsp may indicate a homeostatic mechanism maintaining auxin content in the meristematic tissue of actively growing root tips.

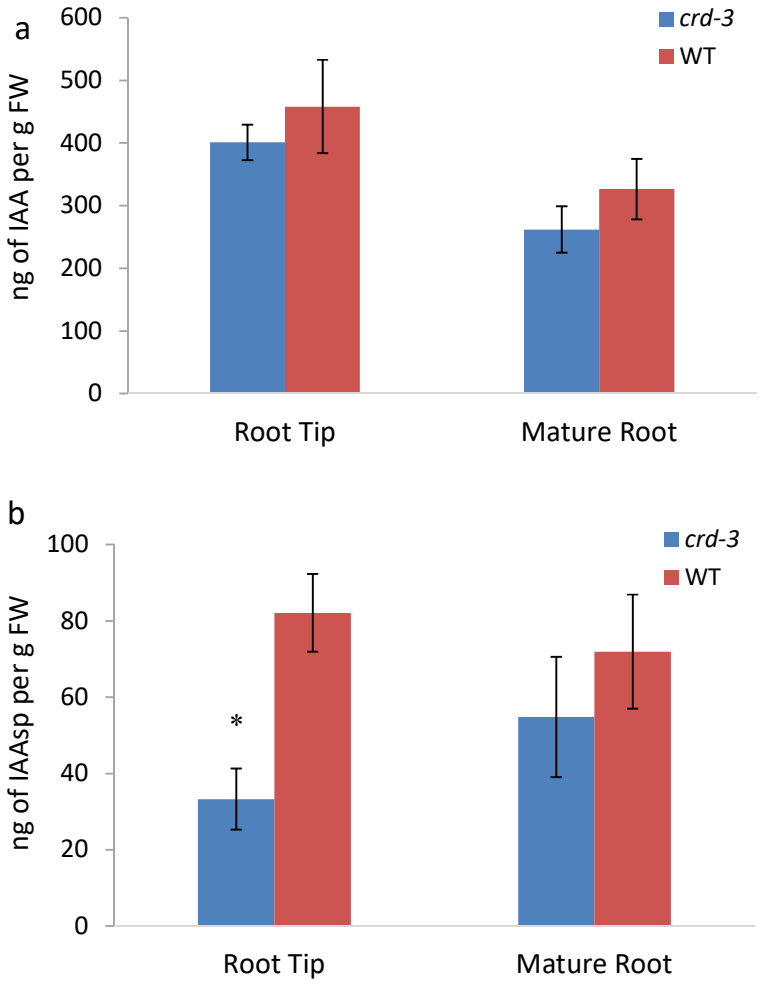

Figure 4.27. Free IAA and IAAsp content from developing tips of lateral roots and differentiated lateral root tissue of *crd-3* mutant and segregating WT plants. a) There is no difference in IAA content between the mutant and WT genotype (n=5). b) The *crd-3* mutant root tip tissue had decreased IAAsp levels when compared with the WT (n=5, p=0.005). Results are means ± S.E. and asterisk denotes significant difference.

IAA and IAAsp contents are reduced in crd-4 *apical portions*

Next, free IAA and the auxin conjugate IAAsp were quantified from apical portions containing developing leaves and meristematic tissue. Seedlings had four fully expanded leaves. Free IAA and IAAsp levels were reduced by approximately 50% and 80%, respectively, in the apical tissue of *crd-4* plants compared to WT-4 plants (Figure 4.28).

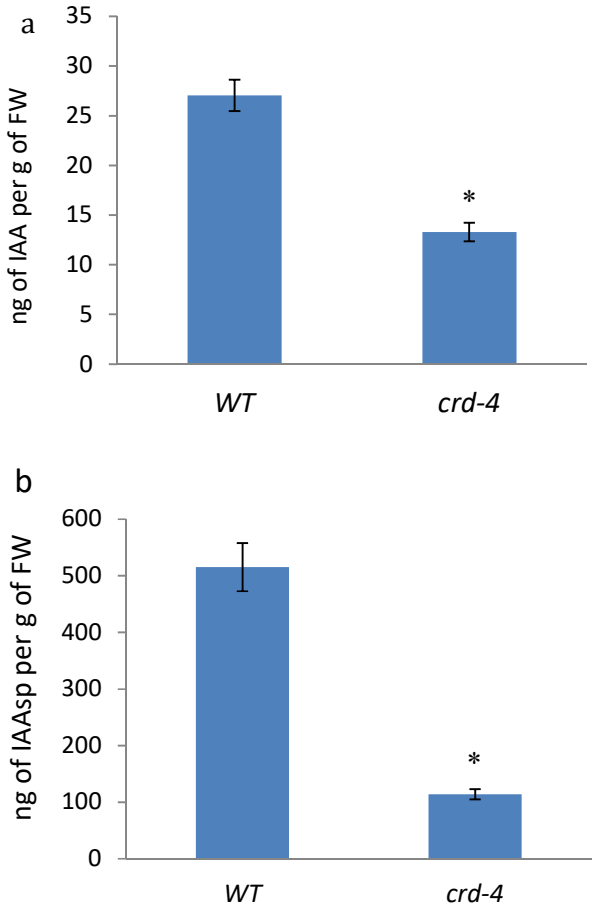

Figure 4.28. Free IAA and IAAsp content from developing apical portions of *crd-4* mutants on the dwarf background and co-segregating WT. (n=4; p=0.0003 and p=9.2E-05 respectively). Results are means ± S.E. and asterisk denotes significant difference.

IAAsp content is decreased in the crd-4 *young flowers*

Similarly, IAA and IAAsp contents were monitored in young flowers prior to anthesis. No significant difference in the IAA content between the *crd-4* mutant and the WT was recorded (Figure 4.29a). However, similarly to the root tip results, IAAsp content was reduced in the mutant when compared with the WT (Figure 4.29b).

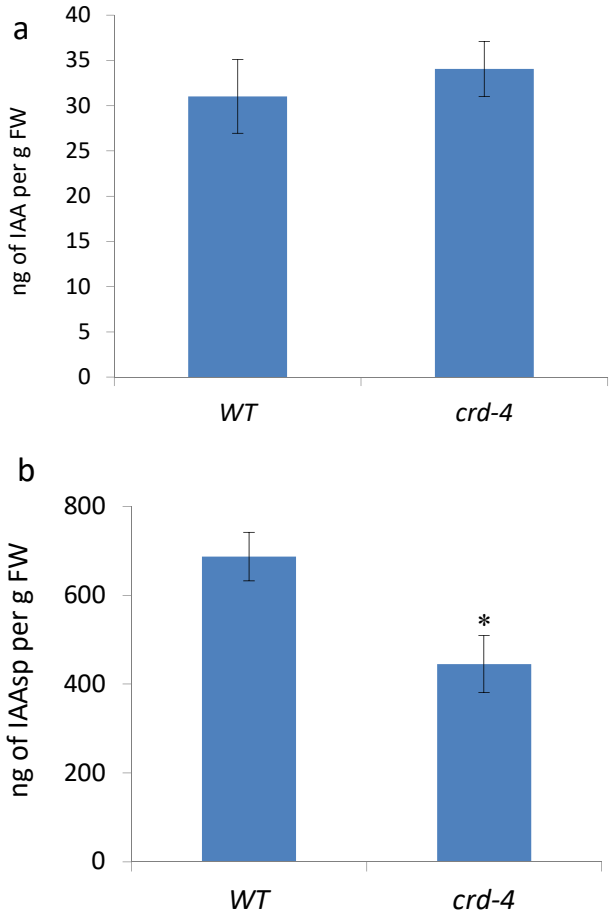

Figure 4.29. IAA and IAAsp content in young *crd-4* and co-segregating WT flowers. IAA did not differ between the two genotypes while IAAsp was decreased in the mutant when compared with the WT (n=5, p=0.7 and p=0.04 respectively). Results are means ± S.E. and asterisk denotes significant difference.

4.4. Discussion

Auxin biosynthesis loss-of-function mutants are invaluable tools for the examination of the potential roles and functions that auxin may exert on plant growth and development. Several routes for the biosynthesis of auxin have been proposed in the past (reviewed in Tivendale et al., 2014). However, the IPyA pathway, now fully characterised, principally based on findings from the *Arabidopsis* model species, is considered the primary route for auxin biosynthesis in plants in general. It is therefore paramount that the IPyA pathway be investigated in a range of plant species to obtain a more inclusive and complete picture of its effects on growth and development in varied plant systems.

In pea, mutants affecting two IPyA-related biosynthesis genes have been reported, a Trp aminotransferase mutant (*tar2-1*, McAdam et al., 2017a) and four mutant alleles with disruptions in a flavin-containing monooxygenase, YUC1 (the *crd* mutant alleles, McAdam et al., 2017b). As mentioned earlier, the *tar2-1* mutant had phenotypes affecting the mature seed but no other classical auxin-deficiency phenotypes were reported in the mutant (McAdam et al., 2017a). Furthermore, auxin derived from another pathway was proposed to operate in WT pea roots (Quittenden et al., 2009). Taken together, these findings suggest that several pathways may contribute to the synthesis of auxin in pea, which by extension, justified the investigation of the effects of the IPyA-related *crd* mutants on pea development.

4.4.1. The lateral roots of *crd* mutants

In the root system of actively growing *crd-3* and *crd-4* mutant seedlings, lateral root number and length were decreased when compared with WT, but taproot length was not (Figures 4.1 to 4.6). There are several lines of evidence demonstrating that auxin participates in lateral root initiation and development. In the primary and lateral roots of *Arabidopsis*, regions of auxin production above the apical meristem tips were identified, indicating that the root has multiple regions with auxin

synthesis capacity (Ljung et al., 2005). The biosynthetic source of the newly synthesised auxin was, however, uncertain.

Furthermore, transgenic pea and Medicago roots carrying DR5 auxin-signalling reporter constructs, were reported to exhibit strong GUS staining in areas where lateral root growth was initiated prior to and post emergence (DeMason and Polowick, 2009; Herrbach et al., 2014). In this instance, it is uncertain if the GUS activity in the transgenic lines was in response to auxin transported through canalisation, to locally produced auxin or to both pools. Indeed, auxin was shown to be actively transported by PIN proteins to sites of lateral root emergence (Blilou et al., 2005). However, in the *Arabidopsis yucQ* mutant, auxin produced in the shoot could not rescue the root phenotypes indicating that auxin produced locally during root development was required (Chen et al., 2014). Furthermore, in decapitated pea plants, root elongation and IAA content in the root tip remained unaffected (Weston et al., 2009).

The present results demonstrate that lateral root development is detrimentally affected in the *crd Psyuc1* mutants and that in the pea system, auxin derived from the IPyA pathway participates in lateral root initiation and formation. In addition, the findings suggest that auxin is likely to be synthesised *de novo* at prebranch sites in the taproot, contributing to lateral root initiation and development (reviewed in Lavenus et al., 2013). Several transcription factors participating in auxin signalling were demonstrated to be highly expressed and required to trigger the initiation of cell division at prebranch sites where incipient lateral root primordia develop (De Smet et al., 2010; Du and Scheres, 2017; Moreno-Risueno et al., 2010). The present results do not, however, exclude a role for polar auxin transport in lateral root growth and development as both sources of auxin might be necessary for the process to occur normally (for reviews, see Jones and Ljung, 2012; Overvoorde et al., 2010). Indeed, in the *crd* seedlings, once a lateral root had emerged it developed somewhat normally but the rate of emergence was reduced in the mutants when compared with the WT.

Auxin production did not appear affected in the root tip of *crd-3* mutants with IAA content being of equivalent concentration in both the WT and the mutant.

However, IAAsp, an important auxin conjugate in pea, was significantly reduced in the root tip although not in the mature and fully differentiated root tissue (Figure 4.27). These results indicate that auxin homeostasis was altered in the *crd-3* root tip when compared to the WT. Potentially, a lower rate of *de novo* auxin synthesis in the root tips is 'counteracted' with a lower rate of conjugation, allowing overall IAA content to be maintained in the root tip. This phenomenon has been previously observed and proposed as an auxin homeostasis feedback loop mechanism (Zheng et al., 2016).

4.4.2. The shoot development of *crd* mutants

Phenotypes pertaining to shoot growth and development were negatively impacted in the *crd* mutants on both the dwarf (*le*) and the tall (*LE*) backgrounds. A diagnostic feature of all crd mutants was the development of abnormal leaves. Indeed, the *crd* compound leaves had a range of morphological defects affecting the stipules, the leaflets and the tendrils. Some of the phenotypes were present only occasionally, such as cupping or tendrils developing as leaflets (Figure 4.12) while others were persistently present. Leaflet vasculature patterning, for example, had obvious defects in the secondary veins (Figure 4.7) and was a reliable diagnostic feature present in all the *crd* mutants (McAdam et al., 2017b). In addition, the various leaf tissues were often deformed, exhibiting placement defects and reduced turgor (Figure 4.8 to 4.11).

Furthermore, leaflet number per leaf were affected in all the monitored mutants, but the reduction was most striking on the tall background (Figure 4.9). Leaflet initiation was affected with leaflets repeatedly being absent from leaves but also, leaflet development was compromised with either protrusions or small structures resembling a petiolule being present at the location where a leaflet should have developed (Figure 4.10 and 4.11). The processes of pea leaflet initiation and development are both thought to require auxin (DeMason et al., 2013). To my knowledge, no *yuc* mutant, in a species with compound leaves, is available at this point in time apart for the *crd* alleles used in this study. Hence, for the first time,

the present results clearly and convincingly indicate that *PsYUC1* is required for leaflet placement and initiation.

The *UNI* gene, proposed to be integral to the pea compound leaf development, is auxin inducible (Bai and DeMason, 2006). *UNI* is expressed according to an acropetal auxin gradient with both auxin and *UNI* displaying strongest concentration/expression at the leaf tip (DeMason et al., 2013). The *uni-tac* mutant leaf phenotypes, a leaky allele with disruptions in *UNI*, has striking parallels to the *crd* leaf phenotypes; though leaflet vasculature was not reported (DeMason and Chawla, 2004). The present GUS staining experiments of the *crd-4* mutant and co-segregating *CRD-4* WT support that, at least to some extent, a portion of the auxin located at the distal end of leaflets is being locally produced (Figure 4.25).

Auxin appears to be integral to the generation of new axes of growth at the apical meristem (Sassi et al., 2014; Scarpella et al., 2010) and at which time interval these events occur (Deb et al., 2015). Potentially, the lower auxin concentration at the SAM of *crd* mutants (Figure 4.28) negatively impacts the transcription of auxin-inducible genes essential to meristematic differentiation or initiation of novel tissue/organ primordial cells. Indeed, in specific locations at the SAM of *Arabidopsis*, auxin accumulated and formed localised regions of high auxin concentration from which novel organ primordia emerged (Benková et al., 2003). The wall of the cells at these sites of auxin maxima are thought to increase in plasticity and to loosen, permitting asymmetric cell expansion (Sassi et al., 2014). Possibly, the auxin maxima required to initiate a new leaf, was not achieved as often in the mutant which could explain the decreased rate of node formation exhibited in the *crd-4* mutant.

Another shoot phenotype described in a *yuc* mutant, was a reduction in apical dominance (Tobeña-Santamaria et al., 2002). Several auxin-related mutants exhibit branching phenotypes, such as the *bushy* (ref) and *rms-2* (ref) mutants of pea. However, apical dominance was not compromised in the dwarf and the tall *crd-4* lines (Figure 4.15). The (still unknown) gene responsible for the *bushy* phenotype (Symons et al., 2002) and the *rms2* mutant, with altered auxin perception (Ligerot et al., 2017) may possibly interact with several auxin pools (produced *de novo* and

polarly transported). On the other hand, the *crd* phenotypes is most likely attributable to a reduction of a local auxin pool that is biosynthesised *de novo* by *PsYUC1* in the meristem/primordia of functional individuals. Auxin content may not actually be deficient in *crd* internodes and remains to be tested.

In *crd-3* and *crd-4* mutant seedlings, total shoot length or number of leaves expanded were decreased but internode length was not (Figure 4.5 and 4.6). Similarly, in the shoot of mature and tall (*LE*) *crd-4* plants, internode length was not affected, but stem length and the number of leaves expanded was reduced (Figure 4.16). These results indicate that growth at the internode is not affected but that the number of nodes laid down as a mutant plant development progress is. Furthermore, the reduced rate of node formation/number of expanded leaves appears to be having an impact on other developmental shoot traits.

Indeed, ontogenetic stage transitions from the vegetative to adult phase and again to the flowering phase occurred at a lower node in the mutants (Figure 4.13 and 4.21). *PsYUC1* may potentially be involved in the determination of the transition stages but the effects were small. Those phenotypes most likely related to the effects of the mutation on the rate of leaf expansion as discussed above.

Furthermore, shoot weight and stem thickness were reduced in the mutant (Figure 4.14 and 4.17). These two traits can be driven by different factors, but nonetheless can both be a measure of biomass and a reflection of photosynthetic rate (McAdam et al., 2017b). It was proposed that the lower auxin content in the *crd* mutants negatively affected leaf vein density, which in turn impacted a leaf photosynthetic capacity, resulting in reduced plant weight (McAdam et al., 2017b). The present findings support this proposition but the fact that overall node numbers are decreased in the mutant must also be considered an influencing factor. Indeed, shoot weight was likely attributable to the decreased stem thickness and overall stem length, driven by the decreased rate of node formation.

Moreover, when taken together, the reduced rate of node formation and leaflet number per leaf support a role for *PsYUC1* in novel and/or lateral organ initiation. The results further suggest that IPyA-derived auxin, produced *de novo* at the SAM

by PsYUC1, participates in the regulation of the pea leaf plastochron/phyllotaxis, or the time interval at which novel leaf primordia are initiated. Clearly, a tight spatiotemporal control of auxin content at a cellular level is required for novel lateral organ initiation and development to occur.

4.4.3. Reproductive traits of *crd* mutants

Flowers are often referred to as specialised shoots with modified leaves (Ditta et al., 2004; Honma and Goto, 2001). The genetic and molecular machinery of the two developmental programmes may have parallels but they do however rely on diversified regulatory networks (Deb et al., 2018). Indeed, in the *crd* mutants, flower development was affected somewhat differently when compared to that of the compound leaves. The first flower emerging from each peduncle was always present and, similarly to the leaves, had missing or deformed organs (Figure 4.18 and 4.19). However, flower initiation did not appear to be affected in the mutants. Potentially, once the shoot transitioned to the flowering phase, flowers continued to be initiated until a certain number of seeds were successfully fertilised (J.J. Ross, pers. comm.).

Flower phenotypes were previously reported to occur in *Arabidopsis* and petunia *yuc* mutants (Cheng et al., 2006; Tobeña-Santamaria et al., 2002). It appears that a critical level of *de novo* auxin is required for floral organs to be determined in a normal way. Indeed, it was previously demonstrated that the *YUC* genes belonging to the YUC1 clade were not ubiquitously expressed in *Arabidopsis* floral organs but were expressed in a temporal and spatial fashion (Cheng et al., 2006). *YUC1* and *YUC4::GUS* lines were mainly active at the apical meristem and in flower primordia. *YUC2* and *YUC6* were active later in the young flower buds with *YUC2::GUS* principally staining the gynoecium and *YUC6::GUS*, the stamen and pollen (Cheng et al., 2006).

The order of organ initiation ascribed to the classical ABCE model of floral organ identity does not necessarily apply in Medicago and pea (Benlloch et al., 2003; Tucker, 2003). A common flower primordium develops, then, in a unidirectional

fashion starting at the abaxial side, sepal primordia are formed followed by the development of two simultaneous primordia: a common primordium that will subsequently differentiate into petals and anthers and the carpel primordium (Tucker, 1989). In line with the petunia *fzy* mutant (Tobeña-Santamaria et al., 2002), the floral defects found in the *crd* mutants were more pronounced and principally affected the three outer whorls indicating that the A and B function genes of pea require auxin produced by PsYUC1.

The carpel of the *crd-4* mutant, on the other hand, only rarely exhibited abnormal phenotypes (Figure 4.19j) despite its primordium being initiated at the same time as the primordia of the abnormally developing petal and anther. This suggests that the C, D and E function genes of pea, such as PsCam038811, an orthologue of the *Arabidopsis AGAMOUS* gene (At4g18960), are not under the same control as the A and B class genes. Most likely, MADS box transcription factors regulating pea gynoecium initiation and differentiation are regulated by other *YUC* genes, as alluded to from *Arabidopsis* by Cheng and colleagues (2006). Hypothetically, auxin from a different biosynthetic pathway may be active in the carpel or other hormones, such as cytokinin, demonstrated to interact with auxin during gynoecium development, may possibly up-regulate the PIN proteins, increasing auxin transport in these tissues (Reyes-Olalde et al., 2017; Zúñiga-Mayo et al., 2014).

Of further interest, the second flower, almost always present in the WT, was mostly absent in the *crd* mutants. On the rare occasion that one was produced, the level of deformities and missing organs was striking, with severe organ identity and placement defects (Figure 4.18). This result alludes to the possibilities that IPyA-derived auxin carries greater influence on the developmental module of second flowers.

The *DR5::GUS* auxin reporter activity in the developing flower clusters of *crd-4* mutant and WT behaved similarly to that of the leaflets (Figure 4.26). GUS staining was weak in the mutant when compared with the WT. However, auxin content was not significantly different in the two genotypes but, as seen in the root tissues and in the apical portion, IAAsp was decreased (Figure 4.29). The decrease in IAAsp content could be the result of a lower rate of conjugation in the mutant.

Indeed, in a recessive *gh3* mutant, *weis1*, levels of several amide-linked conjugates were reduced while the activity of an auxin-reporter was increased, indicating that IAA inactivation, mediated by the GH3s, participates in the modulation of IAA pool and by extension, auxin homeostasis (Park et al., 2007).

4.4.4. GA does not appear to contribute to the *crd* phenotypes

Decreased gibberellin content is known to have detrimental impacts on shoot growth (Ross et al., 1989). To test whether the GA biosynthesis disruptions found in the *crd* mutants dwarf backgrounds contributed to the *crd* shoot phenotypes, the *crd-4* mutation was carried onto a tall background (*LE*). Phenotypic characterisation of the tall *crd-4* mutant revealed that GA had no effects on the monitored phenotypes. Indeed, all the phenotypes present on the dwarf backgrounds were also present in the tall mutant and the severity was of a similar extent. These results indicate that *PsYUC1* and auxin derived from the IPyA pathway are required for normal shoot development in pea and that disruptions in the auxin biosynthesis *PsYUC1* gene were solely responsible for the phenotypes.

Furthermore, the *lh-2* mutant did not exhibit the majority of the *crd-4* shoot phenotypes monitored, indicating that gibberellin does not mediate the effects of the *crd* mutations. Indeed, leaflet venation pattern, leaf morphology and turgor, leaflet placement and number per leaf, ontogenetic phase transitions, and rate of node formation were not affected in the GA mutant.

As expected, overall stem length was decreased in the *lh-2* mutant but the reduced stem height was driven by the markedly shorter internodes while in the *crd-4* mutant, the rate of node formation was the main driver. This evidence further supports a role for *PsYUC1* in localised auxin production. Indeed, in decapitation experiments, polar transport of auxin from the apical portion to the elongating stem was demonstrated to modulate GA biosynthesis. In decapitated plants, the low stem auxin content led to low GA levels and decreased internode length (Ross et al., 2000). In the tall *crd-4* mutant however, internode length was not reduced despite the lower auxin content in the apical portion indicating that the auxin pool produced

by *PsYUC1* may be destined for a local sink, such as lateral organ formation, and is not destined for transport to the subtending stem. The results further suggest that auxin produced by PsYUCs other than PsYUC1, is sufficient to sustain normal internode elongation.

Indeed, the SAM is generally compartmentalised into three zones: an outer layer called the tunica, an internal and central zone (CZ) and sandwiched between the two, an actively growing and dividing peripheral zone (PZ) (Reddy et al., 2004; Sassi and Vernoux, 2013). New primordia arise from the PZ and once a small number of cells are formed, a cell boundary develops, separating the emerging primordia from the rest of the shoot tissue (Gaillochet et al., 2015; Reddy and Meyerowitz, 2005). It is in this zone that *LFY*, the *Arabidopsis* homologue of *UNI* (mentioned in the Introduction) is active (Li et al., 2013; Weigel et al., 1992). Indeed, the establishment of regulatory networks within the newly formed primordia will eventually generate novel lateral organs such as leaves and flowers (Galli and Gallavotti, 2016). *PsYUC1* may participate by synthetising a local auxin pool required for the formation of the organs.

In addition, fewer pods were produced by the *lh-2* mutant when compared with the WT and the *crd-4* mutant (Figure 4.22), while both mutants produced fewer seeds per pod when compared with the WT. A link between seeds and pod growth has been demonstrated in pea (Ozga et al., 1992). Auxin originating from the seeds, is thought to be required for pod growth (Ozga and Reinecke, 1999; Reinecke et al., 1999). Interestingly, while seed yield was affected, mature seed phenotype was unchanged with mutant seeds resembling WT (Figure 4.24).

4.4.5. The *crd-4* mutation is as detrimental as the loss-of-function *crd-3*

The molecular bases of the mutations of the three *crd* mutants used for the phenotypic characterization in this chapter were varied. The *crd-3* mutant is considered a null allele with *PsYUC1* being deleted from the genome, the *crd-1* allele has a point mutation in an important catalytic region of the protein while the

crd-4 mutant impacts the sequence at the C-terminal end of the enzyme, a region with no defined function. The *crd1* and the *crd-4* mutants could potentially be leaky alleles with some enzymatic functionality remaining. However, the phenotypes exhibited by the *crd* mutants were consistent across the three alleles monitored, suggesting that any disruption to the protein is detrimental. Despite the alteration occurring late in *crd-4* sequence, the impact of this mutation on growth and development was substantial. Indeed, lateral root development, node initiation, leaf vasculature and leaflet and flower development were affected to a comparable extent as in the *crd-3* null mutant.

It was previously proposed that defects occurring in areas with no essential catalytic roles may not have an impact on the phenotypes of an affected individual (Hou et al., 2011). However, a *YUC1* mutant allele of maize (*spi1-ref*), with disruptions in a similar location to that of the *crd-4* mutant, had strong vegetative and reproductive phenotypes (Gallavotti et al., 2008). This clearly indicates that the C-terminal region of YUC FMOs is required to the proper functioning of the enzyme.

In Conclusion

The phenotypic characterisation of the *crd* mutant alleles demonstrated that auxin derived from the IPyA pathway does participate in several developmental processes. Disrupting *PsYUC1* delivered a broad range of phenotypes affecting the root system, the shoot and the reproductive organs. Nevertheless, a theme emerged with parallels across the various organs and tissues affected: *PsYUC1* appears to principally participate in lateral organ formation, potentially affecting initiation at the meristematic stage, organ specification or differentiation in the primordial cells and, in some instances, growth. *In situ* hybridisation with an anti-*PsYUC1* probe (or a reporter) could be used to test and demonstrate whether *PsYUC1* is indeed active early on in the SAM.

Auxin activity was reduced in the monitored tissues of the *crd-4* mutant as was IAA content in the apical portion. In the roots and in the young flowers however, IAA levels remained unchanged. Either levels were unchanged as these tissues had

already developed beyond the meristematic and primordia stages or functional redundancy amongst some of the *YUC*s compensated for the disrupted *PsYUC1*. However, IAAsp was reduced indicating that IAA conjugation was altered in *crd-4*. The auxin reporter construct used confirmed that despite IAA content remaining somewhat normal, auxin signalling activity was reduced, suggesting that auxin-inducible gene transcription was also down, including *GH3* activity. Potentially, a lower rate of auxin conjugation in the *crd* mutants permitted IAA levels to be sustained at an optimal level in the affected tissues.

Indeed, auxin homeostasis must be spatially and temporally modulated for developmental processes to occur and for the auxin response to adequately reflect internal and external cues. As auxin is required at different concentrations at different times and in different cells and tissues to elicit the required physiological and morphological responses, metabolism was proposed as an essential regulatory layer for the optimization of auxin gradients at a cellular and tissue level (Ljung, 2013; Stepanova and Alonso, 2016).

Chapter 5 - Inquiries into IAA inactivation in pea and the effects of IPyA breakdown

5.1. Introduction

In Chapter 4, an interesting but counter-intuitive phenomenon was clearly displayed: a decoupling of the phenotype from the auxin content in the *crispoid* mutants. Indeed, if a disruption to IAA biosynthesis is the main driver of the *crd* phenotype exhibited in a range of tissues/organs, then IAA content would be expected to be reduced in the same tissues. However, this was not consistently the case, especially in roots and flowers. This indicates that other mechanisms are participating in cellular auxin dynamics.

The optimisation of active auxin content at a cellular level is critical for the regulation of a plethora of developmental processes (reviewed in Ljung, 2013). As described earlier, biosynthesis, transport, perception, signalling and metabolism all play a part in the maintenance of auxin homeostasis. With the *crd* mutants, IAAsp quantification suggested that auxin conjugation may participate in the maintenance of IAA homeostasis in the affected tissues. An important focus of this chapter will therefore be on aspects of auxin metabolism, within the *crd* context.

5.1.1. Auxin metabolism: making IAA inactive

Auxin content can be increased in a cell through *de novo* synthesis and/or active transport if higher concentrations are required. The auxin content must also be reduced in several instances. For example, auxin minima were reported to be essential for axillary meristem formation during vegetative development in *Arabidopsis* and tomato (Qi et al., 2014; Wang et al., 2014). In both instances,

auxin contents were experimentally manipulated. Auxin depletion was prevented by blocking polar auxin transport with the auxin transport inhibitor, NPA, and auxin was made to accumulate by repressing auxin signalling or up-regulating auxin biosynthesis. These experiments demonstrated that low auxin content is important for certain developmental processes.

Auxin depletion is also necessary to 'recalibrate' a specific cell or tissue/organ so that it may become responsive to the next stimulus. This concept is referred to as signal attenuation (Peer, 2013). Again, auxin can be actively transported out by membrane carriers (reviewed in Friml, 2003). However, mechanisms of auxin inactivation/deactivation have been proposed to impart an extra layer for the regulation of homeostasis, delivering a rapid response in a cellular context. In addition, auxin inactivation would attenuate any developmental process occurring in the specific cell/tissue and would not increase the auxin signal in neighbouring cells as active transport might (Peer et al., 2013). Furthermore, auxin inactivation has been proposed as a mechanism preventing excess active auxin from exerting toxicity, as seen with high applications of exogenous auxin (Woodward and Bartel, 2005).

Several pathways inactivate IAA and numerous modified IAA forms exist in plants (See Figure 1.2). In *Arabidopsis*, IAA can be methylated by the IAA carboxylmethyl transferases 1 (IAMT1) protein (Qin et al., 2005) or oxidised by the IAA dioxygenases *DIOXYGENASE FOR AUXIN OXIDATION 1 (DAO1)* (Porco et al., 2016; Zhang et al., 2016). IAA can also be conjugated by the uridine diphosphate (UDP)-glucose transferases (UGT) (Jackson et al., 2001; Michalczuk and Bandurski, 1982) or by the acyl amido synthetases encoded by the *GRETCHEN HAGEN 3* (*GH3*) genes (Hagen et al., 1991). IAA inactivation can be temporary or irreversible, resulting in storage products, or catabolic/break-down products, respectively. The oxidation of IAA is an irreversible process but conjugate hydrolases were shown to have different amino acid specificities and were able to reverse certain conjugates back to active IAA (Staswick et al., 2005). Methylated auxin was reported to have potent auxinic effects but how and if the compound is reverted back to IAA is unknown (Qin et al., 2005).

5.1.2. IAA oxidation

IAA oxidation is a non-decarboxylative process in which a carbon atom of the indole ring is oxidised. When the second carbon is oxidised, IAA is irreversibly modified to 2-oxoindole-3-acetic acid (oxIAA) by the DAO1 enzymes. The oxIAA catabolite was proposed to be the major inactivation product of auxin in *Arabidopsis* (Mellor et al., 2016; Porco et al., 2016; Zhang et al., 2016). However, the loss-of-function *dao1-1* mutant was reported to exhibit only mild auxin-related developmental defects (Zhang et al., 2016; Porco et al., 2016), even though the oxidation of labelled IAA to labelled oxIAA was impaired. Interestingly, the expression of several of the *GH3* genes for IAA conjugation was up-regulated and the contents of certain conjugates had increased, suggesting that the IAA conjugation pathway can compensate, to some extent, for the disrupted *DAO1* activity in the mutant (Porco et al., 2016).

5.1.3. IAA conjugation

There are three main types of auxin conjugates: ester-linked, amide-linked and peptide- or protein-linked (reviewed in Ljung, 2013; Peer et al., 2013; Rosquete et al., 2012). In all instances, and unlike with oxidised IAA, the indole ring remains intact and an amino acid is conjugated to the hydroxide anion of the carboxymethyl group. There are numerous species of primary and secondary conjugates found in higher plants (reviewed in Peer, 2013). Primary conjugates are the product of a first modification and can be precursors of secondary conjugates if they undergo further modifications. Some primary conjugates were shown to be converted back to free IAA through the hydrolysis of the amino acid by hydrolytic enzymes such as the IAA amidohydrolases ILR1 and IAR3 (Bartel and Fink, 1995; Davies et al., 1999). However, the majority of conjugates are not considered hydrolysable and are thought of as catabolic in nature. Indeed, only a small fraction of all conjugates found in higher plants were reported to be reverted back to active IAA (reviewed in Ljung, 2013).

Ester-type conjugates, such as the primary IAA-glucose and secondary IAA-myo-inositol conjugates, are linked with sugars through the catalytic activity of UGT enzymes (Michalczuk and Bandurski, 1982). Ester-linked conjugates were mainly detected and quantified from the seeds of few species, including maize, Scots pine and *Arabidopsis* (Ljung et al., 2001; Ludwig-Muller, 2011). The two compounds were reported to hydrolyse back to active IAA in maize tissue, suggesting their potential as a storage form and contribution to the IAA pool (Jakubowska and Kowalczyk, 2005).

Amide-type conjugates are the predominant form of conjugates found in plants. Some were reported as reversible and proposed to act as storage forms for IAA (reviewed in Ludwig-Muller, 2011). These conjugates, such as IAA-Leucine (IALeu) and IAA-Alanine (IAAla), can be converted back to the active form of IAA by having the amino acid removed (Bartel and Fink., 1995; Davies et al., 1999). However, most amide conjugates, such as IAA-Aspartate (IAAsp) and IAA-Glutamate (IAGlu), do not appear to be hydrolysed to bioactive IAA and are considered as catabolic products (reviewed in Ljung, 2013).

Pathways regulating the secondary modifications of primary inactivated forms of IAA still remain to be untangled and clarified. For instance, oxIAA-Glucose and oxIAA-Hexose are thought to be synthesized via glucosylation of oxIAA (Kai et al., 2007; Peer et al., 2013) and oxIAA-Aspartate (oxIAAsp) and oxIAA-Glutamate (oxIAGlu) were proposed to be products of further oxIAA degradation (Kai et al., 2007; Östin et al., 1998). However, oxIAA-aspartate (oxIAAsp) was also proposed to result from IAAsp being oxidised in a second step (Ljung et al., 2002; Tuominen et al., 1994), suggesting that a compound could potentially be the product of more than one inactivation pathway.

5.1.4. The *crd* case study

The apparent decoupling between phenotype and auxin content displayed by the *crd* mutants raises an interesting conundrum: why was the IAA content not reduced (or, in the apical portion, only mildly reduced) in tissues exhibiting strong phenotypes (Chapter 4; McAdam et al., 2017b). This disparity between the strong

morphological defects being exhibited and the lack of IAA content difference in *yuc* mutants in comparison to WT, has been highlighted previously (Won et al., 2011). Redundancy amongst the *YUC* genes was proposed as an explanation (Won et al., 2011). The phenomenon of functional redundancy is indeed a prevalent one in developmental biology and can often explain the lack of phenotypes in single mutants (Cheng et al., 2006, 2007; Stepanova et al., 2008). However, how could the *crd* phenotypes be so severe if other PsYUCs maintained IAA content by compensating for the disrupted PsYUC1?

Two propositions that could potentially explain the *crd* phenotype/auxin content decoupling are put forward and tested. As demonstrated in Chapter 4, IAAsp was detected in all tissues tested in both the WTs and the mutants and was present at particularly high concentrations in the apical portion and in the flower of pea. However, the *crd* mutants had decreased IAAsp content in all tissues tested when compared with WTs. It was previously suggested that IAAsp promotes growth in pea. Indeed, root length was reportedly increased with the application of IAAsp (Ostrowski et al., 2016). However, much of the literature states that IAAsp is an irreversible conjugate of IAA in *Arabidopsis* (reviewed in Ljung, 2013). The proposition that IAAsp itself has biological activity in pea must be tested to ascertain that the decreased levels of the conjugate did not impact on and alter the development of the *crd* mutants. In this scenario, the *crd* phenotypes would be a direct result of the low levels of IAAsp and therefore an indirect result of the mutations of *PsYUC1*.

The influence of the degradation of unstable IAA intermediates is another plausible explanation for the phenotype/auxin-content decoupling. The intermediate IPyA is a labile compound known for its instability in aqueous solution and nonenzymatic breakdown to IAA (Dai et al., 2013; Tam and Normanly, 1998). It was previously suggested that the breakdown of IPyA to IAA post-extraction in *Arabidopsis* may boost the IAA content in the higher-order *yuc* mutants and give inflated results. This would lead to results not accurately reflecting *in vivo* IAA biological content (Won et al., 2011). Indeed, IPyA was found at higher concentrations in an *Arabidopsis* triple *yuc* mutant (compared with the WT), and the breakdown of the higher content of IPyA in the mutant was suggested to ‘even-out’ IAA content post-

extraction (Won et al., 2011). This proposition clearly needs to be tested in the *crd* mutants.

5.1.5. Aims

As demonstrated in Chapter 4, the *PsYUC1* disruptions had strong effects on morphology but did not appear to consistently affect IAA content in the mutants when compared with WTs. IAAsp contents were, however, affected in all tissues tested. This raises interesting questions relating to auxin action and homeostasis. However, is IAAsp the main conjugation product in pea, or is oxIAA prevalent in pea as reported for *Arabidopsis*? Is IAAsp further converted to oxIAAsp? Or is it active *per se* in pea, explaining in part the lack of IAA reductions in *crd* tissues with strong phenotypes? Does the IPyA non-enzymatic breakdown contribute to the IAA pool and do *crd* mutants accumulate IPyA, possibly providing an explanation for the phenotype/IAA content decoupling.

Firstly, the presence and prevalence of oxIAA will be tested in the pea system. In 2016, three papers demonstrated the importance of the oxidation pathway in *Arabidopsis* with oxIAA being the main IAA inactivation product (Mellor et al., 2016; Porco et al., 2016; Zhang et al., 2016). In addition, oxIAAsp will be monitored in apical buds. In the pea system, it is theoretically possible that oxIAA is rapidly converted to oxIAAsp.

Secondly, the proposed biological properties of IAAsp on pea root elongation are tested in root growth assays. To do so, the effects of different concentrations of applied IAA and IAAsp will be quantified to compare their respective impacts on root elongation.

As IPyA is an unstable compound, its break-down post extraction may have inflated IAA content in the mutants. The use of a cysteamine-based derivatisation technique developed for *Arabidopsis* will be tested and optimised for the pea system. IPyA will be quantified and IAA content in derivatised and non-derivatised samples will be compared. Furthermore, antioxidants are often added to extraction buffers to

prevent the degradation of analytes. The effects of sodium diethyldithiocarbamate (DEDTCA) antioxidant on IPyA and IAA recovery will therefore be tested.

5.2. Materials and Methods

5.2.1. Chemicals

Standards utilised in this chapter included the precursor IPyA, the active hormone IAA (both from Sigma-Aldrich) and the three conjugates IAAsp (Angene Chemical), oxIAA (kindly provided by Prof. Karin Ljung) and oxIAAsp (synthesised for our research lab by Steve Abel, University of Tasmania). Labelled standards utilised were [$^{13}C_6$]-IAA (Cambridge Isotope Laboratories) and [^{15}N, $^{2}H_5$]-IAAsp (OlChemim).

5.2.2. Plant material

Apical portions from the tall (*LE, LH*) *cv*. Torsdag (line 107) were used for the detection and monitoring of IAA and its metabolites, to test derivatisation techniques and quantify the effects of stabilising labile IAA precursors. In addition, apical portions from the *crd-4* mutant, on the *cv*. Caméor background (McAdam et al., 2017b), the WT parental Caméor (line JI 3253) were used to test the effects of derivatisation in the mutant background. All plant material was grown as described in Chapter 2.

Caméor was used for all root growth assays. In this instance, seeds were nicked, treated with fungicide and germinated communally in potting soil in growth cabinets at 20ºC with a 16 h photoperiod. After 48 hours, the germinating seeds were dug out gently and seedlings were photographed for measurements. Seedlings were then transplanted individually in 50 ml falcon tubes containing potting soil and with holes at the base to allow flow-through. Hormone treatments began from this point onwards.

5.2.3. Growth assays

Growth assays were conducted twice to ascertain the replicability of the results. As mentioned above, once seeds had germinated, pre-treatment measurements of the roots were recorded, and seedlings were allotted to specific treatments: control, 1 µM of IAA, 5 µM of IAA, 5 µM of IAAsp and 100 µM of IAAsp, n=10 for each treatment. Standards in powder form were first suspended in 1 ml of ethanol which was then diluted in 500 ml of Milli-Q grade water. Each seedling was drenched twice, as previously described (Pěnčík et al., 2013; Quittenden et al., 2014) with the solution corresponding to their respective treatment (a total of 40 ml each) and kept in growth cabinet under the same growing conditions.

After seven days of growth in the dark, once all the seedlings had emerged and apical hooks still displayed a level of curvature, seedlings were harvested and photographed for measurements. All root measurements were conducted using the Java-based image processing and analysing programme ImageJ (imagej.nih.gov/ij/). Root length were measured from the tip to the area where the radicle had emerged from the seed (the hilum/the micropyle) following all contours. Pre-treatment measurements were subtracted from post-measurements for each sample to obtain a representation of root growth attained under treatment. Data were analysed using Student's t-tests.

5.2.4. Derivatisation and hormone extraction

Derivatisation and extraction techniques previously described in Chapter 4 (Novák et al., 2012; Novák et al., 2017) were used to stabilise labile compounds and to extract metabolites. IAA, IAAsp, oxIAA and oxIAAsp were qualitatively monitored from Torsdag (line 107) apical portions. Unlabelled standards of the three conjugates were analysed alongside the biological samples to establish that the correct signals and transitions were monitored.

Furthermore, to assess the impacts of derivatisation on IAA quantification and the effects of adding antioxidant to the derivatisation buffer on the stabilisation of labile precursors, biological samples (Torsdag apical portions) were split into several

aliquots, grouped under certain 'conditions', becoming in effect, technical replicates (Figure 5.1). Labelled [$^{13}C_6$]-IAA and [^{15}N, $^{2}H_5$]-IAAsp were used when required to quantify IAA and IAAsp, while standard curves of IPyA-TAZ were used for quantification of IPyA.

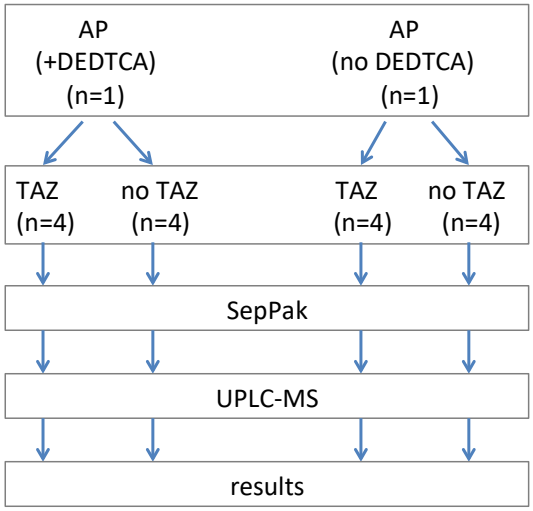

Figure 5.1. Example of the procedure used to derivatise samples and test a range of 'conditions'. On the left, one biological sample (AP=apical portion ~120mg) contains antioxidant in the extraction buffer (DEDTCA), was split into eight aliquots, four of which were derivatised and four that were not.

It is important to note that once all samples were processed, non-derivatised samples were not reintroduced to the derivatised samples as was performed by Novák and colleagues (2012; 2017). In all hormone quantification experiments that follow, IAA was quantified from both derivatised and non-derivatised samples, to enable the comparison of the resuts obtained from both 'conditions/treatments'.

5.2.5. UPLC-MS

Samples were analyzed using a Waters Acquity H-Class UPLC instrument as described in Chapter 4. Two UPLC programs were used to separate the metabolites

of interest, the 'PA Method' (Cook et al., 2016) and the 'IAAsp-Slow Method' described in Chapter 4.

The mass spectrometer was operated in positive and negative ion electrospray mode (Table 5.1) with a needle voltage of 2.8 kV, and multiple reaction monitoring (MRM) was used to detect all analytes.

Analytes levels were calculated as described in Chapter 2.

Table 5.1. MRM transitions, approximate retention time and voltage used to qualify and quantify IAA, precursors and metabolites.

ESI Mode	Analyte	Precursor	Product	Approx retention time (min)
+	Indole-3-acetic acid (IAA)	176.1	130.1	4.6
+	$^{13}C_6$ IAA	182.1	136.1	4.6
-	Indole-3-acetyl-L-aspartic acid (IAAsp)	289.2	132.1/174.1	3.3
-	D5 IAAsp	294.2	132.1	3.3
-	D6 & 13C6 IAAsp	295.2	132.1	3.3
-	13C6 IAAsp	295.2	180.1	3.3
-	D5 15N IAAsp 1	295.2	133.1	3.3
-	D5 15N IAAsp 2	295.2	134.1	3.3
+	Indole-3-pyruvate (IPyA)	204.2	130.1/158.1	7.8
+	IPyA-TAZ	263.1	88.0/132.1	2.6
+	Oxindole-3-acetic acid (oxIAA)	192	132/146	3.2
+	oxindole-3-acetyl-N-aspartic acid (oxIAAsp)	305	146/189	1.9

5.3. Results

5.3.1. IAA oxidation does not appear to be active in the apical portion of pea

As demonstrated in Chapter 4, IAAsp was present in the roots, the apical portions and the flowers of pea. To investigate whether oxIAA is a catabolic product of pea, oxIAA, IAAsp and IAA were monitored in actively developing apical buds of Torsdag seedlings. In addition, oxIAAsp was also monitored as it was proposed to be a secondary catabolite resulting from the oxidation of IAAsp and/or further modification of oxIAA (Ljung et al., 2002; Pěnčík et al., 2013). To do so, oxIAAsp was synthesised and a spectrum of the standard was determined (Figure 5.2). The full scan spectrum from m/z 50 to 400 yielded a molecular ion at m/z 305. The synthesised oxIAAsp yielded a racemic mixture of R- and S- diastereomers that could be separated in the standard with an 80% baseline resolution using the 'IAAsp Slow method'. The two diastereomers could also be analysed as a combined coeluted peak under the 'PA method' described in Chapter 4.

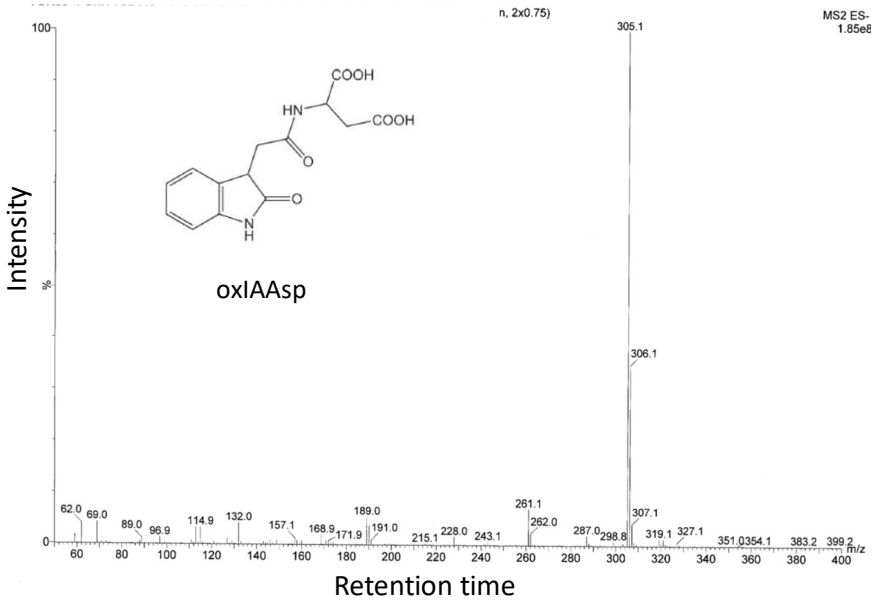

Figure 5.2. Full scan mass spectrum of the synthesised oxIAAsp.

IAA and IAAsp were detected in the apical portion of WT pea but interestingly, oxIAA and oxIAAsp were not (Figure 5.3).

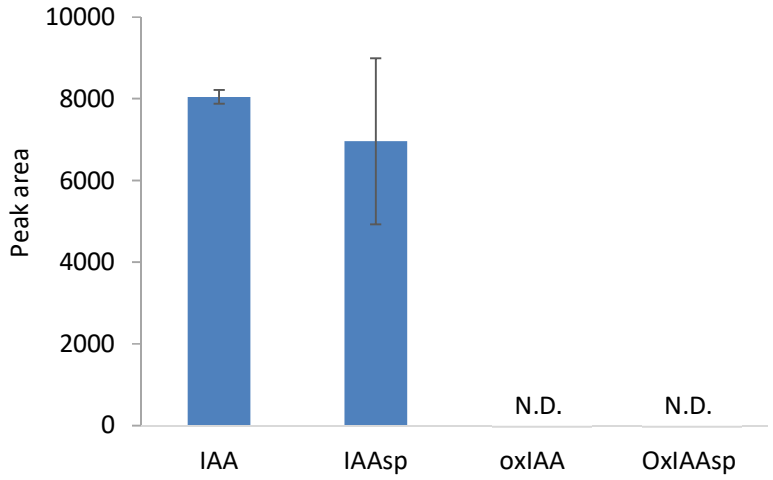

Figure 5.3. Peak areas of IAA and conjugates in apical portions. a) IAA and IAAsp were detected but oxIAA and oxIAAsp were not (n=4). N.D.=not detected. Y axis represents the mean (±S.E.) of the raw data from the peak areas.

No relevant peaks were detected under MRM monitoring of precursors and products for both oxIAA and oxIAAsp while IAAsp was clearly and unequivocally present in the samples (Figure 5.4).

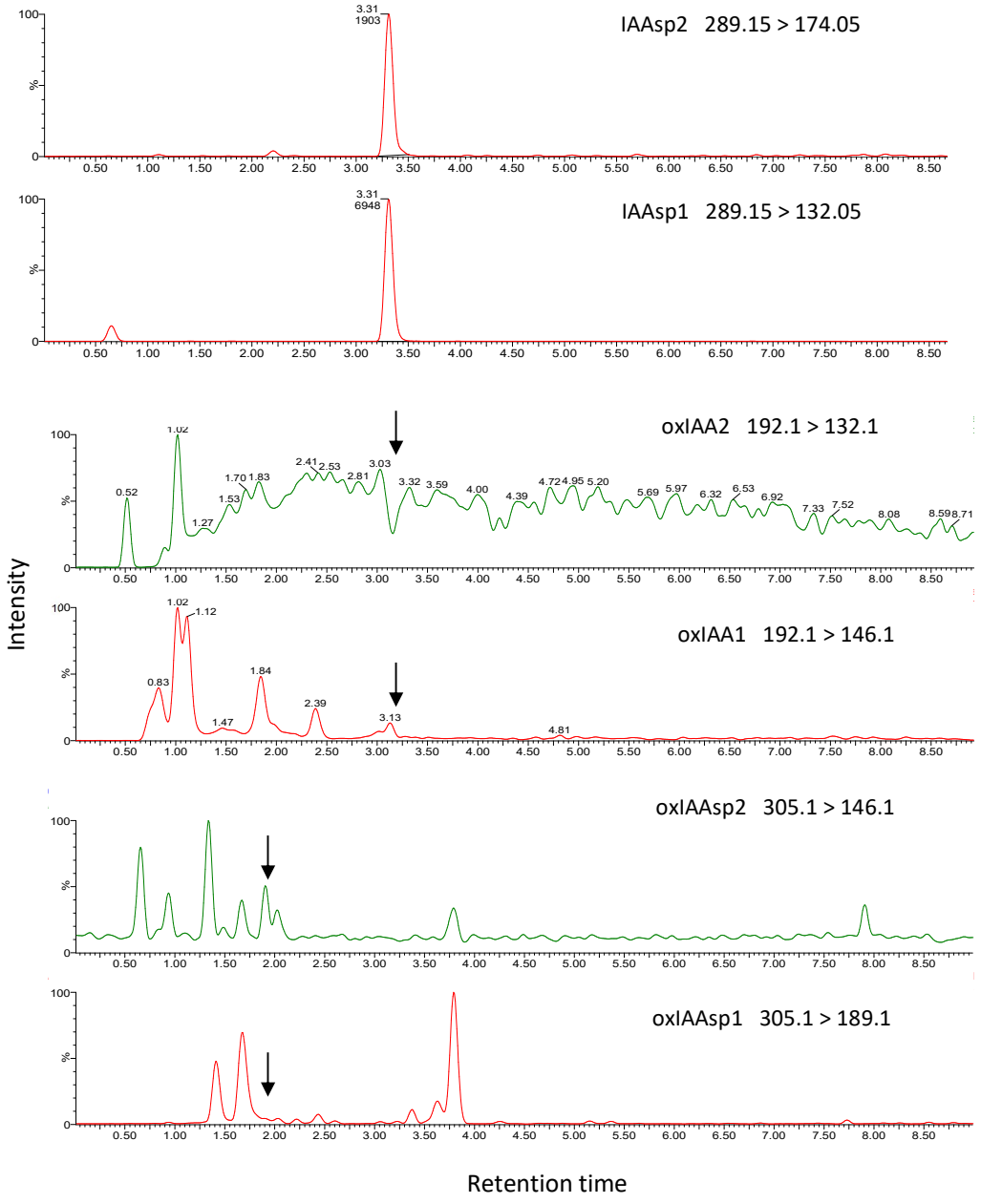

Figure 5.4. Representative MRM chromatograms of IAAsp, oxIAA and oxIAAsp from apical portion of WT pea. Black arrows are located at retention times (RT) where catabolite peaks were expected to elute.

To ascertain the UPLC-MS protocol employed could detect the compounds, samples were 'spiked' with oxIAA and oxIAAsp standards. To do so, small amounts of diluted standards were injected in the UPLC column with the biological samples prior to entering the UPLC column. The two standards were detected in 'spiked' samples with strong and clear peaks. oxIAA eluted approximately at 3.22 minutes and oxIAAsp, at 1.93 minutes (Figure 5.5) confirming that the protocol used was suitable for the detection of the two analytes. The results indicated that that endogenous oxIAA and oxIAAsp were not present in the apical portion of pea. Results further suggested that IAAsp was not oxidised to oxIAAsp in pea shoot apices, or that IAAsp may not be further broken-down in this tissue. Figure 5.5c depicts the approximate times at which the analytes eluted at under the 'PA' method.

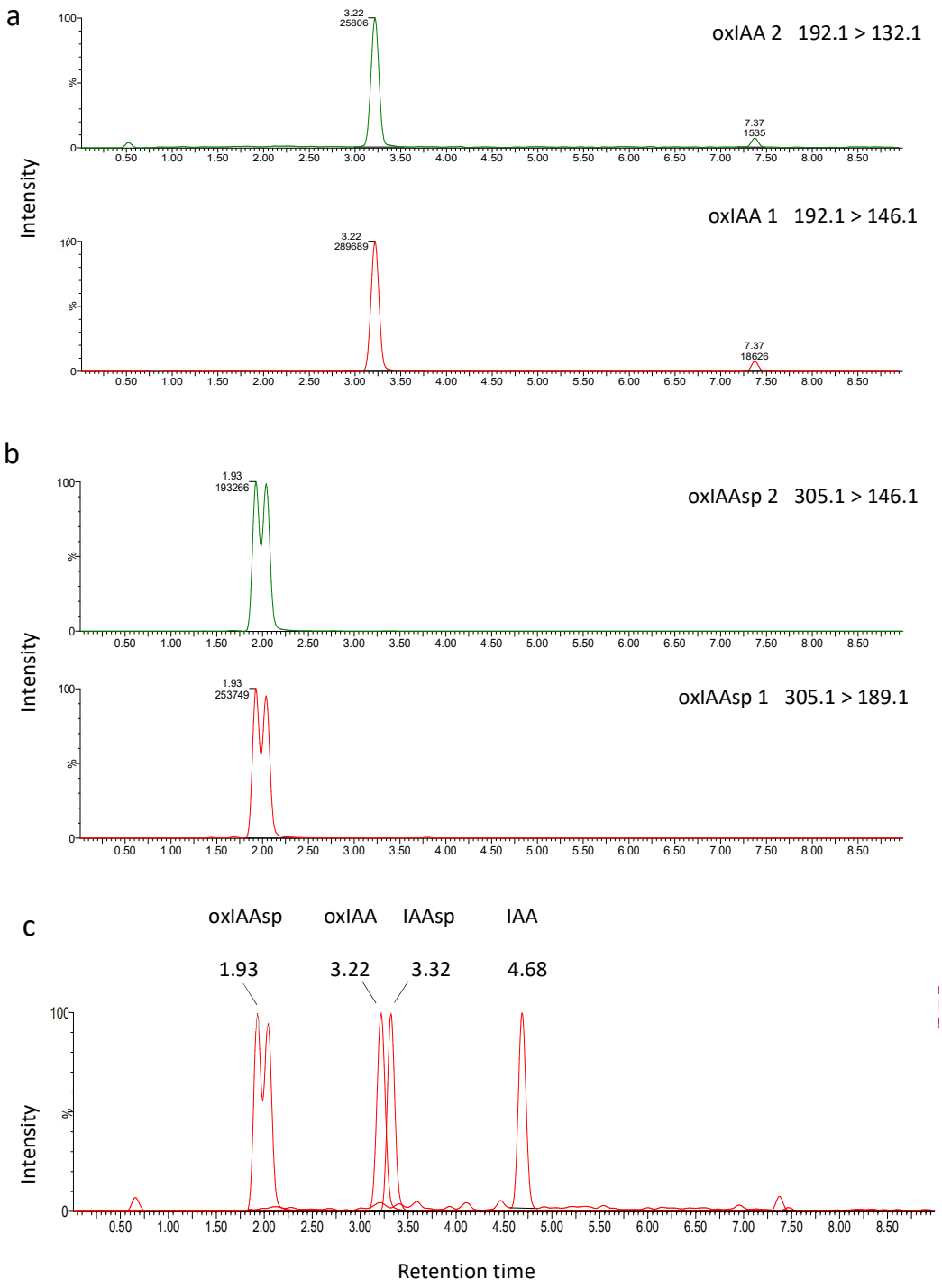

Figure 5.5. IAA and metabolites approximate retention time. a) The oxIAA and b) oxIAAsp standards were detected in spiked samples. c) Representative UPLC-MS chromatograms of IAA, IAAsp, oxIAA and oxIAAsp. The peaks are presented in the order in which the compounds eluted. Note, oxIAAsp was recovered as a co-eluted peak under the UPLC-MS 'PA' method.

5.3.2. Applied IAAsp did not affect root length

IAAsp was suggested to act as a signalling molecule in pea based on its effects on root elongation (Ostrowski et al., 2016). As the *crd-3* mutant had a reduction of IAAsp in the actively growing root tips, the possibility that the lower content may affect root growth and length had to be considered. Using WT pea seeds, IAAsp and IAA were applied at two different concentrations during early seedling development to test their effects on the normal development of root growth. Both concentrations of IAA significantly reduced root length with the highest concentration having strong effects (n=10, 1µM, p=0.04 and 5 µM p=0.03). However, IAAsp applications did not alter root growth (Figure 5.6).

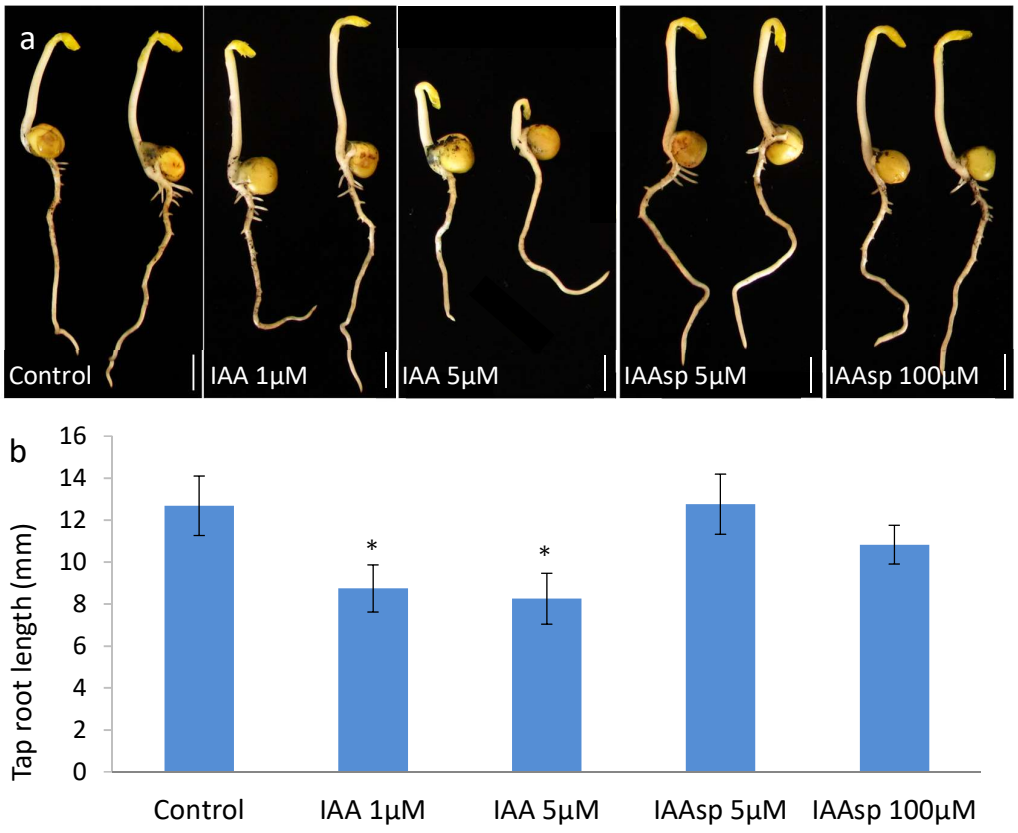

Figure 5.6. The effects of IAA and IAAsp application at different concentrations on pea root elongation. IAA application significantly decreased root growth when compared with control (1µM, p=0.04; 5 µM p=0.03; n=10). IAAsp treated roots were not reduced in length (n=10). Results are means ± S.E. and asterisks denote significant differences.

5.3.3. IPyA and/or IAAld contributes to the IAA pool post-extraction

IPyA is a labile compound that can break down nonenzymatically to IAA (Cooney and Nonhebel, 1989; Tam and Normanly, 1998). Using protocols described in Chapter 2, IPyA could not be detected (data not shown). It was therefore hypothesised that unless IPyA is stabilised, its degradation to IAA would prevent detection. Furthermore, the newly degraded IPyA would contribute, at least in part, to the IAA pool quantified in samples. This could potentially confound IAA quantification. A cysteamine-based derivatisation protocol developed for *Arabidopsis* (Novák et al., 2012; 2017) was optimised for the pea system and used to test the difference in IAA content between derivatised and non-derivatised samples. Apical portions from Torsdag were used for this purpose. The difference in IAA content between the derivatised and the non-derivatised samples was marked and substantial (Figure 5.7).

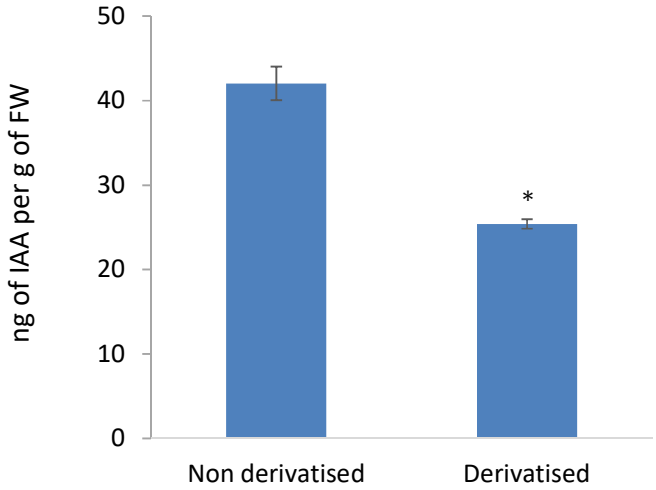

Figure 5.7. IAA content present in non-derivatised and derivatised aliquots from Torsdag apical portions. All samples are technical replicates originating from a single harvest. (n=4, p=0.0002). Results are means ± S.E. and asterisks denote significant differences.

However, despite clearly demonstrating the effect of derivatisation protocols on IAA quantification, the contribution of IPyA was unclear. The contribution of IPyA specifically was tested using technical replicates of IPyA standard; this experimentation clearly showed that underivatised IPyA can contribute to the IAA pool (Adj. Prof. J.J. Ross; unpublished).

Next, the possibility that GH3 enzymes may be active during extraction protocols was considered and tested. If this was the case, GH3 could potentially convert IAA to amide-linked conjugates post-harvest and reduce IAA content in biological samples. Labelled $^{13}C_6$ IAA was added to samples containing apical portions from Torsdag and its potential conversion to $^{13}C_6$ IAAsp was monitored. Labelled IAAsp was not detected indicating that GH3 enzymes were not active post-harvest in the sodium phosphate buffer and did not affect the IAA pool (data not presented).

5.3.4. The antioxidant effect on stabilising IPyA and/IAAld

Most extraction buffers contain antioxidants, principally to prevent the breakdown of compounds of interest during extraction and to a lesser extent, to increase the shelf-life of the buffer. To test if the DEDTCA antioxidant added to the sodium buffer had an effect in limiting the breakdown of IPyA in derivatised samples, IPyA standard was used. During the standard preparation (dissolving the standard, making serial dilutions, partitioning aliquots and adding cysteamine solution), a portion of the IPyA broke down to IAA. Indeed, IAA was recovered in samples whether they contained antioxidant or not (Figure 5.8). However, a smaller proportion of IAA was recovered from samples extracted in buffer with added DEDTCA (n=3, p=4.9E-05). This result indicates that IPyA starts to break down very shortly after being dissolved in aqueous solution.

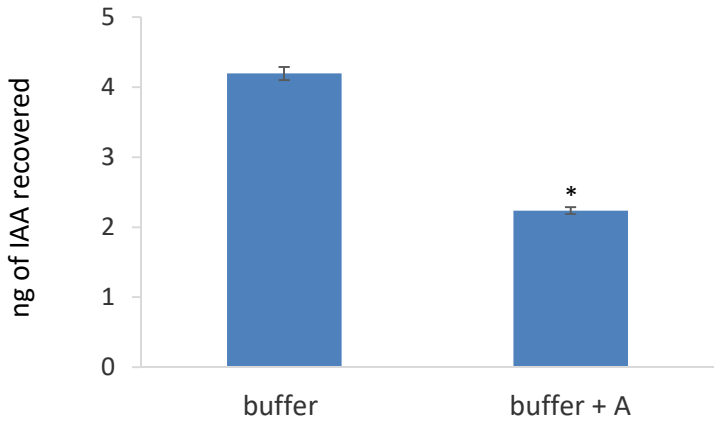

Figure 5.8. Antioxidant effect on IPyA breakdown and on IAA level recovery. Sodium phosphate extraction buffer with DEDTCA antioxidant (+A) and without (buffer). Results are means ± S.E. and asterisk denotes significant difference.

Next, similar conditions were tested using biological samples (Figure 5.9). Derivatised samples with and without antioxidant contained significantly lower IAA content (n=4, p=0.003 and p=0.001 respectively) when compared to non-derivatised samples. In addition, non-derivatised samples containing antioxidant also had a significantly lower content of IAA when compared with samples that were extracted without antioxidant (n=4, p=0.03). However, no difference in IAA content was detected between the two derivatised treatments, with and without antioxidant (n=4, p=0.07). Furthermore, IPyA-TAZ quantified in all treatments was not detected in non-derivatised samples (data not presented) but IPyA-TAZ was detected in derivatised samples, with and without DEDTCA (Figure 5.9). These results indicate that the DEDTCA antioxidant does stabilise the IPyA precursor to some extent, but that cysteamine-based derivatisation is a more powerful and efficient technique to prevent the degradation of IPyA. The results do not however exclude the possibility that the antioxidant may further prevent the break-down of labile compounds other than IPyA, such as IAAld.

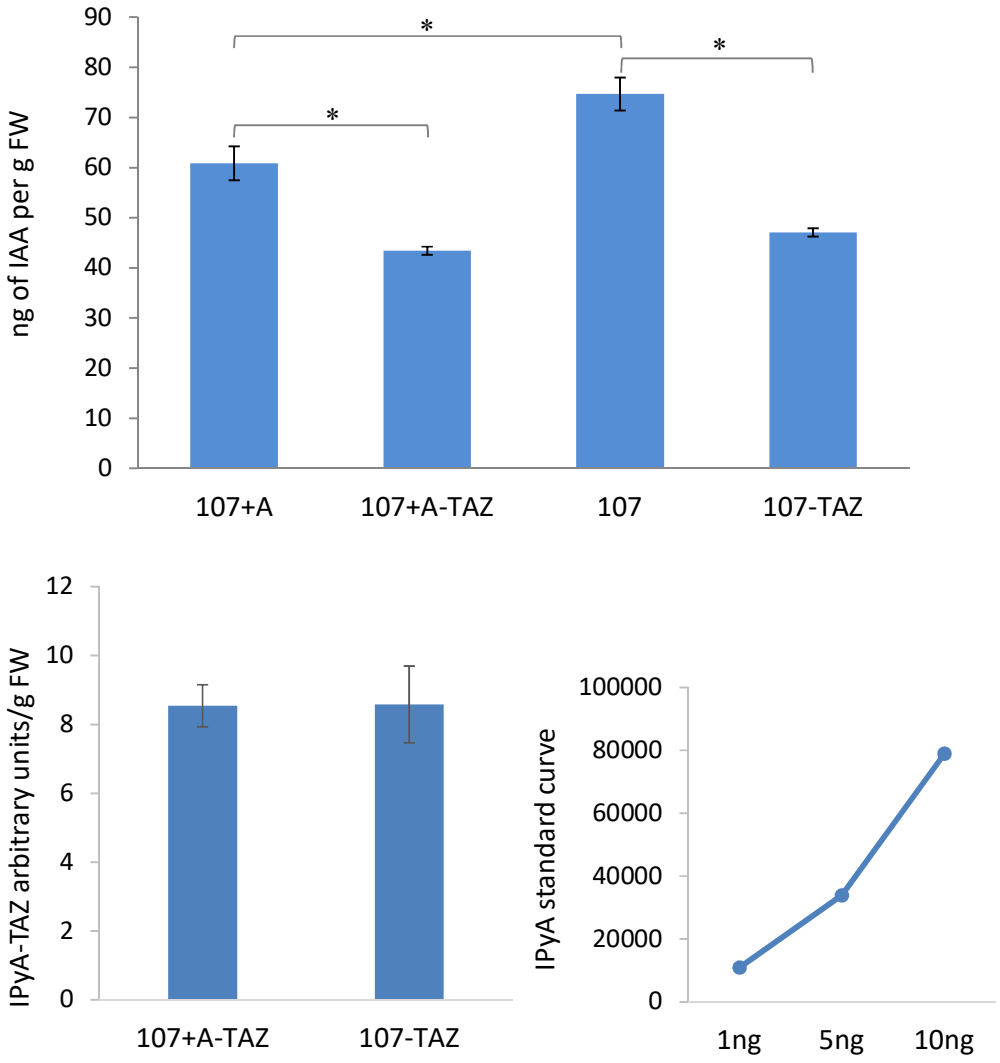

Figure 5.9. The effects of derivatisation and of antioxidant on IAA content. Top: IAA levels; see Figure 5.1 for the experimental design. Two biological replicates, then split into four technical replicates, were extracted from the WT line Torsdag (107). Samples (+A) contained the antioxidant DEDTCA during extraction and samples (-TAZ) were derivatised with cysteamine, (~12 mg, n=4). Bottom: IPyA-TAZ recovered in samples and IPyA standard curve. Results are means ± S.E. and asterisks denote significant differences.

5.3.5. Relative IAA content in *crd-4*

The present results clearly demonstrate that IPyA breaks down during the extraction protocol and contributes to the IAA pool. It was previously reported that the *yuc1*

yuc2 yuc6 mutant accumulated and contained approximately 30% more IPyA than the WT (Won et al., 2011). Won and colleagues (2011) proposed that the lack of reduction of IAA content quantified from *Arabidopsis* higher-order *yuc* mutants, may be due to a greater proportion of IPyA breaking down to IAA in the mutant. This proposition is indeed a plausible explanation. To test if this accumulation occurred in the pea *yuc* mutants, IPyA content was assessed by quantifying its thiazolidine derivative (IPyA-TAZ). However, no difference in IPyA-TAZ content was detected between the two genotypes (Figure 5.10). Surprisingly, the *crd-4* mutant did not accumulate IPyA in the apical portion. The results indicate that the breakdown of IPyA is not sufficient for the IAA contents of the *crd* mutant to reach parity with WT levels.

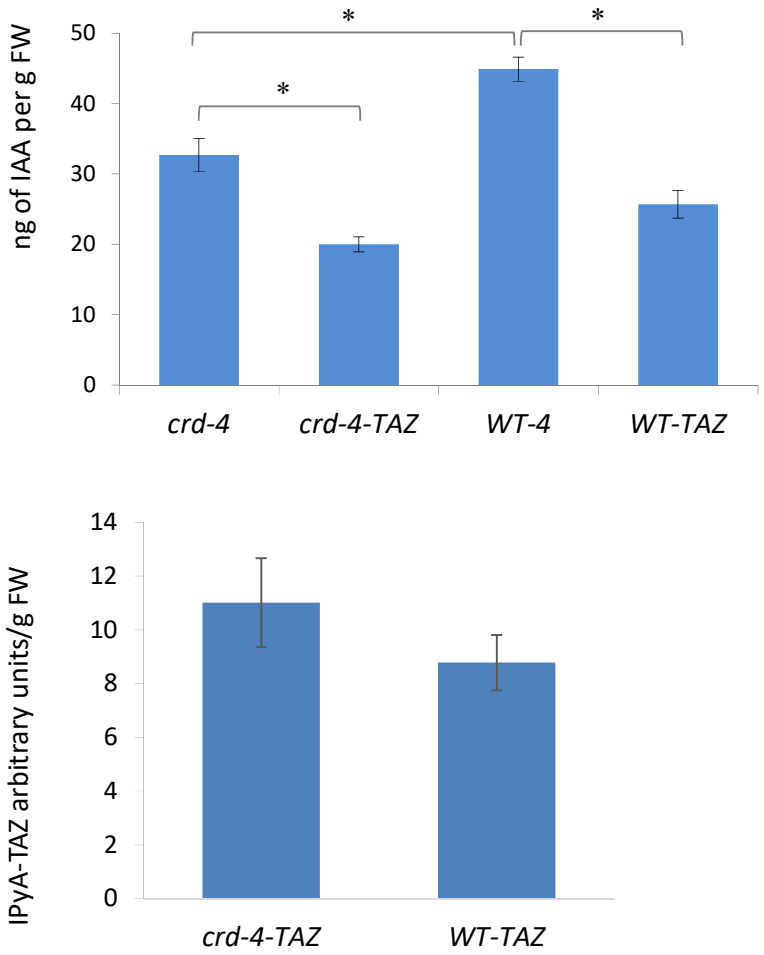

Figure 5.10. IAA and derivatised IPyA content from *crd-4* and co-segregating WT apical buds. a) IAA levels were reduced in the mutant when compared with the WT, regardless of derivatisation (~20 mg, n=5 biological replicates, underivatised: p=0.003 and derivatised: p=0.02), but b) there was no difference in IPyA-TAZ content. Results are means ± S.E. and asterisks denote significant differences.

Furthermore, and importantly to the *crd* context, the effect of the mutation on IAA content was not modified or lost through derivatisation. Indeed, in apical buds, significant but small reductions in IAA levels were obtained in the mutant, when compared with the WT, whether samples were derivatised or not.

5.4. Discussion

The modulation of IAA homeostasis is critical to plant growth and development. Numerous processes underpinning the complex molecular machinery are regulated by a suit of genes and pathways involved in biosynthesis, transport, perception and metabolism. In previous chapters, aspects of IAA biosynthesis were investigated. Some of the results highlighted the likely importance of IAA metabolism for the IPyA pathway and its translation to developmental output in pea. In this chapter, several facets relating to IAA metabolism were therefore investigated.

5.4.1. Evidence that oxIAA is not a catabolic product of IAA in pea apical buds

Labelling and metabolite quantification experiments revealed that the oxidation of IAA to oxIAA is an important mechanism controlling the inactivation of IAA in *Arabidopsis* (Östin et al., 1998; Pěnčík et al., 2013). Phenotypic characterisation of dioxygenase (*DAO*) mutants demonstrated the significance of IAA oxidation for the development and physiology of *Arabidopsis* (Porco et al., 2016; Zhang et al., 2016). Importantly, oxIAA, quantified from actively growing shoots of WT *Arabidopsis*, was reported to be present at higher concentration when compared to other quantified conjugates (Porco et al., 2016; Zhang et al., 2016). For example, the shoot contained approximately 100 picogram (pg) of oxIAA per mg of fresh weight (FW) compared to the negligible levels of IAAsp (0-2pg/mg FW) (Porco et al., 2016; Zhang et al., 2016). In this study, however, oxIAA, was not detected in the apical buds of WT pea plants (Figure 5.3).

MRM transitions monitored in the present metabolite quantification experiments were identical to those used for *Arabidopsis* (Novák et al, 2012; Porco et al., 2016; Zhang et al., 2016). Spiking of samples with standards confirmed that the transitions and retention times monitored were appropriate and relevant for the system used (Figure 5.4a). In this study, oxIAA eluted prior to IAAsp in pea (Figure 5.4c), unlike previously published metabolic profiling showing that oxIAA

eluted after IAAsp (Novák et al., 2012). Derivatisation and extraction protocols used in the present chapter were based on the Novák et al., (2012; 2017) protocol. The discrepancy in elution order may potentially be an UPLC-MS column effect.

If both plant models utilised similar IAA inactivation pathways, apical portions from pea should have contained some level of oxIAA. That oxIAA was not detected in apical portions suggests that IAA oxidation is not an important process in the pea system. Interestingly, a single *DAO* homologue is found in pea and was demonstrated to be mainly expressed in seeds and to some extent in pods (PsCam039164, the pea RNA-seq gene atlas, Alves-Carvalho et al., 2015) suggesting that this gene may be active in these tissues only. The absence of oxIAA in apical buds supports the GH3s as the major players regulating IAA metabolism in pea.

Potentially, the pea *DAO*-like expression may be up-regulated in a scenario where *GH3s* function is impaired. The opposite was demonstrated in the *Arabidopsis dao1-1* loss-of-function mutant. Indeed, the reduction of *DAO* activity in the mutant appeared to be compensated for by an up-regulation of the *GH3*s and a substantial increase in the contents of the IAAsp and IAGlu conjugates, ~280- and ~46- fold respectively (Porco et al., 2016).

To investigate the further catabolism of IAA, the presence of oxIAAsp was qualitatively monitored. Indeed, oxIAAsp was proposed as a secondary metabolite derived from oxIAA (Pěnčík et al., 2013). Possibly, oxIAA is a transient compound rapidly broken down to oxIAAsp in pea, which could explain why oxIAA was not detected. Though no evidence suggesting that the conversion occurs rapidly has been reported. IAAsp was also proposed as a precursor for oxIAA (Ljung et al., 2002). However, endogenous oxIAAsp was not detected in the apical portion of pea (Figure 5.3). The present results suggest two possibilities: 1) IAAsp may not be a precursor for oxIAAsp in pea apical buds (and potentially in other species). 2) oxIAA is likely the precursor for oxIAAsp but there was no evidence for this as the *DAO* pathway did not appear to be active in pea.

5.4.2. IAAsp did not alter root growth

IAAsp was detected in all tissue tested suggesting that this conjugate is prevalent throughout pea plants (Chapter 4 and Figure 5.3). IAAsp was previously proposed to promote root length in pea (Ostrowski et al., 2016) suggesting that IAAsp may itself carry a biological role in the pea system. If this was the case, IAAsp may be required for certain developmental processes to occur. The lower IAAsp content found in the *crd* mutants could potentially have detrimental effects on phenotypes. The proposition that IAAsp can influence root growth was tested by applying different concentrations of IAAsp standard to actively growing WT pea seedlings. No effects on root growth were detected, however (Figure 5.6). Roots drenched with IAAsp were of similar lengths to those of the controls. As expected, root length from the IAA treated seedlings was reduced, indicating that IAA but not IAAsp impacted root development. Thus, IAAsp does not appear to have bioactive properties participating in root elongation and is therefore unlikely responsible for the shorter lateral root length exhibited by the *crd* mutants. However, the hydrolysation of IAAsp to IAA remains to be tested in pea.

5.4.3. IPyA break down contributes to the IAA pool post-extraction

Some IAA precursors are described as labile compounds, such as IPyA and IAAld (Cooney and Nonhebel, 1989; Tam and Normanly, 1998). Indeed, small amounts of IPyA were converted nonenzymatically to IAA and indole-3-carboxaldehyde in *in vitro* assays (Tivendale et al., 2012). With minor modifications to the protocol developed by Novák and colleagues (2012), the thiazolidine derivatives of IPyA could be reliably monitored and quantified from ~12-25 mg of tissue (FW) using UPLC-MS techniques. As previously mentioned by Novák and colleagues (2012), tissue weights above 25 mg per samples gave poorer analyte recovery, potentially due to the matrix effect. Similar levels were previously reported from tomato shoot using pentafluorobenzyl oxime IPyA derivatives to stabilise the precursor (Cooney and Nonhebel, 1989).

The stabilisation of IPyA allowed a comparison of IAA content from both treatments: derivatised versus non-derivatised (Figure 5.7). The contribution of IPyA breakdown to the IAA pool was surprisingly high, up to 40% in some instances. These results highlight the importance of considering the impact of labile compounds when quantifying and interpreting results. Depending on the 'narrative' and the line of logic of a hypothesis or an experimental question, the contribution that labile compounds may have on the quantified levels of compounds of interest could render interpretations completely flawed and even misleading. It is suggested here that IAA quantification is best carried out after labile precursors are stabilised.

To test if stabilising IPyA also impacted IAA recovery in the *crd* mutants and to what extent, IAA and IPyA-TAZ were quantified from *crd-4* and WT apical portions. IPyA was clearly stabilised in both genotypes with IAA recovery being of smaller proportions in the derivatised samples when compared to non-derivatised samples (Figure 5.10). Surprisingly and unlike results reported from *Arabidopsis* (Won et al., 2011), IPyA-TAZ did not appear to accumulate in the *crd-4* mutant. However, results must be interpreted with caution; no labelled internal standard for IPyA or IPyA-TAZ were used for quantifications in the present experiment. All results were obtained utilising IPyA-TAZ standard curves. Nonetheless, the results indicate that in the *crd* mutants, the phenomenon of IPyA degradation, despite contributing to the IAA pool, most likely did not compensate and restore IAA content in the mutants to WT levels. IPyA non-enzymatic degradation post-extraction does not appear to be the cause of the *crd* phenotype/IAA content decoupling.

5.4.4. In conclusion

Considerable progress has been made in the isolation and the characterisation of the enzymes and the genes responsible for the inactivation of IAA and the hydrolysis of the storage species in *Arabidopsis* (reviewed in Ljung, 2013). However, several aspects relating to the interaction between pathways, modes of regulation and biochemistry remain to be clarified. The auxin catabolic/conjugation system in other species requires further investigation to establish whether gene function and

pathways are consistent amongst higher plants (Staswick et al., 2005). For instance, clear differences in the modes for IAA metabolism in pea were demonstrated in this chapter. Indeed, oxIAA and oxIAAsp were not detected in pea apical bud tissue, in contrast to *Arabidopsis*. Instead, IAAsp, and potentially other amide-linked conjugates, appear to predominate in pea. Interestingly, and again unlike results reported for in an *Arabidopsis* higher-order *YUC* mutant (Zhang et al., 2016), the *crd-4* pea mutant did not appear to contain higher levels of IPyA in the shoot when compared with WT.

Other biological processes at play may potentially explain the *crd* phenotype/IAA level decoupling. Based on phenotypic characterisation, *PsYUC1* appears to be a key player at the meristem and primordia level, both of which only involve a small number of cells (Grandjean et al., 2004). If auxin biosynthesis is disrupted in a small number of developmentally pivotal cells, the morphological repercussions may be considerable. Indeed, disruptions to embryo patterning in early developmental stages were shown to lead to morphological deformities (Robert et al., 2013).

Moreover, the quantification of IAA from typically (in this study) at least 20 mg of tissue is unlikely to be impacted if the vast majority of non-meristematic cells contained in the crude extract are not affected. In other words, the number of cells affected by the *Psyuc1* mutations would be disproportionate in comparison to those that are not. The *Psyuc1* effect could therefore be diluted to the extent that it is lost or not perceived. Quantifying and determining hormone profiles within single cells may be the only way to distinguish the impact of disrupting genes involved in the regulation of meristematic and organ initiation processes.

But, against this, is the fact that IAAsp content is typically reduced in *crd* mutants. If the *GH3*s were down-regulated in just a few meristematic or primordial cells with disrupted IAA biosynthesis, IAAsp levels would only be affected in those cells; its effect again, would be lost at the 20-30 mg scale of harvested tissue. This suggests that despite phenotypes being present most likely due to disruptions to IAA biosynthesis early in tissue/organ development and only in a few cells, another

phenomenon is modulating IAA and IAAsp content in fully developed tissues and organs.

Several auxin transporters have been reported to participate in intracellular compartmentalisation of IAA (Barbez and Kleine-Vehn, 2013; Barbez et al., 2012; Dal Bosco et al., 2012; Ding et al., 2012; Feraru et al., 2012; Mravec et al., 2009). PILS for example, are proposed to negatively impact the rate of auxin signalling in the nucleus by limiting the amount of auxin that enters the nucleus (Barbez et al., 2012). Much of the subcellular mechanisms and their biological functions remains to be determined but the possibility that these processes participate in auxin homeostasis is compelling.

Indeed, the endoplasmic reticulum (ER) has been proposed as a gateway to the nucleus (Middleton et al., 2018). Two processes working in concert, involving the ER and auxin carriers, may provide an explanation for the *crd* decoupling phenomenon. Firstly, if less IAA is actively transported by ER carriers into the nucleus of *crd* mutants, when compared with the WT, *GH3* transcription in the nucleus and GH3 amido synthetases activity in the cytosol would be down, resulting in a lower rate of IAA conjugation to IAAsp, preserving IAA in the mutant.

Secondly, in the *crd* mutants, IAA may be sequestered to the ER by the PILS (Barbez et al., 2012) and/or the ER-localised PINs (Mravec et al., 2009), again, preventing IAA from being conjugated by the GH3s in the cytosol. This would prevent the sequestered IAA from being inactivated and could theoretically conserve IAA in the cell. When taken together, these two processes could potentially maintain IAA to near WT levels in the *crd* mutants. Indeed, pathways and/or components, not characterised as of yet, as demonstrated by Middleton and colleagues (2018), may be involved in either the regulation of auxin sequestration to the ER or transport to the nucleus, for the optimisation of IAA homeostasis. Regardless of whether or not these explanations apply, the observations reported here are consistent with the theory that different subcellular compartments might contain different concentrations of auxin.

Chapter 6 – Concluding discussion

The IPyA pathway is now well established as the main route for IAA biosynthesis in a range of species (reviewed in Zhao, 2018). The *TAA1*/*TAR*s and the *YUC*s families are represented widely in angiosperms and encode the catalytic enzymes of this route (Stepanova et al., 2008; Tao et al., 2008; Won et al., 2011). However, as mentioned before, phenotypes exhibited by the available loss-of-function mutants differ substantially between species. Indeed, the single *taa1* mutant of *Arabidopsis* had no obvious phenotypes (Stepanova et al., 2008) while the maize *vt2*, a *TAA1* co-orthologue, had reduced leaf numbers, barren inflorescences and overall reduced cell elongation (Phillips et al., 2011). Similar patterns are observed in *yuc* mutants. Higher-order *yuc* mutants of *Arabidopsis* (Cheng et al., 2006) and *fzy* of petunia (Tobeña-Santamaria et al., 2002) had a branching phenotype while the maize *spi1* produced fewer branches (Gallavotti et al., 2008). These phenotypic juxtapositions indicate that significant diversification of gene/protein function exist across species.

The principal goal of this research was therefore to investigate the effects that mutations to IAA biosynthetic genes, belonging to the IPyA pathway, may have on pea morphology and IAA metabolism.

6.1.1. *PsTAR1* does not appear to be essential for early seed development

The aminotransferase PsTAR1 belongs to a family comprising three other members (Tivendale et al., 2012; the pea RNA-seq gene atlas). It was previously reported that both *PsTAR1* and *PsTAR2* were expressed during seed development with the expression profile of *PsTAR1* correlating with IAA content during the early stages and *PsTAR2* correlating with 4-Cl-IAA in the later stages (Tivendale et al., 2012). In Chapter 2, two *Pstar1* mutant alleles were successfully isolated and used for phenotypic analysis and auxin quantification. The results from the present mutant analysis did not correlate with gene expression profiles and indicated that *PsTAR1* is

not contributing significantly to the biosynthesis of *de novo* auxin or to the maintenance of adequate auxin content in young seeds. Indeed, IAA and 4-Cl-IAA contents, both auxins known to be required for pea seed development, did not vary in content between the *Pstar1-1* mutant and the WT. Furthermore, seed morphology, or any other parts of the plant, were not affected in the mutants.

These present findings do not however preclude a function for *PsTAR1* in early pea seed development. Indeed, *PsTAR1* may contribute to the IAA pool in WT plants while in the mutants, the removal of *PsTAR1* functionality had no effects on auxin content or plant morphology. Possibly, *PsTAR2* and/or its paralogue PsCam057706 and perhaps *PsTAR3*, compensated for any disruption caused by the *Pstar1* mutations. Indeed, both *PsTAR2* and PsCam057706 have higher RNA transcript numbers in pea seed when compared with *PsTAR1* (Alves-Carvalho et al., 2015). Redundancy is an important concept in plant biology and has been proposed as a mechanism that may rescue phenotypes in other *TAA1*-related single mutants (Stepanova et al., 2008).

Of further interest but of a technical nature, HRM analysis, in the *PsTAR1* context, revealed itself as the most reliable and accurate technique for the detection of the single nucleotide polymorphisms. The range of results obtained from the varied genotyping techniques employed highlighted the importance of using a range of protocols when assessing genotypes. Indeed, genetically speaking, most plant species have undergone gene duplication events resulting, in some instances, in highly expanded gene families, with pseudogenes and transposons complicating investigations.

6.1.2. A novel FMO domain is identified

The fortuitous discovery of a novel *crispoid* mutant allele, *crd-4*, from a *Pstar1-1* population permitted the investigation of the effects that disruptions to *PsYUC1* may have on auxin content and pea morphology. Interestingly, the *crd-4* mutation was located late in the sequence, affecting the fourth exon, a region that had not been defined as critical for the functioning of YUC enzymes (Hou et al., 2011) or FMOs

in general (Schlaich et al., 2007). The prospect that *crd-4* was a leaky allele with a degree of functionality had to be considered.

In silico predictions and protein visualisations revealed that a loop, coded for at the beginning of the fourth exon, forms a 'lid' that sits directly above the area where the FAD cofactor locates. This 'lid' is missing in the *crd-4* and in the *crd-2* proteins. Another *YUC1* mutant with strong phenotypes, *spi1-ref* of maize (Gallavotti et al., 2008), was disrupted in a similar location to that of the *crd-4* mutant. This suggests that the C-terminal portion of the protein is also necessary for the YUC1 enzyme of maize. Further supporting the requirement of the C-terminal end of the protein, in Chapter 4, the *crd-4* flower phenotypes were as severe as those exhibited in the loss-of-function *crd-3* mutant. This clearly suggests that phenotypes exhibited by the *crd-4* mutant can be attributed to the loss of function of PsYUC1.

I propose that Loop-30 is required for the functionality of YUC proteins. The nature of the disruption is, however, unknown. Potentially this new domain enhances specificity to FAD, contains binding residues or permits adequate protein folding.

6.1.3. *PsYUC1* is required for normal lateral organ formation

Results from chapter 4 further demonstrated that several important aspects of pea biology require auxin for proper development. The three *crd* mutant alleles were all morphologically affected by their respective mutations, establishing the importance of *PsYUC1* for pea development in general. Indeed, the rate of node initiation was compromised as was lateral root and leaflet formation, leaf venation, flower and reproductive organ development and seed yield. Most of these phenotypes suggested that disrupting IAA biosynthesis during the early stages of lateral organ formation had adverse repercussions on the morphology of mature organs.

Interestingly, IAA levels were not affected in most tissues of the mutants. In apical buds, there were small reductions in IAA content in the *crd-4* mutant, but it is difficult to ascertain whether the statistically significant but nonetheless slight differences can account for the phenotypes. Indeed, the *crd* mutants displayed an

intriguing phenomenon: the decoupling of the phenotypes from the IAA content. This phenomenon was previously noted to occur in higher-order *yuc Arabidopsis* mutants and in the *flz* mutant of petunia (Tobeña-Santamaria et al., 2002; Won et al., 2011). However, auxin activity in the transgenic *crd-4 DR5::GUS* line was markedly reduced in the apical portion and the young flower buds when compared with the WT line, suggesting that auxin signalling activity and gene transcription is strongly reduced in the *crd* mutants.

I propose that *PsYUC1* is responsible for the local biosynthesis of IAA at the meristematic and primordial stages of lateral tissue/organ formation and that the *crd* disruptions to the IAA pool during the early developmental stages are responsible for the mutant phenotypes.

6.1.4. Auxin metabolism is compromised in the *crd* mutants

Levels of the amide IAAsp conjugate was generally reduced, indicating that IAA metabolism is compromised in the *crd* mutants and that, as demonstrated by the *DR5::GUS* auxin reporter construct, the transcription of auxin-inducible genes, including the *GH3*s, was likely down. Furthermore, results suggest that mechanisms involved in intracellular auxin compartmentalisation, such as auxin sequestration to the ER and a lower rate of auxin transport to the nucleus, may be involved in the *crd* mutants. Indeed, these phenomena may be occurring in the *crd* (*Psyuc1*) mutants, reducing the amount of auxin in the nucleus, the level of gene transcription and the rate of conjugation.

Furthermore, results demonstrated that IAAsp is an important conjugate in pea while contrary to *Arabidopsis*, IAA oxidation does not appear to be an active route for IAA inactivation. Indeed, IAAsp was detected in all tissues tested and present in particularly high concentrations in the apical portion and in actively developing flowers but neither oxIAA nor the secondary metabolite oxIAAsp, were detected from the apical portion of pea. Using a positive control known to contain oxIAAsp, such as *Arabidopsis*, would assist in validating the results obtained.

6.1.5. IPyA breakdown contributes to the IAA pool post-extraction

Another interesting aspect emerging from this research is that IPyA, regularly described as an unstable compound, was demonstrated to contribute substantially to the IAA pool post-extraction. The concept of IPyA breaking down nonenzymatically is not new (Cooney and Nonhebel, 1989; Tam and Normanly, 1998) but to my knowledge, it is the first time that the effects of that breakdown, on IAA quantification, are demonstrated empirically. Indeed, when IPyA was stabilised with a cysteamine-based protocol (Novák et al., 2012), lower levels of IAA were recovered when compared with underivatised samples. Furthermore, the importance of using an antioxidant, DEDTCA in this instance, when extracting and quantifying auxin, was also demonstrated.

In addition, IAA content was reduced in the *crd-4* mutant apical portion whether samples were derivatised or not, further demonstrating that in this tissue at least, IAA biosynthesis is altered. Other labile precursors, such as IAAld, are likely to breakdown to IAA nonenzymatically and may also contribute to the IAA pool. This remains to be tested.

6.1.6. Concluding remarks

The findings from this thesis demonstrate the value of investigating hormone metabolism and gene function in a range of species to deliver holistic views pertaining to the developmental biology of plants. Indeed, the novel IPyA-related mutants offered invaluable opportunities for the investigation of auxin biology and metabolism in pea.

The work presented here suggests that *PsTAR1*, despite being principally expressed in the pod and the seed, is not essential for the establishment of IAA content during early seed development. Producing and analysing different *PsTAR* mutant combinations may reveal synergistic or additive functions within the gene family, as demonstrated with the *Arabidopsis* aminotransferases (Stepanova et al., 2008).

Furthermore, the *crd* mutant alleles provided a wide range of investigative scope and will continue to do so in the future. Results presented in this thesis suggest that *PsYUC1* has a very specific role in local auxin biosynthesis and is essential for normal lateral organ formation. The *crd* mutants may reveal themselves to be rich tools for investigating the impacts that auxin action may have on pea development in general and on delineating the contributions of different intracellular IAA pools on plant development and IAA inactivation. Indeed, our understanding of auxin metabolism on the diverse IAA pool and the contributions of those pools to developmental outputs is still incomplete.

Lastly and of paramount importance, when quantifying plant hormones, the possibility of labile precursors confounding results needs to be taken into account. As for IAA, the cysteamine-based protocol was reliable and robust in the pea system. The effects of IPyA degradation on IAA content post-extraction should be tested in a range of species.

Appendices

For Chapter 2

Table S2.1. Expression levels of the four *PsTAR*s in various tissues at different developmental stages. Expression data originating from high throughput Illumina sequencing and deposited in the pea gene atlas portal; bios.dijon.inra.fr/FATAL/cgi/pscam.cgi. (Alves-Carvalho et al., 2015). Expression levels are represented by number of transcripts or reads per kilobase per million reads (RPKM values, Mortazavi et al, 2008).

Organs and developmental stages	*PsTAR1* PsCam038427	*PsTAR2* PsCam045859	*PsTAR3* PsCam017219	PsCam057706
Apical portion- 5-6 opened leaves	0.18	5.72	n.a.	14.96
Root system- Start of flowering	0.04	3.25	2.62	11.67
Nodules- 18 days after sowing	0.01	0.75	0.16	1.22
Shoot- 5–6 opened leaves	0.04	3.89	n.a.	9.34
Leaves- Start of flowering	n.a.	1.60	n.a.	6.61
Flowers- Start of flowering	n.a.	5.10	n.a.	28.03
Pods- 20 days after flowering	4.90	7.28	0.01	2.96
Seeds- 12 days after pollination	8.09	9.74	0.76	9.74

Table S2.2. The TILLING protocol produced 11 mutant alleles for *PsTAR1*. This research focused on the mutant alleles that are predicted to produce truncated proteins (STOP): line 905 and line 2601. Produced by Dr. M. Dalmais and Dr. L. Bataille.

	Base Position[1]	Protein Position	Type of mutation	Line	SIFT score[+]
1	G118A	G40R	Missense	1391	0.07
2	G135A	W45*	STOP	905	-
3	G163A	E55K	Missense	1240	0.02
4	G186A	M62I	Missense	1860	0.02
5	G305A	G102E	Missense	2121	0.00
6	C514T	P172S	Missense	784	0.00
7	G555A	K185K	Silent	2859	-
8	G563A	G188E	Missense	970	0.30
9	G565A	E189K	Missense	2374	0.56
10	G599A	W200*	STOP	2601	-
11	C646T	L216F	Missense	1424	0.00

(1) From the ATG start on the coding sequence.

(+) SIFT score (http://sift.jcvi.org/). The amino acid substitution is predicted damaging is the score is <= 0.05 and tolerated if the score is > 0.05.

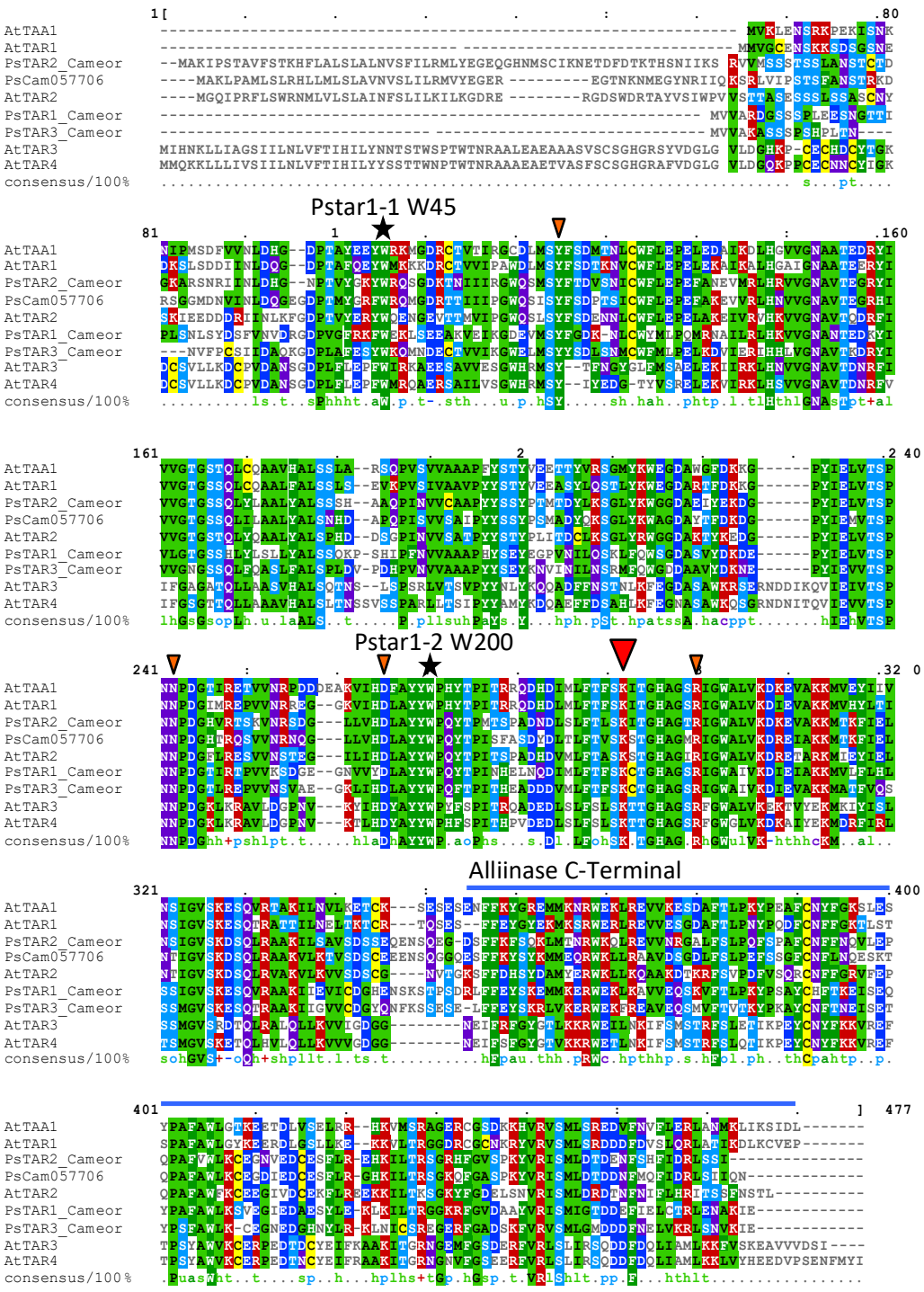

Figure S2.1. Important residues and motifs of PsTAR1 inferred from crystal structure of AtTAA1 (Protein Data Bank: 3BWN, Tao et al, 2008). The 905 and 2601 Pstar1 truncation sites are highlighted with black stars. Small triangles represent putative binding residues and the larger triangle designates the location of the catalytic Lysine residue. Alignment generated with ClustalW and visualised with MVIEW.

Figure S2.2. *PsTAR1* and *PsTAR3* alignment with *PsTAR1* specific primer sequences highlighted. Green: sequencing, yellow: *Pstar1-1* RFLP and cyan: *Pstar1-2* RFLP. Location of the *Pstar1-1* and *Pstar1-2* mutations are encircled.

For Chapter 3

Table S3.1. Expression levels of the *PsYUC*s in various tissues at different developmental stages. Expression data originating from high throughput Illumina sequencing and deposited in the pea gene atlas portal; bios.dijon.inra.fr/FATAL/cgi/pscam.cgi. (Alves-Carvalho et al., 2015). Expression levels are represented by number of transcripts or reads per kilobase per million reads (RPKM values) (Mortazavi et al., 2008).

pea YUC-like gene Tissue and developmental stage	*PsYUC1* ADP88696.2	PsCam036728	PsCam036854	PsCam045906	PsCam038466	PsCam038241	PsCam034710	PsCam039160	PsCam059460	PsCam038488	PsCam000881
Apical portion- 5-6 leaves opened	2.37	3.46	2.43	0.57	n.a.	6.47	13.75	n.a.	n.a.	1.76	10.36
Root system- 8 days after sowing	0.09	2.43	3.85	1.33	2.06	1.30	4.68	0.02	0.08	1.81	2.41
Nodules- 18 days after flowering	0.04	1.04	0.30	2.36	0.04	0.61	1.44	0.02	0.05	0.14	0.73
Shoot- 5-6 leaves opened	0.35	0.83	2.17	0.51	0.07	1.01	6.33	n.a.	n.a.	2.06	32.37
Leaves- Start of flowering	0.35	2.24	2.63	n.a.	0.61	n.a.	2.26	n.a.	0.04	0.04	199.36
Flowers- Start of flowering	0.04	3.58	1.94	0.89	n.a.	8.59	23.17	n.a.	n.a.	1.72	30.07
Pods- 20 days after flowering	n.a.	3.61	2.41	5.57	n.a.	0.42	15.48	2.96	1.63	5.65	17.42
Seeds- 12 days after pollination	2.48	0.05	1.10	2.55	n.a.	0.16	7.72	2.04	0.84	28.07	50.05

References

Abel, S., and Theologis, A. (2010). Odyssey of auxin. Cold Spring Harb Perspect Biol *2*, a004572.

Abu-Zaitoon, Y.M., Bennett, K., Normanly, J., and Nonhebel, H.M. (2012). A large increase in IAA during development of rice grains correlates with the expression of tryptophan aminotransferase OsTAR1 and a grain-specific YUCCA. Physiologia plantarum *146*, 487-499.

Adamowski, M., and Friml, J. (2015). PIN-dependent auxin transport: action, regulation, and evolution. The Plant Cell *27*, 20-32.

Aloni, R., Aloni, E., Langhans, M., and Ullrich, C.I. (2006). Role of auxin in regulating *Arabidopsis* flower development. Planta *223*, 315-328.

Aloni, R., Schwalm, K., Langhans, M., and Ullrich, C.I. (2003). Gradual shifts in sites of free-auxin production during leaf-primordium development and their role in vascular differentiation and leaf morphogenesis in Arabidopsis. Planta *216*, 841-853.

Alves-Carvalho, S., Aubert, G., Carrère, S., Cruaud, C., Brochot, A.L., Jacquin, F., Klein, A., Martin, C., Boucherot, K., and Kreplak, J. (2015). Full-length *de novo* assembly of RNA-seq data in pea (*Pisum sativum L.*) provides a gene expression atlas and gives insights into root nodulation in this species. The Plant Journal *84*, 1-19.

Arumingtyas, E., Floyd, R., Gregory, M., and Mufert, I. (1992). Branching in *Pisum*: inheritance and allelism tests with 17 *ramosus* mutants. Pisum Genetics *24,* 17-31.

Atif, R.M., Boulisset, F., Conreux, C., Thompson, R., and Ochatt, S.J. (2013). In vitro auxin treatment promotes cell division and delays endoreduplication in developing seeds of the model legume species *Medicago truncatula*. Physiologia Plantarum *148*, 549-559.

Bai, F., and DeMason, D.A. (2006). Hormone interactions and regulation of *Unifoliata*, *PsPK2*, *PsPIN1* and *LE* gene expression in pea (*Pisum sativum*) shoot tips. Plant & cell physiology *47*, 935-948.

Barbez, E., and Kleine-Vehn, J. (2013). Divide Et Impera—cellular auxin compartmentalization. Current opinion in plant biology *16*, 78-84.

Barbez, E., Kubes, M., Rolcik, J., Beziat, C., Pencik, A., Wang, B., Rosquete, M.R., Zhu, J., Dobrev, P.I., Lee, Y.*, et al.* (2012). A novel putative auxin carrier family regulates intracellular auxin homeostasis in plants. Nature *485*, 119-122.

Barkoulas, M., Galinha, C., Grigg, S.P., and Tsiantis, M. (2007). From genes to shape: regulatory interactions in leaf development. Current opinion in plant biology *10*, 660-666.

Barlier, I., Kowalczyk, M., Marchant, A., Ljung, K., Bhalerao, R., Bennett, M., Sandberg, G., and Bellini, C. (2000). The *SUR2* gene of *Arabidopsis thaliana* encodes the cytochrome P450 CYP83B1, a modulator of auxin homeostasis. Proceedings of the National Academy of Sciences *97*, 14819-14824.

Bartel, B., and Fink, G.R. (1995). ILR1, an amidohydrolase that releases active indole-3-acetic acid from conjugates. Science *268*, 1745-1748.

Bäurle, I., and Dean, C. (2006). The timing of developmental transitions in plants. Cell *125*, 655-664.

Becker, A., and Theißen, G. (2003). The major clades of MADS-box genes and their role in the development and evolution of flowering plants. Molecular phylogenetics and evolution *29*, 464-489.

Belmonte, M.F., Kirkbride, R.C., Stone, S.L., Pelletier, J.M., Bui, A.Q., Yeung, E.C., Hashimoto, M., Fei, J., Harada, C.M., and Munoz, M.D. (2013). Comprehensive developmental profiles of gene activity in regions and subregions of the *Arabidopsis* seed. Proceedings of the National Academy of Sciences *110*, E435-E444.

Benkert, P., Biasini, M., and Schwede, T. (2010). Toward the estimation of the absolute quality of individual protein structure models. Bioinformatics *27*, 343-350.

Benková, E., Michniewicz, M., Sauer, M., Teichmann, T., Seifertová, D., Jürgens, G., and Friml, J. (2003). Local, efflux-dependent auxin gradients as a common module for plant organ formation. Cell *115*, 591-602.

Benlloch, R., Navarro, C., Beltrán, J., and Cañas, L.A. (2003). Floral development of the model legume *Medicago truncatula*: ontogeny studies as a tool to better characterize homeotic mutations. Sexual Plant Reproduction *15*, 231-241.

Berbel, A., Ferrándiz, C., Hecht, V., Dalmais, M., Lund, O.S., Sussmilch, F.C., Taylor, S.A., Bendahmane, A., Ellis, T.N., and Beltrán, J.P. (2012). *VEGETATIVE1* is essential for development of the compound inflorescence in pea. Nature communications *3*, 797.

Berdnikov, V., Gorel, F., and Kosterin, O. (2000). A new allele at *Crd* disturbs development of the compound leaf. Pisum Genetics *32*, 6-8.

Bernardi, J., Lanubile, A., Li, Q.B., Kumar, D., Kladnik, A., Cook, S.D., Ross, J.J., Marocco, A., and Chourey, P.S. (2012). Impaired auxin biosynthesis in the *defective endosperm18* mutant is due to mutational loss of expression in the *ZmYuc1* gene encoding endosperm-specific YUCCA1 protein in maize. Plant Physiology *160*, 1318-1328.

Bernardi, J., Li, Q.-B., Gao, Y., Zhao, Y., Battaglia, R., Marocco, A., and Chourey, P.S. (2016). The auxin-deficient defective *kernel18* (*dek18*) mutation alters the

expression of seed-specific biosynthetic genes in maize. Journal of plant growth regulation *35*, 770-777.

Bernier, G., Havelange, A.e., Houssa, C., Petitjean, A., and Lejeune, P. (1993). Physiological signals that induce flowering. The Plant Cell *5*, 1147.

Beveridge, C.A., Ross, J.J., and Murfet, I.C. (1994). Branching mutant *rms-2* in *Pisum sativum* (grafting studies and endogenous indole-3-acetic acid levels). Plant Physiology *104*, 953-959.

Biasini, M., Bienert, S., Waterhouse, A., Arnold, K., Studer, G., Schmidt, T., Kiefer, F., Cassarino, T.G., Bertoni, M., and Bordoli, L. (2014). SWISS-MODEL: modelling protein tertiary and quaternary structure using evolutionary information. Nucleic acids research *42*, W252-W258.

Blein, T., Pulido, A., Vialette-Guiraud, A., Nikovics, K., Morin, H., Hay, A., Johansen, I.E., Tsiantis, M., and Laufs, P. (2008). A conserved molecular framework for compound leaf development. Science *322*, 1835-1839.

Blilou, I., Xu, J., Wildwater, M., Willemsen, V., Paponov, I., Friml, J., Heidstra, R., Aida, M., Palme, K., and Scheres, B. (2005). The PIN auxin efflux facilitator network controls growth and patterning in *Arabidopsis* roots. Nature *433*, 39.

Boerjan, W., Cervera, M.-T., Delarue, M., Beeckman, T., Dewitte, W., Bellini, C., Caboche, M., Van Onckelen, H., Van Montagu, M., and Inzé, D. (1995). *superroot*, a recessive mutation in *Arabidopsis*, confers auxin overproduction. The Plant Cell *7*, 1405-1419.

Boisson-Dernier, A., Frietsch, S., Kim, T.-H., Dizon, M.B., and Schroeder, J.I. (2008). The peroxin loss-of-function mutation *abstinence by mutual consent* disrupts male-female gametophyte recognition. Current Biology *18*, 63-68.

Bowman, J.L., Smyth, D.R., and Meyerowitz, E.M. (1991). Genetic interactions among floral homeotic genes of *Arabidopsis*. Development *112*, 1-20.

Bowman, J.L., Smyth, D.R., and Meyerowitz, E.M. (2012). The ABC model of flower development: then and now. Development *139*, 4095-4098.

Byrne, M.E., Kidner, C.A., and Martienssen, R.A. (2003). Plant stem cells: divergent pathways and common themes in shoots and roots. Current Opinion in Genetics & Development *13*, 551-557.

Calderón-Villalobos, L.I., Tan, X., Zheng, N., and Estelle, M. (2010). Auxin perception--structural insights. Cold Spring Harbor perspectives in biology *2*, a005546.

Calderón-Villalobos, L.I.A., Lee, S., De Oliveira, C., Ivetac, A., Brandt, W., Armitage, L., Sheard, L.B., Tan, X., Parry, G., and Mao, H. (2012). A combinatorial TIR1/AFB–Aux/IAA co-receptor system for differential sensing of auxin. Nature chemical biology *8*, 477.

Cannon, S.B. (2013). The model legume genomes. In Legume Genomics (Springer), pp. 1-14.

Caputi, L., Malnoy, M., Goremykin, V., Nikiforova, S., and Martens, S. (2012). A genome-wide phylogenetic reconstruction of family 1 UDP-glycosyltransferases revealed the expansion of the family during the adaptation of plants to life on land. The Plant Journal *69*, 1030-1042.

Chen, Q., Dai, X., De-Paoli, H., Cheng, Y., Takebayashi, Y., Kasahara, H., Kamiya, Y., and Zhao, Y. (2014). Auxin overproduction in shoots cannot rescue auxin deficiencies in *Arabidopsis* roots. Plant and Cell Physiology *55*, 1072-1079.

Cheng, Y., Dai, X., and Zhao, Y. (2006). Auxin biosynthesis by the YUCCA flavin monooxygenases controls the formation of floral organs and vascular tissues in *Arabidopsis*. Genes & development *20*, 1790-1799.

Cheng, Y., Dai, X., and Zhao, Y. (2007). Auxin synthesized by the YUCCA flavin monooxygenases is essential for embryogenesis and leaf formation in *Arabidopsis*. The Plant Cell *19*, 2430-2439.

Choi, H.S., Kim, J.K., Cho, E.H., Kim, Y.C., Kim, J.I., and Kim, S.W. (2003). A novel flavin-containing monooxygenase from *Methylophaga* sp. strain SK1 and its indigo synthesis in *Escherichia coli*. Biochemical and biophysical research communications *306*, 930-936.

Claeys, H., De Bodt, S., and Inzé, D. (2014). Gibberellins and DELLAs: central nodes in growth regulatory networks. Trends in plant science *19*, 231-239.

Coen, E.S., and Meyerowitz, E.M. (1991). The war of the whorls: genetic interactions controlling flower development. Nature *353*, 31.

Colombo, L., Franken, J., Koetje, E., van Went, J., Dons, H., Angenent, G.C., and van Tunen, A.J. (1995). The petunia MADS box gene *FBP11* determines ovule identity. The Plant Cell *7*, 1859-1868.

Conklin, P.A., Strable, J., Li, S., and Scanlon, M.J. (2018). On the mechanisms of development in monocot and eudicot leaves. New Phytologist *221*, 706-724.

Cook, S.D., Nichols, D.S., Smith, J., Chourey, P.S., McAdam, E.L., Quittenden, L.J., and Ross, J.J. (2016). Auxin biosynthesis: Are the indole-3-acetic acid and phenylacetic acid biosynthesis pathways mirror images? Plant physiology *171*, pp. 00454.02016.

Dai, X., Mashiguchi, K., Chen, Q., Kasahara, H., Kamiya, Y., Ojha, S., DuBois, J., Ballou, D., and Zhao, Y. (2013). The biochemical mechanism of auxin biosynthesis by an *Arabidopsis* YUCCA flavin-containing monooxygenase. Journal of Biological Chemistry *288*, 1448-1457.

Dal Bosco, C., Dovzhenko, A., and Palme, K. (2012). Intracellular auxin transport in pollen: PIN8, PIN5 and PILS5. Plant signaling & behavior *7*, 1504-1505.

Dalmais, M., Schmidt, J., Le Signor, C., Moussy, F., Burstin, J., Savois, V., Aubert, G., Brunaud, V., de Oliveira, Y., and Guichard, C. (2008). UTILLdb, a *Pisum sativum in silico* forward and reverse genetics tool. Genome biology *9*, R43.

Davidson, S.E., Smith, J.J., Helliwell, C.A., Poole, A.T., and Reid, J.B. (2004). The pea gene *LH* encodes ent-kaurene oxidase. Plant physiology *134*, 1123-1134.

Davies, P.J. (2010). The plant hormones: their nature, occurrence, and functions. In Plant hormones (Springer), pp. 1-15.

Davies, R.T., Goetz, D.H., Lasswell, J., Anderson, M.N., and Bartel, B. (1999). *IAR3* encodes an auxin conjugate hydrolase from *Arabidopsis*. The Plant Cell *11*, 365-376.

De Jong, M., Mariani, C., and Vriezen, W.H. (2009). The role of auxin and gibberellin in tomato fruit set. Journal of experimental botany *60*, 1523-1532.

De Smet, I., Lau, S., Voß, U., Vanneste, S., Benjamins, R., Rademacher, E.H., Schlereth, A., De Rybel, B., Vassileva, V., and Grunewald, W. (2010). Bimodular auxin response controls organogenesis in *Arabidopsis*. Proceedings of the National Academy of Sciences *107*, 2705-2710.

Deb, J., Bland, H.M., and Østergaard, L. (2018). Developmental cartography: coordination via hormonal and genetic interactions during gynoecium formation. Current opinion in plant biology *41*, 54-60.

Deb, Y., Marti, D., Frenz, M., Kuhlemeier, C., and Reinhardt, D. (2015). Phyllotaxis involves auxin drainage through leaf primordia. Development *142*, 1992-2001.

Del Bianco, M., and Kepinski, S. (2011). Context, specificity, and self-organization in auxin response. Cold Spring Harb Perspect Biol *3*, a001578.

Delarue, M., Prinsen, E., Va, H., Caboche, M., and Bellini, C. (1998). *Sur2* mutations of *Arabidopsis thaliana* define a new locus involved in the control of auxin homeostasis. The Plant Journal *14*, 603-611.

DeMason, D.A., and Chawla, R. (2004). Roles for auxin during morphogenesis of the compound leaves of pea (*Pisum sativum*). Planta *218*, 435-448.

DeMason, D.A., Chetty, V., Barkawi, L.S., Liu, X., and Cohen, J.D. (2013). *Unifoliata-Afila* interactions in pea leaf morphogenesis. American journal of botany *100*, 478-495.

DeMason, D.A., and Polowick, P.L. (2009). Patterns of *DR5::GUS* expression in organs of pea (*Pisum sativum*). International Journal of Plant Sciences *170*, 1-11.

DeMason, D.A., and Schmidt, R.J. (2001). Roles of the *Uni* gene in shoot and leaf development of pea (*Pisum sativum*): Phenotypic characterization and leaf development in the *uni* and *uni-tac* Mutants. International Journal of Plant Sciences *162*, 1033-1051.

Devoghalaere, F., Doucen, T., Guitton, B., Keeling, J., Payne, W., Ling, T.J., Ross, J.J., Hallett, I.C., Gunaseelan, K., and Dayatilake, G. (2012). A genomics approach to understanding the role of auxin in apple (Malus x domestica) fruit size control. BMC Plant Biology *12*, 7.

Dharmasiri, N., Dharmasiri, S., Weijers, D., Lechner, E., Yamada, M., Hobbie, L., Ehrismann, J.S., Jurgens, G., and Estelle, M. (2005). Plant development is regulated by a family of auxin receptor F box proteins. Dev Cell *9*, 109-119.

Di Giacomo, E., Sestili, F., Iannelli, M.A., Testone, G., Mariotti, D., and Frugis, G. (2008). Characterization of *KNOX* genes in *Medicago truncatula*. Plant molecular biology *67*, 135-150.

Ding, Z., Galván-Ampudia, C.S., Demarsy, E., Łangowski, Ł., Kleine-Vehn, J., Fan, Y., Morita, M.T., Tasaka, M., Fankhauser, C., and Offringa, R. (2011). Light-mediated polarization of the PIN3 auxin transporter for the phototropic response in Arabidopsis. Nature cell biology *13*, 447.

Ding, Z., Wang, B., Moreno, I., Duplá Ková, N., Simon, S., Carraro, N., Reemmer, J., Pě Nčí K, A., Chen, X., Tejos, R.*, et al.* (2012). ER-localized auxin transporter PIN8 regulates auxin homeostasis and male gametophyte development in *Arabidopsis*. Nature Communications *3*, 941.

Ditta, G., Pinyopich, A., Robles, P., Pelaz, S., and Yanofsky, M.F. (2004). The *SEP4* gene of *Arabidopsis thaliana* functions in floral organ and meristem identity. Current Biology *14*, 1935-1940.

Domoney, C., Knox, M., Moreau, C., Ambrose, M., Palmer, S., Smith, P., Christodoulou, V., Isaac, P.G., Hegarty, M., and Blackmore, T. (2013). Exploiting a fast neutron mutant genetic resource in *Pisum sativum* (pea) for functional genomics. Functional Plant Biology *40*, 1261-1270.

Doyle, J., and Doyle, J. (1987). CTAB DNA extraction in plants. Phytochemical Bulletin *19*, 11-15.

Du, Y., and Scheres, B. (2017). Lateral root formation and the multiple roles of auxin. Journal of experimental botany *69*, 155-167.

Dubrovsky, J.G., Sauer, M., Napsucialy-Mendivil, S., Ivanchenko, M.G., Friml, J., Shishkova, S., Celenza, J., and Benková, E. (2008). Auxin acts as a local morphogenetic trigger to specify lateral root founder cells. Proceedings of the National Academy of Sciences *105*, 8790-8794.

Duke, J. (2012). Handbook of legumes of world economic importance (Springer Science & Business Media).

Eswaramoorthy, S., Bonanno, J.B., Burley, S.K., and Swaminathan, S. (2006). Mechanism of action of a flavin-containing monooxygenase. Proceedings of the National Academy of Sciences *103*, 9832-9837.

Expósito-Rodríguez, M., Borges, A.A., Borges-Pérez, A., Hernández, M., and Pérez, J.A. (2007). Cloning and biochemical characterization of *ToFZY*, a tomato gene encoding a flavin monooxygenase involved in a tryptophan-dependent auxin biosynthesis pathway. Journal of plant growth regulation *26*, 329-340.

Feraru, E., Vosolsobě, S., Feraru, M.I., Petrášek, J., and Kleine-Vehn, J. (2012). Evolution and structural diversification of PILS putative auxin carriers in plants. Frontiers in plant science *3*, 227.

Ferreira, G.C., Neame, P.J., and Dailey, H.A. (1993). Heme biosynthesis in mammalian systems: evidence of a Schiff base linkage between the pyridoxal 5′-phosphate cofactor and a lysine residue in 5-aminolevulinate synthase. Protein Science *2*, 1959-1965.

Foucher, F., Morin, J., Courtiade, J., Cadioux, S., Ellis, N., Banfield, M.J., and Rameau, C. (2003). *DETERMINATE* and *LATE FLOWERING* are two *TERMINAL FLOWER1/CENTRORADIALIS* homologs that control two distinct phases of flowering initiation and development in pea. The Plant Cell *15*, 2742-2754.

Fraaije, M.W., Kamerbeek, N.M., van Berkel, W.J., and Janssen, D.B. (2002). Identification of a Baeyer–Villiger monooxygenase sequence motif. FEBS letters *518*, 43-47.

Friml, J. (2003). Auxin transport—shaping the plant. Current opinion in plant biology *6*, 7-12.

Friml, J., Benková, E., Blilou, I., Wisniewska, J., Hamann, T., Ljung, K., Woody, S., Sandberg, G., Scheres, B., and Jürgens, G. (2002). AtPIN4 mediates sink-driven auxin gradients and root patterning in *Arabidopsis*. Cell *108*, 661-673.

Friml, J., and Palme, K. (2002). Polar auxin transport–old questions and new concepts? Plant molecular biology *49*, 273-284.

Fujino, K., Matsuda, Y., Ozawa, K., Nishimura, T., Koshiba, T., Fraaije, M.W., and Sekiguchi, H. (2008). *NARROW LEAF 7* controls leaf shape mediated by auxin in rice. Molecular Genetics and Genomics *279*, 499-507.

Gaillochet, C., Daum, G., and Lohmann, J.U. (2015). O cell, where art thou? The mechanisms of shoot meristem patterning. Current Opinion in Plant Biology *23*, 91-97.

Gallavotti, A. (2013). The role of auxin in shaping shoot architecture. Journal of experimental botany *64*, 2593-2608.

Gallavotti, A., Barazesh, S., Malcomber, S., Hall, D., Jackson, D., Schmidt, R.J., and McSteen, P. (2008). *sparse inflorescence1* encodes a monocot-specific *YUCCA*-like gene required for vegetative and reproductive development in maize. Proceedings of the National Academy of Sciences *105*, 15196-15201.

Galli, M., and Gallavotti, A. (2016). Expanding the regulatory network for meristem size in plants. Trends in Genetics *32*, 372-383.

Gould, K.S., Cutter, E.G., and Young, J.P.W. (1991). Modification of pea leaf morphology by 2, 3, 5-triiodobenzoic acid. Botanical gazette *152*, 133-138.

Grandjean, O., Vernoux, T., Laufs, P., Belcram, K., Mizukami, Y., and Traas, J. (2004). *In vivo* analysis of cell division, cell growth, and differentiation at the shoot apical meristem in *Arabidopsis*. The Plant Cell *16*, 74-87.

Guilfoyle, T.J., and Hagen, G. (2007). Auxin response factors. Current opinion in plant biology *10*, 453-460.

Hagen, G., Martin, G., Li, Y., and Guilfoyle, T.J. (1991). Auxin-induced expression of the soybean *GH3* promoter in transgenic tobacco plants. Plant molecular biology *17*, 567-579.

Hansen, B.G., Kliebenstein, D.J., and Halkier, B.A. (2007). Identification of a flavin-monooxygenase as the *S*-oxygenating enzyme in aliphatic glucosinolate biosynthesis in *Arabidopsis*. The Plant Journal *50*, 902-910.

Hartl, F.U. (1996). Molecular chaperones in cellular protein folding. Nature *381*, 571.

Hedden, P., and Thomas, S.G. (2008). Annual Plant Reviews, Plant Hormone Signaling, Vol 24 (John Wiley & Sons).

Heidstra, R., and Sabatini, S. (2014). Plant and animal stem cells: similar yet different. Nature Reviews Molecular Cell Biology *15*, 301.

Hennig, M., Grimm, B., Contestabile, R., John, R.A., and Jansonius, J.N. (1997). Crystal structure of glutamate-1-semialdehyde aminomutase: an α2-dimeric vitamin B6-dependent enzyme with asymmetry in structure and active site reactivity. Proceedings of the National Academy of Sciences *94*, 4866-4871.

Herrbach, V., Remblière, C., Gough, C., and Bensmihen, S. (2014). Lateral root formation and patterning in *Medicago truncatula*. Journal of plant physiology *171*, 301-310.

Hofer, J., Gourlay, C., Michael, A., and Ellis, T.N. (2001). Expression of a class 1 *knotted1*-like homeobox gene is down-regulated in pea compound leaf primordia. Plant molecular biology *45*, 387-398.

Hofer, J., Turner, L., Hellens, R., Ambrose, M., Matthews, P., Michael, A., and Ellis, N. (1997). *UNIFOLIATA* regulates leaf and flower morphogenesis in pea. Current Biology *7*, 581-587.

Hofer, J.M., and Ellis, T.N. (1998). The genetic control of patterning in pea leaves. Trends in Plant Science *3*, 439-444.

Honma, T., and Goto, K. (2001). Complexes of MADS-box proteins are sufficient to convert leaves into floral organs. Nature *409*, 525.

Hou, X., Liu, S., Pierri, F., Dai, X., Qu, L.J., and Zhao, Y. (2011). Allelic analyses of the *Arabidopsis YUC1* locus reveal residues and domains essential for the functions of YUC family of flavin monooxygenases. Journal of integrative plant biology *53*, 54-62.

Inzé, D., and De Veylder, L. (2006). Cell cycle regulation in plant development. Annual Review of Genetics *40*, 77-105.

Irish, V. (2017). The ABC model of floral development. Current Biology *27*, R887-R890.

Ishida, T., Adachi, S., Yoshimura, M., Shimizu, K., Umeda, M., and Sugimoto, K. (2010). Auxin modulates the transition from the mitotic cycle to the endocycle in *Arabidopsis*. Development *137*, 63-71.

Jackson, R.G., Lim, E.-K., Li, Y., Kowalczyk, M., Sandberg, G., Hoggett, J., Ashford, D.A., and Bowles, D.J. (2001). Identification and biochemical characterization of an *Arabidopsis* indole-3-acetic acid glucosyltransferase. Journal of Biological Chemistry *276*, 4350-4356.

Jakubowska, A., and Kowalczyk, S. (2005). A specific enzyme hydrolyzing 6-O (4-O)-indole-3-ylacetyl-β-d-glucose in immature kernels of *Zea mays*. Journal of plant physiology *162*, 207-213.

Jefferson, R.A., Kavanagh, T.A., and Bevan, M.W. (1987). GUS fusions: *B*-glucuronidase as a sensitive and versatile gene fusion marker in higher plants. The EMBO Journal *6*, 3901-3907.

Jones, B., and Ljung, K. (2012). Subterranean space exploration: the development of root system architecture. Current opinion in plant biology *15*, 97-102.

Jung, C., Pillen, K., Staiger, D., Coupland, G., and von Korff, M. (2017). Recent advances in flowering time control. Frontiers in plant science *7*, 2011.

Kai, K., Horita, J., Wakasa, K., and Miyagawa, H. (2007). Three oxidative metabolites of indole-3-acetic acid from *Arabidopsis thaliana*. Phytochemistry *68*, 1651-1663.

Källberg, M., Wang, H., Wang, S., Peng, J., Wang, Z., Lu, H., and Xu, J. (2012). Template-based protein structure modeling using the RaptorX web server. Nature protocols *7*, 1511.

Kasahara, R.D., Maruyama, D., Hamamura, Y., Sakakibara, T., Twell, D., and Higashiyama, T. (2012). Fertilization recovery after defective sperm cell release in Arabidopsis. Current Biology *22*, 1084-1089.

Kater, M.M., Dreni, L., and Colombo, L. (2006). Functional conservation of MADS-box factors controlling floral organ identity in rice and *Arabidopsis*. Journal of experimental botany *57*, 3433-3444.

Kelley, L.A., Mezulis, S., Yates, C.M., Wass, M.N., and Sternberg, M.J. (2015). The Phyre2 web portal for protein modeling, prediction and analysis. Nature protocols *10*, 845.

Kelley, L.A., and Sternberg, M.J. (2009). Protein structure prediction on the Web: a case study using the Phyre server. Nature protocols *4*, 363.

Kepinski, S., and Leyser, O. (2005). The Arabidopsis F-box protein TIR1 is an auxin receptor. Nature *435*, 446.

Kim, M., Pham, T., Hamidi, A., McCormick, S., Kuzoff, R.K., and Sinha, N. (2003). Reduced leaf complexity in tomato wiry mutants suggests a role for *PHAN* and *KNOX* genes in generating compound leaves. Development *130*, 4405-4415.

Koch, M., Vorwerk, S., Masur, C., Sharifi-Sirchi, G., Olivieri, N., and Schlaich, N.L. (2006). A role for a flavin-containing mono-oxygenase in resistance against microbial pathogens in *Arabidopsis*. The Plant Journal *47*, 629-639.

Korasick, D.A., Enders, T.A., and Strader, L.C. (2013). Auxin biosynthesis and storage forms. Journal of experimental botany *64*, 2541-2555.

Kramer, E.M., Jaramillo, M.A., and Di Stilio, V.S. (2004). Patterns of gene duplication and functional evolution during the diversification of the *AGAMOUS* subfamily of MADS box genes in angiosperms. Genetics *166*, 1011-1023.

Kriechbaumer, V., Park, W., Gierl, A., and Glawischnig, E. (2006). Auxin biosynthesis in maize. Plant Biology *8*, 334-339.

Kriechbaumer, V., Wang, P., Hawes, C., and Abell, B.M. (2012). Alternative splicing of the auxin biosynthesis gene *YUCCA4* determines its subcellular compartmentation. The Plant Journal *70*, 292-302.

Krueger, S.K., and Williams, D.E. (2005). Mammalian flavin-containing monooxygenases: structure/function, genetic polymorphisms and role in drug metabolism. Pharmacology & therapeutics *106*, 357-387.

Kuettner, E.B., Hilgenfeld, R., and Weiss, M.S. (2002). Purification, characterization, and crystallization of alliinase from garlic. Archives of Biochemistry and Biophysics *402*, 192-200.

Kumar, P., Henikoff, S., and Ng, P.C. (2009). Predicting the effects of coding non-synonymous variants on protein function using the SIFT algorithm. Nature protocols *4*, 1073.

Lam, H.K., Scott, A., Erin, L.M., and John, J.R. (2015). Evidence that chlorinated auxin is restricted to the *Fabaceae* but not to the *Fabeae*. Plant physiology, pp. 00410.02015.

Lau, S., Slane, D., Herud, O., Kong, J., and Jurgens, G. (2012). Early embryogenesis in flowering plants: setting up the basic body pattern. Annual review of plant biology

63, 483-506.

Lavenus, J., Goh, T., Roberts, I., Guyomarc'h, S., Lucas, M., De Smet, I., Fukaki, H., Beeckman, T., Bennett, M., and Laplaze, L. (2013). Lateral root development in *Arabidopsis*: fifty shades of auxin. Trends in plant science *18*, 450-458.

Lester, D.R., Ross, J.J., Davies, P.J., and Reid, J.B. (1997). Mendel's stem length gene (*Le*) encodes a gibberellin 3 beta-hydroxylase. The Plant Cell *9*, 1435-1443.

Li, W., Zhou, Y., Liu, X., Yu, P., Cohen, J.D., and Meyerowitz, E.M. (2013). *LEAFY* controls auxin response pathways in floral primordium formation. Science Signaling *6*, ra23-ra23.

Ligerot, Y., de Saint Germain, A., Waldie, T., Troadec, C., Citerne, S., Kadakia, N., Pillot, J.-P., Prigge, M., Aubert, G., and Bendahmane, A. (2017). The pea branching *RMS2* gene encodes the *PsAFB4/5* auxin receptor and is involved in an auxin-strigolactone regulation loop. PLoS genetics *13*, e1007089.

Liscum, E., and Reed, J. (2002). Genetics of Aux/IAA and ARF action in plant growth and development. Plant molecular biology *49*, 387-400.

Litt, A., and Kramer, E.M. (2010). The ABC model and the diversification of floral organ identity. Paper presented at: Seminars in cell & developmental biology (Elsevier).

Liu, Y., Xu, M., Liang, N., Zheng, Y., Yu, Q., and Wu, S. (2017). Symplastic communication spatially directs local auxin biosynthesis to maintain root stem cell niche in *Arabidopsis*. Proceedings of the National Academy of Sciences *114*, 201616387.

Ljung, K. (2013). Auxin metabolism and homeostasis during plant development. Development *140*, 943-950.

Ljung, K., Hull, A.K., Celenza, J., Yamada, M., Estelle, M., Normanly, J., and Sandberg, G. (2005). Sites and regulation of auxin biosynthesis in *Arabidopsis* roots. The Plant Cell *17*, 1090-1104.

Ljung, K., Hull, A.K., Kowalczyk, M., Marchant, A., Celenza, J., Cohen, J.D., and Sandberg, G. (2002). Biosynthesis, conjugation, catabolism and homeostasis of indole-3-acetic acid in *Arabidopsis thaliana*. Plant molecular biology *49*, 249-272.

Ljung, K., Östin, A., Lioussanne, L., and Sandberg, G. (2001). Developmental regulation of indole-3-acetic acid turnover in Scots pine seedlings. Plant physiology *125*, 464-475.

Long, J.A., Moan, E.I., Medford, J.I., and Barton, M.K. (1996). A member of the KNOTTED class of homeodomain proteins encoded by the *STM* gene of *Arabidopsis*. Nature *379*, 66.

Ludwig-Muller, J. (2011). Auxin conjugates: their role for plant development and in the evolution of land plants. Journal of experimental botany *62*, 1757-1773.

Luo, J., Zhou, J-J. and Zhang, J-Z. (2018). Aux/IAA gene family in plants: Molecular structure, regulation, and function. International Journal of Molecular Sciences, 19, 259.

Macas, J., Neumann, P., and Navrátilová, A. (2007). Repetitive DNA in the pea (*Pisum sativum L.*) genome: comprehensive characterization using 454 sequencing and comparison to soybean and *Medicago truncatula*. BMC genomics *8*, 427.

Mashiguchi, K., Tanaka, K., Sakai, T., Sugawara, S., Kawaide, H., Natsume, M., Hanada, A., Yaeno, T., Shirasu, K., and Yao, H. (2011). The main auxin biosynthesis pathway in *Arabidopsis*. Proceedings of the National Academy of Sciences *108*, 18512-18517.

MacKenzie-Hose, A.K., Ross, J.J., Davies, N.W., Swain, S.M. (1998). Expression of gibberellin mutations in fruits of *Pisum sativum* L. *Planta*, 204, 397-403.

McAdam, E.L., Meitzel, T., Quittenden, L.J., Davidson, S.E., Dalmais, M., Bendahmane, A.I., Thompson, R., Smith, J.J., Nichols, D.S., Urquhart, S.*, et al.* (2017a). Evidence that auxin is required for normal seed size and starch synthesis in pea. New Phytologist *216*, 193-204.

McAdam, S.A.M., Eleouet, M.P., Best, M., Brodribb, T.J., Carins Murphy, M., Cook, S.D., Dalmais, M., Dimitriou, T., Gélinas-Marion, A., Gill, W.M.*, et al.* (2017b). Linking auxin with photosynthetic rate via leaf venation. Plant Physiology *175*, 351-360.

McMurry, J., and Simanek, E. (2007). Fundamentals of Organic Chemistry 6th ed., Examview and Examview pro are Registered Trademarks of FsCreations. Inc, America, 413-417.

Mellor, N., Band, L.R., Pěnčík, A., Novák, O., Rashed, A., Holman, T., Wilson, M.H., Voß, U., Bishopp, A., and King, J.R. (2016). Dynamic regulation of auxin oxidase and conjugating enzymes AtDAO1 and GH3 modulates auxin homeostasis. Proceedings of the National Academy of Sciences *113*, 11022-11027.

Michalczuk, L., and Bandurski, R.S. (1982). Enzymic synthesis of 1-O-indol-3-ylacetyl-β-D-glucose and indol-3-ylacetyl-myo-inositol. Biochemical Journal *207*, 273-281.

Middleton, A.M., Dal Bosco, C., Chlap, P., Bensch, R., Harz, H., Ren, F., Bergmann, S., Wend, S., Weber, W., and Hayashi, K.-i. (2018). Data-driven modeling of intracellular auxin fluxes indicates a dominant role of the ER in controlling nuclear auxin uptake. Cell reports *22*, 3044-3057.

Mirza, I.A., Yachnin, B.J., Wang, S., Grosse, S., Bergeron, H., Imura, A., Iwaki, H., Hasegawa, Y., Lau, P.C., and Berghuis, A.M. (2009). Crystal structures of cyclohexanone monooxygenase reveal complex domain movements and a sliding cofactor. Journal of the American Chemical Society *131*, 8848-8854.

Moreno-Risueno, M.A., Van Norman, J.M., Moreno, A., Zhang, J., Ahnert, S.E., and Benfey, P.N. (2010). Oscillating gene expression determines competence for periodic *Arabidopsis* root branching. Science *329*, 1306-1311.

Moro, F., Fernández-Sáiz, V., and Muga, A. (2004). The lid subdomain of DnaK is required for the stabilization of the substrate binding site. Journal of Biological Chemistry.

Mortazavi, A., Williams, B.A., McCue, K., Schaeffer, L., and Wold, B. (2008). Mapping and quantifying mammalian transcriptomes by RNA-Seq. Nature methods *5*, 621.

Mravec, J., Skůpa, P., Bailly, A., Hoyerová, K., Křeček, P., Bielach, A., Petrášek, J., Zhang, J., Gaykova, V., and Stierhof, Y.-D. (2009). Subcellular homeostasis of phytohormone auxin is mediated by the ER-localized PIN5 transporter. Nature *459*, 1136.

Normanly, J. (2010). Approaching cellular and molecular resolution of auxin biosynthesis and metabolism. Cold Spring Harb Perspect Biol *2*, a001594.

Normanly, J., Cohen, J.D., and Fink, G.R. (1993). *Arabidopsis thaliana* auxotrophs reveal a tryptophan-independent biosynthetic pathway for indole-3-acetic acid. Proceedings of the National Academy of Sciences *90*, 10355-10359.

Novák, O., Hényková, E., Sairanen, I., Kowalczyk, M., Pospíšil, T., and Ljung, K. (2012). Tissue-specific profiling of the Arabidopsis thaliana auxin metabolome. The Plant Journal *72*, 523-536.

Novák, O., Pěnčík, A., Blahoušek, O., and Ljung, K. (2017). Quantitative auxin metabolite profiling using stable isotope dilution UHPLC-MS/MS. Current Protocols in Plant Biology *1*, 419-430.

Ortiz, A.R., Strauss, C.E., and Olmea, O. (2002). MAMMOTH (matching molecular models obtained from theory): an automated method for model comparison. Protein Science *11*, 2606-2621.

Östin, A., Kowalyczk, M., Bhalerao, R.P., and Sandberg, G. (1998). Metabolism of indole-3-acetic acid in *Arabidopsis*. Plant physiology *118*, 285-296.

Ostrowski, M., Ciarkowska, A., and Jakubowska, A. (2016). The auxin conjugate indole-3-acetyl-aspartate affects responses to cadmium and salt stress in *Pisum sativum L*. Journal of plant physiology *191*, 63-72.

Ouyang, J., Shao, X., and Li, J. (2000). Indole-3-glycerol phosphate, a branchpoint of indole-3-acetic acid biosynthesis from the tryptophan biosynthetic pathway in Arabidopsis thaliana. The Plant Journal *24*, 327-334.

Overvoorde, P., Fukaki, H., and Beeckman, T. (2010). Auxin control of root development. Cold Spring Harbor perspectives in biology *2*, a001537.

Ozga, J.A., Brenner, M.L., and Reinecke, D.M. (1992). Seed effects on gibberellin metabolism in pea pericarp. Plant physiology *100*, 88-94.

Ozga, J.A., and Reinecke, D.M. (1999). Interaction of 4-chloroindole-3-acetic acid and gibberellins in early pea fruit development. Plant growth regulation *27*, 33-38.

Ozga, J.A., van Huizen, R., and Reinecke, D.M. (2002). Hormone and seed-specific regulation of pea fruit growth. Plant Physiology *128*, 1379-1389.

Ozga, J.A., Yu, J., and Reinecke, D.M. (2003). Pollination-, development-, and auxin-specific regulation of gibberellin 3beta-hydroxylase gene expression in pea fruit and seeds. Plant Physiology *131*, 1137-1146.

Parcy, F., Vernoux, T. and Dumas, R. (2016). A glimpse beyond structures in auxin-dependent transcription. Trends in Plant Science, *21*, 574-583.

Park, J.-E., Park, J.-Y., Kim, Y.-S., Staswick, P.E., Jeon, J., Yun, J., Kim, S.-Y., Kim, J., Lee, Y.-H., and Park, C.-M. (2007). GH3-mediated auxin homeostasis links growth regulation with stress adaptation response in Arabidopsis. Journal of Biological Chemistry *282*, 10036-10046.

Peer, W.A. (2013). From perception to attenuation: auxin signalling and responses. Current opinion in plant biology *16*, 561-568.

Peer, W.A., Cheng, Y., and Murphy, A.S. (2013). Evidence of oxidative attenuation of auxin signalling. Journal of experimental botany *64*, 2629-2639.

Pelaz, S., Ditta, G.S., Baumann, E., Wisman, E., and Yanofsky, M.F. (2000). B and C floral organ identity functions require *SEPALLATA* MADS-box genes. Nature *405*, 200.

Pěnčík, A., Simonovik, B., Petersson, S.V., Henyková, E., Simon, S., Greenham, K., Zhang, Y., Kowalczyk, M., Estelle, M., and Zažímalová, E. (2013). Regulation of auxin homeostasis and gradients in *Arabidopsis* roots through the formation of the indole-3-acetic acid catabolite 2-oxindole-3-acetic acid. The Plant Cell, tpc. 113.114421.

Percudani, R., and Peracchi, A. (2003). A genomic overview of pyridoxal-phosphate-dependent enzymes. EMBO reports *4*, 850-854.

Petrášek, J., Mravec, J., Bouchard, R., Blakeslee, J.J., Abas, M., Seifertová, D., Wiśniewska, J., Tadele, Z., Kubeš, M., and Čovanová, M. (2006). PIN proteins perform a rate-limiting function in cellular auxin efflux. Science *312*, 914-918.

Phillips, K.A., Skirpan, A.L., Liu, X., Christensen, A., Slewinski, T.L., Hudson, C., Barazesh, S., Cohen, J.D., Malcomber, S., and McSteen, P. (2011). *vanishing tassel2* encodes a grass-specific tryptophan aminotransferase required for vegetative and reproductive development in maize. Plant Cell *23*, 550-566.

Poethig, R.S. (2013). Vegetative phase change and shoot maturation in plants. In Current topics in developmental biology (Elsevier), pp. 125-152.

Porco, S., Pěnčík, A., Rashed, A., Voß, U., Casanova-Sáez, R., Bishopp, A., Golebiowska, A., Bhosale, R., Swarup, R., and Swarup, K. (2016). Dioxygenase-encoding *AtDAO1* gene controls IAA oxidation and homeostasis in *Arabidopsis*. Proceedings of the National Academy of Sciences *113*, 11016-11021.

Potts, W.C., Reid, J.B., and Murfet, I.C. (1982). Internode length in *Pisum*. I. The effect of the *Le*/*le* gene difference on endogenous gibberellin-like substances. Physiologia plantarum *55*, 323-328.

Poulet, A., and Kriechbaumer, V. (2017). Bioinformatics analysis of phylogeny and transcription of *TAA/YUC* auxin biosynthetic genes. International journal of molecular sciences *18*, 1791.

Qi, J., Wang, Y., Yu, T., Cunha, A., Wu, B., Vernoux, T., Meyerowitz, E., and Jiao, Y. (2014). Auxin depletion from leaf primordia contributes to organ patterning. Proceedings of the National Academy of Sciences *111*, 18769-18774.

Qin, G., Gu, H., Zhao, Y., Ma, Z., Shi, G., Yang, Y., Pichersky, E., Chen, H., Liu, M., and Chen, Z. (2005). An indole-3-acetic acid carboxyl methyltransferase regulates *Arabidopsis* leaf development. The Plant Cell *17*, 2693-2704.

Quittenden, L., McAdam, E., Davies, N., and Ross, J. (2014). Evidence that indole-3-acetic acid is not synthesized via the indole-3-acetamide pathway in pea roots. Journal of plant growth regulation *33*, 831-836.

Quittenden, L.J., Davies, N.W., Smith, J.A., Molesworth, P.P., Tivendale, N.D., and Ross, J.J. (2009). Auxin biosynthesis in pea: characterization of the tryptamine pathway. Plant physiology *151*, 1130-1138.

Rabinkov, A., Zhu, X.-Z., Grafi, G., Galili, G., and Mirelman, D. (1994). Alliin lyase (Alliinase) from garlic (*Allium sativum*). Biochemical characterization and cDNA cloning. Applied biochemistry and biotechnology *48*, 149-171.

Reddy, G.V., Heisler, M.G., Ehrhardt, D.W., and Meyerowitz, E.M. (2004). Real-time lineage analysis reveals oriented cell divisions associated with morphogenesis at the shoot apex of *Arabidopsis thaliana*. Development *131*, 4225-4237.

Reddy, G.V., and Meyerowitz, E.M. (2005). Stem-cell homeostasis and growth dynamics can be uncoupled in the *Arabidopsis* shoot apex. Science *310*, 663-667.

Reid, J.B., and Potts, W.C. (1986). Internode length in *Pisum*. Two further mutants, *lh* and *ls*, with reduced gibberellin synthesis, and a gibberellin insensitive mutant, *lk*. Physiologia Plantarum *66*, 417-426.

Reinecke, D.M. (1999). 4-Chloroindole-3-acetic acid and plant growth. Plant Growth Regulation *27*, 3-13.

Reinecke, D.M., Ozga, J.A., Ilić, N., and Magnus, V. (1999). Molecular properties of 4-substituted indole-3-acetic acids affecting pea pericarp elongation. Plant growth regulation *27*, 39-48.

Reinhardt, D., Pesce, E.-R., Stieger, P., Mandel, T., Baltensperger, K., Bennett, M., Traas, J., Friml, J., and Kuhlemeier, C. (2003). Regulation of phyllotaxis by polar auxin transport. Nature *426*, 255.

Reyes-Olalde, J.I., Zúñiga-Mayo, V.M., Serwatowska, J., Montes, R.A.C., Lozano-Sotomayor, P., Herrera-Ubaldo, H., Gonzalez-Aguilera, K.L., Ballester, P., Ripoll, J.J., and Ezquer, I. (2017). The bHLH transcription factor SPATULA enables cytokinin signaling, and both activate auxin biosynthesis and transport genes at the medial domain of the gynoecium. PLoS genetics *13*, e1006726.

Robert, H.S., Crhak Khaitova, L., Mroue, S., and Benková, E. (2015). The importance of localized auxin production for morphogenesis of reproductive organs and embryos in *Arabidopsis*. Journal of experimental botany *66*, 5029-5042.

Robert, H.S., and Friml, J. (2009). Auxin and other signals on the move in plants. Nature chemical biology *5*, 325.

Robert, H.S., Grones, P., Stepanova, A.N., Robles, L.M., Lokerse, A.S., Alonso, J.M., Weijers, D., and Friml, J. (2013). Local auxin sources orient the apical-basal axis in *Arabidopsis* embryos. Current biology *23*, 2506-2512.

Romero, E., Castellanos, J.R.G., Mattevi, A., and Fraaije, M.W. (2016). Characterization and crystal structure of a robust cyclohexanone monooxygenase. Angewandte Chemie International Edition *55*, 15852-15855.

Rosquete, M.R., Barbez, E., and Kleine-Vehn, J. (2012). Cellular auxin homeostasis: gatekeeping is housekeeping. Molecular plant *5*, 772-786.

Ross, J.J., Murfet, I.C. and Reid, J.B. (1997). Gibberellin mutants. Physiologia Plantarum, *100*, 550-560.

Ross, J.J., O'neill, D.P., Smith, J.J., Kerckhoffs, L.H.J., and Elliott, R.C. (2000). Evidence that auxin promotes gibberellin A1 biosynthesis in pea. The Plant Journal *21*, 547-552.

Ross, J.J., Reid, J.B., Gaskin, P., and MacMillan, J. (1989). Internode length in *Pisum*. Estimation of GA1 levels in genotypes *Le*, *le* and *led*. Physiologia plantarum *76*, 173-176.

Salehin, M., Bagchi, R., and Estelle, M. (2015). SCFTIR1/AFB-based auxin perception: mechanism and role in plant growth and development. The Plant Cell *27*, 9-19.

Sassi, M., Ali, O., Boudon, F., Cloarec, G., Abad, U., Cellier, C., Chen, X., Gilles, B., Milani, P., and Friml, J. (2014). An auxin-mediated shift toward growth isotropy promotes organ formation at the shoot meristem in *Arabidopsis*. Current biology *24*, 2335-2342.

Sassi, M., and Vernoux, T. (2013). Auxin and self-organization at the shoot apical meristem. Journal of experimental botany *64*, 2579-2592.

Scarpella, E., Barkoulas, M., and Tsiantis, M. (2010). Control of leaf and vein development by auxin. Cold Spring Harbor perspectives in biology *2*, a001511.

Schlaich, N.L. (2007). Flavin-containing monooxygenases in plants: looking beyond detox. Trends in plant science *12*, 412-418.

Shao, A., Ma, W., Zhao, X., Hu, M., He, X., Teng, W., Li, H., and Tong, Y. (2017). The auxin biosynthetic *TRYPTOPHAN AMINOTRANSFERASE RELATED TaTAR2.1-3A* increases grain yield of wheat. Plant physiology *174*, 2274-2288.

Shoemaker, R.C., Schlueter, J., and Doyle, J.J. (2006). Paleopolyploidy and gene duplication in soybean and other legumes. Current opinion in plant biology *9*, 104-109.

Sim, N.-L., Kumar, P., Hu, J., Henikoff, S., Schneider, G., and Ng, P.C. (2012). SIFT web server: predicting effects of amino acid substitutions on proteins. Nucleic acids research *40*, W452-W457.

Somers, E., Ptacek, D., Gysegom, P., Srinivasan, M., and Vanderleyden, J. (2005). *Azospirillum brasilense* produces the auxin-like phenylacetic acid by using the key enzyme for indole-3-acetic acid biosynthesis. Applied and environmental microbiology *71*, 1803-1810.

Staswick, P.E., Serban, B., Rowe, M., Tiryaki, I., Maldonado, M.T., Maldonado, M.C., and Suza, W. (2005). Characterization of an *Arabidopsis* enzyme family that conjugates amino acids to indole-3-acetic acid. The Plant Cell *17*, 616-627.

Stepanova, A.N., and Alonso, J.M. (2016). Auxin catabolism unplugged: Role of IAA oxidation in auxin homeostasis. Proceedings of the National Academy of Sciences *113*, 10742-10744.

Stepanova, A.N., Robertson-Hoyt, J., Yun, J., Benavente, L.M., Xie, D.Y., Dolezal, K., Schlereth, A., Jurgens, G., and Alonso, J.M. (2008). *TAA1*-mediated auxin biosynthesis is essential for hormone crosstalk and plant development. Cell *133*, 177-191.

Stepanova, A.N., Yun, J., Robles, L.M., Novak, O., He, W., Guo, H., Ljung, K., and Alonso, J.M. (2011). The Arabidopsis YUCCA1 flavin monooxygenase functions in the indole-3-pyruvic acid branch of auxin biosynthesis. Plant Cell *23*, 3961-3973.

Suh, J.-K., Poulsen, L.L., Ziegler, D.M., and Robertus, J.D. (1999). Yeast flavin-containing monooxygenase generates oxidizing equivalents that control protein folding in the endoplasmic reticulum. Proceedings of the National Academy of Sciences *96*, 2687-2691.

Sun, X.D., Shantharaj, D., Kang, X.J., and Ni, M. (2010). Transcriptional and hormonal signaling control of *Arabidopsis* seed development. Current Opinion in Plant Biology *13*, 611-620.

Sundberg, E., and Ostergaard, L. (2009). Distinct and dynamic auxin activities during reproductive development. Cold Spring Harbor perspectives in biology *1*, a001628.

Swain, S.M., Reid, J.B., and Kamiya, Y. (1997). Gibberellins are required for embryo growth and seed development in pea. The Plant Journal *12*, 1329-1338.

Swarup, R., Friml, J., Marchant, A., Ljung, K., Sandberg, G., Palme, K., and Bennett, M. (2001). Localization of the auxin permease AUX1 suggests two functionally distinct hormone transport pathways operate in the *Arabidopsis* root apex. Genes & development *15*, 2648-2653.

Swarup, R., and Péret, B. (2012). AUX/LAX family of auxin influx carriers—an overview. Frontiers in plant science *3*, 225.

Swiecicki, W. (1989). A new gene *CRISPOID* (*crd*) on chromosome 1. Pisum Newsletter *21*, 73-74.

Symons, G.M., Ross, J.J., and Murfet, I.C. (2002). The bushy pea mutant is IAA-deficient. Physiologia Plantarum *116*, 389-397.

Tam, Y.Y., and Normanly, J. (1998). Determination of indole-3-pyruvic acid levels in *Arabidopsis thaliana* by gas chromatography–selected ion monitoring-mass spectrometry. Journal of Chromatography A *800*, 101-108.

Tan, X., Calderon-Villalobos, L.I., Sharon, M., Zheng, C., Robinson, C.V., Estelle, M., and Zheng, N. (2007). Mechanism of auxin perception by the TIR1 ubiquitin ligase. Nature *446*, 640-645.

Tanaka, H., Dhonukshe, P., Brewer, P., and Friml, J. (2006). Spatiotemporal asymmetric auxin distribution: a means to coordinate plant development. Cellular and Molecular Life Sciences CMLS *63*, 2738-2754.

Tao, Y., Ferrer, J.-L., Ljung, K., Pojer, F., Hong, F., Long, J.A., Li, L., Moreno, J.E., Bowman, M.E., and Ivans, L.J. (2008). Rapid synthesis of auxin via a new tryptophan-dependent pathway is required for shade avoidance in plants. Cell *133*, 164-176.

Tatematsu, K., Kumagai, S., Muto, H., Sato, A., Watahiki, M.K., Harper, R.M., Liscum, E., and Yamamoto, K.T. (2004). *MASSUGU2* encodes Aux/IAA19, an auxin-regulated protein that functions together with the transcriptional activator NPH4/ARF7 to regulate differential growth responses of hypocotyl and formation of lateral roots in *Arabidopsis* thaliana. The Plant Cell *16*, 379-393.

Theißen, G., Kim, J.T., and Saedler, H. (1996). Classification and phylogeny of the MADS-box multigene family suggest defined roles of MADS-box gene subfamilies in the morphological evolution of eukaryotes. Journal of Molecular Evolution *43*, 484-516.

Tivendale, N.D., Davidson, S.E., Davies, N.W., Smith, J.A., Dalmais, M., Bendahmane, A.I., Quittenden, L.J., Sutton, L., Bala, R.K., Le Signor, C.*, et al.*

(2012). Biosynthesis of the halogenated auxin, 4-chloroindole-3-acetic acid. Plant physiology *159*, 1055-1063.

Tivendale, N.D., Davies, N.W., Molesworth, P.P., Davidson, S.E., Smith, J.A., Lowe, E.K., Reid, J.B., and Ross, J.J. (2010). Reassessing the role of *N*-hydroxytryptamine in auxin biosynthesis. Plant physiology *154*, 1957-1965.

Tivendale, N.D., Ross, J.J., and Cohen, J.D. (2014). The shifting paradigms of auxin biosynthesis. Trends in Plant Science *19*, 44-51.

Tiwari, A., Vivian-Smith, A., Ljung, K., Offringa, R., and Heuvelink, E. (2013). Physiological and morphological changes during early and later stages of fruit growth in *Capsicum annuum*. Physiologia plantarum *147*, 396-406.

Tiwari, S.B., Wang, X.-J., Hagen, G., and Guilfoyle, T.J. (2001). AUX/IAA proteins are active repressors, and their stability and activity are modulated by auxin. The Plant Cell *13*, 2809-2822.

Tobeña-Santamaria, R., Bliek, M., Ljung, K., Sandberg, G., Mol, J.N., Souer, E., and Koes, R. (2002). FLOOZY of petunia is a flavin mono-oxygenase-like protein required for the specification of leaf and flower architecture. Genes & development *16*, 753-763.

Tucker, S.C. (1989). Overlapping organ initiation and common primordia in flowers of *Pisum sativum* (Leguminosae: Papilionoideae). American Journal of Botany *76*, 714-729.

Tucker, S.C. (2003). Floral development in legumes. Plant Physiology *131*, 911-926.

Tuominen, H., Ostin, A., Sandberg, G., and Sundberg, B. (1994). A novel metabolic pathway for indole-3-acetic acid in apical shoots of *Populus tremula* (L.) x *Populus tremuloides* (Michx.). Plant physiology *106*, 1511-1520.

Ulmasov, T., Murfett, J., Hagen, G., and Guilfoyle, T.J. (1997). Aux/IAA proteins repress expression of reporter genes containing natural and highly active synthetic auxin response elements. The Plant Cell Online *9*, 1963-1971.

Vallon, O. (2000). New sequence motifs in flavoproteins: evidence for common ancestry and tools to predict structure. Proteins: Structure, Function, and Bioinformatics *38*, 95-114.

Vanneste, S., and Friml, J. (2009). Auxin: a trigger for change in plant development. Cell *136*, 1005-1016.

Wang, B., Chu, J., Yu, T., Xu, Q., Sun, X., Yuan, J., Xiong, G., Wang, G., Wang, Y., and Li, J. (2015). Tryptophan-independent auxin biosynthesis contributes to early embryogenesis in Arabidopsis. Proc Natl Acad Sci U S A *112*, 4821-4826.

Wang, H., Chen, J., Wen, J., Tadege, M., Li, G., Liu, Y., Mysore, K.S., Ratet, P., and Chen, R. (2008). Control of compound leaf development by *FLORICAULA/LEAFY*

ortholog *SINGLE LEAFLET1* in *Medicago truncatula*. Plant Physiology *146*, 1759-1772.

Wang, J.-W., Czech, B., and Weigel, D. (2009). miR156-regulated SPL transcription factors define an endogenous flowering pathway in *Arabidopsis thaliana*. Cell *138*, 738-749.

Wang, Q., Kohlen, W., Rossmann, S., Vernoux, T., and Theres, K. (2014). Auxin depletion from the leaf axil conditions competence for axillary meristem formation in *Arabidopsis* and tomato. The Plant Cell *26*, tpc. 114.123059.

Wang, R. and Estelle, M. (2014). Diversity and specificity: auxin perception and signaling through the TIR1/AFB pathway. Current Opinion in Plant Biology, *21*, 51-58.

Waterhouse, A., Bertoni, M., Bienert, S., Studer, G., Tauriello, G., Gumienny, R., Heer, F.T., de Beer, T.A.P., Rempfer, C., and Bordoli, L. (2018). SWISS-MODEL: homology modelling of protein structures and complexes. Nucleic acids research *46*, W296-W303.

Weeden, N.F., Brauner, S., and Przyborowski, J.A. (2002). Genetic analysis of pod dehiscence in pea (*Pisum sativum L.*). Cellular and Molecular Biology Letters *7*, 657-664.

Weigel, D., Ahn, J.H., Blázquez, M.A., Borevitz, J.O., Christensen, S.K., Fankhauser, C., Ferrándiz, C., Kardailsky, I., Malancharuvil, E.J., and Neff, M.M. (2000). Activation tagging in *Arabidopsis*. Plant physiology *122*, 1003-1014.

Weigel, D., Alvarez, J., Smyth, D.R., Yanofsky, M.F., and Meyerowitz, E.M. (1992). *LEAFY* controls floral meristem identity in *Arabidopsis*. Cell *69*, 843-859.

Weller, J.L., Hecht, V., Liew, L.C., Sussmilch, F.C., Wenden, B., Knowles, C.L., and Vander Schoor, J.K. (2009). Update on the genetic control of flowering in garden pea. Journal of experimental botany *60*, 2493-2499.

Weston, D.E., Reid, J.B., and Ross, J.J. (2009). Auxin regulation of gibberellin biosynthesis in the roots of pea (*Pisum sativum*). Functional Plant Biology *36*, 362-369.

Wild, J., Altman, E., Yura, T., and Gross, C.A. (1992). DnaK and DnaJ heat shock proteins participate in protein export in *Escherichia coli*. Genes & development *6*, 1165-1172.

Wiltshire, R., Murfet, I., and Reid, J. (1994). The genetic control of heterochrony: Evidence from developmental mutants of *Pisum sativum L*. Journal of Evolutionary Biology *7*, 447-465.

Wolbang, C.M., Davies, N.W., Taylor, S.A., and Ross, J.J. (2007). Gravistimulation leads to asymmetry of both auxin and gibberellin levels in *barley pulvini*. Physiologia plantarum *131*, 140-148.

Wollmann, H., Mica, E., Todesco, M., Long, J.A., and Weigel, D. (2010). On reconciling the interactions between *APETALA2*, miR172 and *AGAMOUS* with the ABC model of flower development. Development, 036673.

Won, C., Shen, X., Mashiguchi, K., Zheng, Z., Dai, X., Cheng, Y., Kasahara, H., Kamiya, Y., Chory, J., and Zhao, Y. (2011). Conversion of tryptophan to indole-3-acetic acid by *TRYPTOPHAN AMINOTRANSFERASES OF ARABIDOPSIS* and *YUCCA*s in *Arabidopsis*. Proceedings of the National Academy of Sciences *108*, 18518-18523.

Woo, Y.-M., Park, H.-J., Su'udi, M., Yang, J.-I., Park, J.-J., Back, K., Park, Y.-M., and An, G. (2007). *Constitutively wilted 1,* a member of the rice *YUCCA* gene family, is required for maintaining water homeostasis and an appropriate root to shoot ratio. Plant molecular biology *65*, 125-136.

Woodward, A.W., and Bartel, B. (2005). Auxin: regulation, action, and interaction. Annals of botany *95*, 707-735.

Yachnin, B.J., Sprules, T., McEvoy, M.B., Lau, P.C., and Berghuis, A.M. (2012). The substrate-bound crystal structure of a Baeyer–Villiger monooxygenase exhibits a Criegee-like conformation. Journal of the American Chemical Society *134*, 7788-7795.

Yamada, M., Greenham, K., Prigge, M.J., Jensen, P.J., and Estelle, M. (2009). The *TRANSPORT INHIBITOR RESPONSE2* gene is required for auxin synthesis and diverse aspects of plant development. Plant Physiology *151*, 168-179.

Yamamoto, Y., Kamiya, N., Morinaka, Y., Matsuoka, M., and Sazuka, T. (2007). Auxin biosynthesis by the *YUCCA* genes in rice. Plant Physiology *143*, 1362-1371.

Yang, Y., Xu, R., Ma, C.-j., Vlot, A.C., Klessig, D.F., and Pichersky, E. (2008). Inactive methyl indole-3-acetic acid ester can be hydrolyzed and activated by several esterases belonging to the AtMES esterase family of *Arabidopsis*. Plant physiology *147*, 1034-1045.

Yaxley, J.R., Ross, J.J., Sherriff, L.J., and Reid, J.B. (2001). Gibberellin biosynthesis mutations and root development in pea. Plant physiology *125*, 627-633.

Yoshikawa, T., Ito, M., Sumikura, T., Nakayama, A., Nishimura, T., Kitano, H., Yamaguchi, I., Koshiba, T., Hibara, K.I., and Nagato, Y. (2014). The rice *FISH BONE* gene encodes a tryptophan *aminotransferase*, which affects pleiotropic auxin-related processes. The Plant Journal *78*, 927-936.

Zažímalová, E., Murphy, A.S., Yang, H., Hoyerova, K., and Hosek, P. (2010). Auxin transporters--why so many? Cold Spring Harbor perspectives in biology *2*, a001552.

Zhang, J., Lin, J.E., Harris, C., Pereira, F.C.M., Wu, F., Blakeslee, J.J., and Peer, W.A. (2016). DAO1 catalyzes temporal and tissue-specific oxidative inactivation of auxin in *Arabidopsis thaliana*. Proceedings of the National Academy of Sciences *113*, 11010-11015.

Zhang, R., Wang, B., Ouyang, J., Li, J., and Wang, Y. (2008). *Arabidopsis* indole synthase, a homolog of tryptophan synthase alpha, is an enzyme involved in the trp-independent indole-containing metabolite biosynthesis. Journal of integrative plant biology *50*, 1070-1077.

Zhang, Y., and Skolnick, J. (2005). TM-align: a protein structure alignment algorithm based on the TM-score. Nucleic acids research *33*, 2302-2309.

Zhao, Y. (2012). Auxin biosynthesis: a simple two-step pathway converts tryptophan to indole-3-acetic acid in plants. Molecular Plant *5*, 334-338.

Zhao, Y. (2018). Essential roles of local auxin biosynthesis in plant development and in adaptation to environmental changes. Annual review of plant biology *69*, 417-435.

Zhao, Y., Hull, A.K., Gupta, N.R., Goss, K.A., Alonso, J., Ecker, J.R., Normanly, J., Chory, J., and Celenza, J.L. (2002). Trp-dependent auxin biosynthesis in *Arabidopsis*: involvement of cytochrome P450s *CYP79B2* and *CYP79B3*. Genes & development *16*, 3100-3112.

Zhao, Y.D., Christensen, S.K., Fankhauser, C., Cashman, J.R., Cohen, J.D., Weigel, D., and Chory, J. (2001). A role for flavin monooxygenase-like enzymes in auxin biosynthesis. Science *291*, 306-309.

Zheng, Z., Guo, Y., Novák, O., Chen, W., Ljung, K., Noel, J.P., and Chory, J. (2016). Local auxin metabolism regulates environment-induced hypocotyl elongation. Nature plants *2*, 16025.

Zhou, Z.Y., Zhang, C.G., Wu, L., Zhang, C.G., Chai, J., Wang, M., Jha, A., Jia, P.F., Cui, S.J., and Yang, M. (2011). Functional characterization of the *CKRC1/TAA1* gene and dissection of hormonal actions in the *Arabidopsis* root. The Plant Journal *66*, 516-527.

Zhu, H., Choi, H.-K., Cook, D.R., and Shoemaker, R.C. (2005). Bridging model and crop legumes through comparative genomics. Plant physiology *137*, 1189-1196.

Zhu, X., Zhao, X., Burkholder, W.F., Gragerov, A., Ogata, C.M., Gottesman, M.E., and Hendrickson, W.A. (1996). Structural analysis of substrate binding by the molecular chaperone DnaK. Science *272*, 1606-1614.

Ziegler, D.M. (1993). Recent studies on the structure and function of multisubstrate flavin-containing monooxygenases. Annual review of pharmacology and toxicology *33*, 179-199.

Zúñiga-Mayo, V.M., Reyes-Olalde, J.I., Marsch-Martinez, N., and de Folter, S. (2014). Cytokinin treatments affect the apical-basal patterning of the *Arabidopsis* gynoecium and resemble the effects of polar auxin transport inhibition. Frontiers in plant science *5*, 191.